TAILORING THE ELASTIC POSTBUCKLING RESPONSE OF THIN-WALLED AXIALLY COMPRESSED CYLINDRICAL SHELLS

By

Nan Hu

A DISSERTATION

Submitted to
Michigan State University
in partial fulfillment of the requirements
for the degree of

Civil Engineering - Doctor of Philosophy

2015

ABSTRACT

TAILORING THE ELASTIC POSTBUCKLING RESPONSE OF THIN-WALLED AXIALLY COMPRESSED CYLINDRICAL SHELLS

By

Nan Hu

Recognition of the positive features of elastic instabilities for use in smart and adaptive materials and structures has increased in recent years. Among many unstable events, buckling is one of the oldest and most well-understood types of response and yet this critical condition has been mainly regarded as a failure limit and the afterward response (postbuckling) as a safeguard. However, research on smart/adaptive devices has identified buckling and postbuckling as a favorable behavior. This dissertation explores the potential of cylindrical shells under axial compression, for which mode transitions during the postbuckling response lead to sudden and high-rate deformations from generally smaller changes in the controlling load or displacement input to the system. Such geometric nonlinear responses allow cylindrical shells to be considered as a viable structural prototype for purposes such as energy harvesting, sensing, actuation, etc.

Experimental and numerical studies evaluated three avenues for modifying and controlling the postbuckling response of cylindrical shells: (1) by introducing seeded geometric imperfections (SGI); (2) by introducing non-uniform stiffness distributions (NSD); and (3) by providing lateral constraints and interactions (LCI). An SGI cylinder is obtained by superposing a single mode shape from the eigenvalue analyses on a uniform cylinder to provide a governing role over other initial random imperfections. An NSD cylinder follows a similar concept of introducing artificial imperfections but by strategically placing patterned thickened regions (which alter the stiffness distribution) on the shell surface with the aim of triggering localized buckling events in non-thickened regions. Finally, an LCI cylinder is driven by the desire to gain further control of the

postbuckling response through the interaction of multiple cylinders in nested assemblies. The numerical simulations were conducted through extensions on established methods for simulating nonlinear geometric response in slender structures. Prototyped cylinder were fabricated, first by using laminated composite materials and later through 3D printing and tested under cyclic loading. Further extension of these concepts was explored through a design optimization process.

Numerical and experimental results suggest that SGI and NSD cylinders can attain a controllable postbuckling response due to the governing role of artificial imperfections. For both cases, the localized buckling events can be triggered in predefined regions; and careful selection of the geometry and stiffness distribution can lead to elastic postbuckling responses with tailorable features, which implies diverse design opportunities. Further, simulations and test results demonstrated that the elastic postbuckling response of SGI and NSD shells was less sensitive to initial (manufacturing) imperfections as well as loading variations compared to that of uniform cylinders. Studies on LCI cylinders showed that this concept allows the attainment of a higher number of mode transitions in the elastic postbuckling regime and the post-buckling stiffening behavior increases to levels that surpass the initial buckling load. Optimization results showcased that postbuckling response can be tailored into three types (softening, sustaining and stiffening) and design guidelines were developed to achieve a targeted behavior.

The study has led to knowledge on the possibilities, extent and means to control (and thus design) the elastic far postbuckling response of cylindrical shells with the noted variations in geometry, stiffness and boundary conditions. Full characterization and understanding of these variables in the attainment and control of postbuckling response with desirable features can promote the use of the presented cylindrical shell concepts for a variety of purposes of emerging interest and across scales for various applications.

To my grandpa, Mingsong Hu
For inspiring me to become a lifelong learner
and to my late grandma Dianying Fu
For encouraging me to become an honest person

ACKNOWLEDGMENTS

In spring 2011, my life diverged from the original plan and the offer letter from Michigan State University means a lot to me. At the end of the day, I believe I made a great decision. As I finish this dissertation and complete my doctoral degree at MSU, first and foremost, I would like to acknowledge my adviser, Prof. Rigoberto Burgueño. His expertise and excellence in research was the biggest reason I chose MSU over other schools. Over the past four years, his guidance and encouragement has broadened my training from the traditional research field to a more holistic interdisciplinary platform. He has inspired me to become an independent and hard-working researcher. His passion and continuous push for excellence has made my graduate student career truly rewarding. My success in completing this dissertation and preparing my future academic career would not have been possible without his time and effort. He is not just an academic advisor but a great mentor and a terrific friend. I have determined to pursue a career in academia and I am excited to face the challenges will bring. He planted the ideological seeds for the research presented in this dissertation, and his insight and vision will continue to assist me at developing into the researcher I want to become in the future. As I move forward into the next stage, I will never forget those days I spent with him in East Lansing.

I am grateful for the financial support from the Department of Civil and Environmental Engineering (CEE) at MSU. The CEE Dept. invested in me through teaching assistantship and provided department fellowships. In addition, my doctoral study could not have been completed without funding from the Michigan Department of Transportation and from the U.S. National Science Foundation (Grant number ECCS-1408506). I also gratefully acknowledge the Student Employment Assistance Award and the International Family Health Insurance Award that I received from the Office for International Students and Scholars (OISS) at MSU.

I would like to acknowledge the College of Engineering for numerous resources during my graduate study through seminars, workshops, training, travel grants and fellowships. Special recognition goes to the DECS for their technical services on computer servers and 3D printing.

A special thank you to Dr. Nizar Lajnef as my committee member who, together with Dr. Burgueño, persevered on the promising potential of using elastic instabilities for smart purposes; an effort that was instrumental to the pursuit of this research. Thank you to my other committee members, Dr. Ronald Averill and Dr. Alejandro Diaz for their time, guidance, insight and helpful comments toward the modelling and optimization aspect of this dissertation.

I would like to recognize some instructors I met at MSU, all of whom made my coursework a valuable learning process, not only building my fundamental knowledge but also showing me how to become a better teacher. They are Dr. Rigoberto Burgueño, Dr. Alejandro Diaz, Dr. Dahsin Liu, Dr. Thomas Pence, Dr. Steven Shaw and Dr. Thomas Voice.

I was blessed that I had a rich teaching experience during my graduate study. Being a TA for four years allowed me get to know many smart undergraduate students and I built a great friendship with many of them. This is a valuable training for my future faculty career. Beyond my TA, I have been actively involved in many teaching training programs. I would like to acknowledge Dr. Melissa McDaniels for offering me opportunities to learn advanced pedagogical knowledge and to help new TAs in their early career. I also thank Dr. Joyce Parker and Dr. Katy Colbry in the process of finishing the Certificate of College Teaching at MSU.

I am grateful to Prof. William C. Taylor for his time on editing many of my manuscripts for journal publications and helping me improve my English writing.

I wish to express my thanks to Dr. Ahmed Naguib for his time and assistance in finishing the Master Degree of Science in engineering mechanics at MSU.

I would like to acknowledge our great CEE staff, Margaret Conner, Mary Mroz, Joseph Nguyen, Laura Post, and Laura Taylor for their dedication on administrative support.

I want to express my gratitude to Dr. Julia McAnallen, who appointed me to serve on the Graduate Advisory Board and to plan and run some graduate school events. I would like to acknowledge CEE Dept. committee for nominating me as the student representative at the Engineering Graduate Studies Committee and COGS for selecting me as a standing board member of the University Committee on Graduate Studies. These experiences helped me build more long-term skills for my future career.

My graduate school experience at MSU was so special and grateful because of my colleagues and friends - past and present. It is a great source of friendships as well as good advice and collaboration. Many members in Dr. Burgueño's group offered me their time to share their research and personal experience, including Mansour Alturki, Ata Babazadeh, Lauren Fedak, Annelise Heeringa, Suihan Liu, Erik Ohlsson, David Stringer, Yi Sun, Emily Winn, and Caroline Williams. I would like to particularly acknowledge two of my best friend among them: Yi who helped me in settling down in the beginning and in surviving throughout my graduate program and Suihan for bringing me positive words, attitude and energy toward the end of my program.

Many other colleagues in the CEE Dept. contributed immensely to my personal and professional time at MSU. They offered their time and support. They shared their culture and language with me. They are Ankit Agrawal, Amir Arablouei, Wassim Borchani, Chris Dean, Iman Harsini, Anas Jamrah, Salih Kocak, Tulakemelwa Mhamilawa, Mohannad Naser, Shabnam Rajaei, Duraisamy Saravanathiiban, Libya Ahmed Sbia, Anuj Shakya, Sepehr Soleimani, Berkay

Tascioglu, and Sudhir Varma. It has been a pleasure to share my office with Hande Ozturk, Elaheh Esfahanian, Pegah Rajaei and Jingjun Shen. I enjoyed working with my fellow board members on CEE Graduate Student Organization, including Wouter Brink, Amanda Herzog, Prianca Bhaduri Maggie Kronlein, and Yogendra Kanitkar. The Chinese student community who provided a strong support system: Cui Cheng, Qinqin Ding, Lina Nan, Bing Guo, Jun Liu, Wenyang Liu, Xing Rao, Hang Shi, Yang Song, Di Tang, Fei Teng, Jie Wang, Xiaoyu Wang, Xun Wang, Dejian Xu, Baolin Yu, Danna Yu, Fangyun Zhong, Tao Zhou and Shuzhuan Zheng.

I am also grateful to the following former classmates, for their various forms of support during my graduate study: Xu Gong, Li Gu, Liaoyuan Li, Yuanyuan Luo, Yun Luo, Wei Pei, Yufeng Shi, Wei Wang, Xiao Xiao, and Dongdong Zhao.

Additionally, I would like to offer my sincere gratitude and thanks to my family: Mom, Dad, Mother-in-law, Father-in-law, uncles, aunts and grandparents, for their support and love.

Finally, I would like to offer my deepest gratitude to my wife, Juan. We have spent more than ten years together since our undergraduate study in China. Without her unconditional love, support, and never-ending words of encouragement, I would not have been able to overcome all obstacles and become who I am today. She pushes me become a better person. She believes that I could accomplish anything, regardless of how difficult I thought it was. Early this year in March, she delivered our first daughter, Yiwen. We feel lucky and grateful to become parents and raise her together.

Nan Hu

East Lansing, Michigan, USA

June 2nd 2015

TABLE OF CONTENTS

LIST OF TABLES

LIST OF FIGURES

KEY TO SYMBOLS

A	=	dissipated strain energy (enclosed area of response curve)
K_e	=	end stiffness before the unloading point
K_i	=	initial stiffness before the first bifurcation
P_{cr1}	=	first buckling load
P_{max}	=	maximum buckling load
m	=	the axial half wavenumber
n	=	the circumferential full wavenumber
n_t	=	number of mode transitions
δ	=	spacing between snap-through events
δ_{max}	=	maximum spacing between snap-through events
ΔP	=	load drop between first bifurcation and unloading point
ΔP_{max}	=	maximum load drop between first bifurcation and unloading point
L	=	the effective length of the cylindrical shell
R	=	the radius of the cylindrical shell
t	=	the shell thickness
v	=	the Poisson's ratio

Chapter 1

Introduction

1.1 Motivation and Vision

Elastic instability has been a major concern for centuries in the design of all slender structural elements and systems due to the resulting capacity reduction and associated large deformations. However, a paradigm shift has emerged during the past decade pointing to an exciting research area dealing with the harnessing of elastic unstable events for "smart" purposes, such as the design of actuators, dampers, energy harvesters, sensors, etc. Among many unstable events, buckling is one of the oldest phenomena that is well understood and yet is generally avoided through special design consideration. Increasing interests in the design of smart devices and mechanical systems have identified buckling and postbuckling as a favorable behavior, which leads to the investigation of such response from a brand new perspective.

In the context of buckling-induced smart applications, most studies to date have explored many traditional structural prototypes, such as laterally-loaded arched beams and bi-stable plates, axially-loaded columns and strips, etc. Studies on 3D forms such as cylinders and spheres are limited because the potential of using these forms for smart applications is confined by the uncertainty of the postbuckling response and the difficulty of numerical prediction due to their imperfection sensitivity. The selected prototype for this research was an axially compressed thin-walled cylindrical shell, which has been comparatively less studied for smart purposes than for its use as a load-carrying element. Mainstream research efforts have been made since early in the

20th century mainly focused on determining the critical buckling load with a single stable equilibrium path, or on determining the initial postbuckling path for use as residual capacity. Compared to other existing prototypes, cylindrical shells can attain a higher number of multiple stable configurations (also known as mode jumps or mode transitions) in their postbuckling regime without the need of additional constraints due to the natural transverse deformation restraint provided by their geometry. However, cylinders are embedded in many structural component and system, as shown in Figure 1-1. The research findings presented herein provide guidance on tailoring the postbuckling response of cylindrical shells to achieve desired target responses and open new avenues for using such prototype for potential applications across scales.

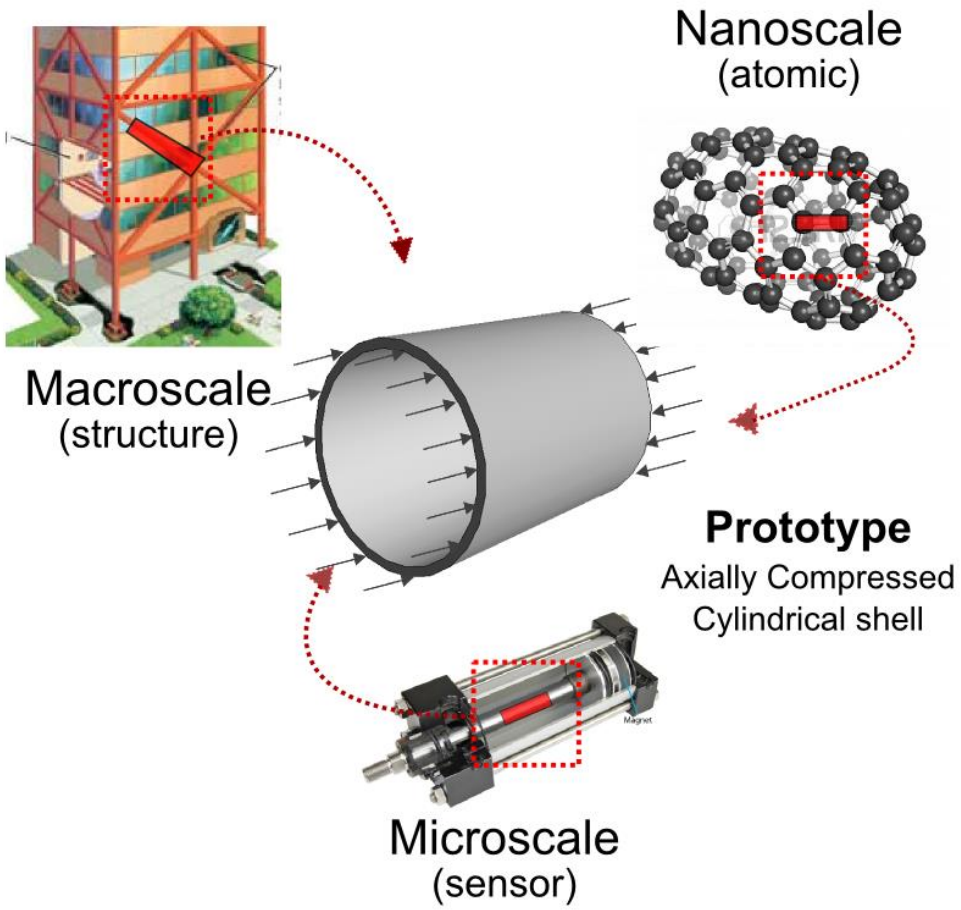

Figure 1-1: Axially compressed cylindrical shells across scales.

1.2 Background

1.2.1 Harnessing elastic instabilities for smart purposes

Even though the theory of elastic stability [1, 2] is considered a mature field of mechanics, a paradigm shift during the past decade is emerging to rekindle the popularity of studying elastic instabilities of many kinds [3], such as snapping, buckling, wrinkling, crumpling, phase transition, cavitation, etc. Among these kinds, buckling is a phenomenon that has been known for centuries, since an equation to determine the critical buckling of a column was derived by Leonhard Euler. Harnessing buckling-induced instabilities for smart purposes is a much less explored yet promising research field. Figure 1-2 shows a concept map of four major aspects in the use of buckling and elastic instabilities including application purposes, application scales, structural prototypes and material prototypes.

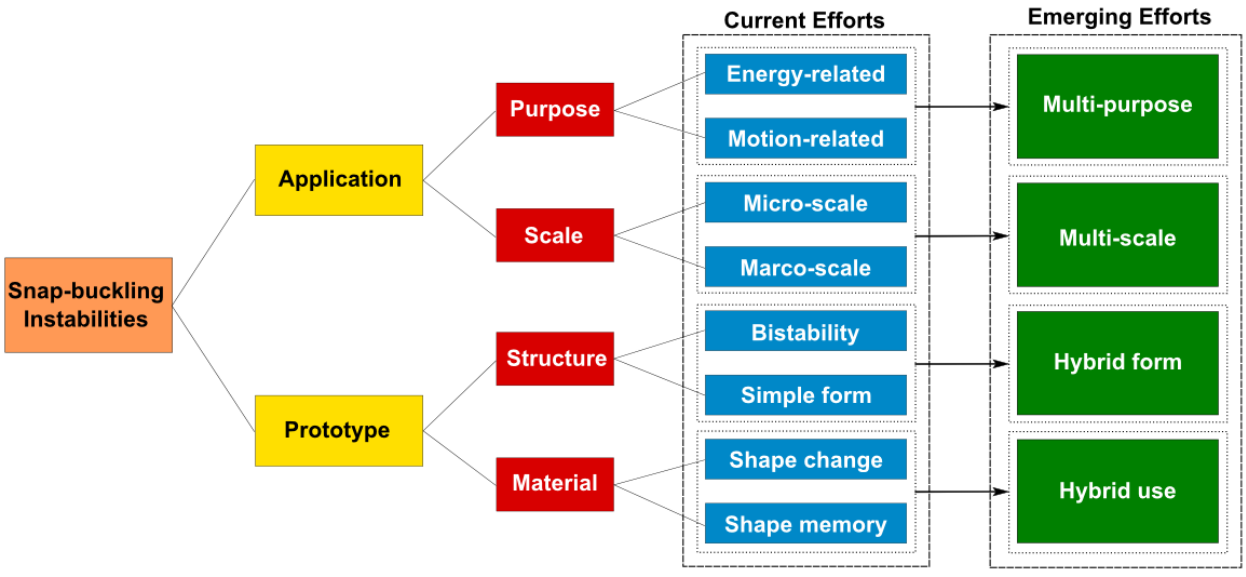

Figure 1-2: Concept map of using elastic instability, applications and prototypes.

Smart applications have recognized buckling-induced nonlinear behavior as favorable due to two encouraging features, namely, high-rate motion and sudden energy release. Within the elastic response domain, structures are capable of snapping from an initial shape to a buckled shape. This feature has been investigated to develop novel design concepts of actuation, micro-optical switching, and structures at multiple scales with switchable functionalities, morphogenesis, etc. [4-6]. The key merit of using snap-buckling is that local and global buckling (in some cases they may happen together) in structural elements can reduce the actuation force during shape recovery. In addition, snap-buckling events release a significant amount of energy from the system as the structure transitions into another stable post-buckled shape. Such behavior has proved to be a very promising phenomenon for the design of energy harvesters, sensors and actuators. For example, micro-electromechanical systems (MEMS) with snap buckling as an energy harvesting mechanism have features such as being able to generate high-frequency impulses over a large frequency interval, self-tuning abilities, and capability of adapting to variable acceleration levels [7]. Recent efforts on self-powered wireless sensors have shown them capable of achieving active sensing due to the actuation from buckling-induced responses (from a buckled wire [8], beam [9], strip [10]). Such active sensors have proven to be a powerful future technology for structural health monitoring (SHM) and non-destructive evaluation (NDE). Emerging trends have shown the promising buckling-induced applications for multiple purposes, such as compliant mechanism for MEMS-based accelerometers [11], increase of solvent transport [12], determination of material properties [13], design of ventricular assistance devices for a better transmission of the pneumatic load to the blood [14, 15], etc. It should be noted that many existing buckling-induced applications are primarily at the micro scale, but the emerging trend is extending similar principles to potentially serve as a platform for some nanoscale

applications, such as triggering an abrupt change in the phononic properties of nano-materials [16], creating unidirectional negative Poisson's ratio behavior within materials with periodic microstructure [17], and to assist nanoscale assembly of a complex structures [18], etc.

It follows that the study of elastic instabilities and its applications is a highly multi-disciplinary problem that includes elements of applied mathematics, biology, material sciences, mechanics, physics, engineering, sustainability, etc. A recent review [19] concluded that many interesting problems within the topic of elastic instability in a broader sense remain to be investigated, including: (1) the mathematical complications in modeling buckling and post-buckling in thin structures; (2) the mechanical instability of materials associated with inhomogeneity and nonlinearity; (3) new phenomena due to the coupling between geometric and material nonlinearities; and (4) the usefulness of mechanical instabilities for broad engineering applications.

The first and major step for using a specific unstable event is to identify the desirable structural prototype. Using the postbuckling response of axially-loaded structures for smart applications has been studied for many structural forms [20-23], including beams, plates, and rods. However, cylindrical shells have been relatively less used due to its more rigorous analytical modeling and their high sensitivity to imperfections. However, cylindrical shells offer some desirable response features in the postbuckling regime that other forms cannot attain with the provision of external constraints. Figure 1-3 plots schematic response curves in the initial postbuckling equilibrium path, which indicates that cylindrical shells can have an initially unstable behavior with a larger load drop and deformation. Recent studies have attempted to use such initial unstable postbuckling behavior of cylindrical shells in the design of energy harvesters [24] and sensors [25]. When considering energy harvesting, the cylindrical

piezoelectric harvester with optimal layout is expected to provide higher energy conversion efficiency than simple forms (e.g., beams or cantilevers). In sensing applications, an axially-loaded cylindrical shell is expected to detect minute loads due to its sudden load drop along the equilibrium path. Another interesting postbuckling feature is the negative stiffness in the response curve, which can be potentially used in the design of advanced dampers and isolators. Such principle has been recently explored in other cylindrical type axially-loaded structures, such as tubes [26], and columns [27, 28].

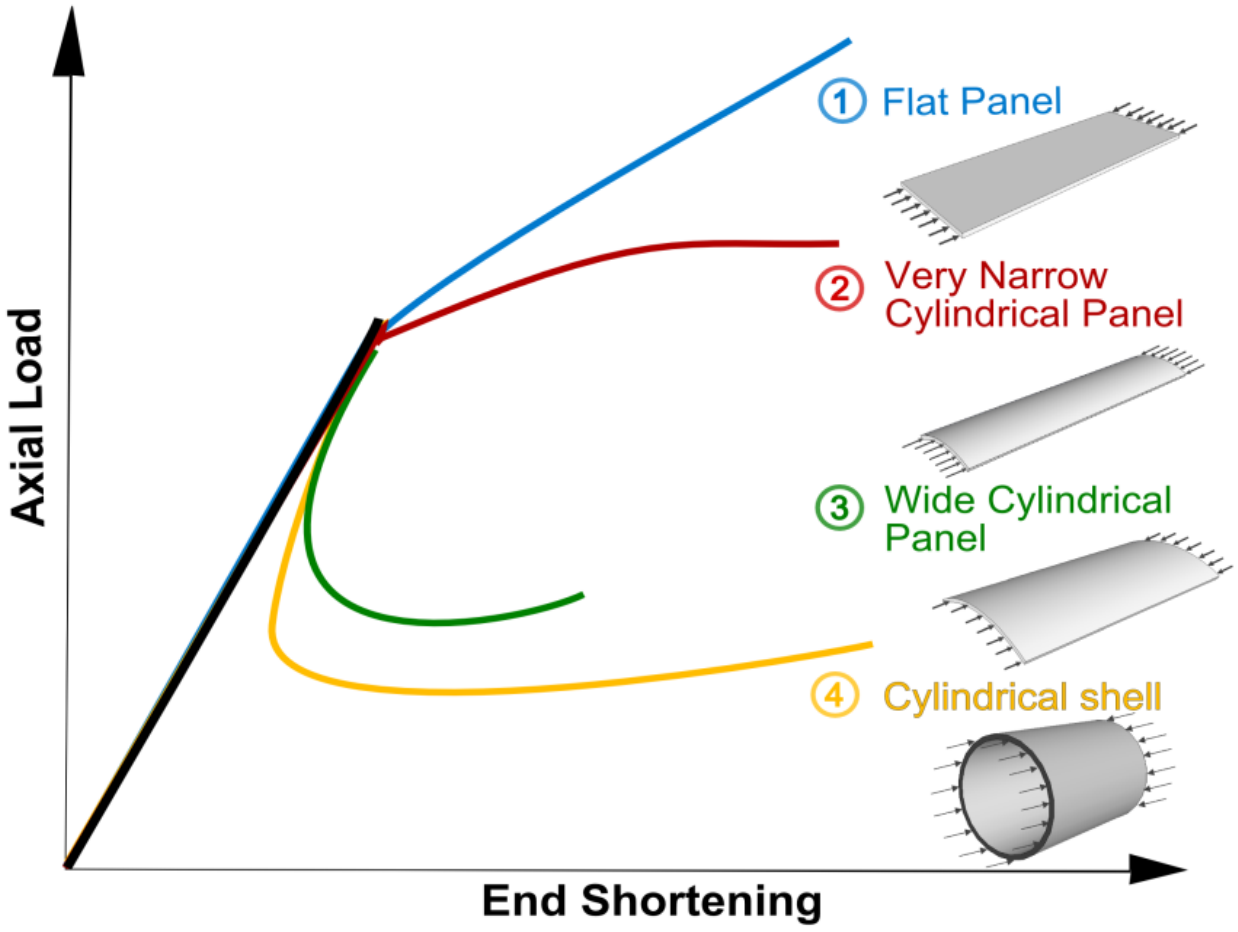

Figure 1-3: Schematic diagram of the postbuckling response of various axially-loaded structures.

1.2.2 Buckling and postbuckling of an axially compressed cylindrical shells

There is a long history of research [29, 30] since the early twentieth century aimed at predicting the critical buckling load of cylindrical shells under axial compression with the goal of determining this limit state with more accuracy. Consequently, most of the efforts have been on determining the critical bifurcation point in the primary static loading branch, shown as path (1) in Figure 1-4. Later, experimental evidence [31, 32] identified the governing role of material and geometric imperfections on the critical load, which challenged the development of analytical and numerical models. Geometric imperfections are known to reduce the critical buckling as shown in path (2). Endeavors to understand the mechanisms behind the postbuckling response of axially compressed cylindrical shells have been carried out analytically since the pioneering work by Koiter in the early 1940's [33]. Due the problem's complexity analytical studies have mainly focused on determining the first or second buckling loads and the initial postbuckling equilibrium paths [34-37]. Recent efforts are motivated by the interest in using the residual strength in the postbuckling regime as a safeguard [38, 39].

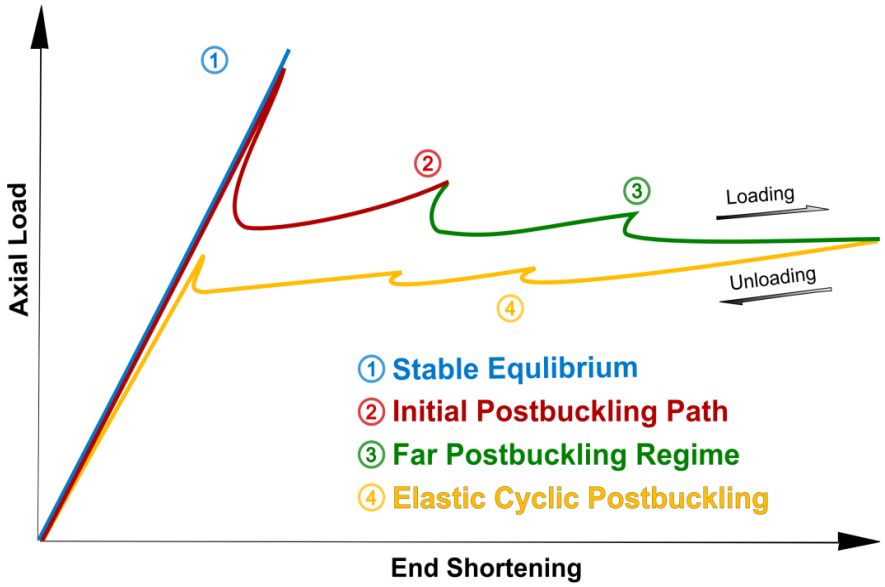

Figure 1-4: Schematic diagram of the postbuckling response of a cylindrical shell.

Aided by advances in computational mechanics and computer technology, investigations on the postbuckling behavior of shells since early 1990s have mostly been carried out through numerical modeling approaches. Several numerical methods have been proposed to trace the equilibrium paths in the postbuckling regime [40-43], as shown in path (3) of Figure 1-4. Rather than a response path with a single bifurcation point and a large critical buckling load, multiple bifurcation points can be observed in the postbuckling response due to changes in the deformed geometry after each critical point. A sudden "load drop" will occur when the equilibrium paths intersect with each other, namely the strain energies corresponding to two successive curves are equal. A localized buckling event in the shell surface releases energy from the system and additional strain energy needs to accumulate to generate a new critical event. As a result, the final response curve will consist of portions from the entire family of paths with a number of jumps. Another interesting feature recognized by several experimental studies [38, 44, 45] is the recoverable nature of the postbuckling response, as shown in path (4). An enclosed area in the force-deformation response exists associated with the energy dissipation from the equilibrium path transitions. Such features are not easily attained by other axially compressed structural prototypes without providing them with additional external constraints.

1.2.3 Effect of geometric imperfections on postbuckling response

The postbuckling response of cylindrical shells is highly imperfection sensitive and difficult to predict due to the random nature of the imperfection profile. In general, geometric imperfections on the shell surface can be considered in four ways: by a mathematically determined "worst" pattern, from actual measurements, through eigenvalue-based simulated shapes, or by probabilistic methods. In the early stages of analytical model development, determination of the "worst" pattern was theoretically demanding and thus geometric imperfections were assumed to

have an asymmetrical shape such that a load deduction could be estimated at a lower capacity. The well-known knock-down factor was introduced to consider the imperfection sensitivity and ensure a lower bound of residual capacity. The existence of imperfection leads to discrepancy between analytical model predictions and experimental data. The most significant modeling performance gain comes from the ability to scan the initial geometric imperfections and thickness variations of manufactured shells for use as input to analytical and numerical models. From a practical point of view, measured imperfections using laser scanning techniques are not always available. Thus, mode shapes from eigenvalue buckling analyses are commonly used to define artificially generated imperfections as small perturbations on the perfect shell. Typically the first eigenmode is chosen to simulate an imperfection with a symmetric shape because the lowest mode is assumed to have the largest effect on the first buckling load. However, it has been shown that improved agreement with experimental data is obtained by seeding imperfections from the superposition of multiple mode shapes [43]. The seeded imperfection amplitude can range from 5% to 50% of the shell thickness and is selected based on known knowledge of experimental response [46]. Thus, in spite of the significant advances in numerical modeling approaches for predicting the buckling and postbuckling response of cylindrical shells, without the measurement of actual geometric imperfection, the disagreement of predicted and measured responses still exists [47-49]. Most of the recent studies on imperfection sensitivity have featured the use of probabilistic methods (such as Monte Carlo) to develop less conservative guidelines for the design of axially compressed cylindrical shells [50-52] and more localized types of imperfection have been considered for calculating the postbuckling response, such as cutouts, dimples, dents, mid-surface imperfections, etc.

The governing role of imperfection sensitivity has limited the potential use of unstiffened cylindrical shells for the design of smart devices and mechanical systems. Given that imperfections cannot be avoided, at least under current manufacturing technologies, the design of cylindrical shells for smart purposes requires the transition from imperfection sensitive structures to imperfection insensitive structures. Such attempt has been made in the design of stiffened cylindrical shells where the buckling events are to occur between stringers even though the load-carrying capacity is still reduced by the imperfection [53]. The possibility of the noted transition (from imperfection sensitive to imperfection insensitive) has been demonstrated in a two-part paper series [54, 55]. Several recent studies on shape optimization have thus explored the opportunity of designing the pattern and amplitude of imperfections. Lindgaard et al. [56] carried out shape optimization with buckling mode shapes as the design variables. The resulting mode shapes were used to define a "worst" imperfection pattern for a thin-walled cylindrical shell such that the axially compressed cylinder would minimize the buckling load. Ning and Pellegrino [57] explored the concept of imperfection-insensitive cylindrical shells by designing a wavy cross-section using structural optimization. It follows that, overall, the role of the geometric imperfection may not be necessary regarded as a detrimental factor for the purpose of designing smart materials and structures.

1.2.4 Modification and control of postbuckling response

The generation of multiple mode transitions in the postbuckling response of axially compressed cylindrical shells highly depends on material, geometry and constraint features. To achieve a targeted postbuckling response, existing avenues to modify and potentially control such behavior includes: (1) varying the material properties; (2) using hybrid material systems; (3) using hybrid material combinations and (4) adding lateral constraints.

A prior study [58] identified that an isotropic shell may only be stable in its initial configuration but that it will exhibit second or more stable configurations if made from fiber-reinforced composites. The variation of fiber orientations, layer thicknesses and stacking sequence of laminated composites has a significant effect on the first buckling load and near bifurcation postbuckling behavior. Tailoring laminated composite to achieve tristability has been investigated for multiple shell forms, such as corrugated shells [59], orthotropic shells [60], double curved shells [61], etc. Multi-stable mechanisms have also been reported by using hybrid systems. A quadri-stable compliant mechanism was designed and tested by using a bi-stable curved-beam embedded in an arch beam [62]. A bi-stable switching mechanism was achieved through a hybrid system of curved strips attached to a center beam [63]. A multi-stable lattice structure consisting of a tri-stable lattice cell made with bi-stable laminates has also been developed [64]. Buckling and postbuckling response has also been studied with the combination of two materials for achieving sustainable snapping events, such as shape memory alloy wire actuators embedded in laminated composites [65, 66], composite plates with piezoelectric actuators and sensors [67, 68]. Similar effects have been achieved by using Macro-Fibre Composites (MFC) to provide activation load. MFC bonded onto another structure has also been used for developing energy harvesting prototypes due to their flexibility at large deformations and shown to have higher power generating efficiency compared to traditional piezoelectric materials [69]. Four major materials with the ability of shape change reported in the literature [6] are metals (including metalloid), fiber-reinforced composites, polymers and piezoelectric materials. In other cases, a smart structure also requires the ability of shape memory (i.e., snap back to the original shape without external stimulus). Shape memory alloys (SMAs) [70] and shape-memory polymers (SMPs) [71, 72] are well-known candidates among many smart

materials. An ongoing trend is using soft and super-elastic materials to trigger snap-buckling, such as dielectric elastomers (DEs), graphene, and ionic polymer–metal composites (IPMCs). Finally, a way to induce multiple bifurcation events in the postbuckling response of slender elements is to provide them with external lateral constraints that limit transverse deformations [73, 74]. Prior studies have studied the addition of rigid constraints to provide additional boundary conditions in order to achieve sustained snap-through and snap-back response in the far postbuckling regime. For example, the disordered packing behavior of an elastic rod constrained by a cylindrical chamber was studied to develop a prototype for a folding mechanism [75]. A bilaterally constrained axially loaded CFRP strip can also exhibit snap through behavior between the multiple buckling modes [10].

Optimization techniques have been devloped to seek the best material/stiffness distributions or, in this case, an optimal shell geometry for a given objective [76] and general theories are well-documented [77]. A recent review [78] shows that topology optimization has been used to solve many multidisciplinary problems in the past decade. A paradigm shift of topology optimization from a static problem with a strength goal to a buckling objective, considering a nonlinear large deformation problem for smart purposes, has also emerged. Numerical algorithms for tracking a nonlinear response path that exhibits snap-through behavior have been developed [79-83]. Optimization studies towards tailoring the postbuckling response of cylindrical shell has not been equally explored compared to plates because it always fails to the clichés of imperfection sensitivities and manufacturing difficulties. Recent efforts showcase the use of topology optimization to find material layouts to obtain larger displacement and energy release from the snap-through events for different purposes, such as actuators [84-88], energy harvesters [24, 89, 90], dampers [91], multi-stable compliant mechanisms [92, 93],

thermoelectric generators [94] and flutter control [95]. Thus, topology optimization is a promising technique to find new structural and material layouts that satisfy a targeted snap-buckling response. Shape and topology optimization techniques can thus provide synergistic features to explore optimal geometric shapes and material distributions for harnessing instabilities in the postbuckling behavior of shells.

1.2.5 Research gap

The buckling and postbuckling response of axially-loaded cylindrical shells has been a topic of study for over a century. Yet, Figure 1-5 indicates that most studies have primarily focused on determining the first critical buckling capacity. Studies beyond the initial equilibrium path have increased only recently and deal mostly with the evaluation of residual capacity. The far postbuckling regime is usually regarded as a failure and associated with plastic buckling if the cylindrical shells are used as load-carrying components.

The focus of this research is in the vein of increasing interests in smart structures, which turns elastic buckling from an undesirable feature into a desirable opportunity. Rather than a buckling criterion, the first research gap is attaining multiple mode transitions and a recoverable response in the far elastic postbuckling regime. The background presented in this section has shown that axially-loaded cylindrical shells as a prototype for smart purposes are much less explored. The largest barrier for using the elastic postbuckling domain in shells is that the occurrence of multiple mode transitions and their spacing cannot be accurately predicted and controlled due to the high degree imperfection sensitivity. The second research gap is thus to study cylindrical shells with varied stiffness (material and geometry) such that postbuckling response can be tailored and controlled. Figure 1-6 provides the evidence that isotropic unstiffened cylindrical

shells have been highly studied due to their associated purpose as load-carrying components; but in this kind of behavior they are most likely not an appropriate prototype.

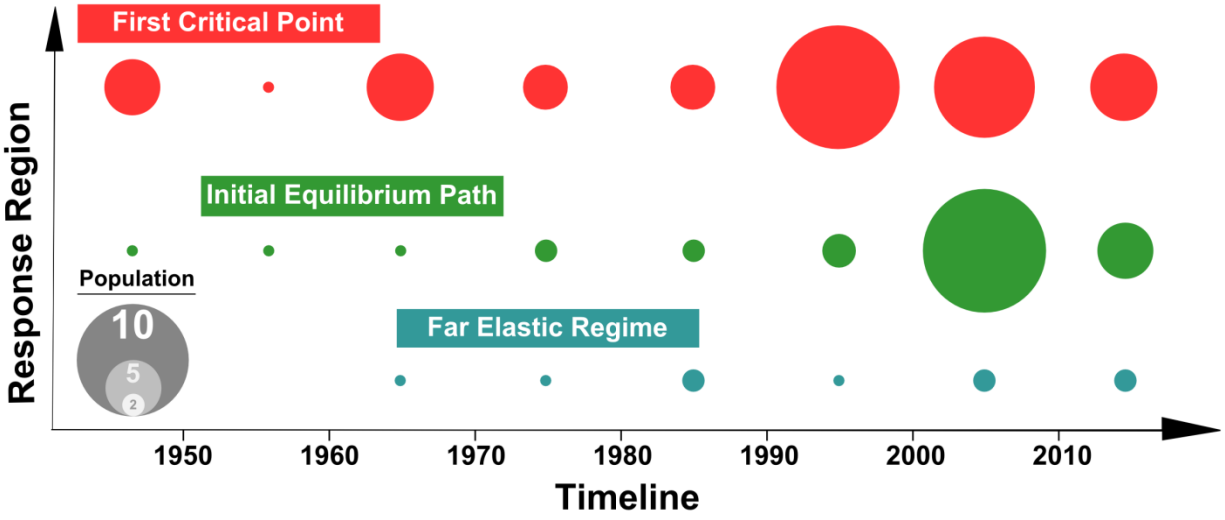

Figure 1-5: Response domain on postbuckling behavior of axially-loaded cylindrical shells.

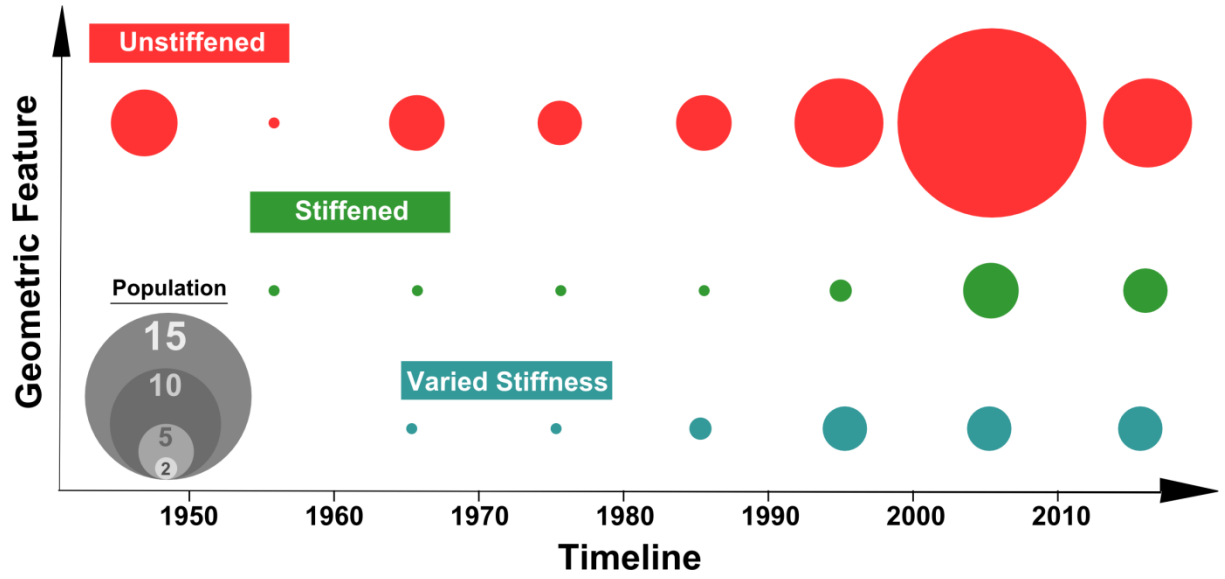

Figure 1-6: Geometric feature on the study of postbuckling behavior of cylindrical shells.

1.3 Hypothesis and Objectives

1.3.1 Hypothesis

The elastic postbuckling response of cylindrical shells can be tailored and the sensitivity to imperfections as a traditional challenge in the design of cylindrical shell can be reduced *if* the geometric features, material systems and external constraints can be properly designed; thus transforming a behavior traditionally seen as undesirable into an opportunity for use in smart materials and structures.

1.3.2 Objectives

Harnessing elastic postbuckling response features in cylindrical shells is a less explored yet promising avenue for the development of novel materials and devices. The research goal is to generate a new understanding for the means by which the elastic postbuckling response of cylindrical shells can be tailored, i.e., modified, controlled and designed for specific features.

1.4 Scope

The scope of this research is to study the elastic postbuckling regime of cylindrical shells under axial compression through three key design approaches as shown in Figure 1-7. Again, the postbuckling response regime is the focus of this study, particularly the attainment of multiple mode transitions. It is proposed that the elastic postbuckling response of axially compressed cylindrical shells can be categorized in three types, as shown in Figure 1-8: stiffening, sustaining and softening. These definitions are based on a ratio of the total load drop (between the first buckling event and the end of the loading phase) to the magnitude of first critical buckling load. As discussed later, each postbuckling response type has its own potential application features.

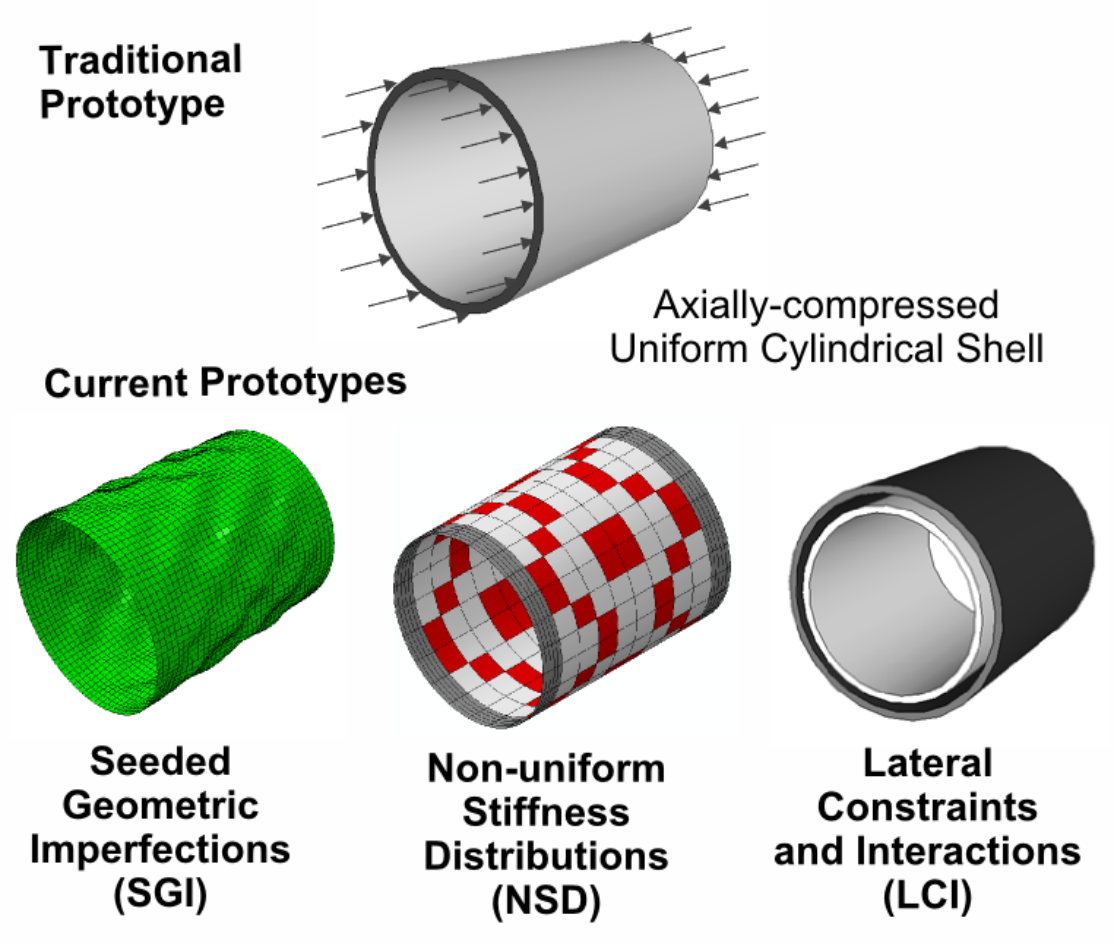

Figure 1-7: Schematic of the three design concepts for cylindrical shells..

Three prototypes (SGI, NSD, and LCI) are proposed (see Figure 1-8) to achieve a targeted elastic postbuckling response. The SGI concept was inspired by a well-known numerical approach of modeling the postbuckling behavior with the consideration of imperfections. An SGI cylinder is thus obtained by superposing single or multiple mode-shapes from an eigenvalue analysis on a uniform cylinder such that a predefined geometric imperfection provided to the original geometry has a governing role over other initial random imperfections. The NSD cylinder follows a similar concept of introducing artificial imperfections but in this case by strategically placing patterned thickening regions (which alter the stiffness distribution) on the

shell surface with a focus of triggering localized buckling events in non-thickened regions. The LCI cylinder concept emerged from the desire to obtain more mode transitions in the postbuckling regime, compared to SGI and NSD cylinders, since the provision of multiple walls leads to their interaction in the elastic postbuckling regime. With the noted variations in geometry, stiffness and boundary conditions, the elastic postbuckling responses of these three cylindrical shell types are expected to be tunable, that is, they can be modified and controlled.

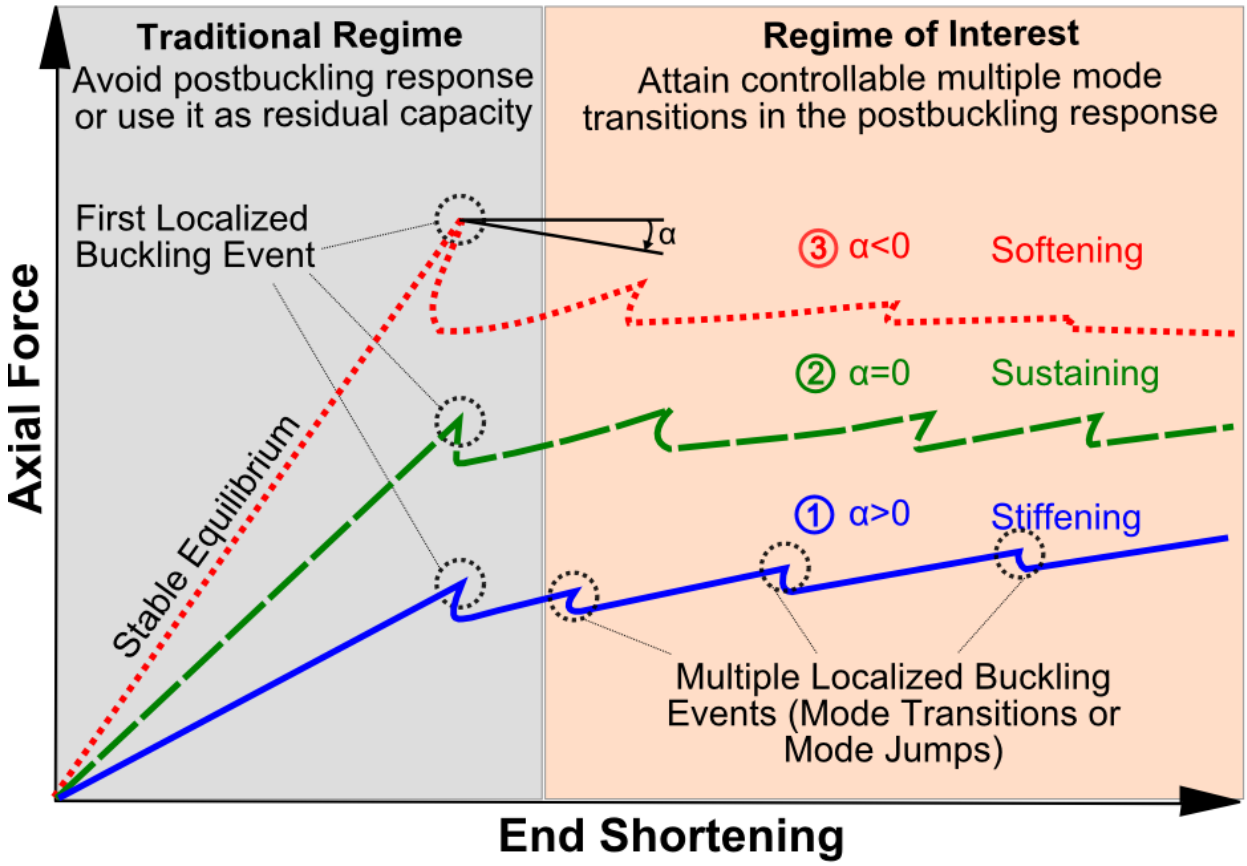

Figure 1-8: Schematic of the target postbuckling response of axially-loaded cylindrical shells.

1.5 Organization

This dissertation has been organized into eight chapters. The remainder of this dissertation is organized as follows. Chapter 2 provides a background and literature review for the advances and trends on using buckling and elastic instabilities in general, including key applications, structural prototypes, material uses, etc. Chapter 3 introduces the state-of-the-art approaches of understanding and predicting the postbuckling response, including theoretical considerations, numerical modeling and experimental testing. Chapter 4 presents the concept of using seeded geometric imperfection (SGI) designs to modify and control the elastic postbuckling response. Chapter 5 explores the concept of using non-uniform stiffness distributions (NSD) numerically and experimentally. Chapter 6 presents the concept of providing internal lateral constraints and interactions (LCI). Chapter 7 discusses the potential applications for using cylinders with the assistance of an optimization tool and advanced manufacturing. Chapter 8 provides the research significance, conclusions and future research needs.

Chapter 2

Buckling-Induced Smart Applications

2.1 Overview

This chapter presents a state-of-the-art review to showcase the recent advances on buckling-induced smart applications and to explain why a buckling response offers certain advantages to fit their purpose. Interesting prototypes in terms of structural forms and material uses associated with those applications are summarized. Finally, this review identifies potential research avenues and emerging trends for using buckling and other elastic instabilities (EI) for future innovations. This chapter was partially published as a topical review paper in the journal *Smart Materials and Structures* [96].

2.2 Why Buckling?

For centuries, buckling has been a major concern in the design of all slender structural elements and systems due to the resulting capacity reduction, associated large deformations and catastrophic failure. The structural response beyond the first bifurcation, i.e., the postbuckling response, has been of most common interest only as residual capacity but otherwise not given much attention and in most cases thought of little practical meaning. This is because it is difficult to predict and control due to its high sensitivity to initial conditions, namely geometric imperfections. Other than load-carrying capacity, two encouraging features of many buckling phenomena are high-rate motion and sudden energy release. Within the elastic region, structures are capable of snapping from their initial shape to a buckled shape along with a significant

amount of energy release from the system, represented as a load drop in the force-deformation response curve. These two features make buckling an ideal mechanism for adaptive and smart applications. Increasing studies are demonstrating the use of such behavior across disciplines, which can be divided into two main categories: energy-related and motion-related applications (see Figure 2-1).

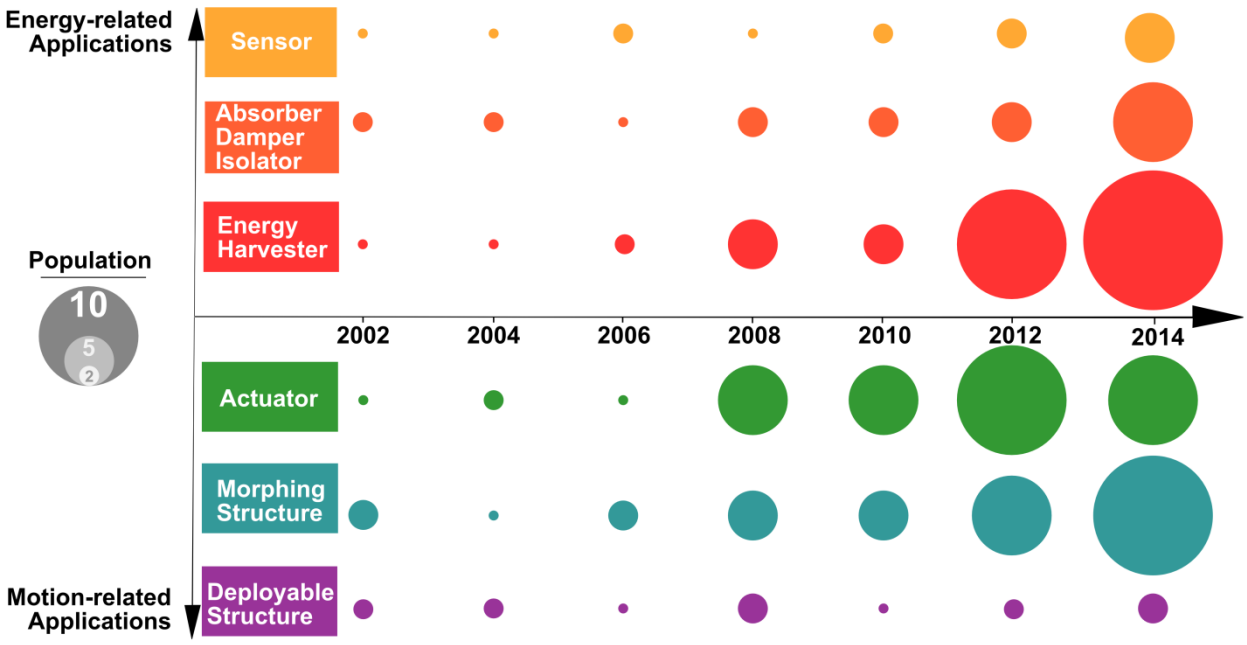

Figure 2-1: Research publications on the use of elastic instability for different purposes.

2.2.1 Energy-related applications

Energy-related applications can be further categorized into energy production and energy dissipation. Energy released from the buckling events can be used in the design of energy harvesters and sensors for micro-electromechanical systems (MEMS) while the energy dissipated can be useful for the design of absorbers, dampers, stabilizers and isolators.

Buckling events have been shown as a very promising source for nonlinear energy harvesters by featuring the generation of high-frequency impulses over a large frequency interval, self-

tuning features, and the capability of adapting to variable acceleration levels [7]. Energy harvesting (EH) is a very attractive technique for a wide variety of self-powered microsystems. Compared to macro-EH technology (such as the kW or MW level of power generated by energy plants), micro-EH technology focuses on the development of alternative solutions for the conventional battery [97]. The source for the EH technology can come from mechanical, thermal, frictional, photic, chemical or biological sources and the corresponding harvested power ranges from mW to μW. Energy harvesting from mechanical vibration has gained considerable interest in recent years by converting mechanical energy into electrical energy [98]. A smart energy harvester should be able to respond with large amplitude motions to increase power generation as well as EH efficiency. The harnessing of buckling events offers advantages in the design of an EH device because the nonlinear behavior can be excited at high-energy orbits from low-frequency broadband vibrations, or quasi-static deformations, at which linear harvesters are usually only weakly excited. Buckling events explored for use in nonlinear harvesters include the snap-through mechanism in laterally-loaded clamped-clamped beams and bistability in thin laminated composite plates. This applications have also found that the excitation frequency of the harvester becomes less sensitive to frequency changes compared to linear harvesters, such as a cantilever excited at its natural frequency [23]. Such buckling-induced prototypes have proved suitable for many MEMS applications because the subject nonlinear response can broaden their application bandwidth, modify the device performance and control resonant frequencies.

The benefit of buckling events has been the catalyst for much recent research on MEMS applications. With the advances in integrated circuit technology, MEMS applications find wide applications and the production cost have been significantly reduced [99]. The use of buckling-induced response has been demonstrated to be reliable and capable of delivering useful power to

MEMS devices. However, MEMS devices are susceptible to the well-known “pull-in” instability if the applied electrostatic voltage reaches a critical level. Since it is widely accepted that the “pull-in” instability is unavoidable, a latest review [100] identified that an increasing number of studies have explored the feasibility of using “pull-in” instability to design special sensors and actuators. More examples on buckling-induced MEMS systems are presented in Section 2.3.

Increasing research activities have focused on the development of wireless sensors and sensor networks through the use of buckling and snapping for structural health monitoring (SHM) and non-destructive evaluation (NDE). A comprehensive review [101] has shown that researchers started to explore self-power wireless sensors because power operation based on batteries is their major drawback. The emerging concept of wireless sensors with actuation interfaces is an important step in the evolution of wireless sensor technology because it closes the gap between traditional SHM and NDE methods. Recent efforts have demonstrated the capability of active sensing due to the actuation from buckling events in different structural types such as wires [8], beams [9], strips [10] and cylinders [25]. The actuation provides the interaction between the wireless sensors and the system in which they are attached to or embedded in. With advances in smart materials, such as piezoelectric materials, power harvesting (conversion of mechanical to electrical energy) becomes possible. Buckling events provide the function of modifying the input to smart materials by serving as a trigger. Under this concept, active sensors are likely to become a promising technology in the future.

Promising endeavors on the use buckling events for energy dissipation have also been conducted, but to a lesser extent as compared to the energy production purposes. Recent studies have explored the possibility of taking advantage of such response for the design of absorbers [102-104], dampers [26, 27], and isolators [28, 105-107]. It should be noted that in all of those

applications the structural elements suffering buckling and postbuckling response are in the elastic response region. Plastic buckling along with progressive failure mechanisms are out of the scope of this dissertation.

2.2.2 Motion-related applications

The high-rate motion associated with snap-through buckling is another promising feature that has been investigated to develop novel design concepts for actuators and micro-optical switching in MEMS devices. Small perturbations can generate sudden snapping behavior in elastic elements that enables the structure to dynamically change its configuration. The onset of the snap-buckling transition can provide actuation output in terms of out-of-plane displacements, which provides a new route to design materials and structures at multiple scales with switchable functionalities, morphogenesis, etc. The key merit of using snap-buckling is that local and global buckling (some cases may happen together) in structural elements can reduce the actuation force during shape recovery and in most cases no additional stabilizing element is required during the transformation between the equilibrium states.

The efforts noted above can be found in several recent reviews on morphology in materials and structures. Kuder et al. [5] showed the increasing interest of using buckling-induced response in terms of multistability to design morphing features in materials and devices. Friedman et al. [4] showed that snap-through instabilities can lead to the development of self-deploying or self-locking structures depending on the stability of their packed configuration. Huang et al. [6] discussed switching in polymeric materials and their structures due to instability/collapse phenomena in their shape changes. More buckling-induced mechanisms and structure are expected to be explored with advances in novel fabrication technologies.

2.2.3 Multi-purpose applications

The spectrum of smart applications covered in Section 2.2.1 and 2.2.2 has profiled the increasing interests in buckling responses and the ongoing trend is to take the fundamental aspects behind energy and motion related applications into diverse purposes. Another interesting trend is on the use of elastic instabilities across multiple scales, particularly at the nano-scale.

Beyond the fundamental design of actuators and energy harvesters, several recent endeavors have shown the promising potential of using buckling-induced behavior for multiple other purposes (see Figure 2-2). Figure 2-2(a) presents a bi-stable compliant mechanism for a MEMS-based accelerometer in which the mechanism can switch from one position to another when the force on the accelerometer exceeds a threshold value [11]. Figure 2-2(b) shows a half section view of a curved water-soluble polyethylene beam that is designed to increase the rate of solvent transport. Snap-buckling of the beam is trigged by the release of internal elastic energy due to the swelling and shrinking processes when the solvent diffuses into the water-soluble polyethylene [12]. Such mechanism can also be used in the design of artificial muscles. The schematic picture in Figure 2-2(c) shows a new experimental approach to determine the bending rigidity of graphene using the snap-buckling instability in a prebuckled graphene membrane. Such concept offers an interesting method to predict the properties of nanoscale materials [13]. For example, Sadeghian et al. [108] experimentally estimated the Young's Modulus of a silicon nanocantilever from the instability induced by electrostatic pull-in forces. The approach has substantial advantages over other methods used for the characterization of nanoelectromechanical systems. Figure 2-2(d) shows an experimental setup to examine the snap-through instability of a membrane subjected to an axially symmetric load simulated through water inside an acrylic column. This prototype was developed to harness the nonlinear behavior of snap-buckling for the

design of a ventricular assist device for better transmission of the pneumatic load to the blood [14, 15]. A sensor relying on the elastic buckling of a thin wire (Figure 2-2(e)) was designed and tested for memorizing peak strains in structures to identify damage. Such mechanical-memory mechanism is a promising concept for damage index sensors [8]. Figure 2-2(f) shows a biomimetic responsive surface inspired by the Venus flytrap leaves that can snap from concave to convex states [109]. The sphere snaps by swelling elastic network with an organic solvent to develop an osmotic stress. Such snapping surfaces can impact a variety of applications, such as coatings, adhesives, drug delivery, etc.

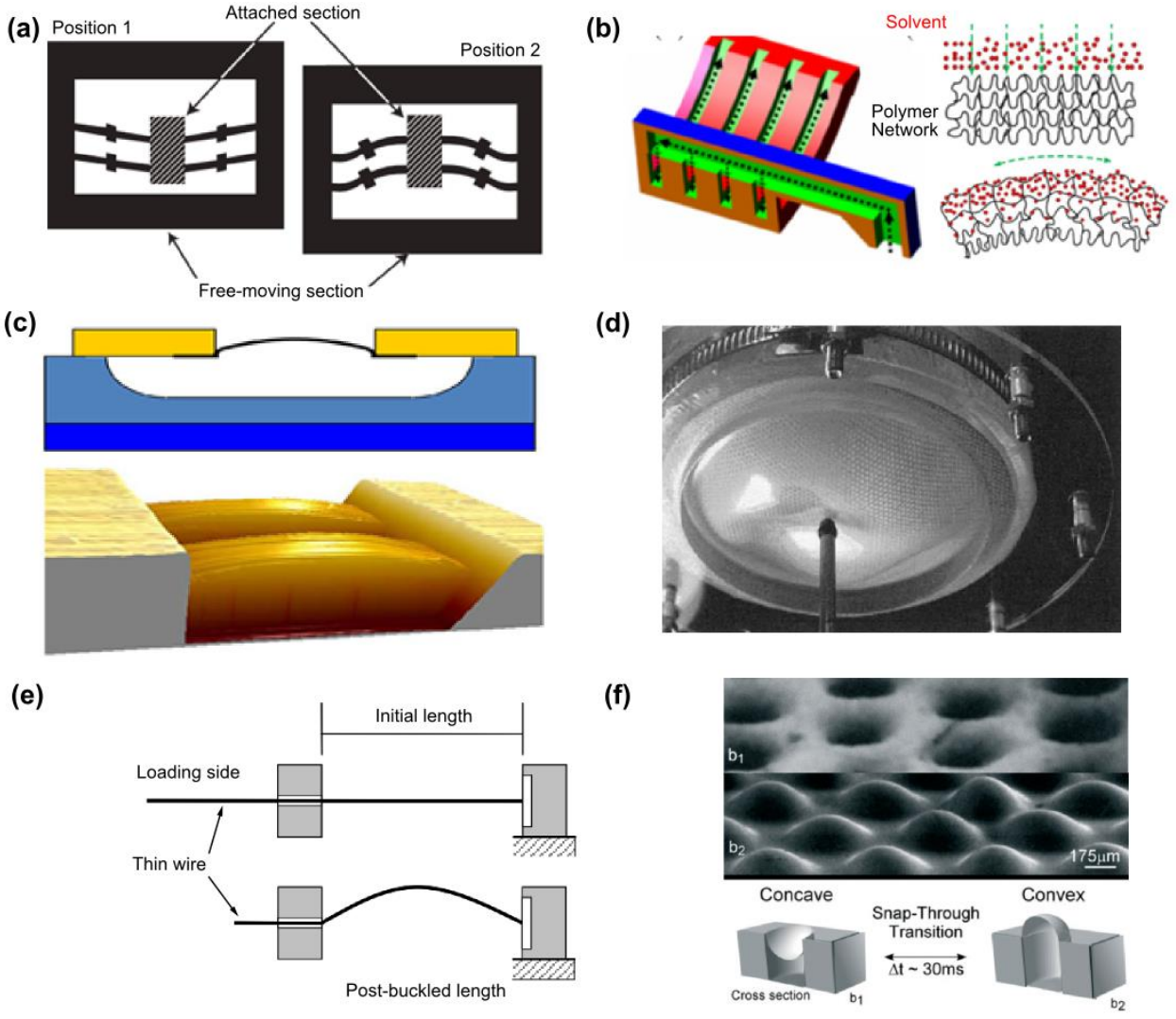

Figure 2-2: Harnessing of elastic instabilities for diverse purposes. (a) A bi-stable compliant mechanism for a MEMS-based accelerometer (Reprinted from [11], Copyright (2007), with permission from IOP Publishing). (b) A curved water-soluble polyethylene beam that to increase solvent transport (Reprinted from [12], Copyright (2010), with permission from IOP Publishing). (c) A method of determining material properties using snap buckling (Reprinted from [107], Copyright (2012), with permission from American Chemical Society). (d) A ventricular assist device using snap buckling (Reprinted from [14], Copyright (2003), with permission from Elsevier). (e) A smart sensor with memorizing peak strain for damage identification (Reprinted from [8], Copyright (2003), with permission from IOP Publishing). (f) A biomimetic responsive surface based on snap-through buckling of domes (Reprinted from [108], Copyright (2007), with permission from John Wiley and Sons).

Harnessing buckling has been explored for many micro-scale applications; yet the emerging trend is to extend the instability principles for uses across multiple scales, particularly the nanoscale. For example, dramatic mechanically triggered transformations in a 2D periodic elastomeric structures using unstable events have been used to transform phononic band gaps [110]. In a similar line, microstructure elastic buckling responses have been used to trigger abrupt changes in the phononic properties of nano-materials [16] to create unidirectional negative Poisson's ratio behavior in materials with periodic microstructures [17] and to assist the nanoscale assembly of a complex structures [18]. A similar idea [111] was numerically investigated by using a two-phase transition to design a viscoelastic material with negative elastic modulus to be used as inclusions in a positive elastic modulus matrix. Elastic instabilities have been found in many nanoscale structures [112, 113], such as nanowires, nanotubes, etc. The major issue at such scale is surface effects, and they should be accounted as part of the total energy potential of the system [19]. On the other hand, the success of micro-scale buckling-induced applications has been extended toward the discussion of possibly using similar concepts for large-scale applications. For energy-related applications, the increasing number of published literature has shown the great potential of self-powered smart sensors based on snap-buckling for wireless structural monitoring networks on buildings and bridges [10, 114-118]. For motion-induced application, several reviews have identified opportunities for using buckling behavior to design morphing components for different structures, such as automobiles [119], wind turbine blades [120] and infrastructure [4].

2.3 Prototype: geometry

The use of buckling and snapping events is diverse and this section summarizes various manifestations of structural prototypes related to recent smart applications that have been designed and experimentally investigated. Based on their configuration, structural prototypes can be categorized into classic forms and emerging forms. From a geometrical point of view, the buckling phenomenon can be found in all slender members, including one-dimensional members (arches, beams, columns, rods, wires, etc.), two-dimensional members (membranes, plates, shells, etc.) and three-dimensional members (cylinders, tubes, spheres, etc.). Some notes of interest regarding these structural forms are: (1) laterally-loaded beams and bi-stable plates have been well studied for the purposes of energy harvesting; (2) cylinders/columns/tubes have been heavily investigated for energy dissipation purposes; (3) 3D forms are more favorable for use in motion-based applications such as morphing structures, deployable structures and adaptive structures; and (4) novel prototypes have been proposed under each form type to address multiple potential applications. The following section highlights some of the examples to identify the changing role of some classic buckling phenomena and to present emerging efforts on new forms for potential applications.

2.3.1 Structural forms for energy-related applications

The loss of stability in a structure depends on the prescribed form and its geometrical imperfections. In most cases, snap-through buckling occurs at a limit point rather than at a bifurcation point. Figure 2-3 shows a classic structure that is known to exhibit unstable behavior once its subjected to external loading. A laterally-loaded beam/arch/strip is the simplest 1D structural form reported in energy-related applications [9, 23, 121-126]. Such phenomenon is

familiar to engineers and has only one limit point on the initial loading path. Physically, external loading at the critical state leads to snap-buckling along the loading direction.

Another common structural form for energy harvesting is the bi-stable panel/plate. Snap-through buckling in a bi-stable system can also cause large amplitude motion due to its transition from one stable state to another, which can significantly improve the efficiency of energy harvesters. Compared to a laterally-loaded beam, the snap-through behavior of a bi-stable plate depends on both its bending and in-plane stiffness. A recent review [23] highlights the increasing body of literature on energy harvesting from bi-stable plates. Buckling in 3D forms (such as cylinders and spheres) has been far less studied for energy harvesting purposes. One of the reasons is that postbuckling behavior in cylinders and spheres is usually an asymmetric bifurcation response that exhibits random behavior. Prediction and control of such behavior is more difficult due to its high imperfection sensitivity.

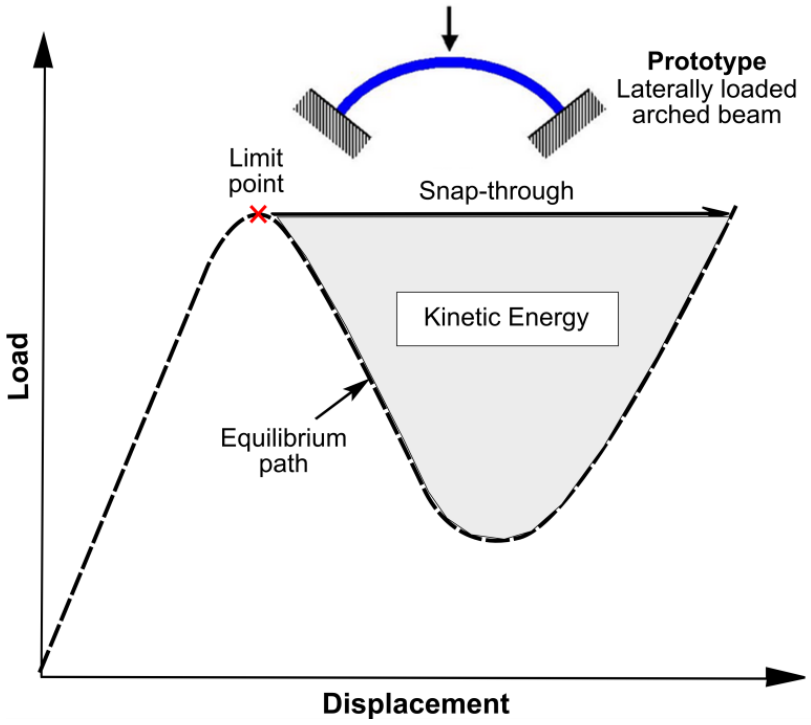

Figure 2-3: Schematic snap-through buckling of a laterally-loaded arch beam.

Many recent studies [12, 21, 22, 127-133] have explored various techniques to trigger snap-buckling triggered by non-mechanical loading for the development of MEMS devices or energy harvesters, see Figure 2-4. Figure 2-4(a) shows snap-through buckling of a curved double-clamped beam from the electrostatic actuation of a fringing field engendered by symmetrically located electrodes [130]. Figure 2-4(b) demonstrates a semi-flexible strip made of 115 μm-thick curved bimetals designed to snap at 47 ℃ and to snap-back at 42.5 ℃, whereby a hysteretic thermal gradient can trigger snap-through behavior between the two positions [21]. Figure 2-4(c) displays a steel buckled-beam subjected to a magnetic levitation system repelled by top and bottom magnets to trigger the second buckling mode and thus enhance energy harvesting at low frequency and small excitation conditions [22]. Two classes of azobenzene-functionalized polymers (Figure 2-4(d)) were investigated to design contactless photo-initiated snap-through events in bi-stable arches, leading to orders-of-magnitude enhancement in the actuation rates (~102 mm/s) and powers (~1kW/m^3) under moderate irradiation intensities (<<100 mW/cm^2) [134]. For micro-device design, the capillarity-induced snapping of elastic beams and the solvent-induced snapping of a beam (see Figure 2-4(e)-(f)) was reported in [12] and [129], respectively. However, one of the noted drawbacks in these systems is that the external source may not always be available and/or suitable for applications at different scales. For example, it is difficult to integrate permanent magnets at the nanoscale and magnetic fields could strongly interact with other components in electronic devices [20]. In addition to triggering from external sources, structural prototypes using smart materials offer the features of self-tuning and self-adapting and more discussion on this aspect of their development is presented in Section 4.

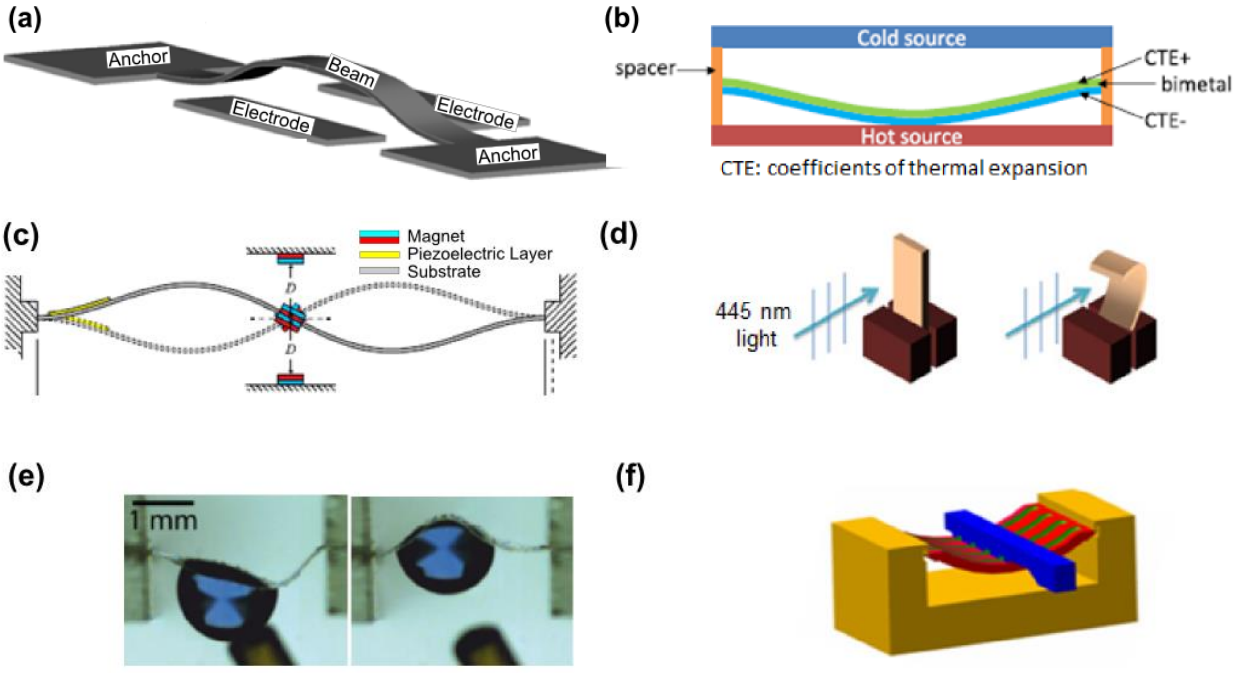

Figure 2-4: Snap-through buckling of arch/beam forms triggered by various sources other than mechanical loading: from (a) electrode-induced (Reprinted from [130], Copyright (2011), with permission from Springer), (b) Thermal-induced (Reprinted from [22], Copyright (2013), with permission from IOP Publishing), (c) Magnetic-induced (Reprinted from [23], Copyright (2013), with permission from AIP Publishing), (d) Photo-induced (Reprinted from [134], Copyright (2013), with permission from PNAS), (e) Capillarity-induced (Reprinted from [13], Copyright (2013), with permission from IOP Publishing), and (f) Solvent-induced (Reprinted from [129], Copyright (2013), with permission from the American Physical Society).

Another well-documented prototype form class with postbuckling behavior is that of axially-loaded structures. Such prototypes have not been extensively studied for energy harvesting purposes but they have been used for energy dissipation purposes such as absorbers, dampers and isolators. For these purposes, 3D forms, particularly cylinders and tubes are more frequently used as a structural prototype over 1D and 2D forms. Figure 2-5 shows the load-deformation curve of an axially-compressed cylindrical shell, which exhibits a postbuckling response with multiple bifurcation points (also termed mode transitions) due to changes in the deformed geometry after each critical point. Cylindrical shells can attain multiple local buckling events, or

mode jumps, in their postbuckling regime due to the natural transverse deformation restraint provided by their geometry. Dealing with such complex nonlinear behavior has proven to be a challenging task due to the high imperfection sensitivity that this prototype form suffers from, which has limited the practical design of thin-walled structures using this behavioral feature. Nonetheless, 3D prototypes could gain more attention if the static and dynamic response from mode branch switching in their postbuckling response can become predictable and possibly modified and tailored.

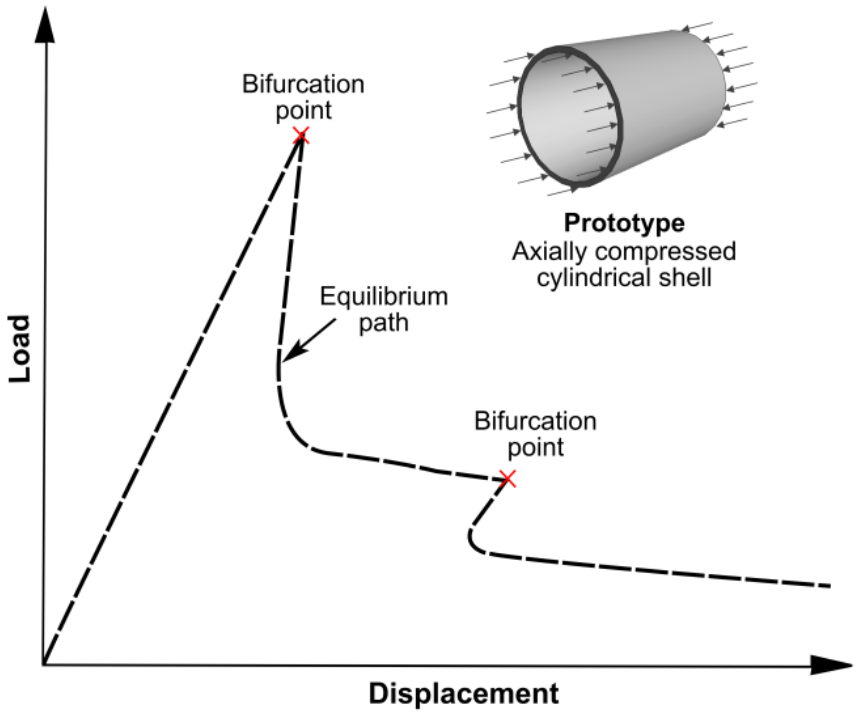

Figure 2-5: Schematic postbuckling response of an axially compressed cylinder.

Many experimental and numerical studies have provided valuable knowledge towards characterizing the elastic postbuckling response of axially-loaded structures. With increased understanding of the behavior in the postbuckling regime, a wide variety of structural forms have

been explored for energy dissipation purposes. For example, the postbuckling response of axially compressed cylindrical shells (Figure 2-6(a)) can occur at a lower energy level and efforts to characterize this response experimentally and numerically have been motivated by the interest of using the residual strength as a safeguard [38, 135, 136]. A recent study [137] may inspire using a group of cylinders connected by ligaments for use as an energy absorber (Figure 2-6(b)). The bifurcation and snap-through collapse of a variety of thin-walled structures can be found in a comprehensive review [138]. An inspiring study [105] has investigated several vertical vibration isolation designs by using the Euler buckling springs (Figure 2-6(c)). A recent endeavor [139] uses a composite bi-stable plate as part of vibration isolator subjected to harmonic base excitation (Figure 2-6(d)). Another interesting feature in prototypes displaying buckling events is that they give rise to negative stiffness, which can be potentially used for the design of advanced dampers. For example, an interesting damping system (Figure 2-6(e)) was designed with negative stiffness and large hysteresis by using the snap-buckling of a column with flat ends [26]. A negative stiffness device using snap-buckling under a similar framework was recently attempted to use as seismic protection for structures (Figure 2-6(f)) [140, 141]. Similar buckling-induced responses in various structural prototypes can also be used as isolators.

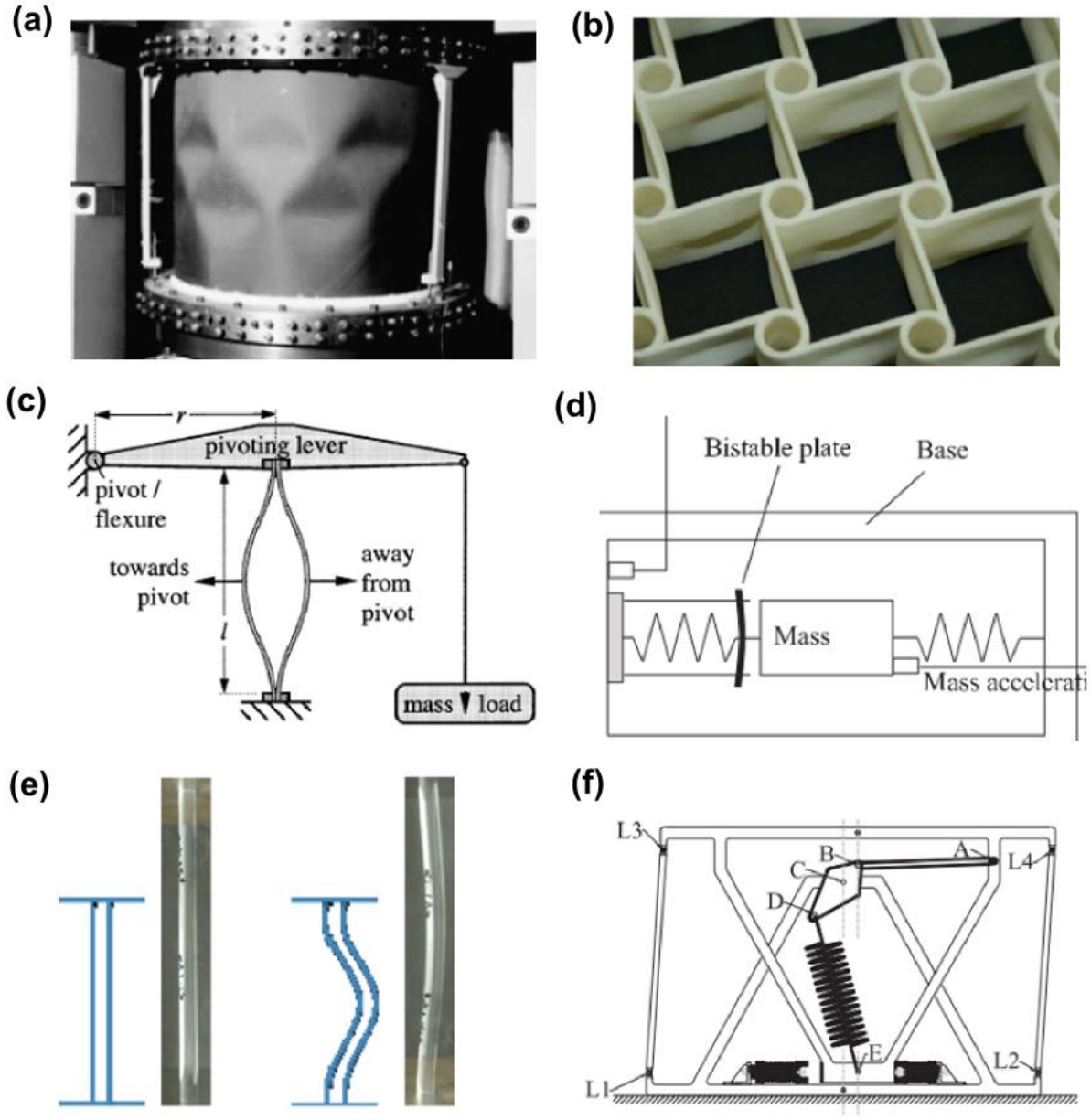

Figure 2-6: Harnessing buckling-induced behavior for the different energy dissipation purposes. (a) Postbuckling of a CFRP cylindrical shell (Reprinted from [39], Copyright (2003), with permission from Elsevier). (b) Buckling of a cylinder group connected by ligaments (Reprinted from [137], Copyright (2010), with permission from Elsevier). (c) Buckling of a column used for an isolator (Reprinted from [105], Copyright (2002), with permission from Elsevier). (d) Bi-stable plate used as an isolator (Reprinted from [139], Copyright (2013), with permission from Elsevier). (e) Buckling of a column designed for a damper (Reprinted from [27], Copyright (2013), with permission from Elsevier). (f) Spring-based negative stiffness device for seismic protection (Reprinted from [140-141], Copyright (2013), with permission from ASCE).

2.3.2 Structural forms for motion-related applications

One of the key features of snap-buckling is their capacity of actuation. Many classical buckling phenomena have been incorporated into the design of energy harvesters and MEMS devices. Figure 2-7(a) shows a widely used example of using an arch-shaped beam as an actuator [87]. In this case, a magnetic field normal to the chip surface creates a Lorentz force to trigger snap-through buckling of the arch-shaped leaf spring. Similar snapping behavior can also be found in many plate designs [120] for adaptive and morphing structures (Figure 2-7(b)). Brinkmeyer et al. [142] explored the snap-through buckling of an isotropic spherical dome to design morphing structures with pseudo-bistable behavior (meaning that snap-buckling occurs slowly due to the use of a viscoelastic material). This dome can recover its original state without further actuation due to the use of a macro polymer composite (Figure 2-7(c)).

Nature has long made use of elastic instabilities for functionality and it has generated an important research are during the past decade. For example, a recent study [143] found that the mosquito fascicle is laterally supported throughout the penetration process such that the Euler buckling load is increased by a factor of 6. The results showed the importance of lateral supports for modifying the stability of elastic structures, which is similar to man-made laterally constrained systems. Within the subject of this review, bio-inspired concepts and biommetics have been used in the development of structures and mechanisms with two major features: snapping and folding. With inspiration from the Venus flytrap's fast closure [144], a biomimetic responsive surface was developed that can snap from one curvature to another [109]; a hingeless flapping device (Figure 2-7(d)) was developed and patented under the name Flectofin® [145]; and a flytrap-inspired robot and novel actuation mechanism was designed [146]. Other recent biomimetic lessons on snapping behavior include the design of an initially flat pod valve that

turns into a helix, which was inspired from the mechanical process of seed pods opening in Bauhinia variegate [147], and the development of a dragonfly-inspired flapping strip with piezoelectric patches [148]. Folding is another interesting mechanism that can be useful for the design of deployable and morphing structures. Leaf-folding patterns have been investigated to create new fold patterns for thin membrane structures [149]; a multi-stable composite cylindrical lattice structure (Figure 2-7(e)) was designed to mimic the bi-stable behavior of the virus bacteriophage T4 [150]; and the design of a bi-stable cell (Figure 2-7(f)) capable of reversibly unfolding from a flat configuration to a highly textured configuration was inspired by natural systems through origami design principles [151].

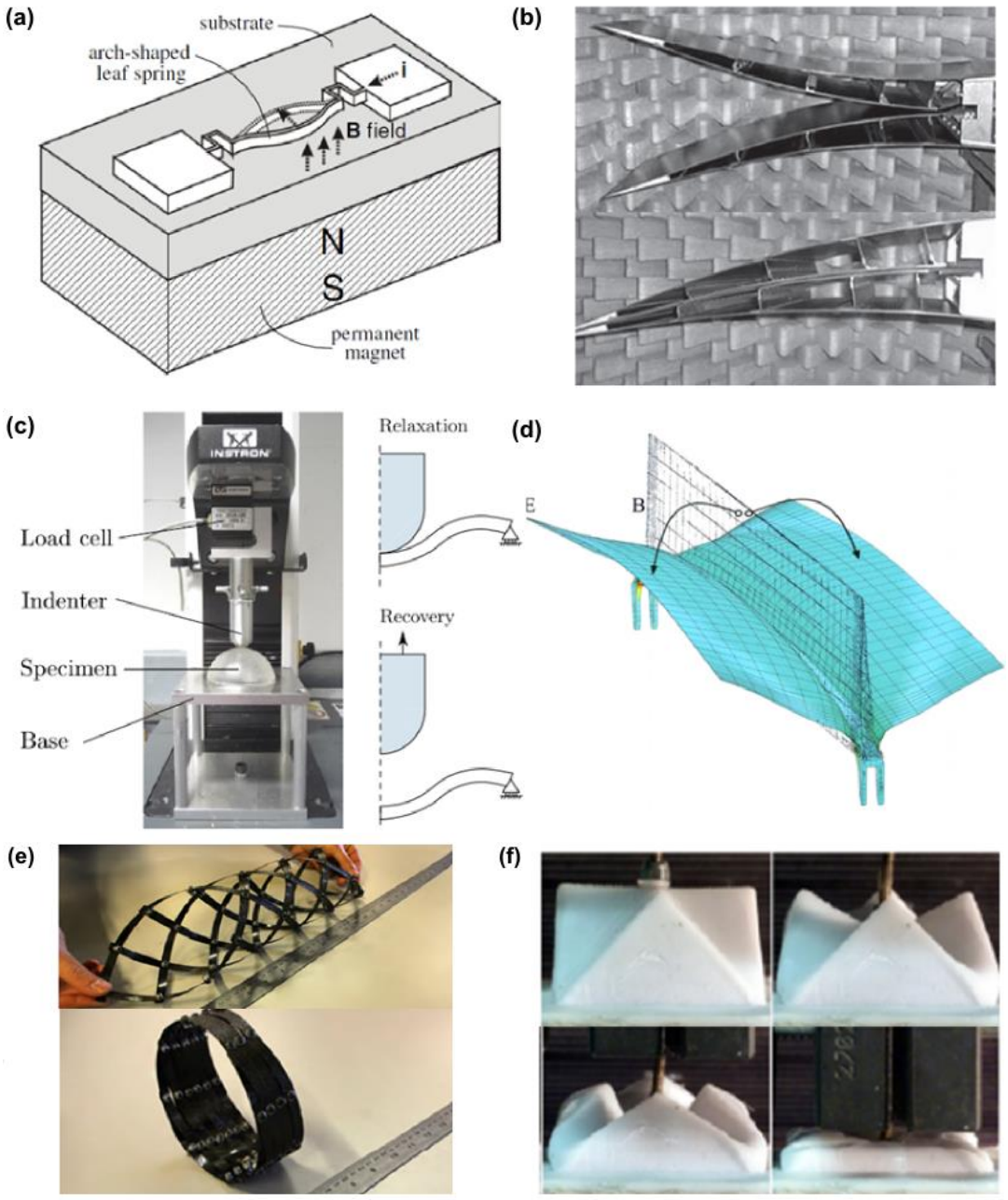

Figure 2-7: Harnessing snap-buckling instabilities for motion-based purposes. (a) Snap-through buckling of beam for actuator (Reprinted from [88], Copyright (2004), with permission from IOP Publishing). (b) Snapping behavior of adaptive morphing trailing edge (Reprinted from [120], Copyright (2013), with permission from John Wiley and Sons). (c) Snap-through buckling of a dome with self-recovery ability (Reprinted from [142], Copyright (2012), with permission from Elsevier). (d) A biommetic design of hingeless flapping device using snap-buckling (Reprinted from [145], Copyright (2012), with permission from IOP Publishing). (e) Multi-stable cylindrical lattices inspired from the bi-stable behavior of a virus (Reprinted from [150], Copyright (2013), with permission from Elsevier). (f) Depolyable cell by using snap-buckling behavior (Reprinted from [151], Copyright (2013), with permission from IOP Publishing).

2.3.3 Emerging forms

Beyond the extensively studied classic forms, structural form-finding for new prototypes are part of a parallel research avenue on harnessing snap-through buckling for potential applications. Buckling-induced applications have sparked advancements in the development of novel forms that can attain elastic instabilities. A recent review [19] concluded that many interesting problems within the topic of snap-through instability remain to be investigated, including: (1) the mathematical complications in modeling buckling and post-buckling in thin structures; (2) the mechanical instability of materials associated with inhomogeneity and nonlinearity; (3) new phenomena due to the coupling between geometric and material nonlinearities; and (4) the usefulness of mechanical instabilities for broad engineering applications.

Recent contributions considered elastic instabilities in a variety of structural forms, ranging from 1D to 3D, on their opportunities and feasibilities to be used as structural prototype, as shown in Figure 2-8. Featured examples include slackening of a twisted thin rod [152] (Figure 2-8(a)), buckling of an elastic planar rod penetrating into a sliding sleeve [153], snapping of an elastic arched beam inspired by a popper [154], snapping of a simple stretched bi-strip of elastomers [155], the buckling and folding of over-curved rings [156], shrinking and buckling of thin sheets with non-Euclidean metrics [157, 158], buckling of a planar sheet with a negative-curvature liquid interface [159], the 3D shape of a sheet with a series of prescribed concentric curved folds [160], multi-stability in spontaneous helical ribbons [161] (Figure 2-8(b)), the postbuckling of a thin cylindrical shell under torsional loading to fold to a flat 2D form [162] Figure 2-8(c)), buckling-induced encapsulation of a spherical shell patterned with a regular array of circular voids [163] (Figure 2-8(d)), the secondary buckling instability of an initially spherical elastic capsule [164], periodic beam lattices [165], periodic porous structures [166], etc.

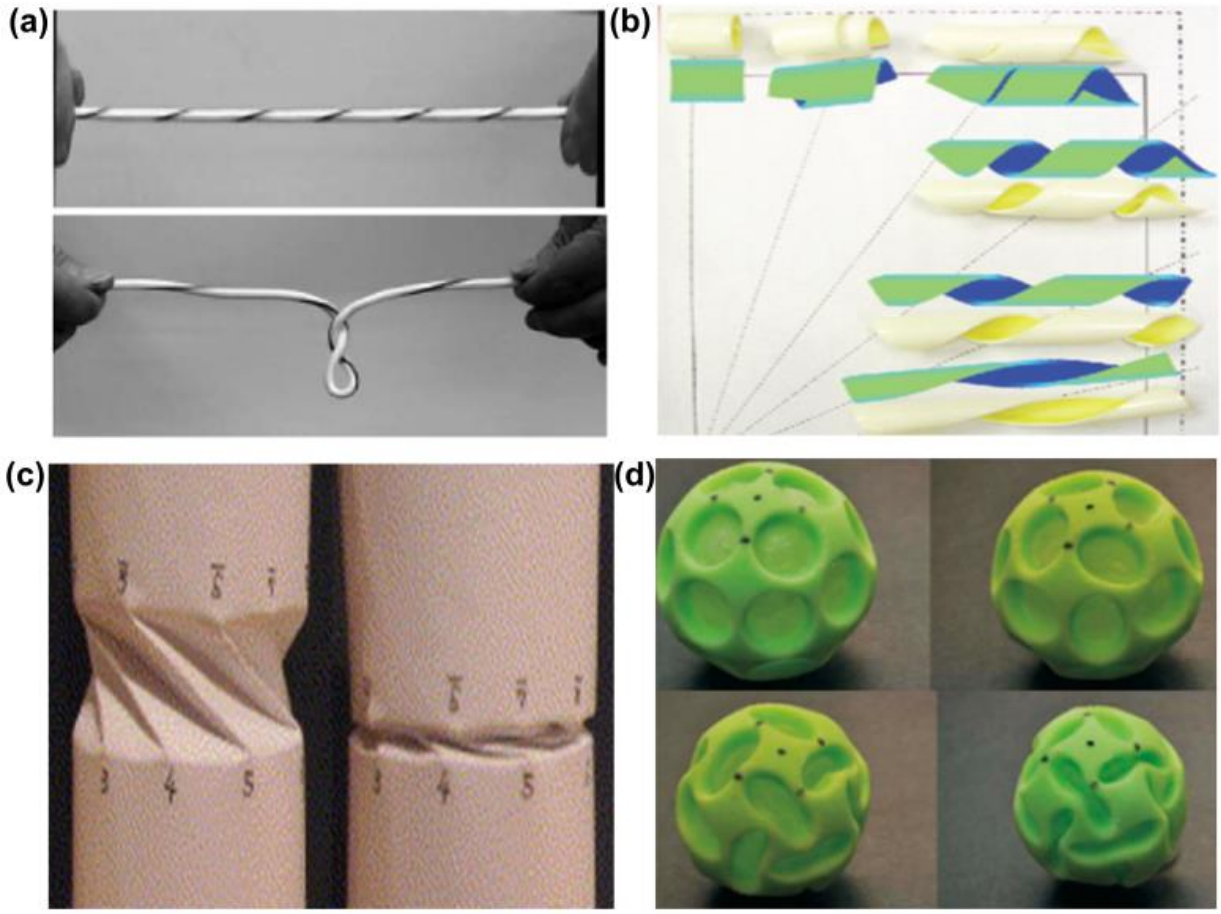

Figure 2-8: Explorations on structural prototypes for smart applications. (a) Twisting buckling of a thin rod (Reprinted from [152], Copyright (2005), with permission from Springer). (b) Multistability in a helical ribbon (Reprinted from [161], Copyright (2014), with permission from AIP Publishing). (c) Postbuckling of an origami-inspired cylinder (Reprinted from [162], Copyright (2005), with permission from Elsevier). (d) Buckling-induced deployable sphere, Buckliball (Reprinted from [163], Copyright (2012), with permission from PNAS).

Future buckling-induced smart applications require the development of prototypes with tailored geometric configurations and material distributions. The snap-through buckling response in the structural prototypes presented thus far shows no more than two stable states. Research efforts are emerging to explore the possibility of achieving multiple stable events through four different approaches: (1) varying material and geometrical properties; (2) using hybrid systems; (3) using hybrid material combinations and (4) adding constraints.

A study [58] identified that an isotropic cylindrical shell may be only stable in its initial configuration, but that it can exhibit second or more stable configurations as a result of the anisotropy that can be attained by using fiber-reinforced polymer composites. Tailoring laminated composite to achieve tristability has also been investigated for multiple shell forms, such as corrugated shells [59], orthotropic shells [60], double curved shells [61], and shells with piezoelectric patches [167].

More multi-stable mechanisms have been reported by using hybrid material systems. A quadri-stable compliant mechanism was designed and tested by using a bi-stable curved-beam embedded in an arch beam [62]. A bi-stable switching mechanism was achieved through a hybrid system of curved strips attached to a center beam [63]. A multi-stable lattice structure (Figure 2-9(a)) was developed based on a tri-stable lattice cell made from bi-stable laminates [64]. Hybrid carbon fiber/E-glass/epoxy cylindrical shells have been shown to obtain multiple mode transition in the postbuckling regime with a certain degree of control [45]. Finally, rather than proposing an actual physical model, recent studies explored the design of smart structures by connecting multiple unstable configurations through a representative model, namely the use of heteroclinic connections between unstable equilibria [168, 169].

Buckling and postbuckling response has also been studied by the combination of two materials for achieving sustainable snapping events, such as shape memory alloy wire actuators embedded in laminated composites [65, 66], and composite plates with piezoelectric actuators and sensors [67, 68]. Many studies have successfully investigated snap-bucking in structural prototypes with piezoelectric patches and applied them to the design of novel adaptive multi-stable composites. Figure 2-9(b) shows a prototype of bi-stable composite plates with four piezoelectric patches such that the bi-stable structure can snaps back to its initial configuration

without the need of an external actuation force [89]. A similar effect has been achieved by using another emerging smart material to provide the actuation load – macro-fiber composites (MFC) [167, 170, 171]. Bonded MFC onto other structures is also being used for developing energy harvesting prototypes due to their large deformation capacity and their high energy conversion efficiency compared to traditional piezoelectric materials [69].

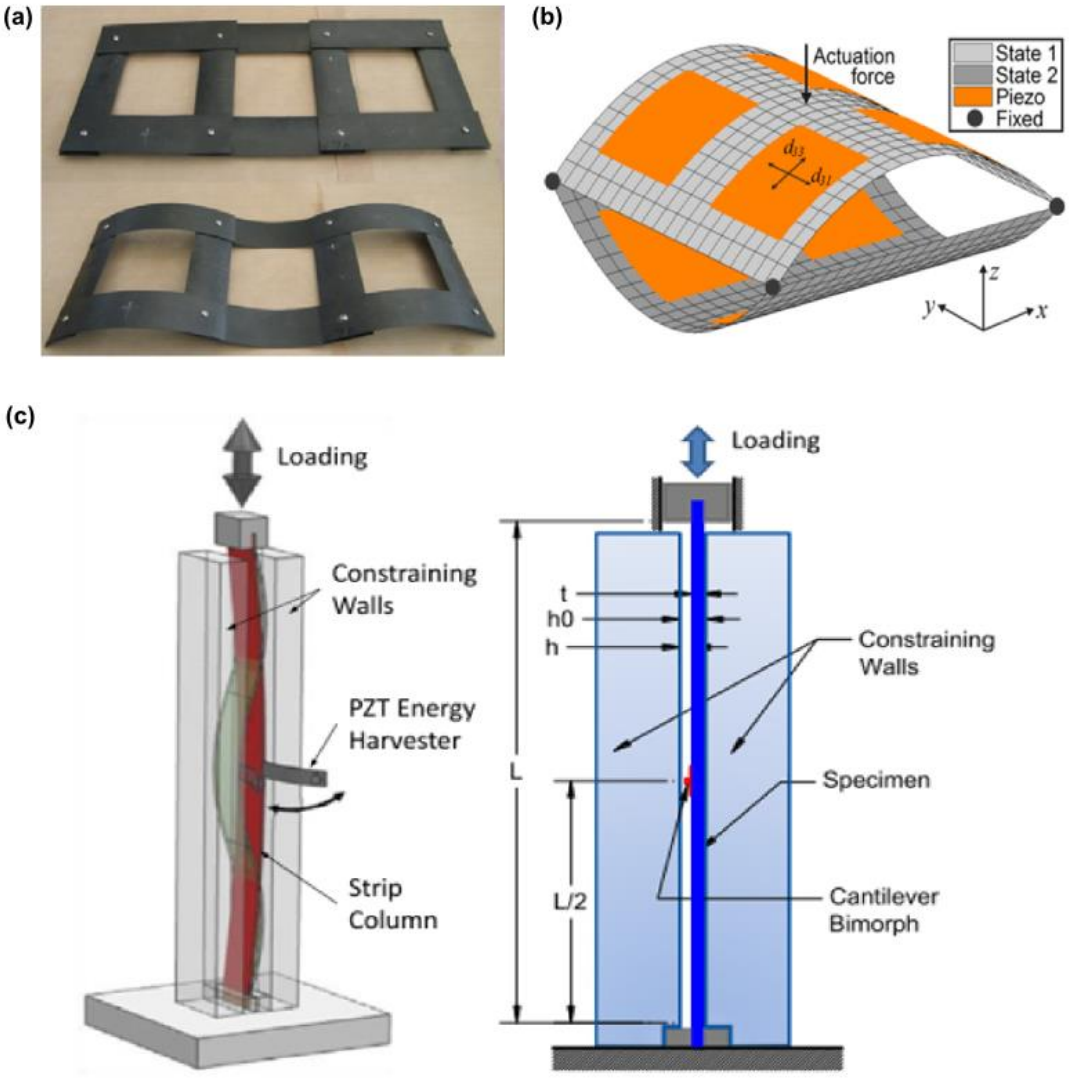

Figure 2-9: Structural prototypes for obtaining multi-stable behavior. (a) A bi-stable composites concept for energy absorption (Reprinted from [112], Copyright (2013), with permission from Elsevier). (b) Bi-stable composites attached with four piezoelectric patches (Reprinted from [65], Copyright (2012), with permission from AIP Publishing). (c) A bilaterally constrained axially loaded CFRP strip (Reprinted from [46], Copyright (2014), with permission from IOP Publishing).

The use of lateral constraints has also been shown effective for achieving sustained snap-through and snap-back response in the far postbuckling regime. For example, the disordered packing behavior of an elastic rod constrained by a cylindrical chamber was studied to develop the prototype for a folding mechanism [75]. Bilaterally constrained axially loaded strips, which can exhibit snap through behavior between multiple buckling modes [172] have been shown to be efficient for devices that could harvest energy from pseudo-static motions [10]. Such behavior has been exploited for energy harvesting purposes (Figure 2-9(c)) as well as its use in self-powered sensors [10, 118]. Inner constraints have also been shown as a viable mechanism to modify, and potentially tailor, the postbuckling response of axially compressed composite cylindrical shells [45].

Searching structural forms for achieving snapping and buckling can be assisted by design optimization methods. Topology optimization techniques has been developed to seek the best material/stiffness distribution for a given objective [76] and its fundamental principles are well-documented [77]. A recent review [173] showed that topology optimization has been extensively used to solve a variety of multidisciplinary problems in the past decade. Topology optimization methods with a buckling response objective are also emerging; thus shifting the concept from the search of maximum strength or stiffness under static loading demands to problems dealing with obtaining nonlinear large deformations for smart purposes. Numerical algorithms that can track the nonlinear structural response following a path that exhibits snap-through behavior have been developed [79-83]. Recent efforts have also showcased the use of topology optimization to find material layouts that lead to larger displacement and energy release from the snap-through behavior for different purposes, such as actuators [84-88], energy harvesters [24, 89, 90],

dampers [91], multi-stable compliant mechanisms [92, 93], thermoelectric generators [94] and for flutter control [95].

2.4 Prototype: material

This section summarizes various endeavors on buckling-induced applications from a material point of view. A recent review [6] distinguished materials for morphing application into two categories: by either having the ability of shape change or the ability of shape memory. A material may have these two features separately or simultaneously. It can be seen from Section 2.3 that buckling response in either energy-based or motion-based applications can be trigged suddenly, in an elastic manner, or gradually, in a viscous-elastic fashion. When an external stimulus is not available a smart structure should be able to snap back to the original shape with the use of shape memory materials. The applications involving shape changing materials, shape memory materials and emerging soft material are discussed in this section.

2.4.1 Shape-changing and shape-memory material

The four major reported materials with the ability of shape change are metals (including metalloids), fiber-reinforced composites, polymers and piezoelectric materials. Conventional metals (such as steel, aluminum, etc.) are still a material option for many motion-based applications. The major drawback of these isotropic materials is their lack of property tailoring features, and that they are usually used as a base material requiring the aid of some shape memory material for smart applications. Research studies on bi-stable shells [58] has proved that, for a given configuration, a structure made from isotropic materials has only one stable configuration, while it can have two stable configurations by introducing material anisotropy.

Fiber-reinforced composites have been widely used for smart structures due to the possibility of varying their stiffness via selection of the individual ply material properties, fiber orientation and laminate stacking sequence. While anisotropic coupling effects are known to reduce the buckling capacity of many structural forms, and are generally avoided through special laminate designs, new and emerging smart applications like the many pursued in this review have seen their influence as favorable, as shown in Figure 2-10.

Winkelmann [103] explored an energy absorbing mechanism by using composite bi-stable strips. The waiting links, made of ultra-high molecular weight polyethylene (Figure 2-10(a)), were designed to provide a redundant load path and provide a higher ductility to the mechanism through snap-buckling behavior. Shaw et al. [139] experimentally investigated a passive vibration isolator with the concept of high static stiffness but low dynamic stiffness via the snap-buckling behavior of a composite bi-stable plate (Figure 2-10(b)). The nonlinear behavior was shown to support substantial load and to significantly reduce the natural frequency of the system. Figure 2-10(c) presents an experimental study on the tristable response of a doubly curved orthotropic shell and it shows the use of curvature and anisotropy to achieve multistability [61]. Lachenal et al. [174] investigated an adaptive structural concept using a multi-stable twisting grid of carbon fiber reinforced plastic (CFRP) strips (Figure 2-10(d)). More interesting studies on the bistability and multistability of composite structures for morphing and adaptive application can be found in the review by Daynes and Weaver [119].

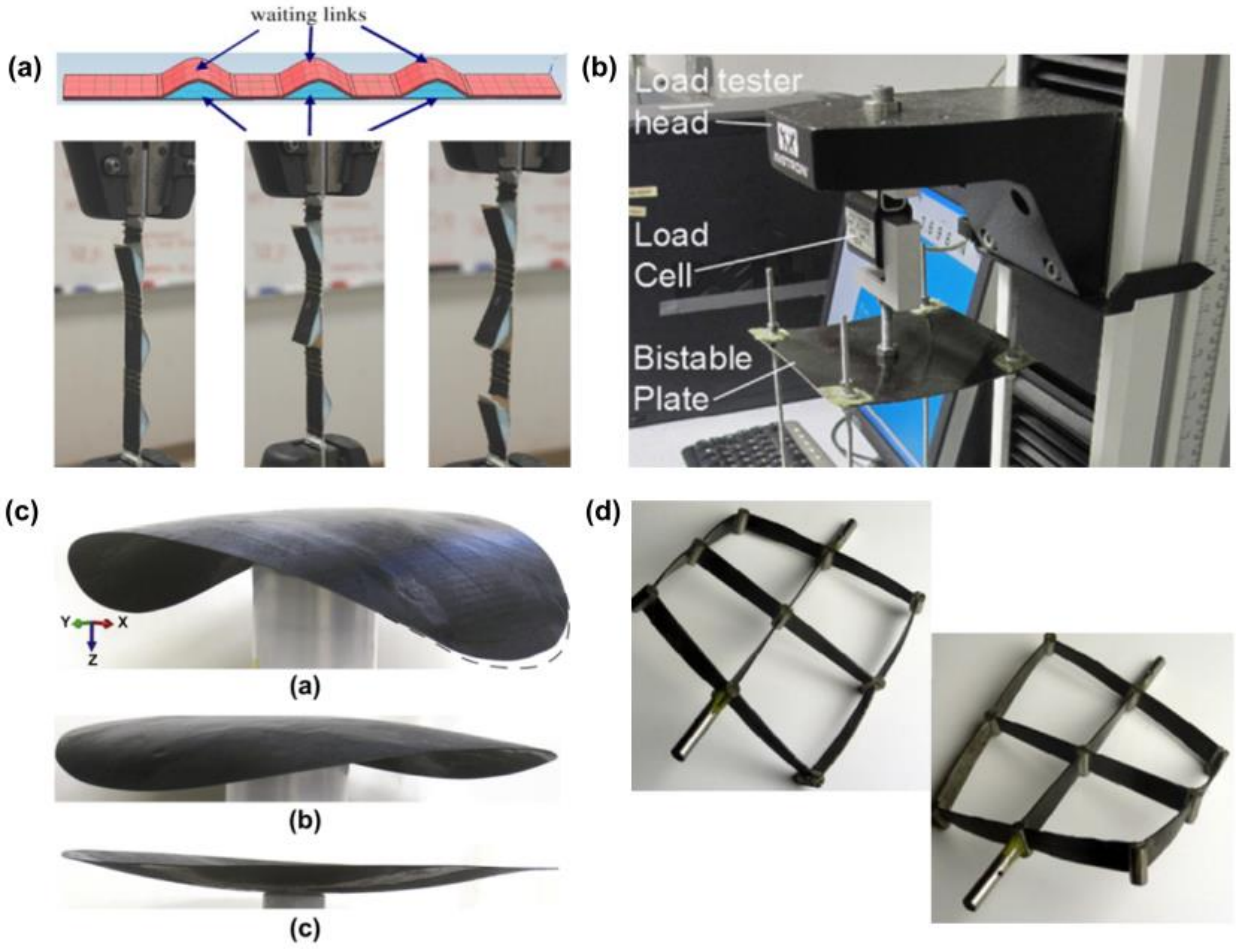

Figure 2-10: Explorations on structural prototypes for smart applications. (a) A bi-stable composite strip for energy absorption (Reprinted from [103], Copyright (2013), with permission from Elsevier). (b) A spring mechanism incorporating a bi-stable composite plate for vibration isolation (Reprinted from [139], Copyright (2013), with permission from Elsevier). (c) Three stable states for an orthotropic shallow shell with constant curvature (Reprinted from [62], Copyright (2013), with permission from Elsevier). (d) A multi-stable twisting grid of carbon fiber reinforced plastic strips (Reprinted from [174], Copyright (2013), with permission from SAGE Publications).

The potential of polymeric materials for smart applications is similar to that of fiber-reinforced composites, particularly in the development of micro devices and mechanisms. Two major types of polymers used for buckling-induced applications are glassy polymers and rubbery polymers. A comprehensive review on instability phenomena in polymeric materials and their structures can be found in [6].

Piezoelectric materials have received the most attention for buckling-induced applications due to their ability to directly convert applied strain energy into usable electric energy, particularly for integration into micro-scale devices. Several reviews [97, 175-177] have shown that the high compliance associated with piezoelectric materials is very attractive for the design of energy harvesters, actuators and self-powered sensors. Another interesting research avenue is the active control of snap-buckling instabilities in structures through piezoelectric actuator-induced loading. Similar concepts have been explored on various structural prototypes and they have shown the possibility of instability control in columns [178, 179] and beams [123, 180].

As discussed in Section 2.2, self-adaptation and self-recovery are preferable features for buckling-induced applications such that the structure can have a snap back behavior after snap buckling. Shape memory alloys (SMAs) are one of the well-known candidates among many smart materials for such purpose. The shape recovery of SMAs can be induced by either a stress or a temperature change, which results in transformation between its two main phases due to its different crystal structure. It has been reported that SMAs can regain their original shape after being deformed well beyond 6-8% strain and magnetic shape memory alloys (MSMA) can even result in reversible strain levels to up 10% [181]. SMAs have a number of unique properties that make them appealing for a wide variety of applications in the biomedical and aerospace industries, including large energy dissipation capacity, good fatigue and corrosion resistance, large damping capacity, and availability in many configurations [182, 183]. Advances and challenges for the use of SMAs can be found in a recent review paper [70]. Another promising candidate for buckling-induced applications is shape-memory polymers (SMPs). Compared to thermal-induced and mechanical-induced SMAs, SMPs can also be activated by electricity, light, moisture and even certain chemical stimulus. The shape recovering capacity of SMPs can reach

up to 400% in recoverable strain and, more importantly, they cost less than SMAs. More smart applications using SMPs can be found in two recent comprehensive reviews [71, 72].

2.4.2 Soft materials

Another growing research trend pertains to the use of soft and superelastic materials for triggering elastic instabilities. It should be noted that the following discussion is not solely focused on buckling-induced but EI-induced applications in general. Two major materials reported in the literature for the above-noted purpose are dielectric elastomers (DE) and graphene. DEs are ideal candidates for high performance and low cost applications due to their characteristics of lightweight, ease of fabrication and low cost. General behavioral theory and applications of DEs can be found in [184] and [185], respectively. Research studies [186-188] have shown that DEs are capable of having large voltage-induced snap-through instabilities (Figure 2-11(a)) and their potential has been demonstrated for different purposes, such as actuators [189-192], energy harvesters [193-195], soft generators [196] and morphing in elastomer systems (Figure 2-11(b)) [155]. More endeavors on harnessing snap-through instabilities with DEs can be found in two recent reviews [197, 198].

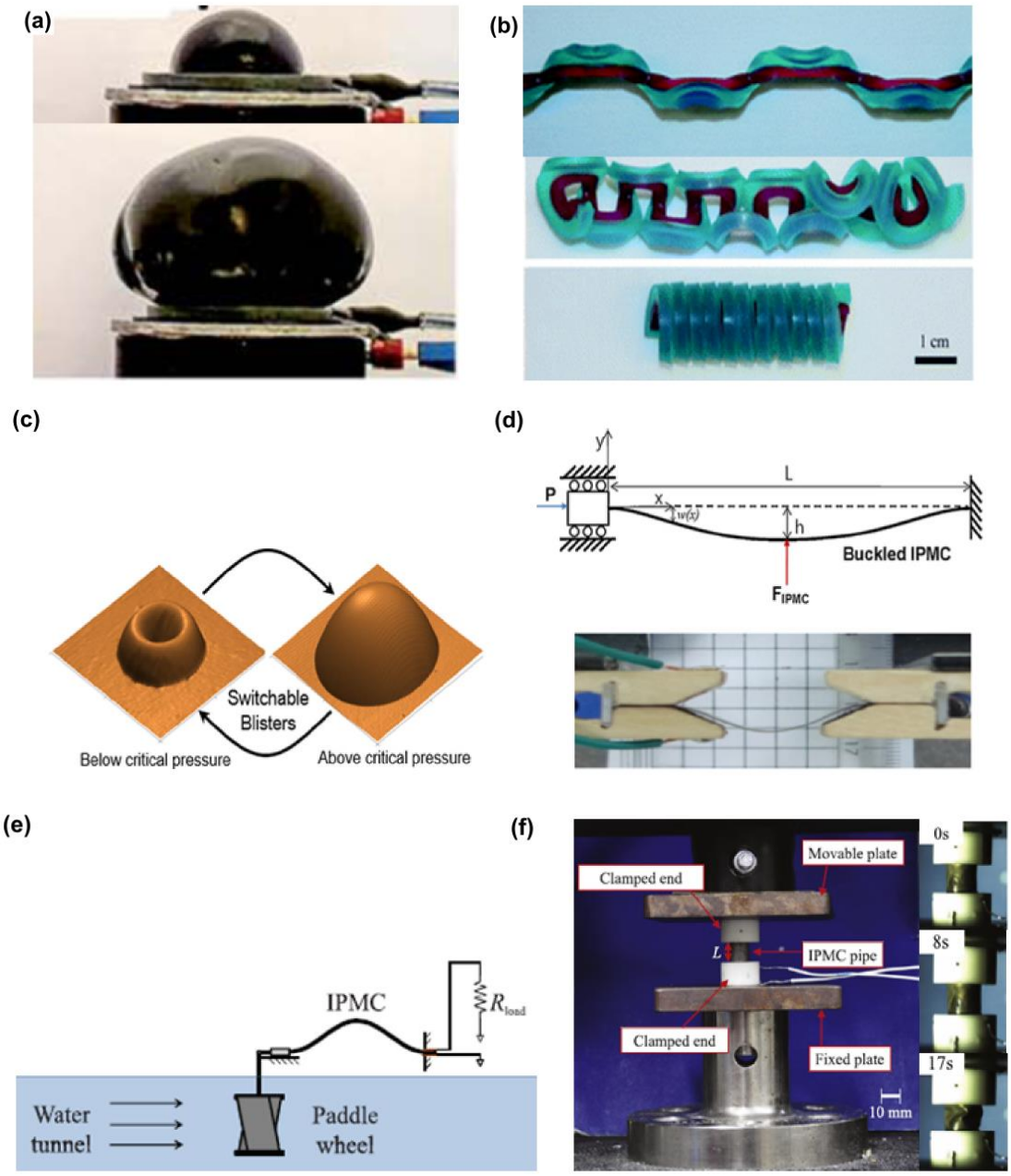

Figure 2-11: The potential use of emerging soft material on buckling-induced applications. (a) A bi-stable compliant mechanism for a MEMS-based accelerometer (Reprinted from [90], Copyright (2012), with permission from RSC Publishing). (b) Snapping a simple stretched bi-strip of elastomers (Reprinted from [115], Copyright (2012), with permission from RSC Publishing). (c) A graphene blister with switchable snap-buckling feature (Reprinted from [125], Copyright (2013), with permission from American Chemical Society). (d) A double clamped IPMC actuated beam (Reprinted from [209], Copyright (2010), with permission from Elsevier). (e) An energy harvesting concept with two IPMC sliding cranks (Reprinted from [55], Copyright (2013), with permission from SAGE Publications). (f) An experimental study on buckling of IPMC pipes (Reprinted from [17], Copyright (2013), with permission from IOP Publishing).

Graphene is a monolayer of carbon atoms densely packed in a honeycomb crystal lattice [199]. Studies [112, 200, 201] have recognized that the morphology of grapheme can lead to a sudden snap-through transition and that it has great potential for the development of graphene-based interfaces and devices (Figure 2-11(c)). Another soft material that has caught the attention of researchers for buckling-induced applications is ionic polymer–metal composites (IPMC). The features of IPMCs are their light weight, their ability to sustain large deformations, and their ability to be used in wet conditions. Typical IPMC materials include Nafion and Flemion [185]. Figure 2-11(d) presents a double-clamped buckled beam under the electrical actuation of an IPMC [202]. Cellini et al. [127] explored the feasibility of using the snap buckling of two IPMC sliding cranks induced by a steady fluid flow for energy harvesting purposes (Figure 2-11(e)). Beyond snap-through buckling of beam-like IPMC samples, a recent study by Shen et al. [25] has showcased a prototype, along with a novel fabrication method, for sensors based on the buckling of axially-compressed IPMC pipes (Figure 2-11(f)). A comprehensive review on IPMC can be found in [203], while studies [157] also indicate that there is plenty of room left for material science researchers to develop artificial materials to achieve elastic instabilities.

2.5 Summary

Harnessing elastic instabilities is a promising technique that is yet to be fully explored. Four major aspects include application purposes, application scales, structural prototypes and material prototypes. This chapter presented state-of-the-art developments on the harnessing of buckling for smart purposes. The increasing interest in various disciplines for developing smart applications during the past decade has motivated creative researchers to transform buckling behavior into a promising phenomenon for the design of novel materials and mechanical systems.

The following findings can be drawn from this chapter:

(1) Existing endeavors on buckling-induced applications can be generally divided into two main categories: energy-related and motion-related. Energy-related applications can be further categorized into energy production and energy dissipation. Energy released from snap-through buckling can be used in the design of energy harvesters, sensors, actuators and micro-electromechanical systems (MEMS), while the energy dissipated from buckling events can be used for the design of energy dissipaters, dampers, stabilizers, isolator, etc. For motion-related applications, snap-buckling instabilities have been proven to be useful in the design of morphing, adaptive and deployable structures.

(2) The compiled research efforts have shown that buckling and other elastic instabilities can be found across scales: from nanostructured materials to macro-scale structural elements. Energy- and motion-related applications using snapping and buckling have been primarily explored at the micro scale. However, an emerging trend is to extend the basic principles as a platform for nanoscale applications. Prototypes of EI-induced sensors and actuators are also gaining momentum for the monitoring of large structures.

(3) The key step for using a specific unstable event is to identify a desirable structural prototype. The studies highlighted in this review have shown that laterally-loaded beams and bi-stable plates are the most frequently used structural forms for the purpose of energy harvesting, while cylinder-type structures have been heavily studied for energy dissipation purposes. 3D forms, by their nature, are more favorable for motion-based applications with morphing or deployable features. Extending beyond the bistability featured by many existing forms, a research trend is emerging to explore the structural systems that can feature multi-stable events by: varying material properties, using hybrid

structural/mechanical systems, using hybrid materials, and adding constraints. The search for structural forms to achieve desirable snap-through instabilities is also being assisted by optimization methods, such as topology optimization.

(4) Another key step for using a specific unstable event is to select a suitable material. Two major features in the selection of a material for EI-induced purposes are the ability of shape change and the ability of shape memory. A material may have these features separately or simultaneously. Four major reported materials with the ability of shape change are metals (including metalloids), fiber-reinforced composites, polymers and piezoelectric materials. Shape memory alloys (SMAs) and shape-memory polymers (SMPs) are well-known candidates among many smart materials. An ongoing trend is using soft and superelastic materials, such as dielectric elastomers (DEs), graphene, and ionic polymer–metal composites (IPMCs), to trigger elastic instabilities.

This chapter has covered diverse studies under the overarching concept of harnessing buckling and elastic instabilities. However, it should be noted that snap buckling is only one type of instability phenomena. This narrower treatment follows from the fact that it is not easy to classify, or unify, all kinds of instabilities into a single category. Nonetheless, the research trend is on the exploration of many kinds of instabilities. Continuous advances in materials processing and fabrication methods are likely to motivate the creativity of researchers seeking to harness EI-induced mechanisms, indicating increasing growth and development in this research field for several years to come.

Chapter 3

Approach

3.1 Overview

The previous chapter featured the great body of experimental works on the subject of elastic instabilities for smart applications and focused on conceptual and physical aspects, but it did not highlight fundamental aspects. This chapter presents the theoretical background, experimental approach and numerical tools based on which the current work is established. Figure 3-1 presents a review of the method used to study this problem and it can be seen that while research activities are still ongoing they have shifted from analytical approaches toward finite element methods. The contents of this chapter are used and referenced in the following chapters.

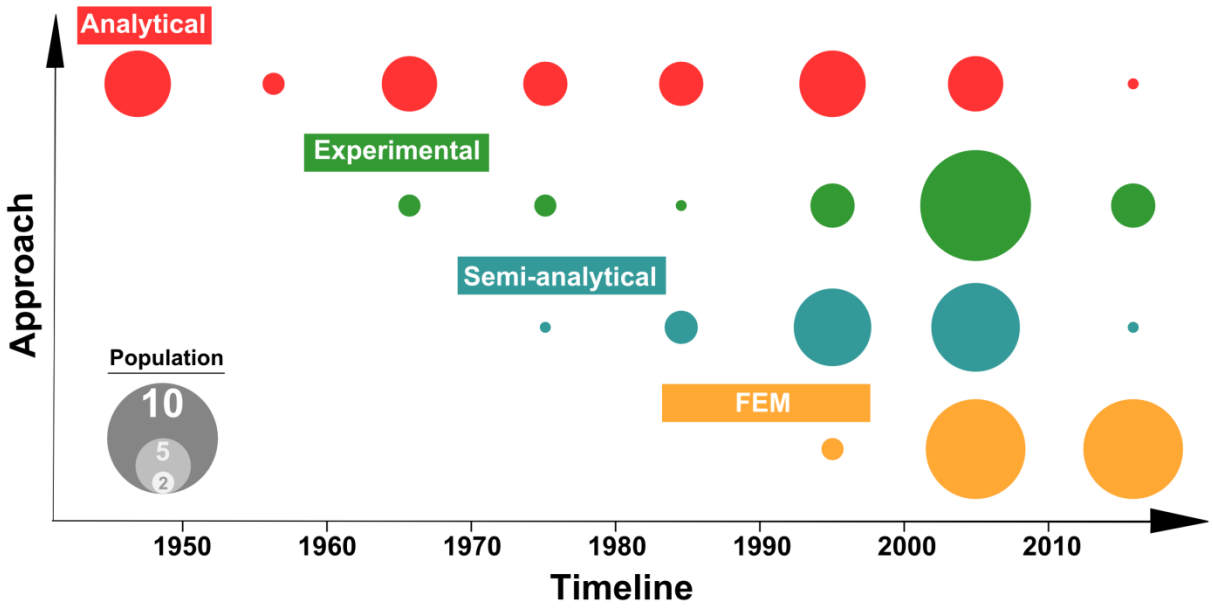

Figure 3-1: Research approach on postbuckling behavior of axially-loaded cylindrical shells.

3.2 Theoretical background

Buckling of cylindrical shells under axial compression is perhaps one of the most studied problems in mechanics, with thousands of publications since the early twentieth century [204]. Due to the geometrical symmetry present in cylindrical shells, their buckling is a phenomenon related to the occurrence of an unstable symmetric point of bifurcation in the equilibrium path. In this type of bifurcation buckling even a small imperfection plays a significant role and has a large effect in modifying the equilibrium path; which leads to a new position of equilibrium at a much lower buckling load. A localized buckling event on the shell surface is due to the difference between the membrane stiffness and bending stiffness. Typically, the membrane stiffness of the cylindrical shell is several orders of magnitude greater than the bending stiffness. When a cylinder is subjected to axial compression, it will absorb a great deal of membrane strain energy without large deformation in the axial direction. However, the thin shell will buckle when the large stored-up membrane energy is converted into an equivalent amount of bending strain energy. In reality, the uneven edge of the cylinder may create an initial uplift at the base, which tends to produce a local and inward-directed “dimple” at a low axial load level. The “dimple” then tends to grow larger both in extent (area) and in depth and moves gradually up along the shell surface. Further generation of these local buckling events finally leads to a buckled configuration of the shell into a more-or-less diamond pattern.

As a classic problem, a shell buckling analysis consists of determining the maximum load a cylinder can support before it collapses, or significantly loses is load carrying ability. Contributions to this field started early last century and were made by Donnell [29], von Karman and Tsien [30]. Donnell was the first to explore large-displacement theory to achieve a closer agreement with experimental data. von Karman and Tsien developed the governing equations

that are based on classical shell theory with a Karman-Donnell type of kinematic nonlinear equations. With the use of an Airy stress function ϕ, the problem is reduced to solving two governing equation subjected to appropriate boundary conditions as shown in Equation 3-1 and Equation 3-2; where $D = 2Et^3/3(1-\nu^2)$; E is the Yong's modulus, ν is the Poisson's ratio; 2*t* is the shell thickness; *r* is the radius; and ω is the radial displacement of any points in the middle surface. It consists of two coupled nonlinear partial differential equations in terms of the transverse displacement ω and the Airy stress function ϕ.

$$D\nabla^4\omega = 2t\left[\frac{\partial^2\phi}{\partial y^2}\frac{\partial^2\omega}{\partial x^2} - 2\frac{\partial^2\phi}{\partial x\partial y}\frac{\partial^2\omega}{\partial x\partial y} + \frac{\partial^2\phi}{\partial x^2}\left(\frac{\partial^2\omega}{\partial y^2} + \frac{1}{r}\right)\right] \quad \text{Equation 3-1}$$

$$\nabla^4\phi = E\left[\left(\frac{\partial^2\omega}{\partial x\partial y}\right)^2 - \frac{\partial^2\omega}{\partial x^2}\frac{\partial^2\omega}{\partial y^2}\right] - \frac{E}{r}\frac{\partial^2\omega}{\partial x^2} \quad \text{Equation 3-2}$$

The assumed radial deformation ω in the first equation is approximately estimated in terms of a number of parameters by using a minimum strain energy condition. Those parameters are solved by applying the static analogue of Kelvin's minimum energy theorem. Then, the Airy stresses in the second equation are solved such that the stresses in the middle plane are obtained. This procedure laid a significant basis for many following studies on the buckling and postbuckling of cylindrical shells under axial compression.

Using the boundary condition of the membrane state, the governing equation can be reduced to a standard eigenvalue problem with the eigenvalues

$$\lambda_{c,mn} = \frac{1}{2}\left\{\frac{(\alpha_m^2 + \beta_n^2)^2}{\alpha_m^2} + \frac{\alpha_m^2}{(\alpha_m^2 + \beta_n^2)^2}\right\} \quad \text{Equation 3-3}$$

and eigenfunctions:

$$\omega(x,y) = t \sin m\pi \frac{x}{L} \cos n\pi \frac{y}{R} \quad \text{Equation 3-4}$$

$$\phi(x,y) = -\frac{Et^3}{2\sqrt{3(1-\nu^2)}} \frac{\alpha_m^2}{(\alpha_m^2+\beta_n^2)^2} \sin m\pi \frac{x}{L} \cos n\pi \frac{y}{R} \quad \text{Equation 3-5}$$

where

$$\alpha_m^2 = m^2 \frac{Rt}{2\sqrt{3(1-\nu^2)}} \left(\frac{\pi}{L}\right)^2 \quad \text{Equation 3-6}$$

$$\beta_n^2 = n^2 \frac{Rt}{2\sqrt{3(1-\nu^2)}} \left(\frac{1}{R}\right)^2 \quad \text{Equation 3-7}$$

Another significant theoretical contribution towards understanding the postbuckling behavior of cylindrical shells was made by Koiter [205] by proposing the use of an asymptotic method to track the postbuckling path of cylindrical shells with the consideration of imperfections**.** Solution of the equilibrium equations near bifurcation points were derived on the basis of the potential energy expansion. Koiter's theory served as a groundbreaking theoretical solution for most following investigations on postbuckling behavior. Budiansky and Hutchinson [206] identified a complete family of bifurcation modes and then formulated an exact analytical solution for a limited case of modes with infinitely long wavelengths while other cases are solved by numerical analysis. Such analytical framework is also available based on the procedure of a perfect cylindrical shell with an additional effect from thickness variation [207]. Similar studies have been conducted to evaluate the critical buckling load with effect of the axisymmetric thickness variations and periodic variations on anisotropic cylindrical shells [208, 209] and cylindrical shells with arbitrary axisymmetric variations [210].

The nonlinear equilibrium equations (Equation 3-1 and Equation 3-2) can also be derived based on the principle of minimum potential energy. Researchers led by Thompson and Hunt introduced another analytical approach based on general postbuckling stability theory and focused on the tracing of branching phenomena [2, 211]. A conservative system is described by a potential energy function Π, which is the combination of the strain energy U of the cylindrical shell and the loss of the potential energy of the applied load V. The strain energy U includes two parts: from bending (U_b) and from membrane action (U_m). The determinant of Π will vanish at a discrete critical point that lies on the fundamental equilibrium path. With assumptions of boundary conditions and geometric imperfections, the equilibrium equations are established by the Ritz Method by considering the total potential energy to be stationary with respect to all the independent degrees of freedom.

Pedersen [212] extended the asymptotical solution into the advanced postbuckling region by using the Galerkin method, where each bifurcated load and postbuckling function are associated with axial wavelength. Sheinman and Simitses [34] described a framework to predict the post limit points in the equilibrium path with the consideration of imperfections. Numerical results showed that short (low L/R) and thin (high R/t) imperfect cylindrical shells have more significant change in the wave number in the postbuckling regime. The imperfection sensitivity decreases with increasing L/R and R/t. Under the same avenue, more recent studies has explored the postbuckling behavior of cylindrical shells on multiple materials, such sandwich shells [213], anisotropic laminated shells [37] and functional graded shells [214]. Energy methods are thus most commonly used for predicting the postbuckling response of slender structures because it is naturally compatible with the FEM formulation and has been incorporated in general-purpose codes.

3.3 Numerical modeling

Advances in computational mechanics and computer technology have decreased the difficulty of simulating the chaotic postbuckling response of structures. Reports on numerical investigations [46, 215, 216] have shown that equilibrium states in the postbuckling regime can be tracked and predicted by general purpose finite element programs by conducting a second-order nonlinear analysis of a shell with imperfection considerations, as shown in Figure 3-2. The procedure requires two types of analyses: (1) an eigenvalue analysis to obtain estimates of the buckling loads and modes, and (2) a load-deformation analysis to trace the postbuckling behavior.

Buckling eigenvalues and mode shapes were predicted and then linearly superposed to define and seed an imperfection to a perfect shell. Geometric imperfections on the shell surface can be introduced in the numerical model in three ways: from actual measurements, by a mathematically determined "worst" pattern, or through eigenvalue-based simulated shapes [217]. From a practical point of view, measured imperfections using laser scanning techniques are not always available, while the determination of the "worst" pattern is theoretically demanding. Thus, mode shapes from eigenvalue buckling analyses are commonly used to define artificially generated imperfections as a small perturbation on the perfect shell. This requires that the mesh be adequate to model the buckling modes. Typically, the first eigenmode is chosen to simulate an imperfection with a symmetric shape because the lowest mode is assumed to have the largest effect on the first buckling load. However, it has been shown that improved agreement with experimental data is obtained by seeding imperfections from the superposition of multiple mode shapes [43]. The seeded imperfection amplitude can range from 5% to 50% of the shell thickness and is selected based on known knowledge of experimental response [46].

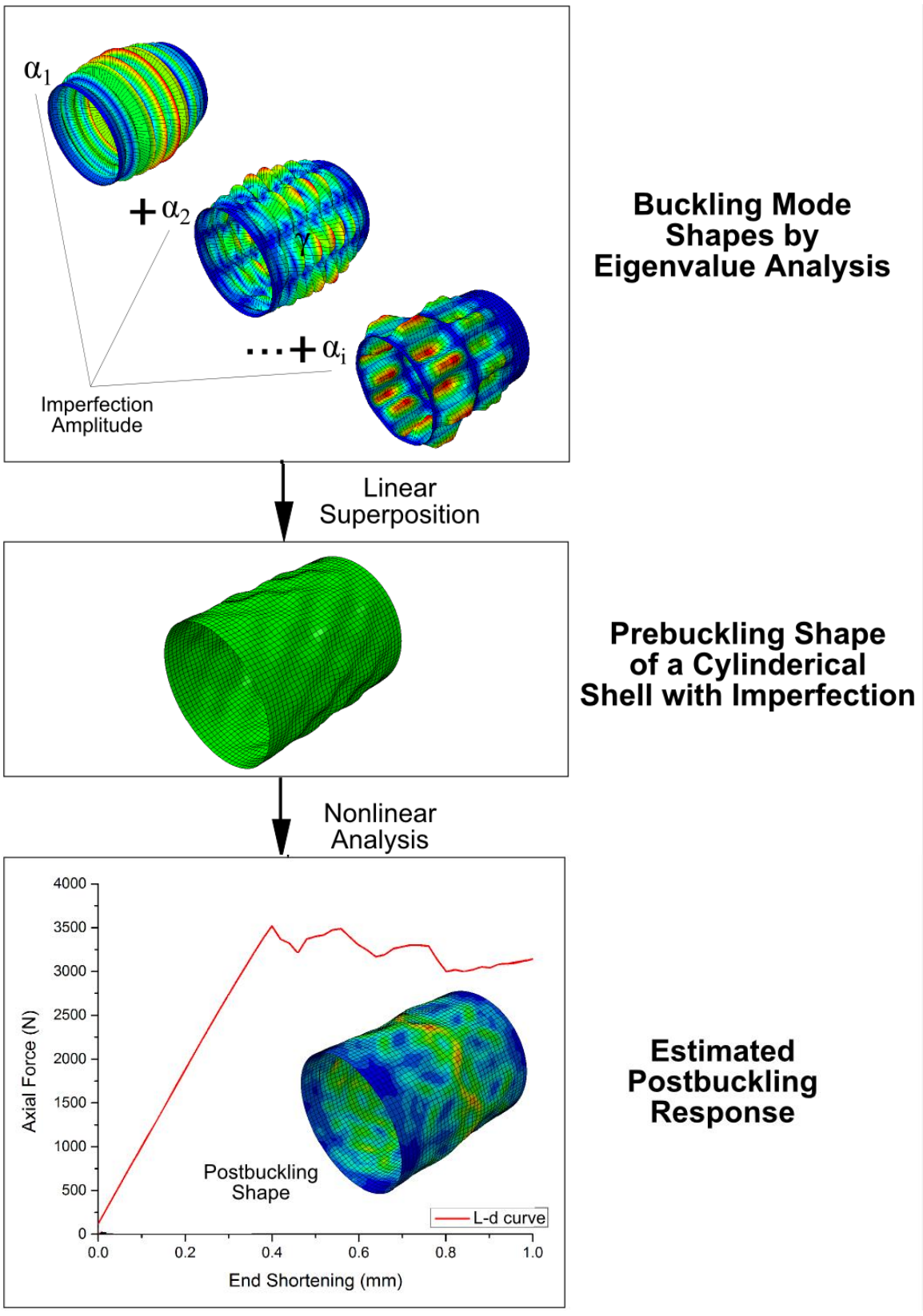

Figure 3-2: Established numerical approach for predicting postbuckling response.

The numerical simulations presented in this dissertation were conducted using the approach generally introduced in the above paragraph with slight modifications. The modifications in the approach used are: (1) the use of asymmetric buckling mode shapes, (2) the use of higher-order modes, and (3) the use of a statistical approach to determine the most likely response. A pilot experimental study [218] showed that the postbuckling mode shapes were always asymmetric due to the high sensitivity to localized imperfections on the shell surface. Thus, the biased mesh seed method [219] was used to generate a non-uniform (size) mesh in the finite element model. The cylinders were modeled with 4-node quadrilateral finite-membrane-strain elements with reduced integration (S4R). Asymmetric buckling mode shapes were thus obtained from the eigenvalue analysis. In addition, higher-order modes (up to 100) were considered to generate the seeded imperfections because these shapes have a large number of waves in the circumferential and axial direction. Finally, given the uncertainties of real imperfections, a statistical approach is preferred to capture the general predictive response [220-222]. After eliminating repeated mode shapes (i.e., with the same eigenvalue), mode shapes from the eigenvalue analysis were organized in different groups and used as an imperfection. In ABAQUS, this step uses the *IMPERFECTION option to define the imperfection and the model definitions for the buckling prediction analysis and the postbuckling analysis be identical.

Tracing the postbuckling behavior requires conducting a second-order nonlinear analysis. All analyses were conducted using the general-purpose finite element program ABAQUS [223]. Options include static solvers, arc-length methods (e.g., Riks) and dynamic solvers. All of these methods have been shown to be suitable and offer advantages and disadvantages that depend on the analysis goals [224]. Most numerical results in this dissertation were simulated using a static

solver with an empirical damping ratio, which was proven to capture the postbuckling behavior from test data.

3.4 Experimental plan: test units

It is well-known that the occurrence of multiple mode transitions and their spacing is highly depended on the shell's geometry, namely the length/radius ratio (L/R) and the radius/thickness ratio (R/t). Prior experiments [32, 38, 44, 45, 225, 226] have established an empirical range of these two ratios where multiple mode transitions were observed (see Table 3-1), which indicates that short thin-walled cylindrical shells ($L/R \leq 2$ and $R/t \geq 100$) are more likely to have multiple mode jumps under small end shortening. With respect to materials, two types were used in this study. A pilot study was conducted on shells fabricated from carbon/epoxy and carbon-E-glass/epoxy laminates. Subsequent studies were conducted on prototypes fabricated through 3D printing using polylactic acid (PLA). Details on these two test unit groups are presented in the following sections.

Table 3-1 Experiments on axially-compressed cylinders featuring multiple mode transitions.

Source	L (mm)	L_e* (mm)	R (mm)	t (mm)	L_e/r (mm)	r/t (mm)
[32]	51-160.9	-	100	0.247	0.51-1.61	404
[225]	800	600	300	3.2	2	93.8
[38]	700	520	350	0.33	1.5	265
[44]	530	510	250	0.5	2.04	500
[45]	254	203	101.5	0.28	2	363
Range	-	-	-	-	0.5-2	94-500
Mean Value	-	-	-	-	1.7	330

* Note: L_e is the effective length of the cylindrical shell, obtained by subtracting the reinforcing boundary regions from the total length.

3.4.1 Laminated composite cylinders

Two structural prototypes were considered using laminated composites during initial pilot studies for this research: a carbon/epoxy cylindrical shell and a hybrid carbon/E-glass/epoxy cylindrical shell (see Figure 3-3). The geometry of the carbon/epoxy cylinders had a L/R ratio of 1 and an R/t ratio of 363. All tests of the laminated composite cylinders had an inner diameter of 203 mm and a total length of 254 mm (including stiffened end regions of 25.5 mm each). The effective length of the central part of the shell was thus 203 mm. The shell end regions were strengthened (thickened) to attach the shell onto loading platens and consisted of 12 plies of unidirectional carbon/epoxy placed in the cylinder hoop direction. The stiffened regions were tapered such that each had four 25.4 mm plies, four 20.6 mm plies and four 15.9 mm plies

Figure 3-3: Carbon/epoxy cylinder (left) and hybrid carbon/E-glass/epoxy cylinder (right).

The baseline carbon/epoxy test unit had a [45/-45] laminate design. The 2-ply design was chosen to obtain a shell with relatively flexible axial stiffness in order to obtain the desired postbuckling response. The laminate sequence was chosen based on numerical studies that evaluated the effects of coupling stiffness terms in laminated composites on triggering multiple mode jumps in the postbuckling response of cylindrical shells [218]. The presence of extension-twist coupling terms (B_{16}, B_{26}) was found to be desirable for the sought-after behavior. Thus, while anisotropic coupling effects are known to reduce the buckling capacity of cylindrical shells, and are generally avoided through special laminate designs, new and emerging applications like the one pursued in this research may see their influence as favorable [227].

The design of the hybrid carbon/E-glass/epoxy cylindrical shells was inspired by the use of stiffeners for improving the load-carrying capacity of shells. Linear and nonlinear buckling

analyses on isotropic cylinders [218] showed that mode jumps in the postbuckling regime were more likely to occur when the seeded imperfection mode shapes had a relatively small number of waves in the longitudinal direction but a large number of waves in the circumferential direction. Thus, a hybrid cylinder concept was developed by using a chopped E-glass fiber mat with spaced unidirectional carbon/epoxy strips. It was of interest to have a matrix system with high compliance for the E-glass mat. Thus, an Epon 828 epoxy resin (Momentive Specialty Chemicals Inc., Columbus OH) with a Jeffamine D-400 hardener (Hunstman Advanced Materials, Lansing MI) and a ratio of hardener to resin of 0.6 was used. The hybrid cylinders were cured in an autoclave as noted above for the carbon/epoxy cylinders. The average thickness of the cured E-glass region was about 1.64 mm. Material properties for the E-glass-mat/epoxy material were obtained through coupon testing and they were: E = 7. 95 GPa and v = 0.25.

3.4.2 PLA cylinders

The baseline PLA cylindrical shell also considered the geometrical constraints (L/R and R/t ratio) from Table 3-1 and the size constraint of the available 3D printer. The baseline cylinder had a length of 100 mm, a radius of 40 mm and a thickness of 0.5 mm, as shown in Figure 3-4. Like the laminate composite cylinders, stiffened/thicker ring regions of 10 mm were built on each end of the cylindrical shell because pilot experiments found localized buckling events occurring at the edges can cause damage. The reinforced region had a step-wise geometry to transition from the edge to the center part of the cylindrical shell (i.e., effective length region). The effective length (L_{eff}) of the cylinder was thus 80 mm. The cylinder had a L_{eff}/R ratio of 2 and an R/t ratio of 80. The Young's modulus E was 1.8 GPa and the Poisson's ratio v was 0.2. All specimens used the baseline dimension just described yet variations were made for some prototypes.

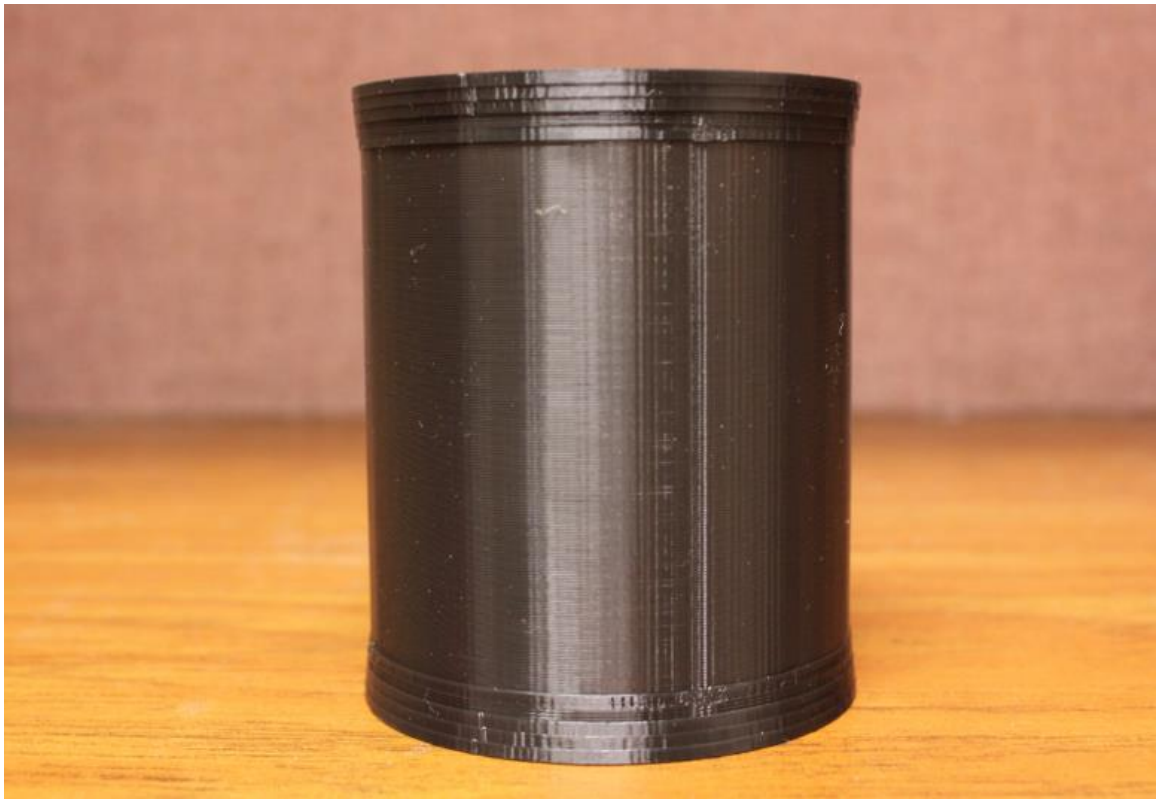

Figure 3-4: PLA uniform cylinder.

Studies on PLA-based 3D printing products [228, 229] have reported that the printing orientation and fill pattern have an important effect on the mechanical properties of the printed part due to the anisotropic nature of this fabrication technique. Therefore, tensile tests on PLA printed coupons were conducted before the fabrication of the PLA cylindrical shells. The test coupons were printed following the Type IV dimensions described in the ASTM D638 standard. The coupons were fabricated in the same region of the printer to minimize variability. Two sets of specimens were built with different printing orientation (see insets in Figure 3-5): one in the XYZ direction and the other in the ZXY direction. Tensile test results are given in Table 3-2 and Figure 3-5. It can be seen that the tensile strength and elastic modulus of the coupons is affected by the printing orientation. The strength and modulus of coupons printed in XYZ direction are

slightly higher (10%) than those printed in ZXY direction. It should be pointed out that the elastic modulus for PLA printed material has been reported to be higher in tension than in compression [228].

Table 3-2 Tensile test results of 3D printed coupons.

Specimen	Modulus of Elasticity (GPa)	Peak Stress (MPa)	Break Strain (%)
XYZ-1	3.045	50.98	4.08
XYZ-2	2.722	51.56	2.69
XYZ-3	3.317	52.15	2.39
XYZ-Mean	**3.028**	**51.56**	**3.05**
ZXY-1	2.569	46.89	2.42
ZXY-2	2.475	46.26	2.77
ZXY-3	2.709	48.71	2.58
ZXY-Mean	**2.592**	**47.28**	**2.59**

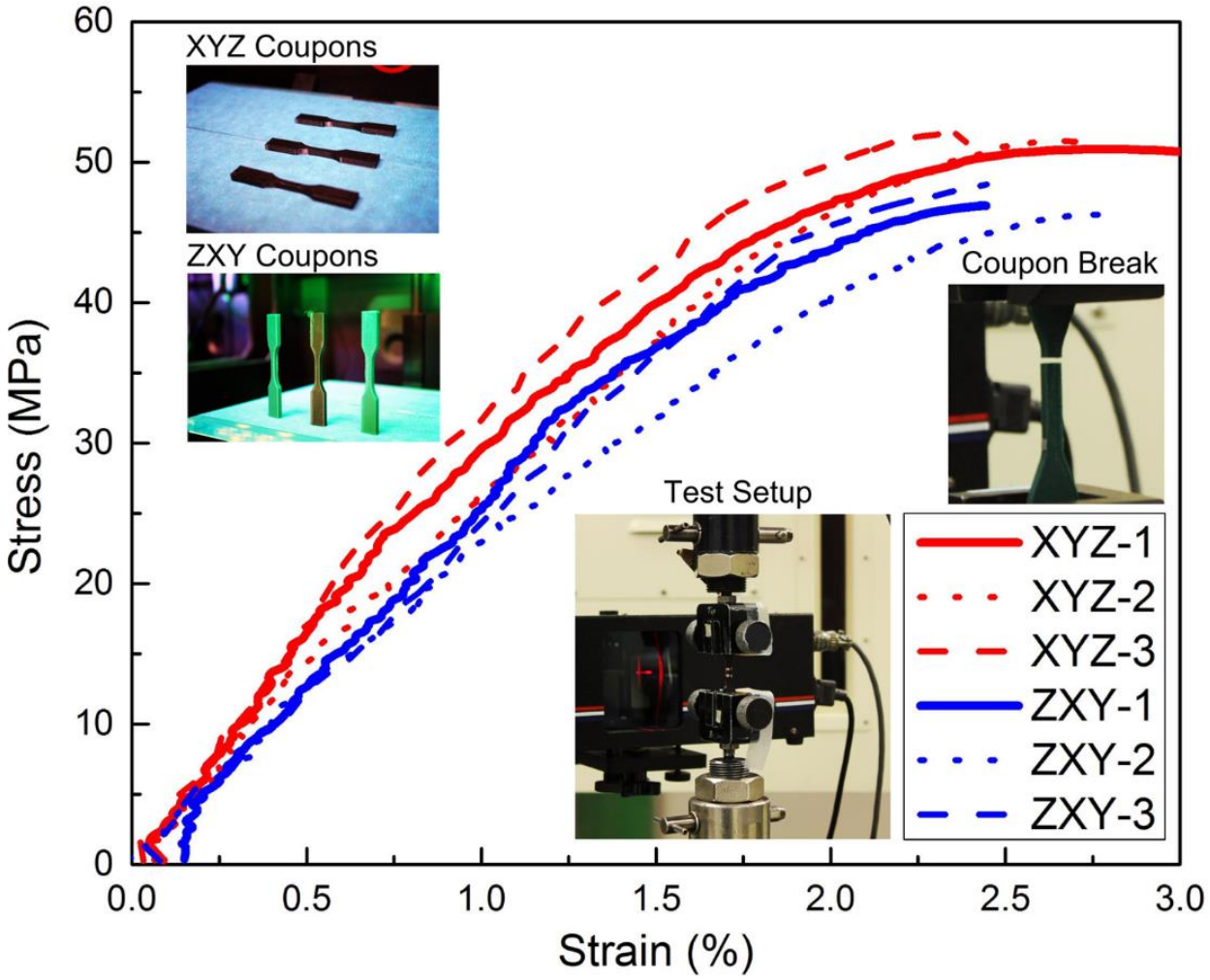

Figure 3-5: Results from tensile tests on PLA coupons printed in different directions.

3.5 Experimental plan: fabrication

3.5.1 Laminated composite cylinders

The cylindrical shells were manufactured from carbon-epoxy prepregs at the Composite Materials and Structures Center (CMSC) at Michigan State University. The carbon/epoxy cylinders were manufactured with unidirectional prepreg material (Item No. C-PP150; CST Inc., Tehachapi CA). The ply properties were: t_{ply} = 0.14 mm, E_{11} = 144.8 GPa, E_{22} = 9.655 GPa, G_{12} = 5.862 GPa, and ν_{12} = 0.25. The carbon/epoxy prepregs were cut into suitable rectangular

shapes (see Figure 3-6) and then assembled by placing them around a steel cylindrical mandrel in the proper direction (0° refers to the axial direction). The curing schedule includes applying 0.276 MPa of pressure inside the autoclave. The temperature inside the autoclave was ramped to 120 ℃ at 6 degree/min., and then held for 120 minutes. The samples were then cooled to 65 ℃ at 10 degree/min. The autoclave pressure was removed once the sample cooled to 65 ℃.

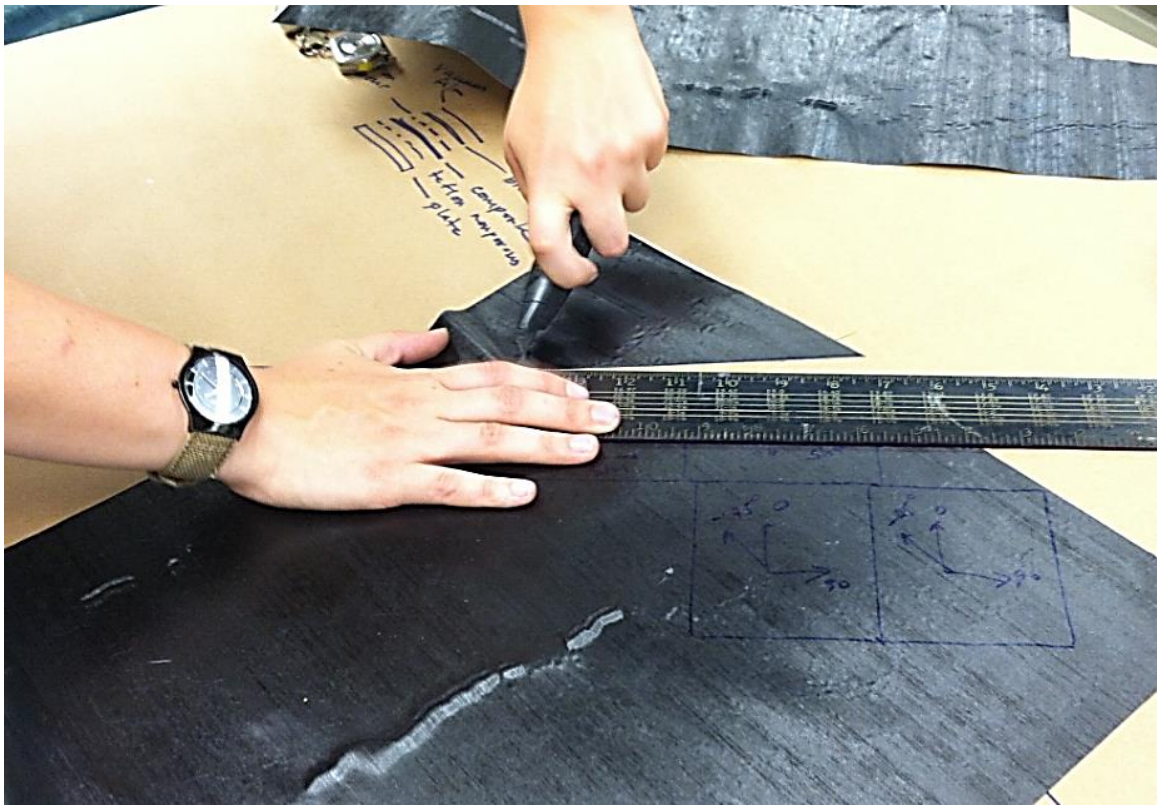

Figure 3-6: The cutting of CFRP prepregs.

The hybrid carbon/E-glass/epoxy cylinders were manufactured by placing 9.5 mm wide strips of the carbon/epoxy unidirectional tape (the same used for the carbon/epoxy cylinders) with a spacing of 41 mm on either side of an epoxy-saturated short-fiber E-glass mat. Manufacturing of the hybrid cylinder started by cutting out E-glass mat and all carbon fiber prepreg strips (including strips for hoop boundaries). Key steps on the layup of the CFRP strips on the E-glass mat are shown in Figure 3-7. After placing the strips to the cylinder, it was found advantageous

for the specimen to sit in the freezer for several hours, or overnight, so that the resin became less mobile for curing. The curing procedure was as described for the carbon/epoxy cylinders.

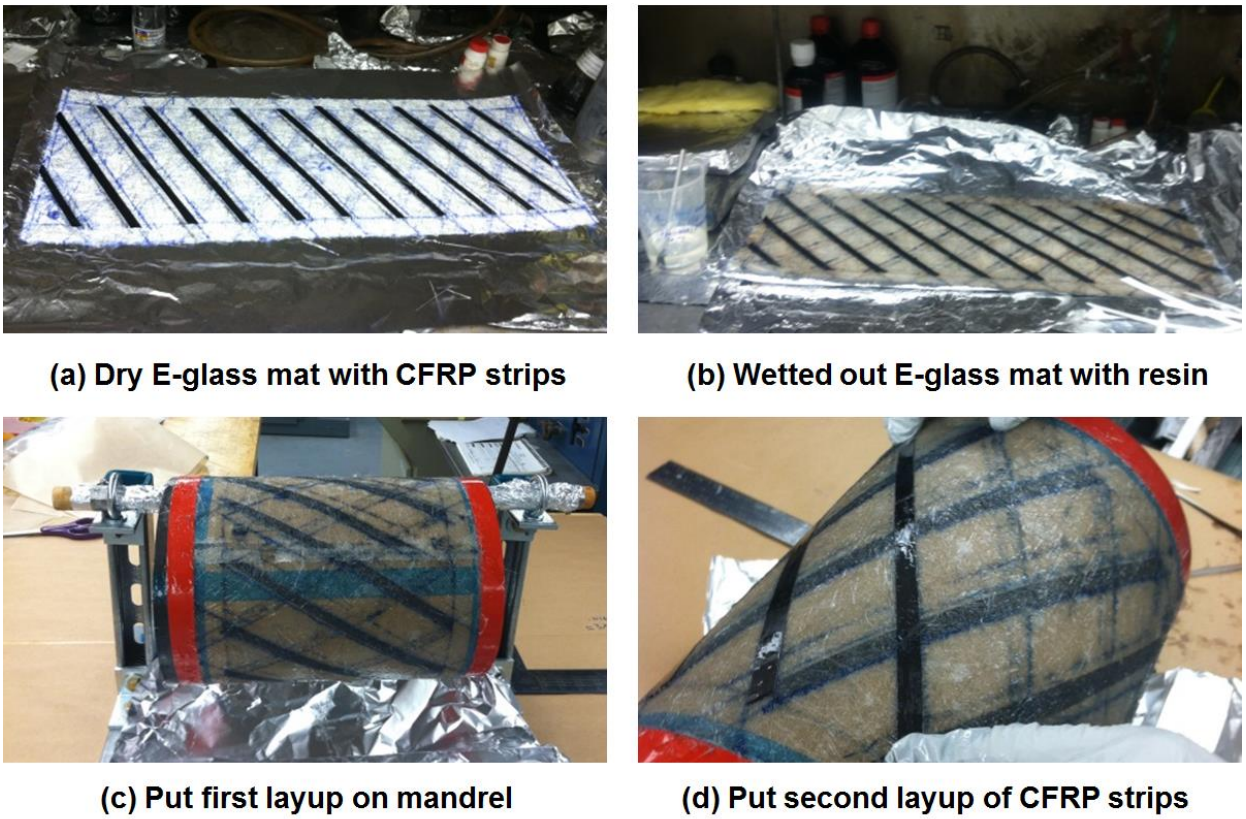

Figure 3-7: Key manufacturing steps for hybrid cylinder.

3.5.2 PLA cylinders

All of the cylindrical shells were fabricated with a 3D polymer-based printer (MakerBot Replicator 2, MakerBot Industries, New York City) using a PLA (polylactic acid) filament. The geometry file is created in SolidWorks [230]. The SolidWorks model was then converted into a STL type file before sending it to the 3D printer. The 3D printer heats the PLA filament and squeezes it out through a nozzle (0.4 mm in diameter). The filament cools down rapidly once it's placed on the building plate. The process is repeated to make a solid object layer by layer as shown in Figure 3-8.

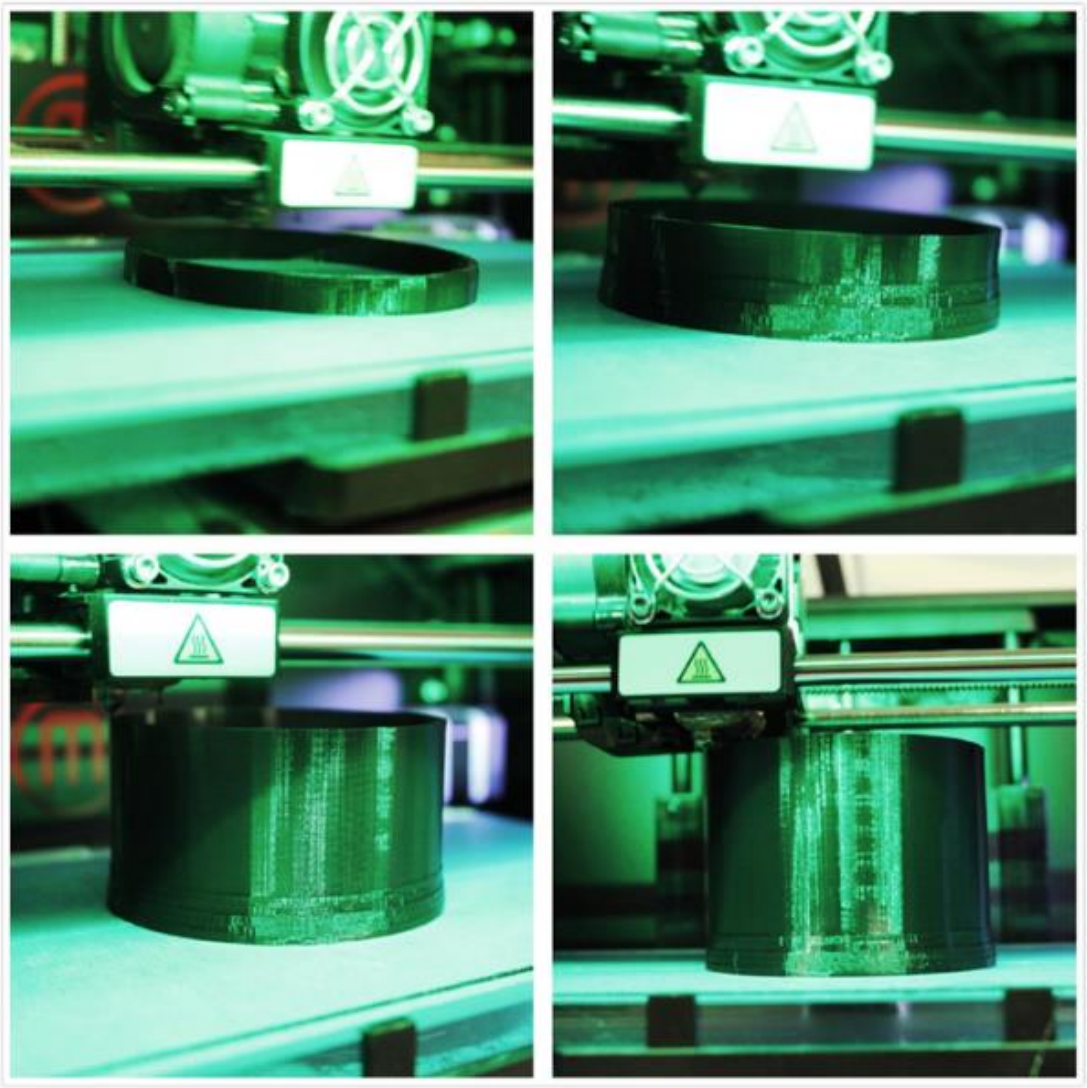

Figure 3-8: Representative images of the 3D printing of a cylindrical shell.

3.6 Experimental plan: test procedure

The laminated composite cylinders were tested under uniform axial compression in a universal testing frame as shown in Figure 3-9. The cylinders were prepared for testing by attaching them to two (top and bottom) aluminum loading platens to avoid damage to the cylinder edges, provide a uniform edge loading pressure and create a condition of fixity at the cylinder boundaries. The loading platens were $229 \times 229 \times 13$ mm and they were provided with a circular

(203 mm average diameter) groove (4.8 mm deep and 8 mm wide) to allow connection with the test unit. A bismuth alloy was used to attach the cylinder to each platen. During testing the bottom loading platen was supported by a rigid surface while loading was applied at the top through a spherical bearing placed at the center of the platen. The cylinders were subjected to axial compression under displacement control and then unloaded. The load and displacement records obtained from the load cell and displacement transducer of the universal testing frame were the only measurements taken.

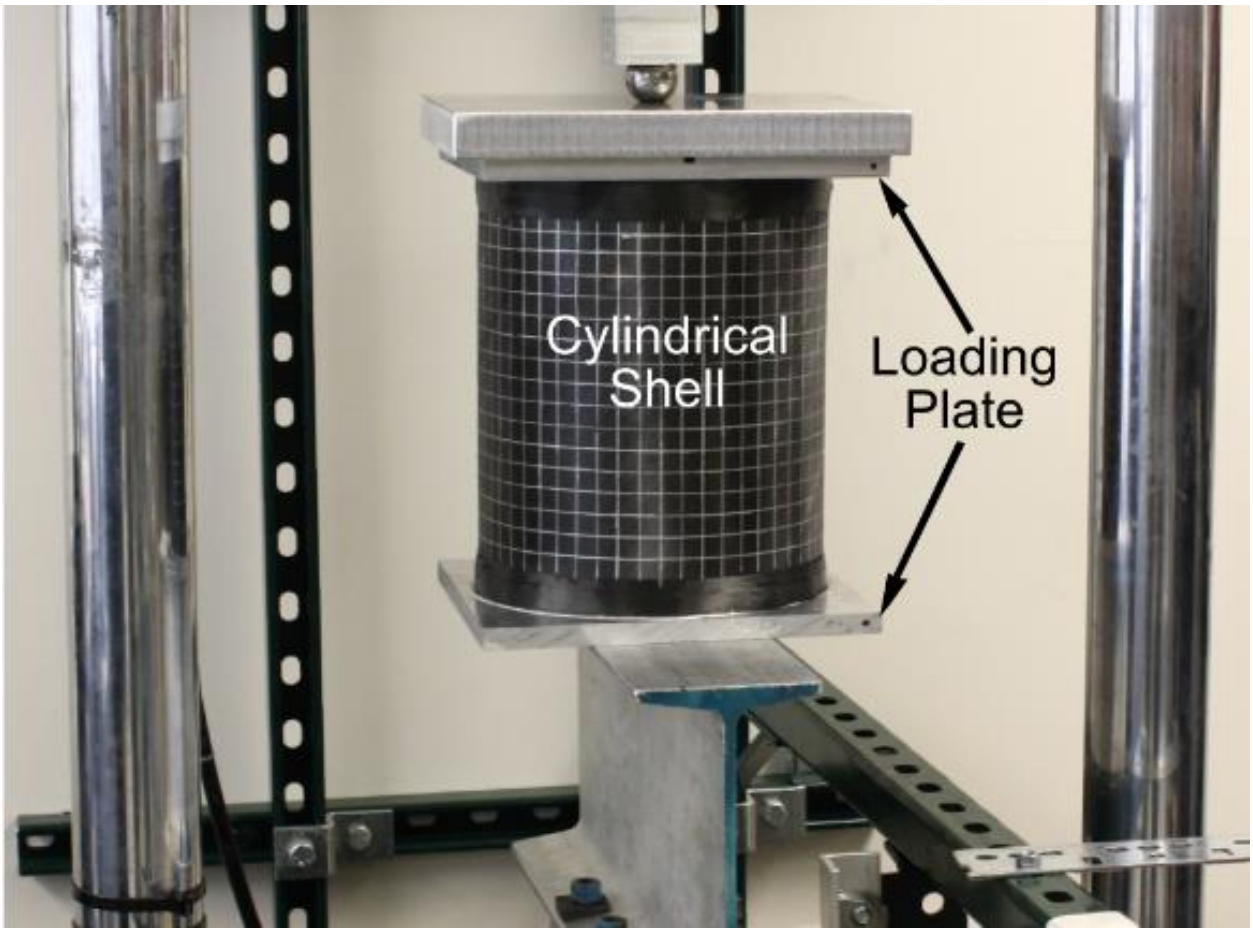

Figure 3-9: Test setup of a CFRP cylinder subjected to axial compression.

All PLA cylinders were axially compressed in same universal testing frame as shown in Figure 3-9. Since the PLA cylinders have smaller size than composite cylinders, the loading fixtures for PLA cylinders were different. The test setup made use of top and bottom loading fixtures with a pressure-tight fit to the test cylinder ends (see Figure 3-10). Again, the fixtures helped avoid damage to the cylinder edges, provided a uniform edge loading pressure and created a condition of fixity at the cylinder edges. The bottom loading fixture was supported by a rigid surface while loading was applied through a spherical bearing placed at the center of the top fixture.

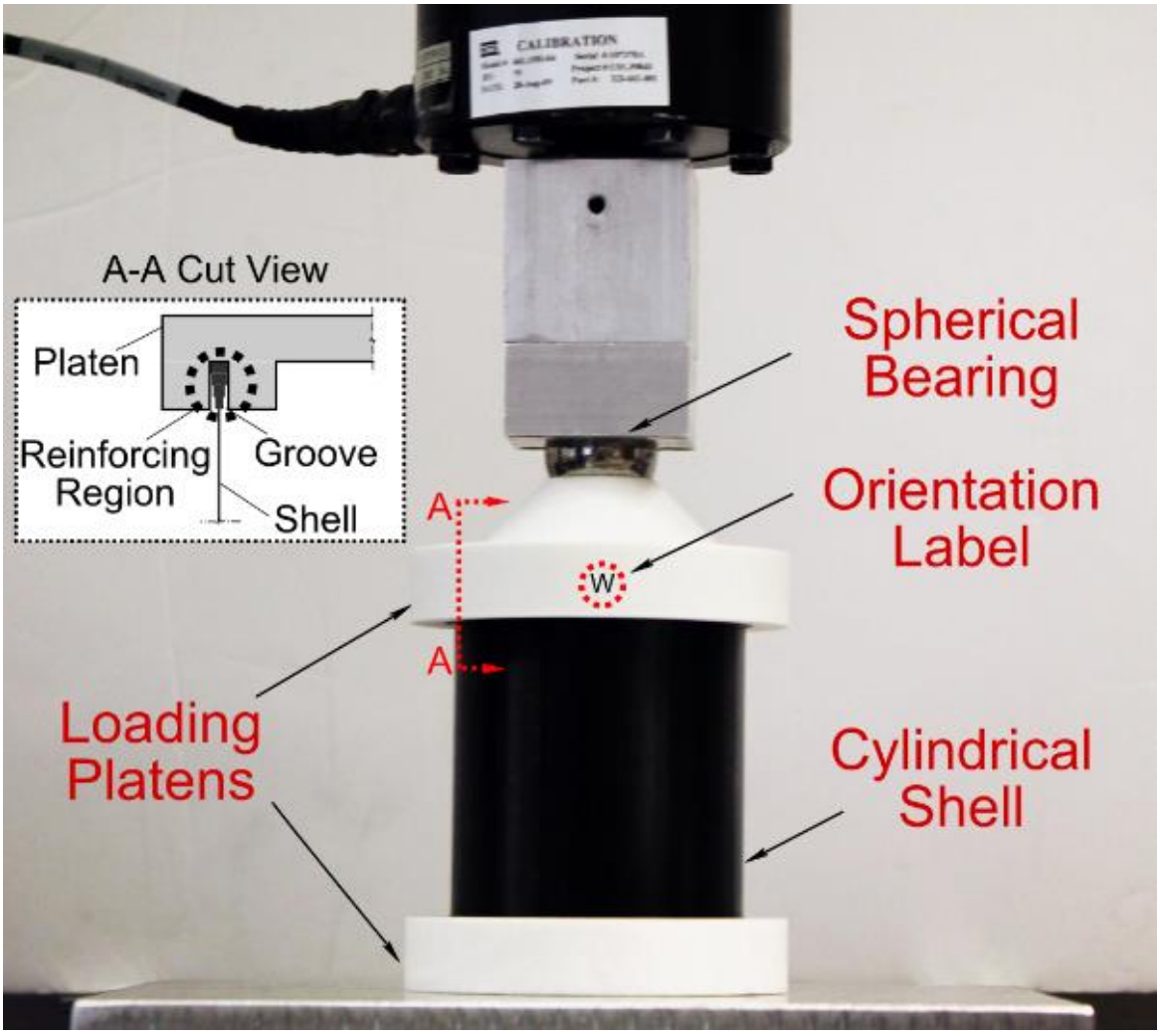

Figure 3-10: Test setup of a PLA cylindrical shell subjected to axial compression.

Bottom and top loading fixtures for the PLA cylinders were fabricated using a ceramic-based 3D printer (ZPrinter 250, 3D Systems, Rock Hill). The bottom loading fixture was a 20 mm thick circular plate with a radius of 53 mm, provided with a circular (40.25 mm average diameter) groove (10 mm deep and 4 mm wide) to allow connection with the test unit. The top fixture had the same features as the bottom one but in addition it was provided with a 20 mm cone in the center to uniformly distribute the load from a metallic sphere attached to the universal testing frame.

The printing process for the loading fixtures was different than that used for the cylindrical shells, as shown in Figure 3-11. The loading fixtures need to be stiff such that their deformations during testing are minimized. The ZPrinter 250 uses a plaster-ceramic composition that allows printing sand casting-like molds and builds samples through layers from the bottom up. The printing process consists on alternating layered depositions of a ceramic powder and a binder solution. After building the part, the specimen is allowed to dry and cool down.

Figure 3-11: Representative images of the 3D printing of loading fixture.

3.7 Postbuckling response characteristics

Understanding how the postbuckling behavior can be modified is the first step towards harnessing such instability phenomenon. The desired load-deformation response in the postbuckling regime is schematically shown in Figure 3-12 and the behavior of the cylindrical shells studied in this dissertation was evaluated under the features and variables defined here.

First, the equilibrium path is expected to have multiple critical points or mode transitions (n), manifested in the load-deformation response as load drops, rather than a single bifurcation point. It should be noted that the magnitude of the first bifurcation event (P_{cr1}) is not of primary interest. Rather, maximizing the number of critical points is of more importance. A second feature of

interest is the magnitude of each load drop (ΔP), which is associated with the area of the region exhibiting localized snap-through buckling, and the separation of the snap-through events as indicated by the relative end shortening (δ). The maximum load drop (P_{max}) and the maximum separation of these critical points (δ_{max}) are of particular interest for use of the postbuckling response in smart structures. It should be noted that δ_{max} is usually associated with the occurrence of P_{max} because a larger amount of strain energy needs to accumulate to generate a new critical event if the previous snap-buckling event has released a significant amount of energy from the system. The third feature of interest is the change in axial stiffness of the cylinder from its initial value (K_i) to the unloading point (K_e). Lastly, it is of interest to maximize the enclosed area (A) in the force-displacement response as it is associated with the dissipated strain energy from the equilibrium path transitions.

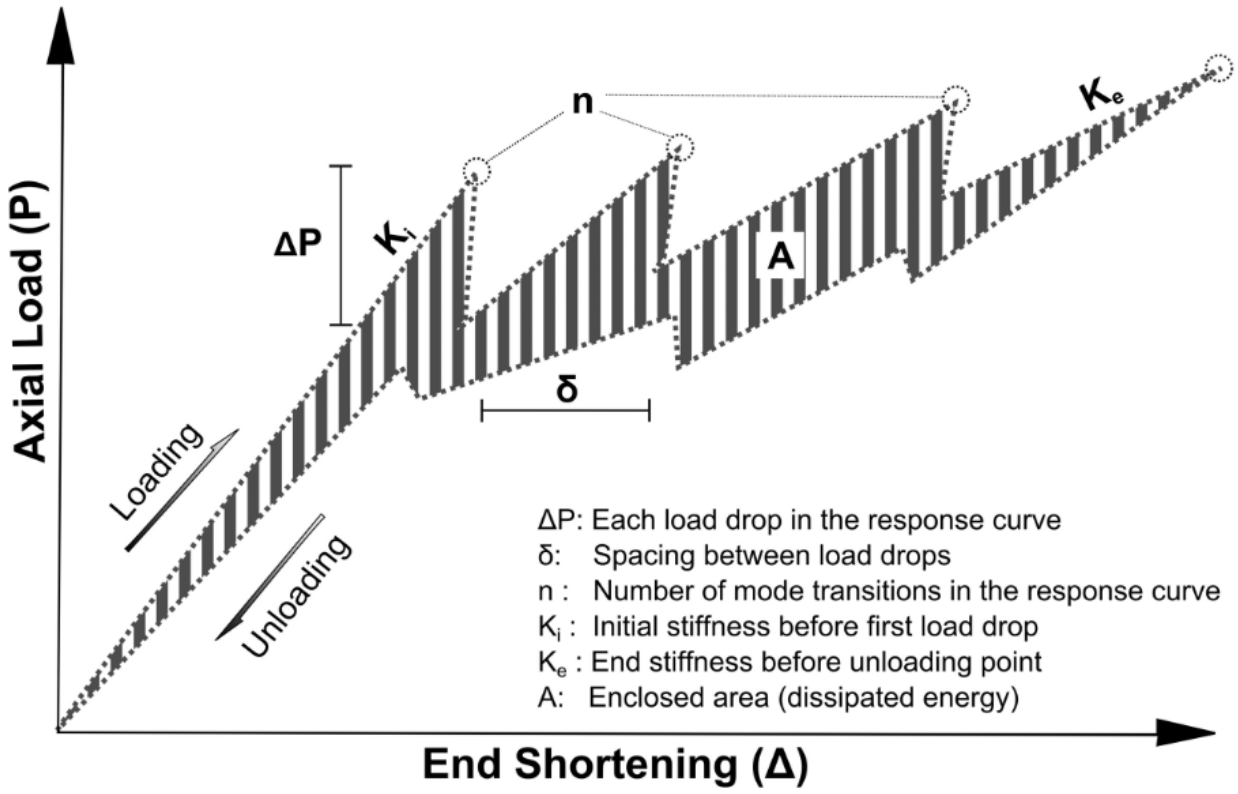

Figure 3-12: Schematic of key response features in the postbuckling behavior of an axially-compressed cylindrical shell.

3.8 Summary

The chapter described how the theoretical basis for tracing the postbuckling response of axially-compressed cylindrical shells are well-established and how numerical frameworks for modeling the postbuckling response are available in general-purpose finite element programs. Laminated composite cylinders and PLA cylinders were used as baseline designs according to an empirical range of length/radius (L/R) and radius/thickness (R/t) ratios based on published literature. The key parameters of interest in the postbuckling response were also presented. The approaches presented in this chapter are used and referenced in the following chapters.

Chapter 4

Seeded Geometrical Imperfection (SGI)

4.1 Overview

This chapter introduces the concept of a seeded geometric imperfect (SGI) design for cylindrical shells so as to obtain an elastic postbuckling response with targeted features. The research hypothesis is that the elastic postbuckling response of a cylindrical shell can be modified and made less sensitive to small material and geometric imperfections by providing them with large and strategically placed deformation patterns. The elastic postbuckling response can then be controlled and opportunities for using such cylindrical shells for the design of smart structures can be increased. This chapter presents a numerical and experimental study on the elastic postbuckling response of SGI cylindrical shells. Geometric imperfections were seeded from eigenvalue analyses and the obtained SGI cylindrical shells were fabricated by using 3D printing for experimental studies. The imperfection sensitivity of the SGI cylindrical shells under axial compression was then numerically and experimentally evaluated. The material presented in this chapter was submitted to the journal *Thin-walled Structures* for publication consideration.

4.2 Design concept

4.2.1 Eigenvalue-based shapes as imperfection

It can be seen in Equation 3-3 that eigenvalue $\lambda_{c,mn}$ depends not only on the geometric parameters but also on the axial and circumferential wave numbers m and n. The theories presented in Section 3.2 (both equilibrium and energy approaches) are capable of predicting the postbuckling response that yields a family of equilibrium paths due to different buckled wave numbers, as shown in Figure 4-1. These buckling patterns are predicted under the assumption of an axisymmetric shape, which does not match actual imperfection patterns. Thus, the postbuckling response should follow a predefined equilibrium path if the imperfection is seeded in terms of a fixed circumferential wavenumber with larger amplitude over other initial imperfections. This is the theoretical foundation for the concept of SGI design in this chapter.

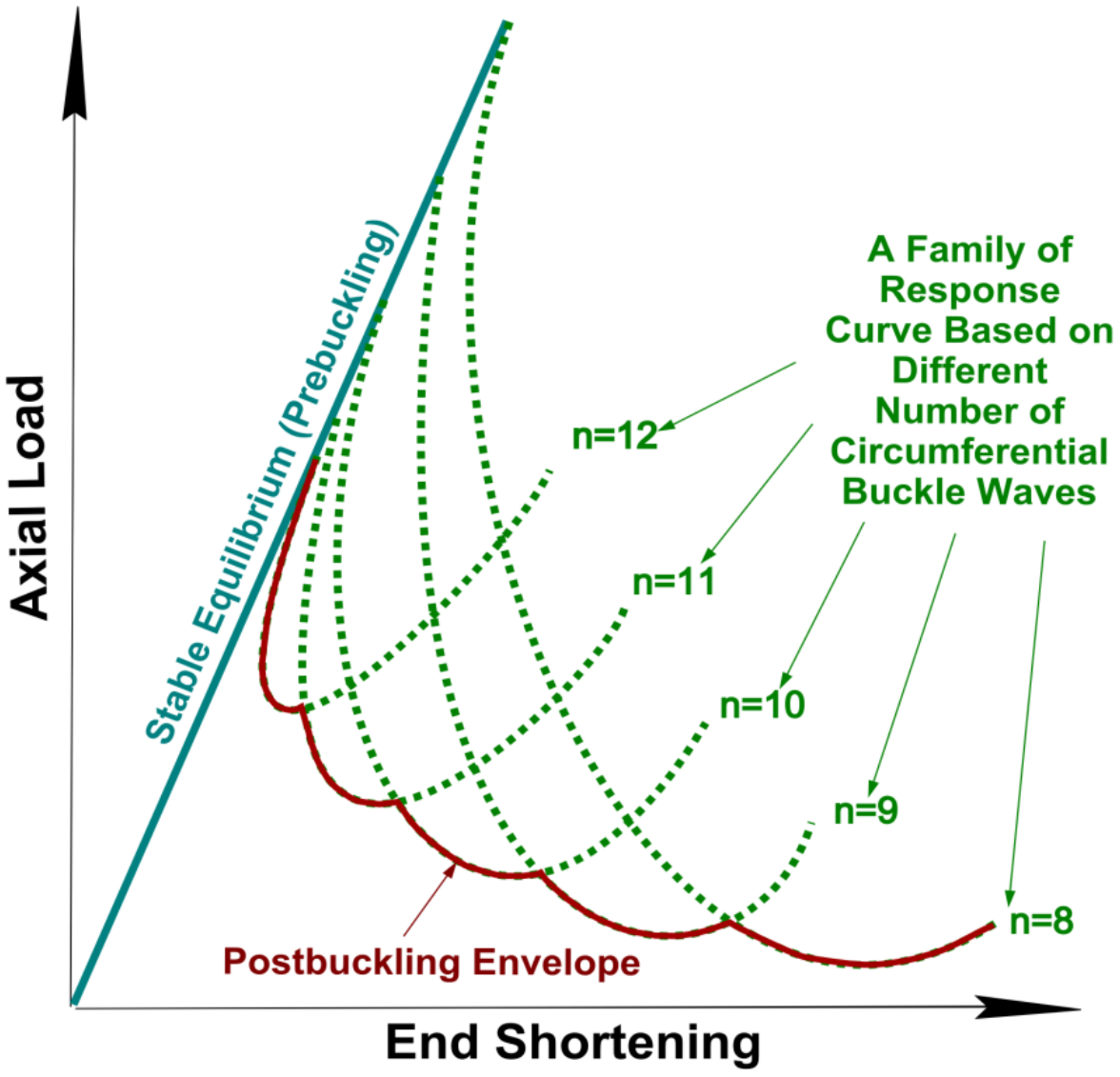

Figure 4-1: Family of equilibrium paths due to different buckled wave numbers.

The concept of using a seeded geometry is also inspired by the analysis approach presented in Section 3.3 and schematically shown in Figure 3-2. Mode shapes from eigenvalue analyses are the most common method to define artificially generated imperfections as a small perturbation on a perfect shell. Two other major methods to introduce geometric imperfections to a perfect shell are: (1) a mathematically determined "worst" pattern and (2) actual measurements [217]. In

the early stages of analytical model development, determination of the "worst" pattern was theoretically demanding and thus geometric imperfections were assumed to have an axisymmetric shape such that a critical buckling load could be estimated and a knock-down factor could be used in practice to ensure a lower bound of residual capacity. The most significant modeling performance gain comes from the ability to scan the initial geometric imperfections and thickness variations of manufactured shells for use as input to analytical and numerical models. From a practical point of view, measured imperfections, typically using laser scanning techniques, are not always available. Thus, using eigenvalue-based shapes have certain advantages over the other two methods.

The first eigenmode is commonly chosen to simulate an imperfection with a symmetric shape because the lowest mode is assumed to have the largest effect on the first buckling load. However, it has been shown that improved agreement with experimental data is obtained by seeding imperfections from the superposition of multiple mode shapes [43]. The seeded imperfection amplitude can range from 5% to 50% of the shell thickness and is selected based on knowledge of the experimental response [46]. Without measurement of the actual geometric imperfections, disagreement between predicted and measured responses still exists [47]. Most of the recent studies on imperfection sensitivity have featured the use of probabilistic methods to develop less conservative guidelines for the design of axially compressed cylindrical shells [50-52]; and more localized types of imperfection have been considered for calculating the postbuckling response, such as cutouts, dimples, dents, mid-surface imperfections, etc. Clearly, the large number of closely spaced eigenvalues and innumerable combinations of eigenmodes is part of the difficulty in tracing the postbuckling behavior.

Based on above-mentioned methods for the selection of imperfections, the discrepancy

between simulations and experiments in predicting the first critical buckling load, or lower-bound capacity, has been significantly reduced. However, a pilot experimental and numerical study [45] by the authors has shown that a discrepancy still exist in the far elastic postbuckling regime and that numerical simulations do not closely trace the postbuckling response. Therefore, a predefined geometric imperfection is introduced here in order to reduce the effort of selecting appropriate shapes to match the actual response. The selected geometry is expected to have a governing role over other initial imperfections on the postbuckling behavior of cylindrical shells.

4.2.2 Koiter circle as seeding variables

The imperfection profile and its amplitude have a bigger role on governing the postbuckling response. An axisymmetric imperfection profile was used in early theoretical studies [30, 205] to predict the critical buckling load. Periodic buckling modes and their locus can be interpreted along a half circle known as the Koiter circle in terms of a dimensionless axial and circumferential wavenumber. The classical view considers that all waves on the Koiter circle are possible, but it fails to distinguish what might occur in reality. Later, Hunt et al. [42] mentioned that predominately localized imperfections can more easily trigger buckling and the fundamentals behind the stability theory is quite different. They thus extended the Koiter circle to predict all possible buckling patterns in terms of a circumferential wavenumber as represented in Equation 4-1:

$$n^2 = m\pi\sqrt[4]{12(1-\nu^2)}\frac{R}{L}\sqrt{\frac{R}{t}} - m^2\pi^2\left(\frac{R}{L}\right)^2 \qquad \text{Equation 4-1}$$

where n is the circumferential full wavenumber; m is the axial half wavenumber; ν is the Poisson's ratio; R is the radius of the cylindrical shell; L is the effective length of the cylindrical shell; and t is the shell thickness.

The baseline PLA cylinder (see Section 3.5.2) had an effective length of 80 mm, a radius of 40 mm and a thickness of 0.5 mm. Again, the selected geometry was based on data of L/R and R/t ratios shown to trigger multiple mode transitions. Figure 4-2 shows the Koiter circle for the baseline shell (obtained from Equation 4-1) along with 200 buckling modes (determined using ABAQUS).

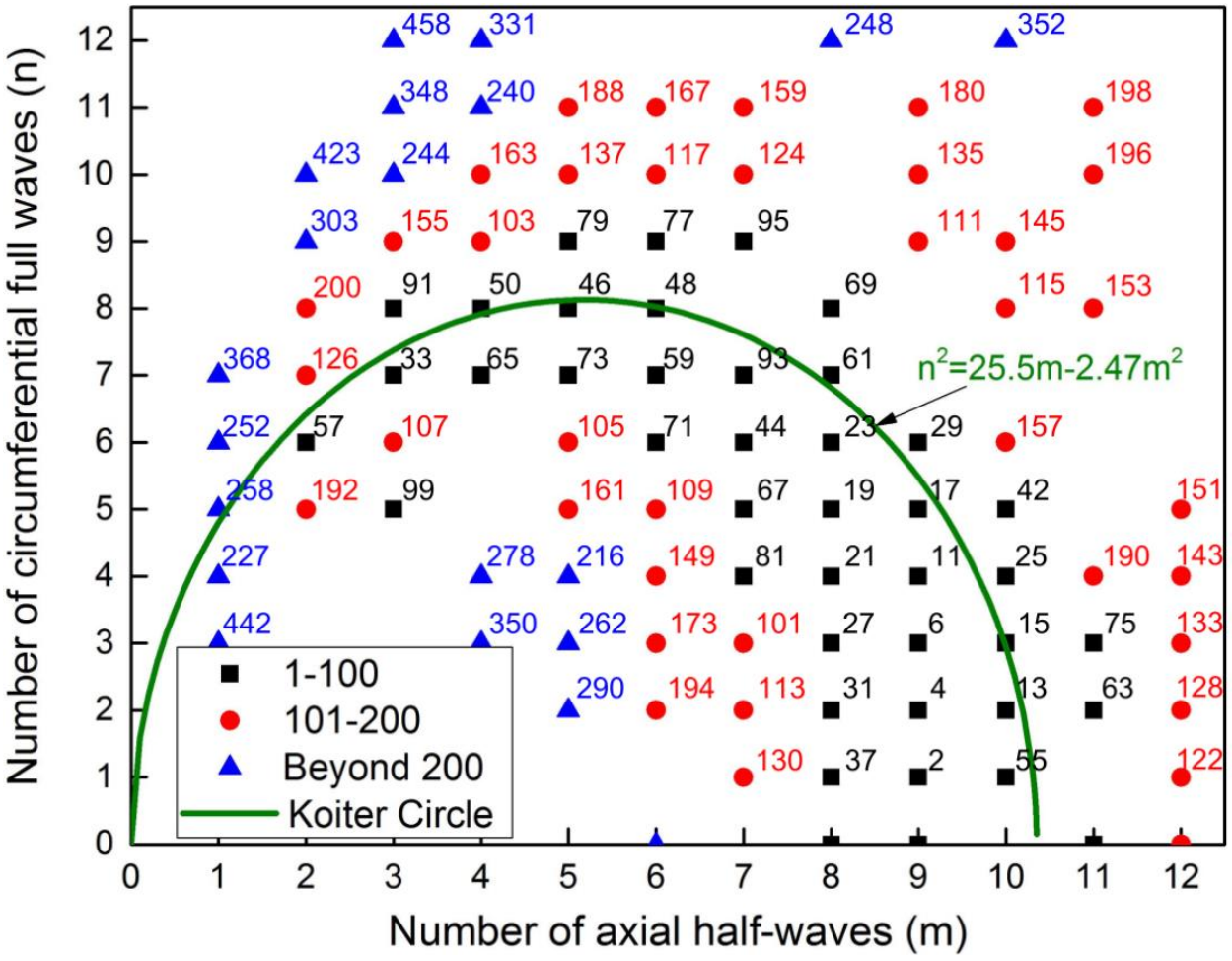

Figure 4-2: Koiter circle for the baseline cylindrical shell and mode shapes as seeded geometry.

Low buckling modes (below 50) are commonly used to estimate the critical buckling load of shells. However, it is known that the eigenvalues of cylindrical shell are closely spaced. In this

case, the maximum load difference between modes 1 and 200 is only 45%. Thus, higher-order modes (up to 200) were considered in order to provide more geometric options for seeded designs. It can be seen that the first 100 modes are along the perimeter of the half circle while the next 100 modes are slightly offset from the perimeter. The design of SGI cylindrical shells presented in the following section of the chapter uses single and multiple mode combinations from this Koiter circle.

4.3 Numerical results

4.3.1 Approach evaluation

Before evaluating the SGI concept, a full numerical procedure was evaluated against a published experimental test on a uniform cylindrical shell. The uniform cylindrical shell was studied in an earlier work [231] following the procedure described in Section 3.3. The shell was originally investigated in an experimental study by Yamaki et al. [32]. It had a length (L) of 113.9 mm, a radius (R) of 100 mm and a thickness (t) of 0.247 mm. The cylinder had a L/R ratio of 1.14 and an R/t ratio of 405. The Young's modulus E was 5.56 GPa and the Poisson's ratio v was 0.3. The classic buckling critical load is given by Equation 4-2 [215]:

$$P_{cl} = \frac{2\pi E t^2}{\sqrt{3(1-\nu^2)}} = 1290\ N \qquad \text{Equation 4-2}$$

The numerical model had a fine mesh resolution, with 400 elements in the circumferential direction and 80 elements in the axial direction. The cylinder was clamped along both edges. The buckling eigenvalue and mode shapes were predicted by the Lanczos method and the postbuckling response was simulated using an explicit dynamic solver. The cylinder was

subjected to axial compression under displacement control to a shortening of 1.0 mm (same as in the experiment). It should be noted that only elastic response was considered.

Arbitrary choice of eigenmodes as imperfections may lead to a reasonable first buckling load, but postbuckling paths would be drastically affected by the different choices of imperfections. It is thus of interest to solve the problem in an inverse manner to find an optimal combination of mode shapes that yield the best curve fitting with test data. Thus, 18 modes were chosen as design variables after eliminating repeated shapes (i.e., with the same eigenvalue). Some of selected mode shapes are shown in Figure 4-3, where *m* and *n* are the number of full sine waves along the axial and circumferential direction, respectively.

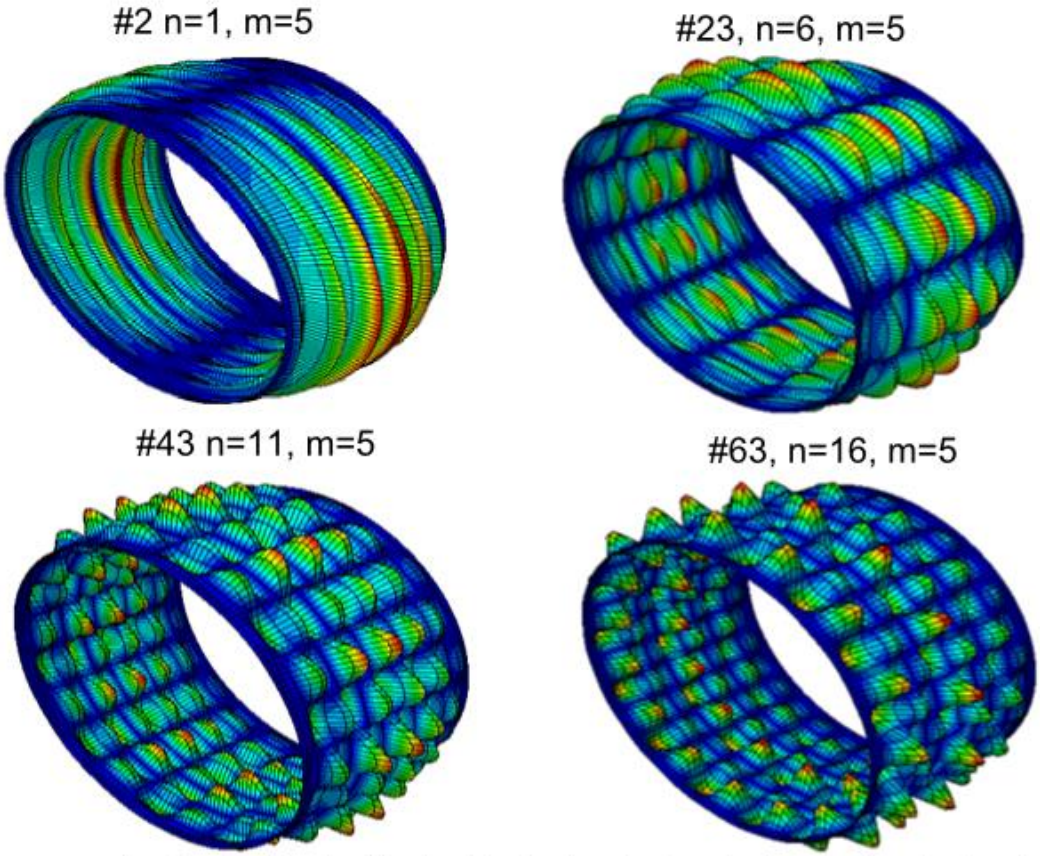

Mode	2	4	9	15	19	23	27	31	35	39	43	47	51	55	59	63	67	77
n	1	2	3	4	5	6	7	8	9	10	11	12	13	14	15	16	17	18

*Note: m=5 for all the selected mode shapes

Figure 4-3: Sample seeded buckling mode shapes.

After evaluating multiple combinations, the optimized superposed geometry included the contributions from 5% of mode 2, 5% of mode 15 and 10% of mode 63. The postbuckling response is plotted in Figure 4-4 along with test data and baseline/initial design. The comparison of postbuckling response parameters is given in Table 4-1, from which it can be seen that the optimized results better capture the key response features shown in Figure 3-12, including the initial stiffness (K_i), magnitude of fist mode jump (ΔP_1) and the total number of mode transitions (n). Although there are still differences between the simulated curve with optimal imperfections and the test curve, it can be seen that the area (A_{total}) below the force-deformation curves (which corresponds to the total work) are very close to each other. In addition, the postbuckling shape obtained by the numerical model matched well the diamond-shaped buckling wave patters observed in the test (as shown in Figure 4-4). This implementation confirmed the validity of using the nonlinear analysis procedure to match a targeted postbuckling response and indicates potential for using the approach toward the efforts of tailoring and controlling the postbuckling equilibrium path and mode transitions in a cylindrical shell under axial compression.

Table 4-1 Postbuckling response of cylinders.

Item	K_i (N/mm)	P_1 (N)	$\lvert\Delta P_1\rvert$ (N)	δ_1 (mm)	A_{total} (J)	n
Test	7297	908	535	0.13	211	4
Simulation	7448	1195	791	0.16	269	6

Note: P_1, ΔP_1 *and* δ_1 are associated with first bucking event. A_{total} is the area below each curve (correspond to the total work)

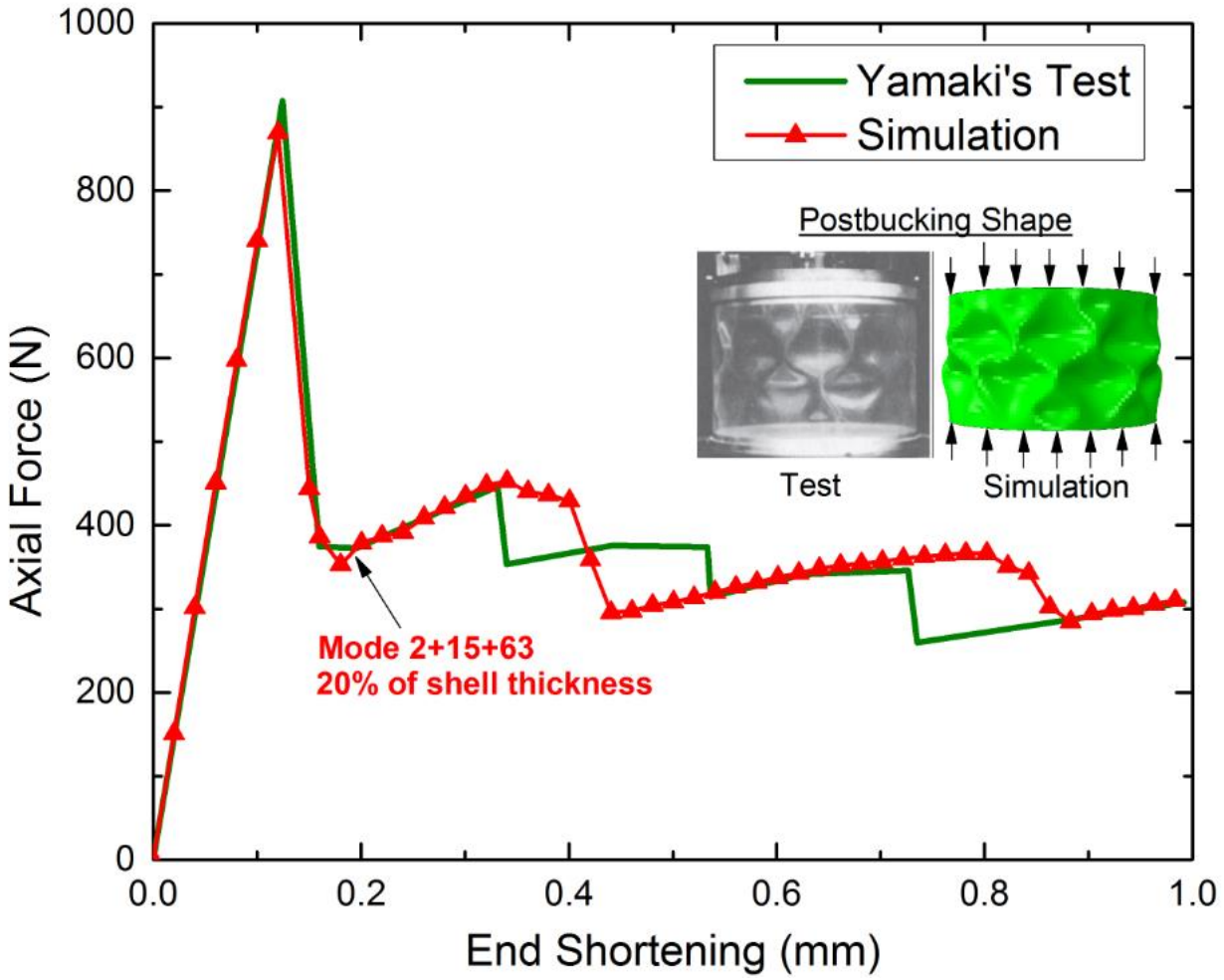

Figure 4-4: Comparison of postbuckling response from numerical simulations and experiment.

Three additional simulations were conducted using the same modeling approach on cylinders with all of the pre-selected 18 mode shapes for imperfection seeding but with different scaling factors (0.01%, 1% and 100% of the shell thickness for each mode). Figure 4-5 shows the resulting simulated postbuckling responses. The nearly perfect cylinder with a linear elastic postbuckling response can be considered as the upper bound case while the cylinder with large imperfections has no significant load drop which can be regarded as the lower bound case. For the cylinder with small imperfections (1% case), the postbuckling response has a number of load

drops. It is clear that the simulation results are very sensitive to the prebuckling mode shape selection and imperfection amplitudes, but such uncertainty also offers a variety of opportunities with the resulting design domain, which is identified as a hatched area in Figure 4-5.

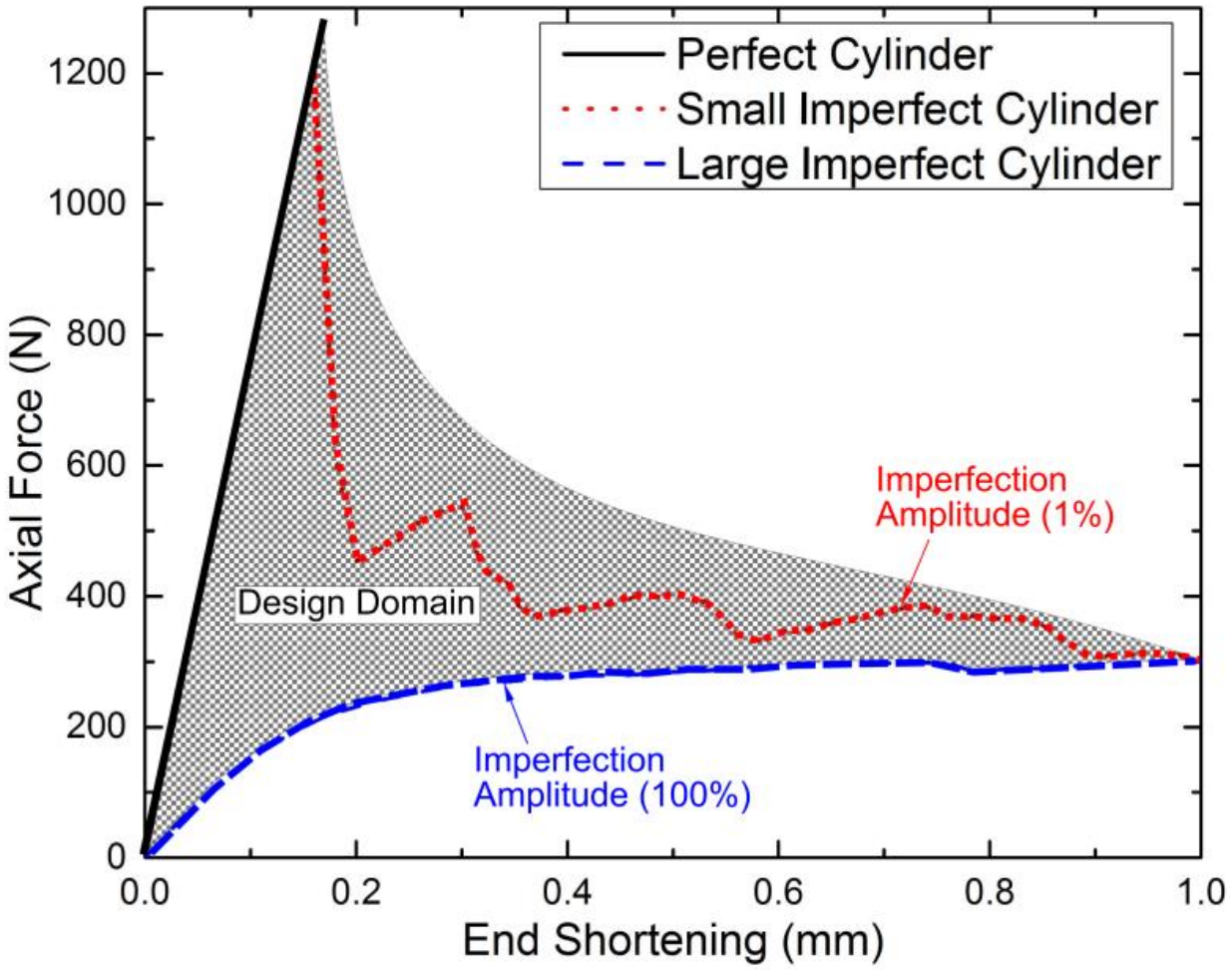

Figure 4-5: Postbuckling response of cylinders with identical mode imperfection seeding but different amplitudes.

4.3.2 Sensitivity analyses

A follow-up numerical simulation was conducted on a uniform cylindrical shell and a SGI cylindrical shell to evaluate the concept of SGI designs and their sensitivity to the initial imperfections. For consistency, the cylinders' geometry and material properties were the same as

those used in the evaluation study. Seeking a higher *n* in the postbuckling regime requires the seeded imperfection to be larger. Thus, another simulation was run with relatively larger amplitudes. The obtained imperfections were seeded from 12 out of 18 mode shapes (see Figure 4-3). The load-deformation response along with the time history of kinetic energy release of the best design is plotted in Figure 4-6. It can be observed that the number of mode jumps (*n*) obtained in this case was much higher than was obtained in the initial/baseline design conducted in the evaluation section. A detailed discussion can be found in an earlier paper [231].

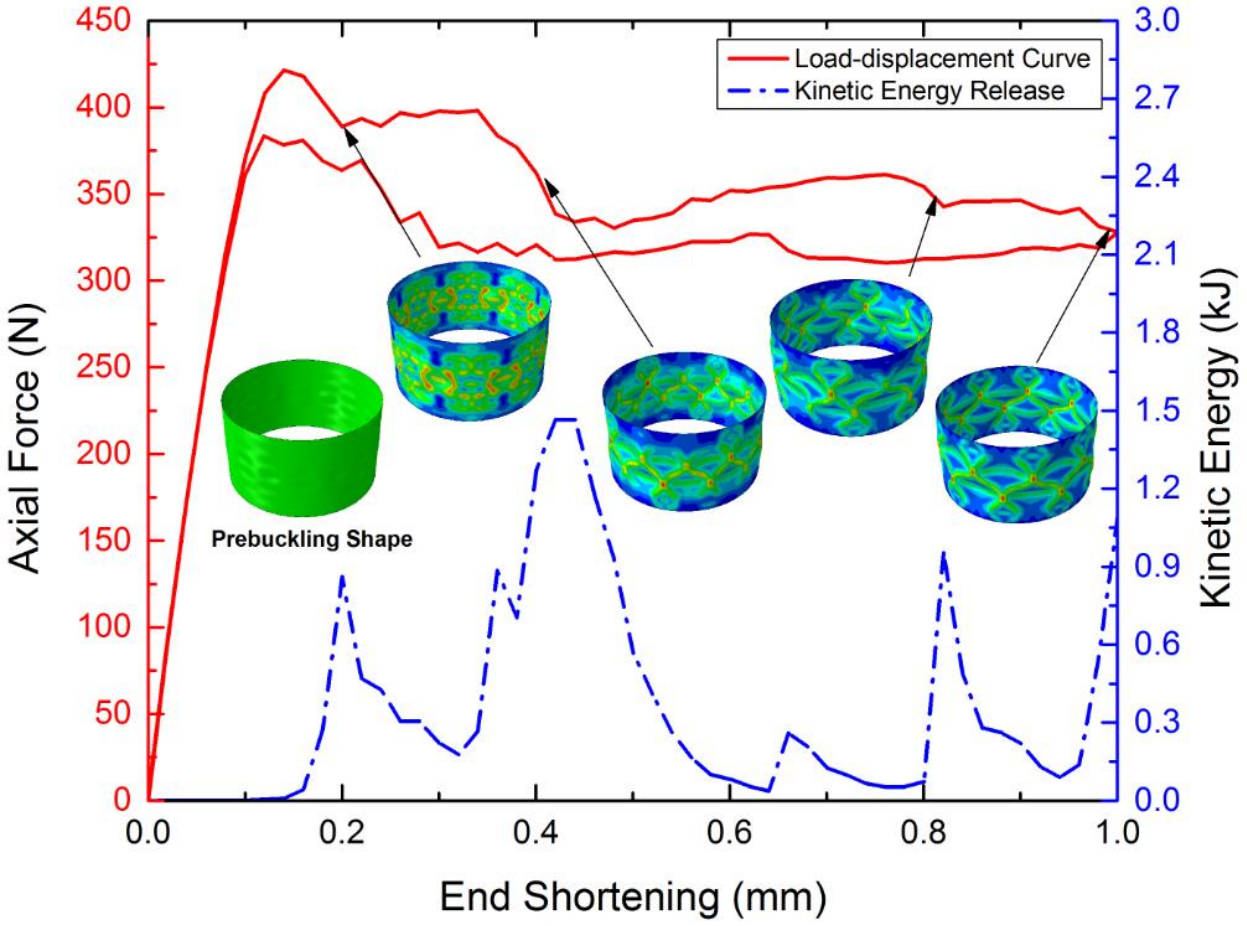

Figure 4-6: Obtained postbuckling response of cylinders with the objective of maximizing the number of mode jumps (n).

Based on the understanding of the role of imperfection design, two additional simulations were conducted for the uniform cylindrical shell and the obtained SGI cylindrical shell to compare their sensitivity to initial imperfections. Both shells were subjected to two sets of imperfection considerations: (1) the same total imperfection amplitude but varied imperfection profile, and (2) a fixed imperfection profile but with varied amplitude. Figure 4-7 and Figure 4-8 show the normalized postbuckling response for both cases. The first simulation group (Figure 4-7) featured cylinders subjected to four different imperfection sets where each set was seeded from a total of 10 mode shapes. It is interesting to note (see insets in Figure 4-7) that the buckling mode shapes of the uniform shells were typically axisymmetric while the SGI cylindrical shells exhibited asymmetric mode shapes. The second simulation group (Figure 4-8) considered cylinders subjected to an imperfection amplitude with a mean value of 200% of the shell thickness, and then varied by 100% to estimate the response deviation. In both cases the size of the shaded area indicates the response variation. The results clearly show that the SGI cylindrical shell has a relatively lower sensitivity in the postbuckling regime.

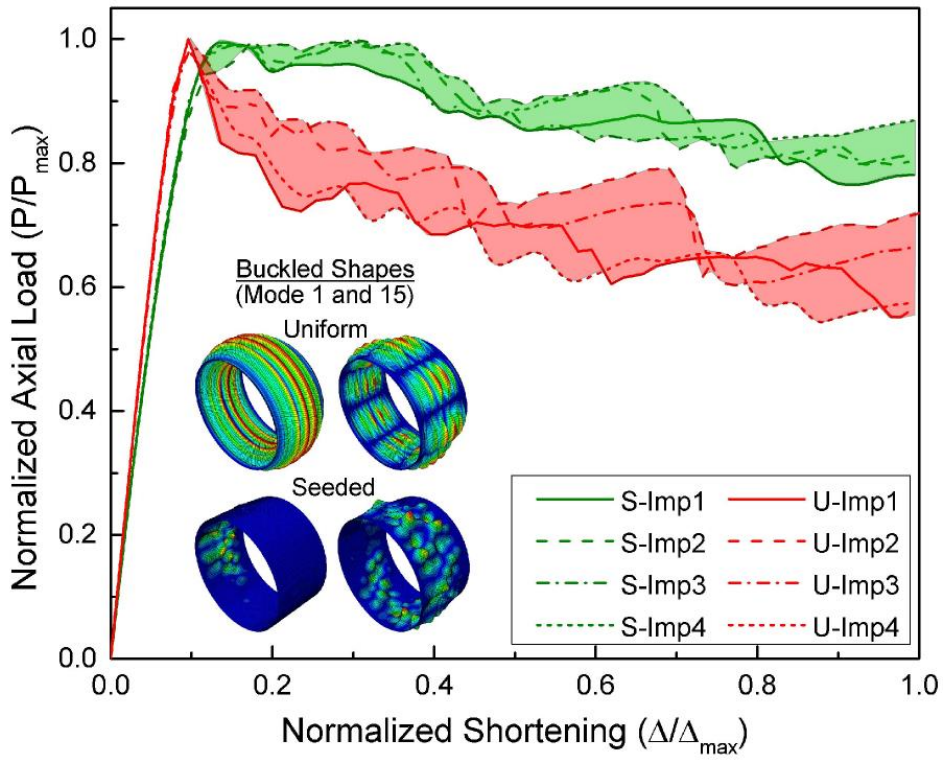

Figure 4-7: Numerical comparison of the sensitivity to initial imperfections between a uniform and a SGI cylindrical shell with same amplitude but varied imperfection profile.

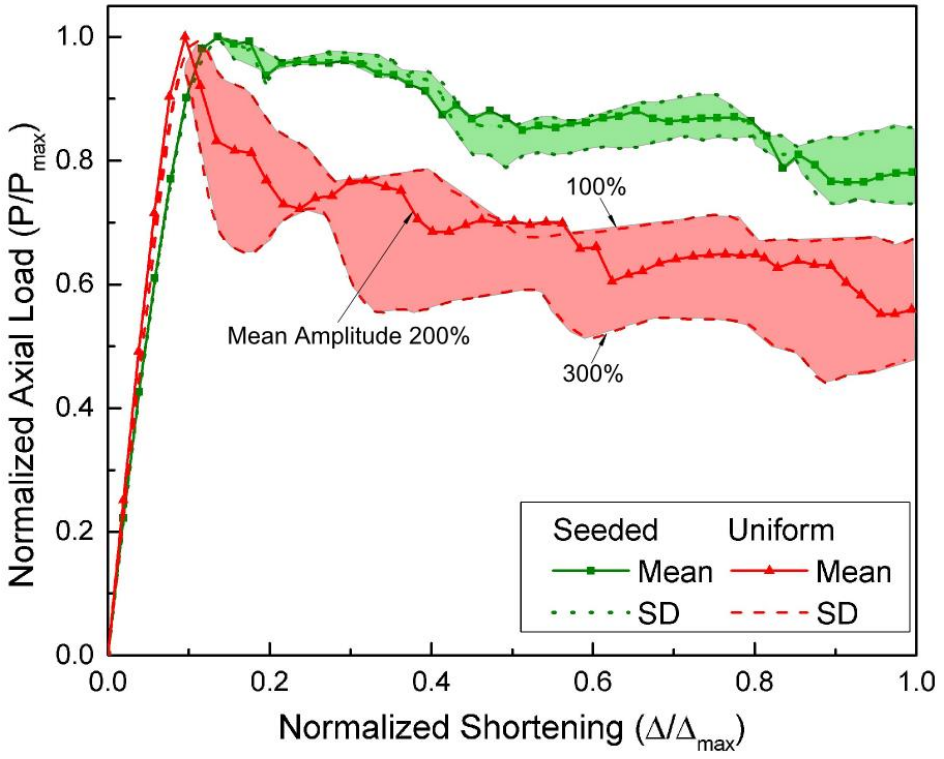

Figure 4-8: Numerical comparison of the sensitivity to initial imperfections between a uniform and a SGI cylindrical shell with same imperfection shape but varied amplitude.

4.4 Experimental results

Eight cylindrical shells, organized in four design groups, were printed and tested. The first group consisted of two uniform cylindrical shells (U1 and U2) to compare the postbuckling response against a baseline. These two cylinders were printed in different 3D printers to evaluate fabrication sensitivity. The second group were two baseline SGI cylindrical shells (M69-1 and M69-2) seeded from a single mode with an amplitude of 200% of the total shell thickness (No. 69, m = 8 and n = 8). The shell thickness was 0.5 mm, which lead to a 1 mm maximum amplitude variation from the mid-plane of the shell. The third group consisted of two SGI cylinders (M192 and M200) seeded from a single mode shape. Cylinder M200 (m = 2, n = 8) was used to compare the baseline design and study the effect of axial wavenumber on the postbuckling behavior, while cylinder M192 (m = 2, n = 5) was studied to understand the effect of the circumferential wavenumber. The final group contained two SGI cylinders (MD64 and MD77) seeded from mode combinations. The purpose of studying these two cylinders was to showcase the variety of opportunities to modify the postbuckling response within a design domain. The three key steps in the fabrication procedure are shown in Figure 4-9.

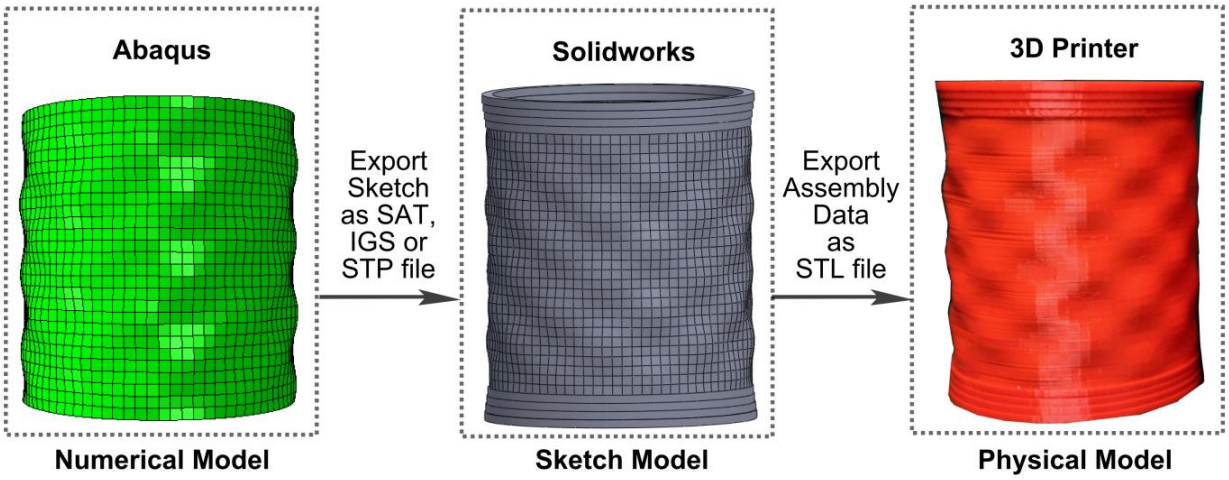

Figure 4-9: Key steps in the fabrication procedure of a SGI cylindrical shell.

4.4.1 Uniform cylinders vs SGI cylinders

The use of the seeded geometry on the shell surface is expected to have certain advantages, compared to a uniform shell surface, in controlling the element's elastic postbuckling response. To test this hypothesis, a uniform cylindrical shell (U1) was printed and subjected to a series of axial compression tests (U1-W1, U1-W2 and U1-W3) under displacement control to a shortening of 1.0 mm. The label "W" in the specimen's identification name is an orientation mark, meaning that the front side of the specimen was facing west. Labels "N" and "E" represent north and east, and indicate that the cylinder's position was rotated 90 ° and 180 ° from the position of U1-W1.

Specimen U1-W was subjected to three loading and unloading cycles and then rotated 90 ° for another two loading cycles. Results from the five tests, where each loading cycle is considered a test, were statistically combined to determine an average response and standard deviations for specimen U1. Table 4-2 gives the postbuckling response for the experimental cases in terms of the key parameters (K_i, P_{max}, ΔP_{max}, δ_{max}, A, and n) shown in Figure 3-12. As expected, there was significant variation between the test results, even though some tests had exactly same test setup and loading sequence. The discrepancy in results follows from the well-known fact that the postbuckling behavior of cylindrical shells is highly sensitive to geometrical imperfections as well as changes to loading and boundary conditions.

The same test protocol was used for specimen series M69-1 with a total of three reloading cycles. Response variation also occurred between the SGI cylinder tests, but the sensitivity was smaller than for the uniform cylinder (details are provided at the end of this section). Figure 4-10 shows the axial load vs. end shortening responses of a uniform cylinder (U1-W1) versus a SGI cylinder (M69-1-W2). It can also be seen that the applied axial deformation and the initial stiffness were recovered upon unloading in both tests. Due to the predefined imperfection, the

initial stiffness of the SGI cylinder was lower compared to the uniform cylinder. A prior numerical study [231] found that initial stiffness has a strong correlation with other key response parameters, including ΔP_{max}, δ_{max}, and A. These observations were confirmed by the test reported here as can be seen in Table 4-2.

Table 4-2: Postbuckling response of uniform and SGI cylindrical shells.

Specimen	K_i (N/mm)	P_{max} (N)	ΔP_{max} (N)	δ_{max} (mm)	A (mJ)	n
U1-W1	1610	620.1	65.6	0.31	89.8	6
U1-W2	1572	681.3	85.2	0.29	109	5
U1-W3	1716	608.9	66.5	0.31	90.3	6
U1-N1	1762	626.1	85.0	0.46	117	4
U1-N2	1740	571.7	97.3	0.49	90.6	4
U1-Mean	**1680**	**621.6**	**79.9**	**0.37**	**99.3**	**5**
U1-S.D.	**84**	**39.5**	**13.6**	**0.09**	**12.8**	**1**
M69-1-W1	697.1	339.1	28.0	0.18	33.2	6
M69-1-W2	650.2	433.2	23.7	0.13	51.9	6
M69-1-E	621.3	404.6	56.13	0.17	40.4	4
M69-1-Mean	**656.2**	**392.3**	**35.9**	**0.16**	**41.8**	**5**
M69-1-S.D.	**38**	**48.2**	**17.6**	**0.03**	**9.4**	**1**

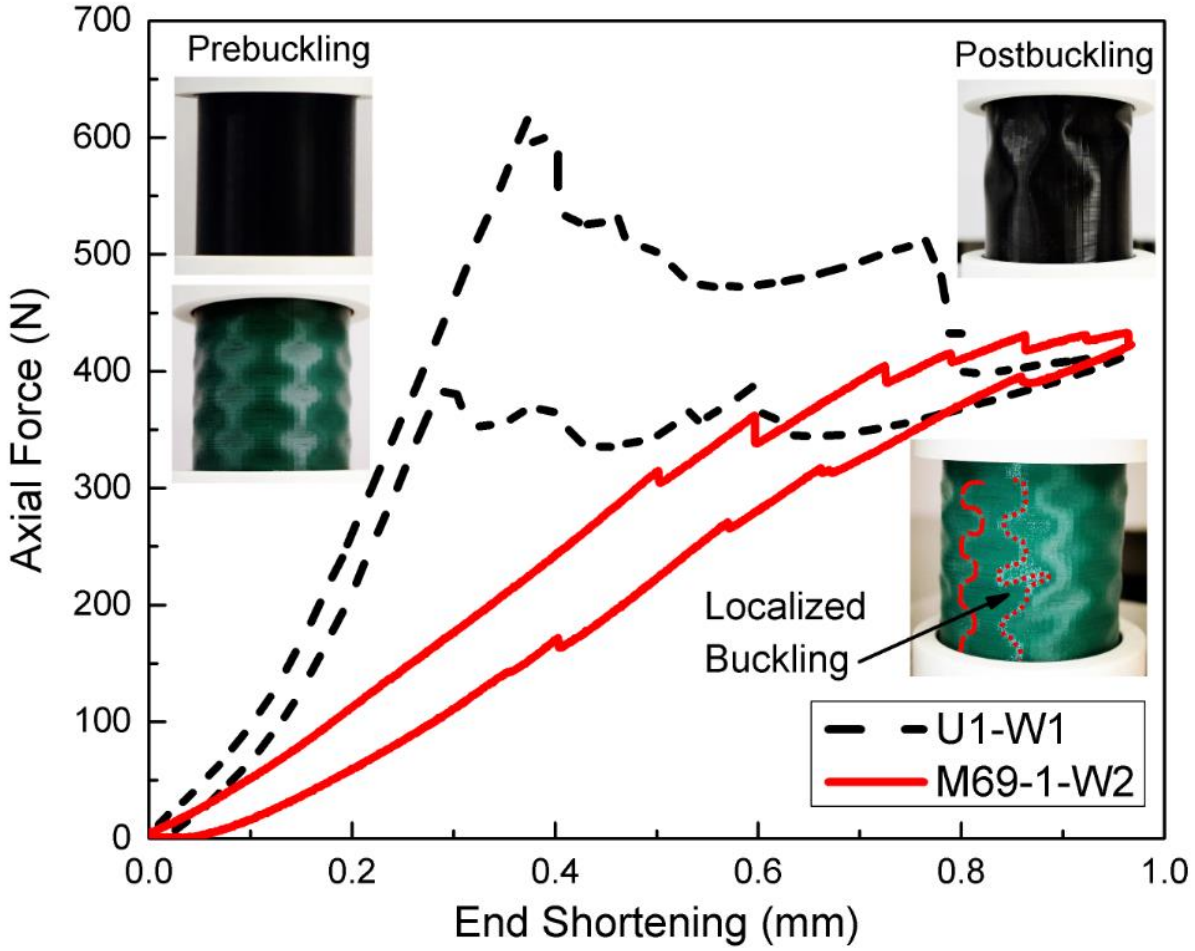

Figure 4-10: Obtained postbuckling responses of a uniform cylinder and a SGI cylinder.

The most interesting finding from the results shown in Figure 4-10 is that the occurrence of the buckling events was quite different for both cases. For the uniform cylinder, stiffness decreased significantly after each critical event, and the end stiffness was nearly zero; while the stiffness of the SGI cylinder varied gradually and a residual stiffness was still observed at the end of the loading process. In other words, the uniform cylinder had a significant total load drop in the response curve and the first buckling load was usually the maximum critical load; while a

post-buckling response with stiffening behavior was observed in the SGI cylinder, with the load capacity tending to a plateau at a level that surpassed the initial buckling load.

Another interesting observation is that the number of mode transitions for both cylinders was similar but the SGI cylinder had equally-spaced localized buckling events. It can also be noted that the magnitude of the load drops due to mode transitions for the SGI cylinder was approximately the same. The seeded geometry plays an important role for such phenomena because the buckling events propagate within small predefined regions. Two curved lines are marked along the axial direction of the SGI cylinder in the postbuckling shape insert of Figure 4-10, where the dotted line indicates a localized buckling event. In contrast, the larger load drop in the uniform cylinder is associated with a bigger snap-through buckling region on the shell surface. In this way, the postbuckling response of the SGI cylinder is more favorable because the occurrence of the mode transitions and their spacing exhibit more controllable features.

The first test series only showed the sensitivity of the postbuckling response within a single cylinder. The purpose of the second test series was to study the effect of the seeded geometry on the postbuckling response of different printed shells. Thus, a second uniform cylinder (U2) and second baseline seeded cylinder (M69-2) were fabricated and tested. Specimen U2 was tested twice with the same orientation and then the cylinder was rotated by 90 ° (U2-N) and later rotated by 180 ° (U2-E). Even though the postbuckling response of the four tests on specimen U2 still had significant variation, the mean response values of specimen U2 were similar to the mean response of specimen U1 (see Table 4-3). The obtained postbuckling responses from the four tests on cylinder U2 had a similar initial stiffness, maximum load drop, number of mode transitions and enclosed area as obtained from the five tests on specimen U1. The only large difference was the maximum spacing between the buckling events. This discrepancy is

reasonable because uniform cylinders by nature have a chaotic behavior in the postbuckling regime. Specimen M69-2 was similarly tested seven times and Table 4-4 compares the mean values for the key response features of cylinders M69-1 and M69-2. It shows that the variation was relatively small compared to the differences between cylinders U1 and U2. In spite of the noted variations, the conducted tests indicate that the elastic postbuckling response of an SGI cylinder is less sensitivity to initial imperfections and load variations than a uniform cylinder.

Table 4-3: Postbuckling response variation between two uniform cylindrical shells.

Specimen	K_i (N/mm)	P_{max} (N)	ΔP_{max} (N)	δ_{max} (mm)	A (mJ)	n
U1-Mean	**1680**	**621.6**	**79.9**	**0.37**	**99.3**	**5**
U2-W1	1819	721.3	92.2	0.12	132	6
U2-N	1903	608.7	95.9	0.11	91.8	6
U2-E	1941	560.7	61.3	0.14	82.2	6
U2-W2	1884	555.4	86.1	0.13	83.1	6
U2-Mean	**1886**	**611.5**	**83.9**	**0.13**	**91.3**	**6**
Difference	11%	2%	5%	65%	8%	17%

Table 4-4: Postbuckling response variation between two SGI cylinders seeded from mode 69.

Specimen	K_i (N/mm)	P_{max} (N)	ΔP_{max} (N)	δ_{max} (mm)	A (mJ)	n
M69-1-Mean	**656.2**	**392.3**	**35.9**	**0.16**	**41.8**	**5**
M69-2-E1	665.7	475.4	56.7	0.09	73.8	4
M69-2-E2	677.8	406.7	46.8	0.16	39.2	5
M69-2-E3	688.1	392.2	43.7	0.18	38.8	5
M69-2-E4	706.4	374.2	49.2	0.17	34.7	5
M69-2-E5	716.5	365.5	62.1	0.18	33.6	5
M69-2-N	702.9	363.1	77.2	0.20	40.5	4
M69-2-W	724.1	340.3	28.7	0.12	32.1	6
M69-2-Mean	**696.4**	**392.4**	**40.9**	**0.15**	**42.0**	**5**
Difference	6%	0%	14%	6%	0%	0%

4.4.2 Seeded design evaluation

From the results presented in Section 4.4.1 it is clear that postbuckling response after the first bifurcation can be modified by introducing seeded geometric imperfections. The following test series was carried out to explore the postbuckling response of SGI cylinders with different seeded shapes under the same imperfection amplitude.

The shell geometry was seeded from a single mode shape other than that used for baseline design M69. Two new SGI cylinders (M192 and M200) were thus fabricated with a low number of axial half-waves (in this case m = 2), as shown in Figure 4-11. Both cylinders had the same imperfection amplitude: 200% of the shell thickness (0.5 mm).

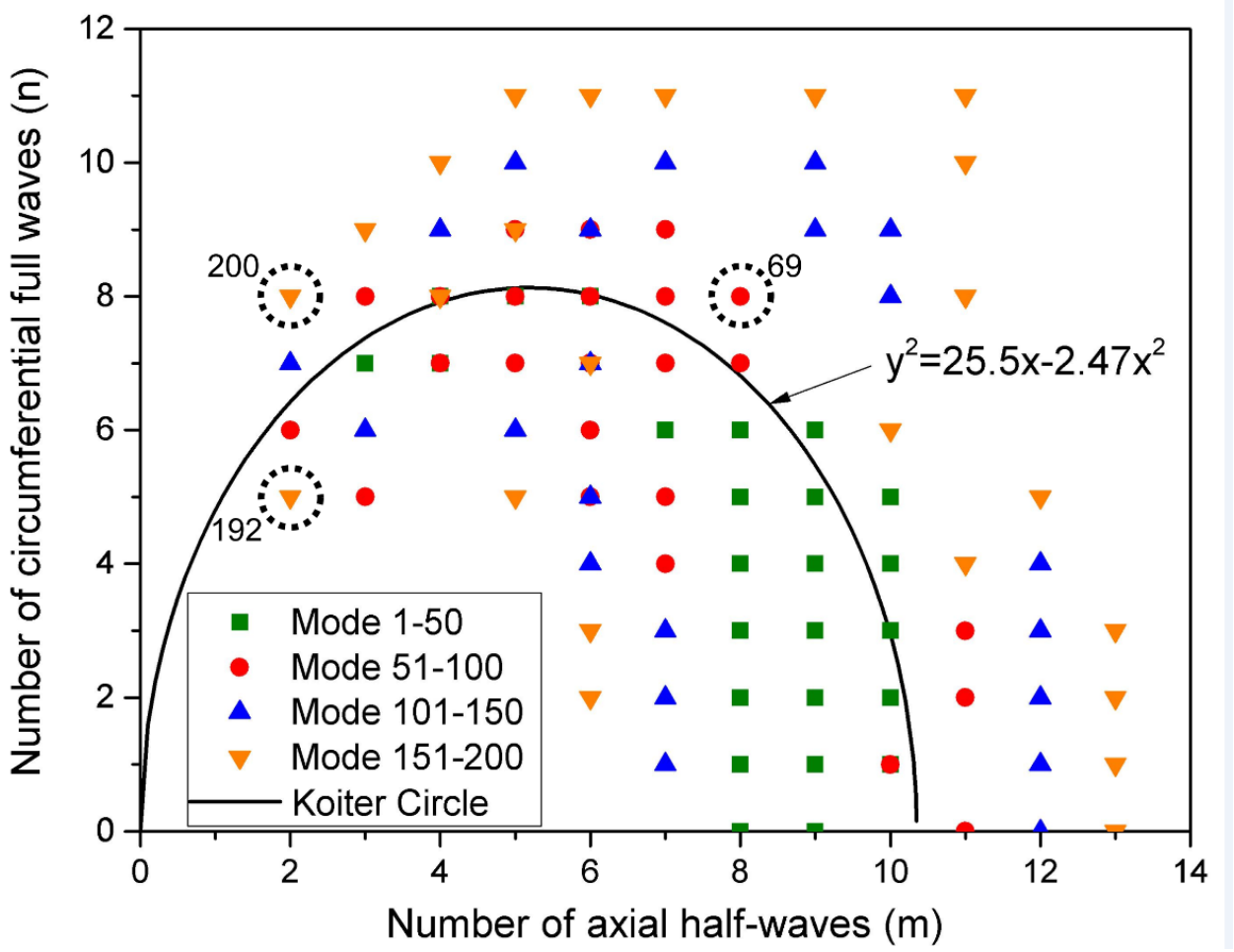

Figure 4-11: Koiter circle for the baseline cylinder and selected mode shapes as seeded geometry.

According to the Koiter circle presented in Figure 4-2, the wavenumber of the baseline SGI cylinder was eight in the circumferential (*n*) and axial (*m*) directions. Prior numerical studies [231] found that a perfect cylinder superposed with a shape of axisymmetric rings (e.g., *m* = 8, *n* = 2) as an imperfection cannot exhibit mode transitions because the large imperfection of this shape usually governs the postbuckling behavior and eventually leads to crushing of the shell under large end shortening. Thus, this kind of mode shape was not evaluated in this study. The resulting force-displacement responses of cylinders M192 and M200 are shown in Figure 4-12.

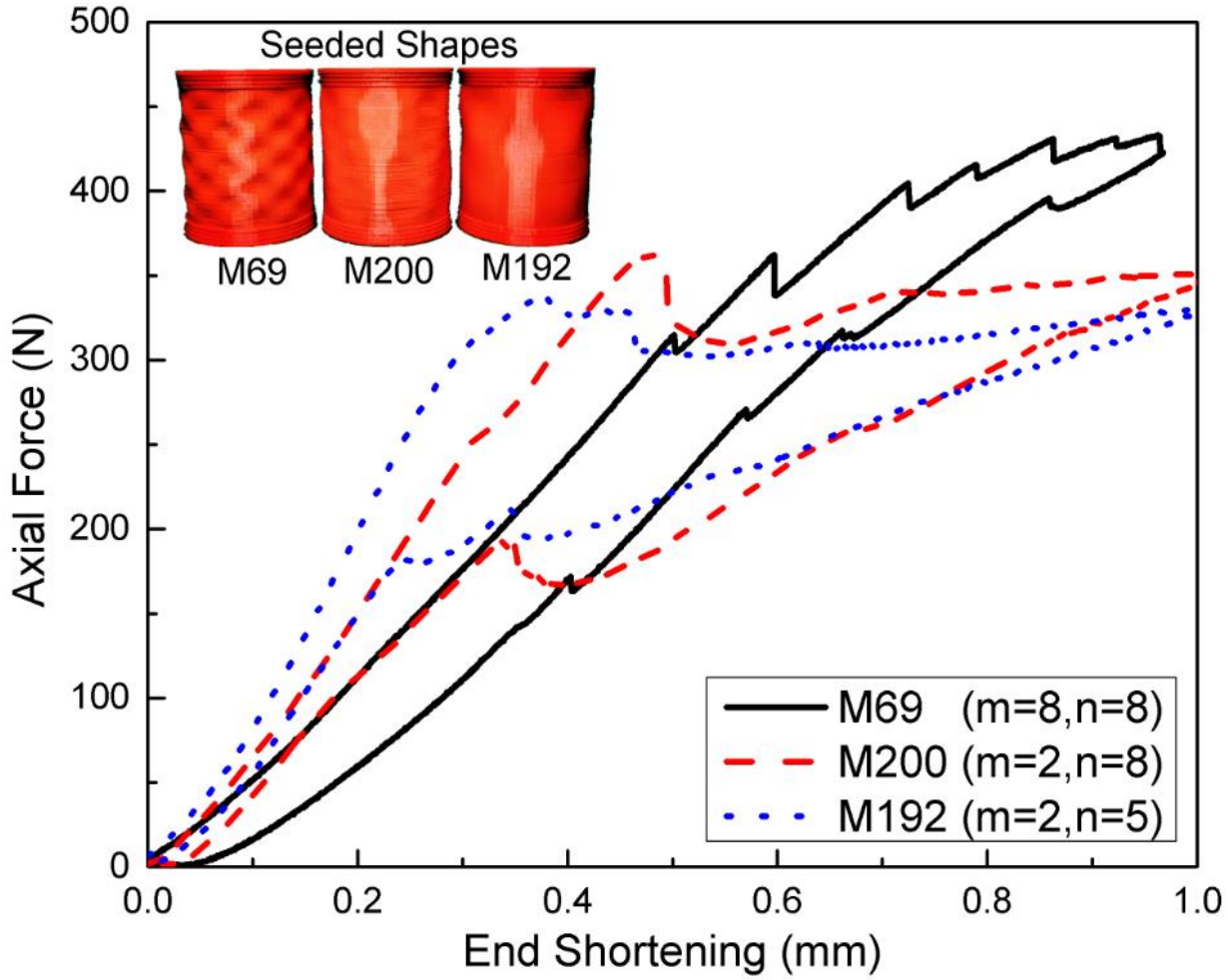

Figure 4-12: Effect of seeded shape on the global postbuckling response of SGI cylinders under axial compression.

It can be seen in Figure 4-12 that the postbuckling responses of both specimens had a smaller number of mode transitions (load drops in the load-displacement response) compared to the baseline cylinder (M69). The buckling pattern for cylinders M192 and M200 started with localized buckling towards the inward region. However, local buckling in these two designs had difficulty propagating along the circumferential direction. Nonetheless, buckling in the SGI cylinders occurred in specific regions rather than at random locations. A summary of results is provided in Table 4-5. From these results it can be seen that, compared to cylinder M69, the

mean responses of M192 and M200 had a higher initial stiffness and a larger enclosed area, but the number of the mode transitions significantly dropped. Thus, the reduction in axial wavenumber (m) increased the structural axial stiffness, the initial loading stiffness (K_i) and the dissipated energy (A). This experimental study indicated that a SGI cylinder can allow for localized snap-buckling events to be triggered in certain regions of the shell due to the patterned seeding geometry.

Table 4-5: Postbuckling response of SGI cylinders seeded with different mode shapes.

Specimen	K_i (N/mm)	P_{max} (N)	ΔP_{max} (N)	δ_{max} (mm)	A (kJ)	n
M69-Mean	**676.3**	**392.4**	**41.9**	**0.16**	**41.9**	**5**
M200-W	870.8	426.7	9.94	0.31	103	2
M200-N	833.3	363.7	38.5	0.33	65.2	2
M200-Mean	**852.1**	**395.2**	**24.2**	**0.32**	**84.1**	**2**
M192-W	1201	415.6	19.5	-	66.4	1
M192-N	1315	380.6	20.7	-	59.3	1
M192-E	1093	336.5	21.5	0.18	56.1	2
M192-Mean	**1203**	**377.6**	**20.6**	**0.18**	**60.6**	**1**

4.4.3 Design domain exploration

This section explores the shape seeded from multiple mode combinations. The buckling shapes introduced in Figure 4-2 were revisited to generate design variable sets as shown in Figure 4-13. Rather than selecting a single mode shape, the design variables are 10 modes to be linearly superposed with equal (empirical) imperfection amplitude. The ten modes were chosen from ten

variable sets with three modes in each one. Each mode set had the same circumferential wavenumber but different axial wavenumber. The design variable sets were discretized based on the circumferential wavenumber (from n = 1 to n = 10). For example, design variable set one included mode 163 (m = 4, n = 10), mode 124 (m = 7, n = 10) and mode 196 (m = 11, n = 10). As a result, a total of 30 modes were used to generate design variables.

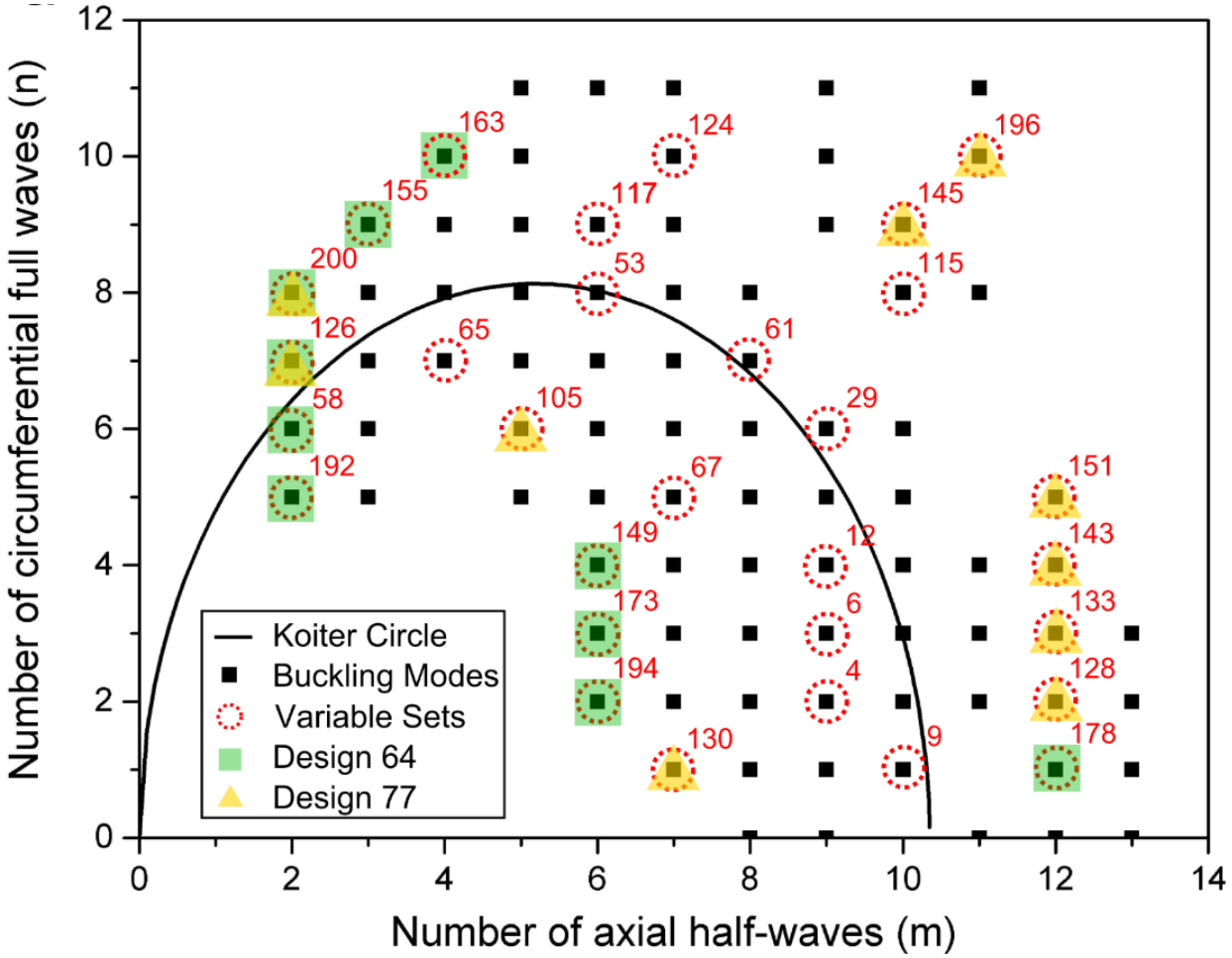

Figure 4-13: Design domain and variables of seeded shape based on mode combinations.

Two cylinders with mode combination (MD64 and MD77) were evaluated. Cylinder MD64 was contributed from the majority of mode shapes with low axial wavenumber (see the square shaded regions in Figure 4-13) while cylinder MD77 included most of mode shapes with a high axial wavenumber (see the triangle shaded regions in Figure 4-13). Both cylinders were

fabricated and tested for multiple loading cycles. The postbuckling responses of one test from each of the multi-mode cases are plotted in Figure 4-14.

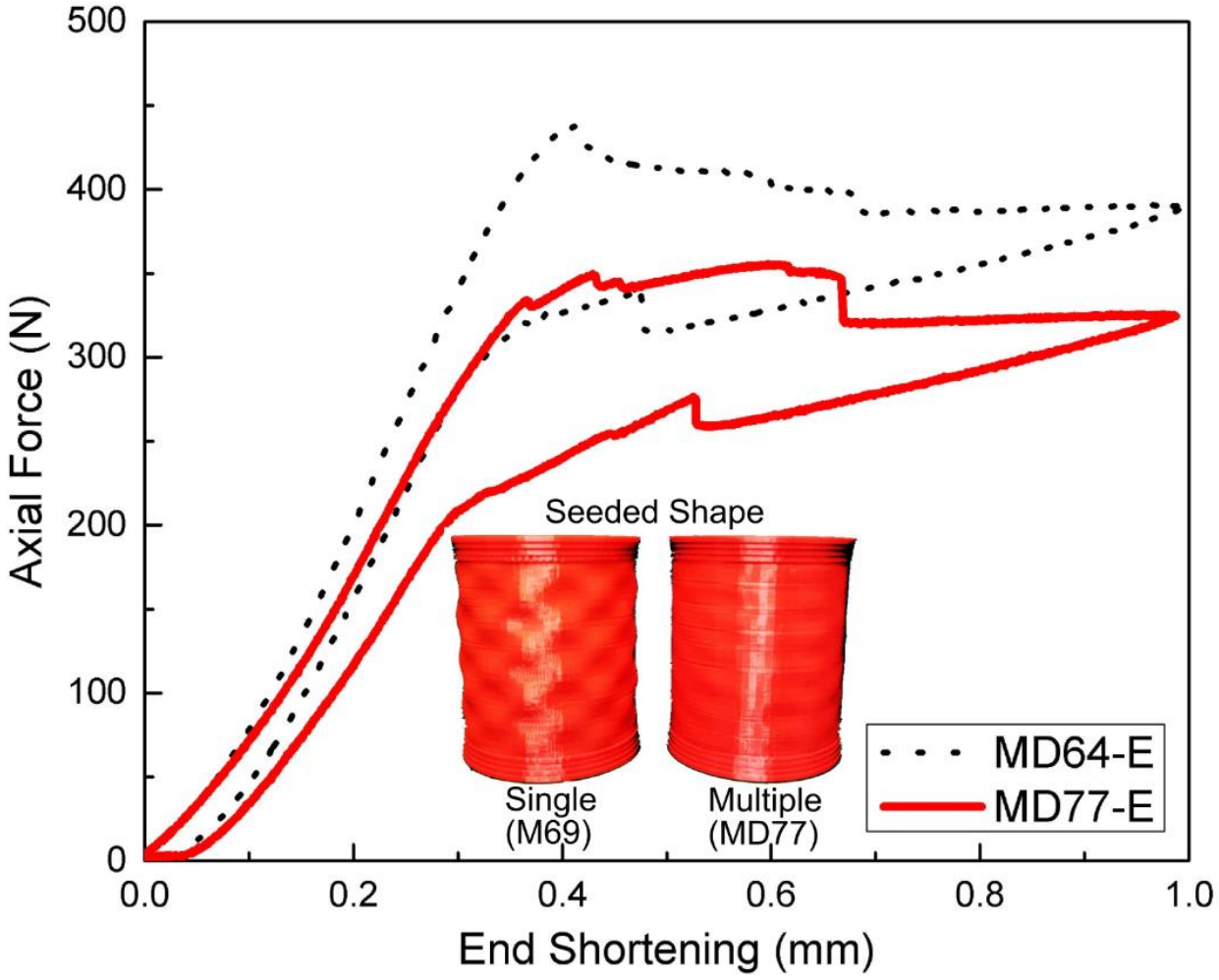

Figure 4-14: Obtained postbuckling responses of two SGI cylinders seeded from multiple modes.

Compared to the baseline case M69, seeded from a single mode shape, the cylinder seeded from multiple modes does not have a significant wave pattern (see the image insets in Figure 4-14). Table 4-6 summarizes the average characteristic features of the postbuckling response. The results are consistent with the evaluation of the single mode shape SGI cylinders in Section 4.4.2 (see Table 4-6) and again indicate that a reduction in the axial wavenumber (m) for SGI cylinders will reduce the number of mode transitions but increase the enclosed area in the

response curve. On the other hand, the superposition of mode shapes with high axial half-wave number for the seeded geometry will create a checkerboard-like imperfection that can trigger localized buckling events while also having high energy dissipation.

Table 4-6: Postbuckling response of SGI cylinders seeded with multiple mode combinations.

Specimen	K_i (N/mm)	P_{max} (N)	ΔP_{max} (N)	δ_{max} (mm)	A (kJ)	n
MD64-W1	1204	500.7	10.8	0.18	102	4
MD64-W2	1167	417.2	8.43	0.31	71.1	3
MD64-W3	1314	464.2	11.4	0.27	58.9	3
MD64-W4	1312	437.7	11.9	0.19	50.1	3
MD64-N	1341	398.3	11.9	0.28	50.9	3
MD64-E	1332	405.2	11.3	0.31	52.2	3
MD64-Mean	**1245**	**437.2**	**11.0**	**0.26**	**64.2**	**3**
MD77-W1	1030	451.1	20.7	0.09	80.8	6
MD77-W2	1212	401.3	23.5	0.09	61.9	5
MD77-W3	1135	358.2	26.7	0.12	53.4	5
MD77-N	1007	326.5	25.6	0.16	52.1	5
MD77-E	1115	355.5	26.3	0.16	53.7	5
MD77-Mean	**1100**	**378.5**	**24.6**	**0.12**	**60.4**	**5**

The most important lesson learned from the study presented in this section is that a seeded geometry from a preselected set of 30 mode shapes limited the postbuckling response within a certain range (i.e., an upper and lower bound). The reason is that each mode was given with the same value of 0.1 mm as an imperfection amplitude (20% of the shell thickness). Additional simulations were conducted using the same modeling approach on cylinders with the same pre-selected 10 mode shapes for imperfection seeding but with different scaling factors (from 0% to 50% the shell thickness for each mode). The resulting simulated postbuckling responses showed the majority of the designs having either two or three mode transitions. Overall, it is clear that a targeted postbuckling behavior can be achieved if a seeded shape is properly selected, offering a variety of opportunities within the design domain.

4.4.4 Effect of seeding amplitude

Additional tests on an SGI cylinder (m = 8 and n = 8) were conducted using the same seeding geometry but with three different amplitude factors (A20 = 0.1 mm; A200 = 1 mm; and A500 = 2.5 mm). The resulting postbuckling responses are shown in in Figure 4-15, from which it can be seen that variation of the seeding amplitude for a fixed seeding geometry can also generate diversity in the postbuckling response within a certain range (i.e., an upper and lower bound). In terms of mode transitions, the cylinder with smaller seeding amplitude (M8N8-A20) had a much larger number of localized buckling events (nine) compared to the other two cylinders. It can also be seen that seeding amplitude has a knockdown effect on the initial stiffness, the magnitude of the load drops and the area of the hysteretic loop. Overall, a targeted postbuckling behavior can be achieved if a seeded initial shape is properly selected.

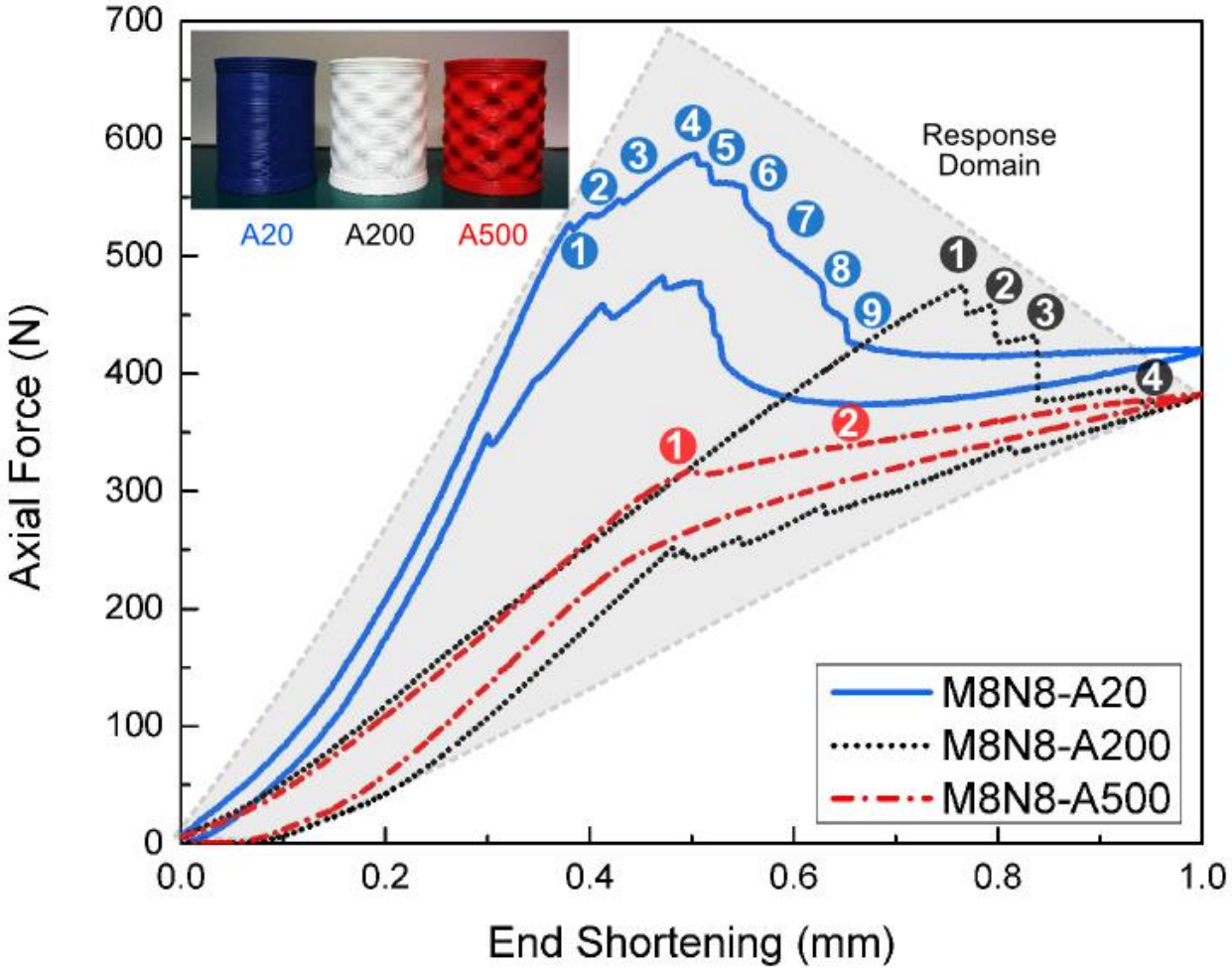

Figure 4-15: Effect of varied seeding amplitude for cylinder with same seeded geometry.

4.4.5 Effect of loading variation

The studies reported in Sections 4.4.1 to 4.4.3 were aimed at evaluating the hypothesis that a cylindrical shell with a seeded geometry on its surface can reduce the sensitivity of the postbuckling behavior to initial imperfections. The presented experimental results have shown that SGI shells can display an elastic postbuckling response with less sensitivity compared to a uniform cylinder. However, the issue of loading position emerged for both uniform and SGI shells, as can be seen from the test data in Table 4-3 to Table 4-6. Considering that a change in loading position essentially amounts to a change on the loading distribution to the shell edge due to slight differences in the test setup, the effect of loading variation on uniform and SGI cylindrical shells was thus be evaluated and is discussed herein.

The loading and unloading response of the MD64 cylindrical shell rotated by 90 °and 180 °are compared in Figure 4-16. Even though all three test cases had a different postbuckling response, several similarities can be observed. The first similarity is related to stiffness. It can be observed that the initial stiffness of all three tests was essentially equal and that the end stiffness was nearly zero. The second similarity is related to the mode transitions. Even though the first buckling event for all tests had large variation in load and deformation values and that the number of mode transitions was three for all tests. Finally, the maximum single load drop and enclosed area in the response curve was also similar. Further, the variations from changes in the boundary conditions are reduced if the specimen was loaded in the same position. Three postbuckling responses of the baseline M69 cylinder under same loading position are given in Figure 4-17. It was interesting to find that the load-deformation curves had little variation.

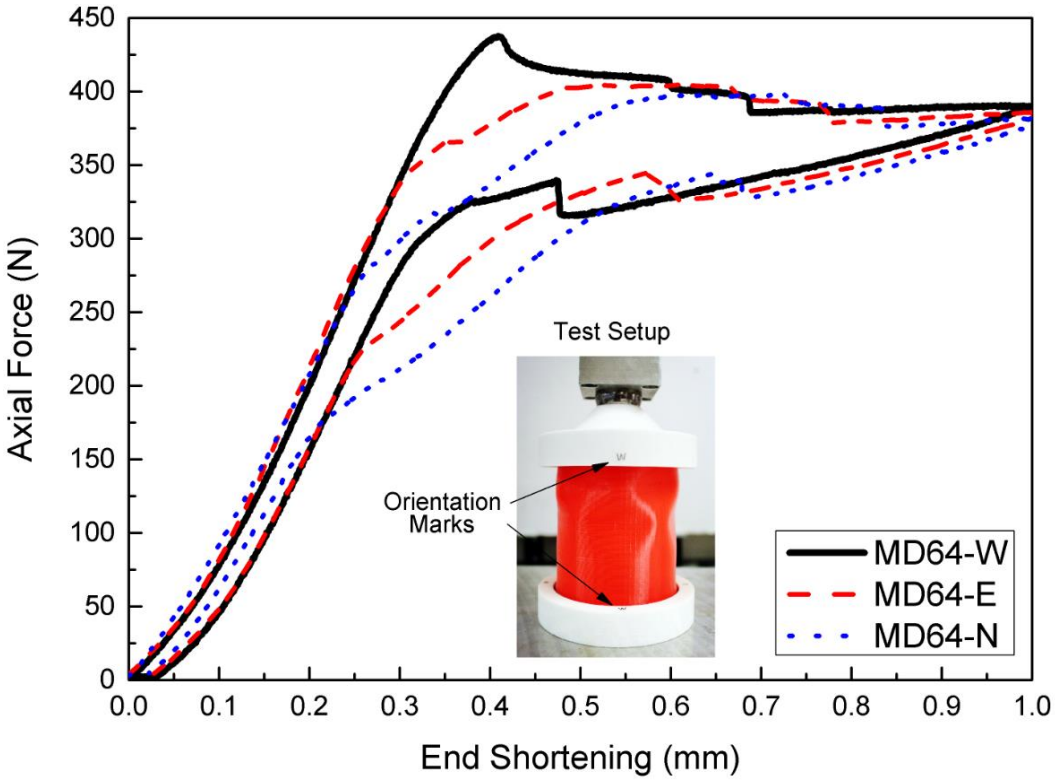

Figure 4-16: Sensitivity to loading variation of SGI cylinders under varied loading position.

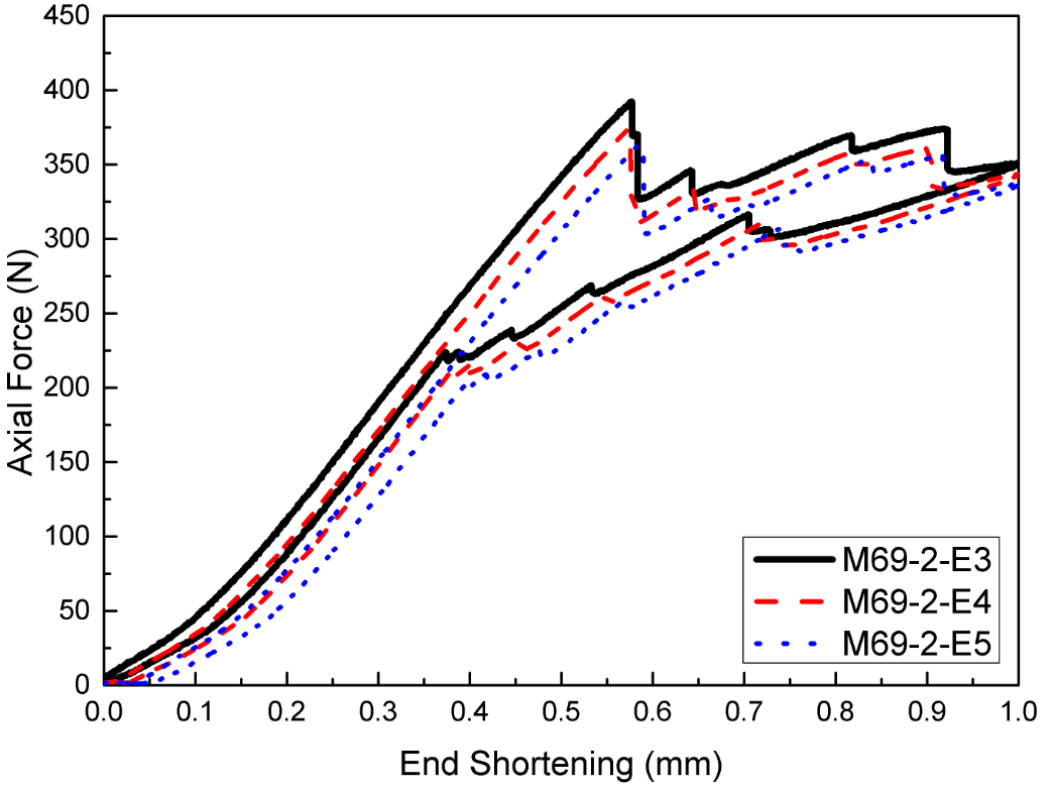

Figure 4-17: Sensitivity to loading variation of SGI cylinders under same loading position.

The normalized postbuckling responses of a uniform cylinder (U2) and a SGI cylinder (MD64) in their original loading orientation (W) and then rotated by 90 ° (N) and 180 ° (E) are compared in Figure 4-18. Only the loading branch of the response curve is shown because the variations within the unloading branch are small. It can be seen that for both cylinder types the loading variations lead to a different postbuckling response. Yet, two major similarities can be observed. The first similarity is that the initial stiffness for the three tests of each case was essentially equal and that the end stiffness was nearly zero. The second similarity is that the number of mode transitions was the same (for a given cylinder type) even though there was large variation on the first buckling event. The shaded areas in Figure 4-18 indicate the response variation and it can be seen that the size of the shade area for the SGI cylinder is smaller than the one for the uniform cylinder. Another indication of the reduced sensitivity of the SGI cylinder to load variations is that the maximum single load drop in the response curve was similar for the three loading cases, while the uniform cylinder had significant variation in this parameter.

The effect of loading variation within the same loading position was evaluated for both uniform and SGI cylinder by considering the repetition of tests, where load variation is introduced by settlement of the test setup, i.e., relative motion between the load fixtures and the test specimen after a test. The normalized postbuckling responses of a uniform cylinder (U1) and a SGI cylinder (M69-2) are compared in Figure 4-19. It can be seen that the response curves for the repeated tests were similar for each cylinder type, but the SGI cylinder had a relatively lower sensitivity compared to the uniform one (see size of shaded area). It is clear that the response variation for this kind of load variation was much smaller than when the specimens were rotated Figure 4-18). Nonetheless, in general, SGI cylinders display a postbuckling response with less sensitivity to loading variation.

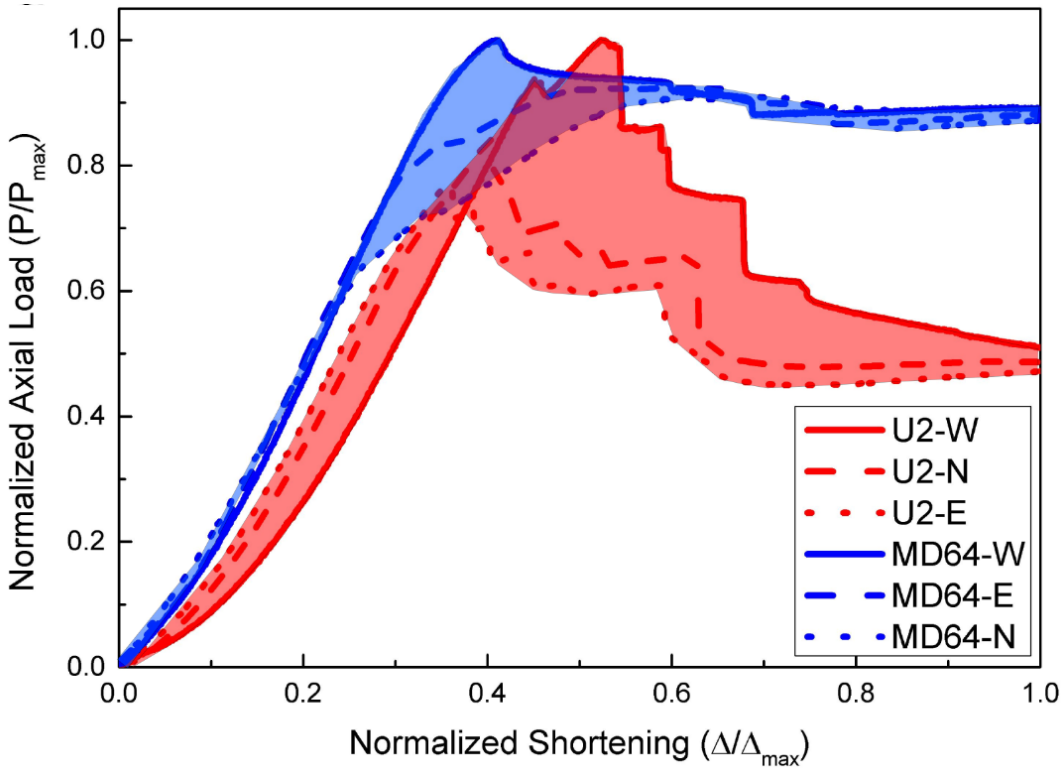

Figure 4-18: Normalized response of uniform and SGI cylinders under varied loading position.

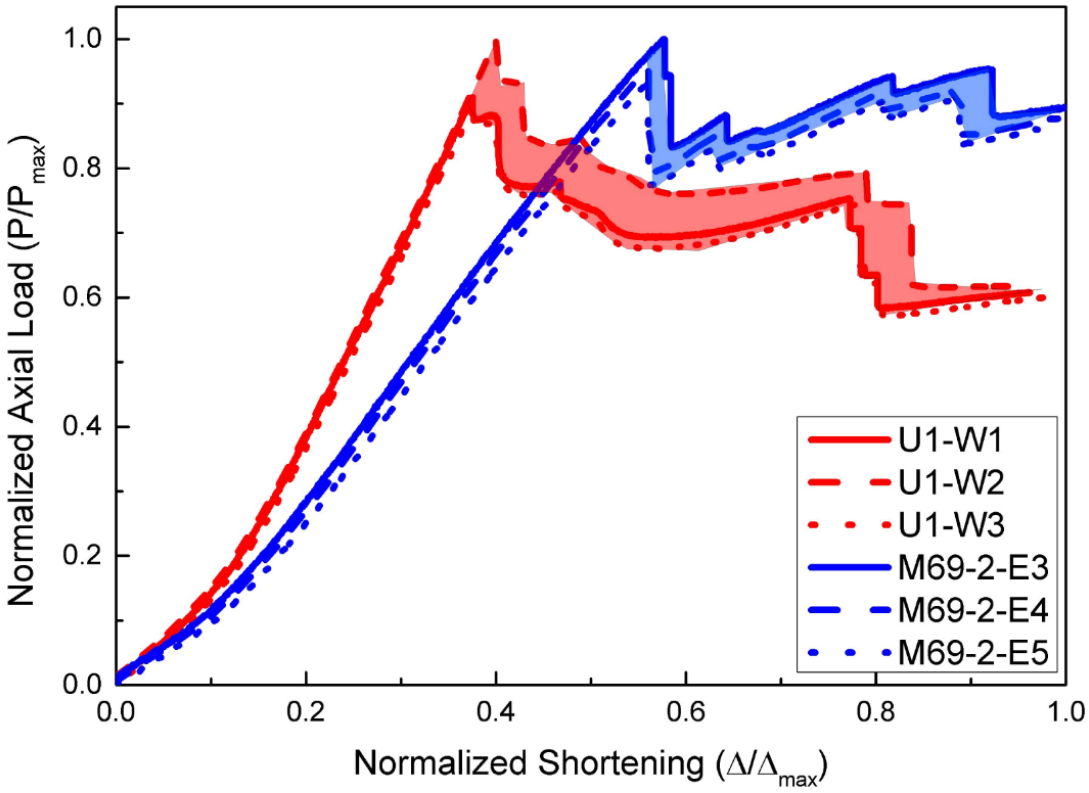

Figure 4-19: Normalized response of uniform and SGI cylinders under same loading position.

4.5 Summary

The experimental and numerical studies presented in this chapter evaluated the hypothesis that seeded geometric imperfect (SGI) designs are a viable approach for modifying and controlling the postbuckling response of cylindrical shells under axial compression. The following conclusions were drawn:

(1) The concept of SGI cylindrical shells was proposed by adding a predefined geometric imperfection to the shell's surface in order to introduce a governing role over other initial imperfections on postbuckling behavior. Eigen-shapes provide diverse design opportunities and careful selection among them can tailor the elastic postbuckling response to desirable features.

(2) Two seeding approaches for SGI designs (single-mode and multi-mode combination) were evaluated. Single-mode designs showed that a reduction in the axial wavenumber (m) increases the structural axial stiffness and leads to an increase of the initial loading stiffness and the dissipated energy, but it reduces the number of snap-through buckling events. Multi-mode designs demonstrated the possibility of using a wide design space to satisfy a targeted postbuckling response.

(3) Numerical simulations and experimental studies on 3D printed cylinders validated the hypothesis that SGI designs provide advantages for controlling the elastic postbuckling response of axially compressed cylindrical shells. The results demonstrated that the elastic postbuckling response of SGI shells was less sensitive to initial (manufacturing) imperfections as well as loading variations compared to that of uniform cylinders.

(4) Experimental observations indicated that SGI cylinder designs display a postbuckling response that is more predictable and reliable than that of uniform cylinders by allowing tailoring of the time and location of buckling events. Namely, SGI designs featured localized buckling in

specific regions of the shell surface rather than at random locations, and in some cases SGI cylinders featured equally-spaced mode transition events rather than the chaotic sequence typical of uniform designs. Thus, SGI designs allow predefining the number and location of localized buckling of cylindrical shells under axial compression even though the exact occurrence of the buckling events was not achieved.

Chapter 5

Non-Uniformed Stiffness Distribution (NSD)

5.1 Overview

This chapter introduces the concept of using non-uniform stiffness distributions (NSD) on the surface of cylindrical shells to control their elastic postbuckling response. Given that imperfections cannot be avoided, at least with current manufacturing technologies, the design of cylindrical shells for smart purposes requires a relatively less imperfection sensitive structure. The NSD concept, which uses patterned thickening patches (PTP), was evaluated with the aim of turning cylindrical shells into a desirable structural prototype for smart applications. Acting as artificial imperfections, the introduced PTP allow changing the postbuckling response of cylindrical shells from high imperfection sensitive to less sensitive. A numerical approach was used to evaluate the sensitivity of NSD cylinders and prototyped NSD cylindrical shells were fabricated through 3D printing to understand rules for PTP designs and then tested under loading-unloading cycles. The study presented in this chapter was submitted to the journal *Thin-walled Structures* for the consideration as a technical publication.

5.2 Design concept

5.2.1 Background

Similar to the effect of geometry on the postbuckling response of cylindrical shells, the equilibrium paths depend on the distribution of stiffness on the shell surface. On the assumption of axisymmetric buckling modes, the classical critical stress can be expressed by Equation 5-1.

$$\sigma_{cl} = \frac{Et}{r\sqrt{3(1-\nu^2)}} \qquad \text{Equation 5-1}$$

The buckling and postbuckling behavior of cylindrical shells with constant thickness and uniform stiffness distribution has been extensively studied for almost a century. Comparatively, the concept of variable stiffness (geometry/material) in the design of the thin-walled structures has caught less attention. Three major response features have motivated the study of non-uniform stiffness distributions on the surface of shells: elastic or critical buckling, plastic buckling and adaptive response. A brief overview of the research progress in these fronts follows.

Most early research related to the use of variable stiffness distributions in cylindrical shells has focused on increasing their load-carrying capacity through axial stiffeners [232]. Later, a series of studies were done to evaluate the critical load of cylinders with small thickness variations, including axisymmetric [207], periodic [208, 233] and arbitrary modifications [210]. Analytical studies have also been carried out on cylindrical shells with anisotropic laminated composites [53, 234] and functionally graded thru-thickness properties [214, 235].

Since the 1980s the concept of variable stiffness on cylindrical shells has primarily focused on the use of composite materials, which can offer increased strength-to-mass ratio by tailoring fiber

orientation and stacking sequence [236, 237]. Recent efforts [238-242] are motivated by the interest of maximizing localized strength and stiffness so as to maximize the performance of composites for a specific structural application, particularly for the design of aerospace structures. Such work has led to novel concepts for using varying fiber orientations to control stiffness properties, which has become feasible with the capability of advanced manufacturing technologies.

In addition to the mainstream research efforts on improving the critical buckling load, two important branches for using patterned stiffness on the shell surface are folding mechanisms and energy absorption. A folding/deploying mechanism is one of the essential features for the design of space structures. Many folding mechanisms have been inspired by origami concepts and have been explored on cylindrical shells [162, 243-245]. A recent review [5] highlights the increasing interests of using variable stiffness material and structural concepts for morphing applications. The use of patterned stiffness on cylindrical shells has also been investigated to optimize energy absorption performance and control crushing behavior in the design of structural components for energy absorption purposes [246-248].

Another promising research avenue for composite materials with variable stiffness is on the topic of bistability and multistability. A plate/shell made from fiber-reinforced composites can be designed to exhibit two or more stable configurations [58]. Tailoring laminated composites to achieve tristability has been investigated for multiple shell forms, such as corrugated shells [59], orthotropic shells [60], double curved shells [61], etc. A new kind of variable stiffness concept for a composite tube was also studied recently with shape memory polymers, which was explored for the design and manufacturing of morphing skins in aircraft designs [249].

5.2.2 NSD design

As mentioned in Chapter 3, the research reported in this dissertation focuses on elastic buckling. Thus, the cylindrical shells studied here are projected for use in smart devices rather than as load-carrying or energy-absorbing components. The core idea (shown in Figure 5-1) is that the postbuckling response of cylindrical shells under axial compression can be tailored through the design and optimization of varied stiffness distributions on their surface, in this case, by using patterned thickening patches (PTP).

By providing variations in thickness and controlling their spatial distribution, the postbuckling behavior of an NSD cylindrical shell is expected to obtain multiple mode transitions in a controllable manner, namely a predefined sequence and location of localized buckling events. In this way, an NSD cylinder is expected to have lower sensitivity to random geometric imperfections compared to a uniform cylindrical shell. Further, novel postbuckling shapes for cylindrical shells can be created by tailoring the distribution of the thickening patches.

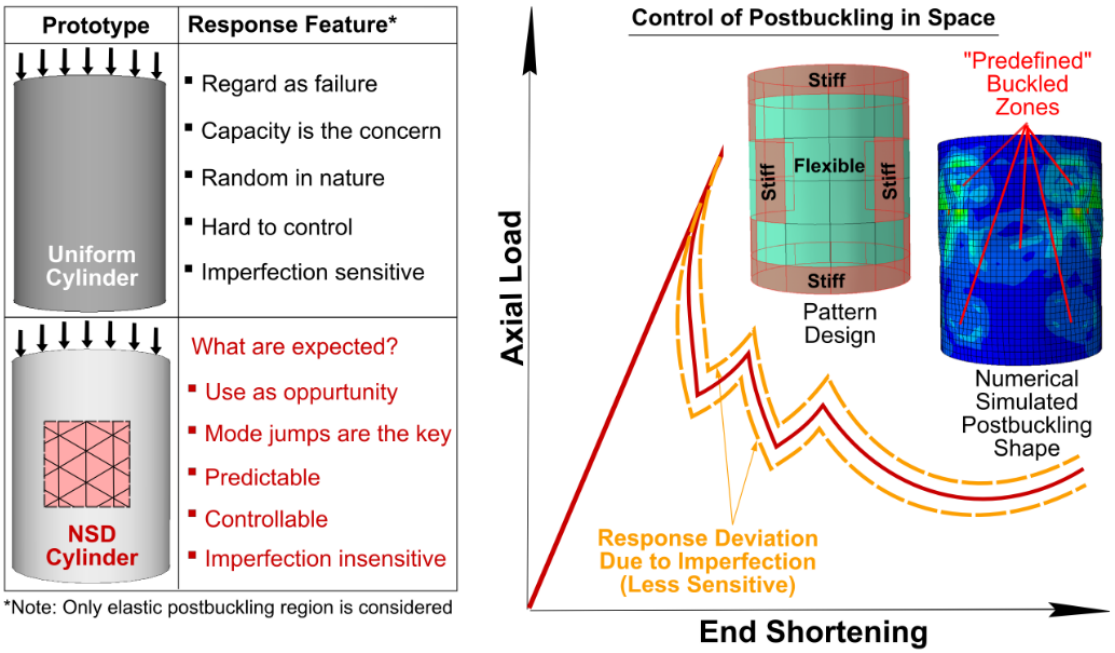

Figure 5-1: The concept figure of advantages by using NSD cylinder over uniform cylinder.

5.2.3 Pilot experiment

In this section, experimental and numerical studies aimed at evaluating the effects of locally varying material stiffness on the postbuckling response of hybrid carbon/E-glass/epoxy cylindrical shells are presented. The goal was to promote localized buckling in certain regions of the shell surface through deliberate changes in the material properties and their distribution on the cylinder such that the dominant postbuckling shape can be triggered. Three hybrid carbon/E-glass/epoxy cylinders (see Figure 5-2) with patterned material stiffness were experimentally evaluated under uniform axial compression. Details on the design and manufacturing of these test units was given in Section 3.5.1.

Figure 5-2: Hybrid cylinders with patterned material distributions.

The resulting force-displacement responses are shown in Figure 5-3. It can be seen that the postbuckling responses of the hybrid cylinders had a number of mode transitions (load drops in the load-displacement response). The [0/G/90] cylinder was subjected to an axial shortening of

0.7 mm. The buckling pattern for this cylinder started on the carbon strips and then triggered a significant snap-through buckling event in the neighboring E-glass zones. Seeking to increase the number of mode transitions in the postbuckling regime the [45/G/-45] cylinder was subjected to a shortening of 0.95 mm. However, no significant increase in the number of snap-buckling events were observed (two major snap-buckling events) as local buckling occurred in the E-glass zones and the buckling waves in this design had difficulty propagating along the circumferential direction. The [30/G/-30] cylinder was shortened 50% more compared to the [0/G/90] cylinder (1.4 mm). This design was found to have a more desirable behavior in the postbuckling regime than the other two cases by presenting a large number of distinct snap-buckling events.

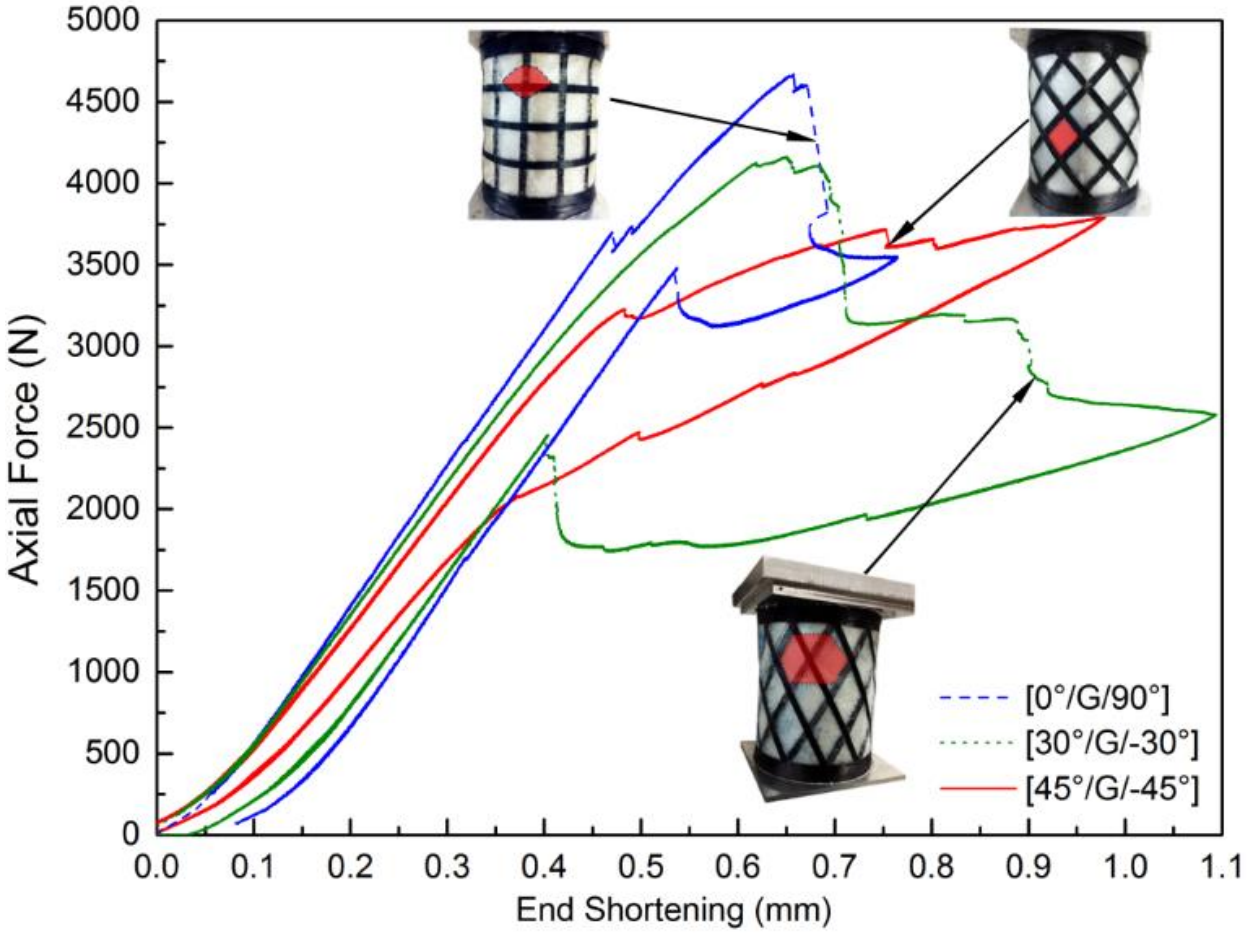

Figure 5-3: Effect of patterned material distributions on the global and local postbuckling response of hybrid cylinders under axial compression.

Table 5-1: Postbuckling response of hybrid cylinders with patterned material distributions.

Laminate Sequence	K_i (N/mm)	P_{max} (N)	ΔP_{max} (N)	δ_{max} (mm)	A (kJ)	n
[45°G/-45°]	6715	3795	108	0.19	438	3
[0°G/90°]	8750	4671	1002	0.27	501	4
[30°G/-30°]	7340	4163	904	0.16	1035	7

A summary of results is provided in Table 5-1. This experimental study indicates that the hybrid design concepts can allow for localized snap-buckling events to be triggered in certain regions of the shell due to the use of carbon/epoxy strips as artificial imperfections. Even though the cylinders were still sensitive to imperfections (mainly due to manufacturing flaws) it was interesting to see that buckling occurred in specific regions rather than at random locations on the shell surface.

5.3 Numerical analysis

5.3.1 Approach evaluation

From the results presented in Section 5.2 it is clear that postbuckling response after the first bifurcation can be modified by locally varying material stiffness. However, it was also observed that the effect of initial geometric imperfections is so large that the explored stiffness patterns could not achieve the targeted postbuckling behavior. Another issue for such artificial imperfection (i.e., strips and hoops) is that the patterns for the three experimentally evaluated hybrid cylinders have axisymmetric theoretical eigen-shapes, which may not trigger the desired

multiple mode-jumping phenomena. Thus, a numerical study was carried out to explore the postbuckling response of hybrid cylinders with non-uniform material/stiffness distributions

As described in Section 3.3, the second-order nonlinear analysis on the imperfect shell was conducted using a dynamic solver. A large damping factor (i.e., linear bulk viscosity parameter) was used to reduce the high oscillations created during the snap-buckling events. Eight non-uniform pattern (NP) designs with similar geometric features to the hybrid cylinders presented in Section 5.2.3 (L = D = 200 mm and t = 0.6 mm) were modeled with discrete patches of two different material as shown in Figure 5-4.

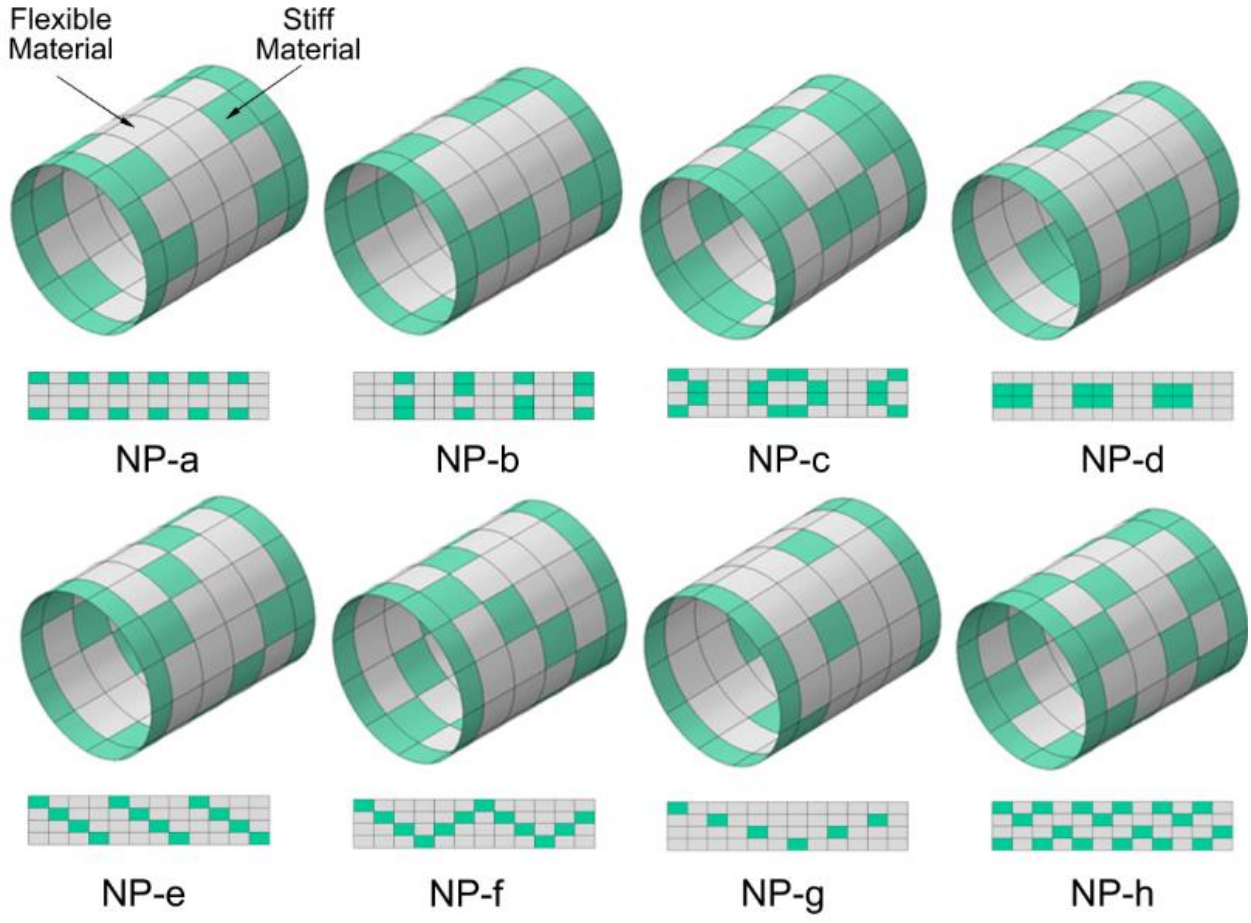

Figure 5-4: Non-uniform material pattern designs for cylinders.

The purpose of the NP designs was to evaluate simple cases with patterned material stiffness layouts and recognize if mode transitions can be triggered in targeted regions. Stiff material patches (cyan/dark zones) were assumed to be isotropic with E = 50 GPa and ν = 0.25, and the flexible patches (grey/light zones) were assumed to have isotropic properties with E =10 GPa and ν = 0.25. The designs were determined empirically based on the lessons learned from the previous cases. Designs cases (a) through (d) were aimed to identify the postbuckling response of cylinders with flexible material layouts predominantly along the axial and circumferential directions, while design cases (e) through (h) explored the behavior of cylinders with an inclined distribution of the stiff material.

Table 5-2: Estimated postbuckling response of hybrid cylinders with non-uniform patterned material distributions.

Case	Connection of flexible patches	K_i (N/mm)	P_{max} (N)	ΔP_{max} (N)	δ_{max} (mm)	A (kJ)	n
a	Y	20336	5198	595	0.51	330	2
b	Y	24804	6033	382	0.23	305	5
c	N	24838	7508	875	0.31	627	9
d	Y	22788	7059	383	0.21	229	5
e	N	22341	6118	686	0.22	384	5
f	N	20518	5974	279	0.15	137	5
g	Y	19133	5764	568	0.19	300	6
h	Y	25659	6755	581	0.21	613	7

Numerical simulations were carried out with the initial imperfection amplitude as 150% of the shell thickness. Table 5-2 summarizes characteristic features of the postbuckling response for all eight cases when axially shortened to 1.0 mm. The initial stiffness for all cases was similar, yet the maximum loads were quite different. The results for cases (a) and (b) indicate that placing the stiff material along the axial direction leads to more mode jumps than placing it in the circumferential direction. Although cases (c) and (d) had a similar maximum buckling load, the postbuckling response of case (c) had a bigger enclosed area and a larger number of mode transitions, which shows that the stiff material distribution should be arranged in a distributed and not clustered pattern. The next four designs had different inclined, or diagonal, patterns of stiff material distribution. It can be observed that the response of case (e) had large load drops and a large amount of energy dissipation compared to case (f). Nonetheless, the buckling events could not propagate along the circumferential direction due to the lack of continuity among the flexible regions. Thus, case (g) and (h) were designed to trigger more interaction between the flexible patches. This approach was successful as it increased the number of mode transitions and the dissipated energy. Overall, cases (c) and (h) were the designs with larger energy dissipation and a larger number of mode transitions; while cases (a) and (f) were the worst patterns according to the aims of this study. Figure 5-5 shows the postbuckling responses of cases (a), (c), (e) and (g). It can be seen that localized events in all of the NP cylinders occurred in the ‘design’ regions. The results confirm that appropriate stiffness patterns can be utilized for controlling postbuckling behavior.

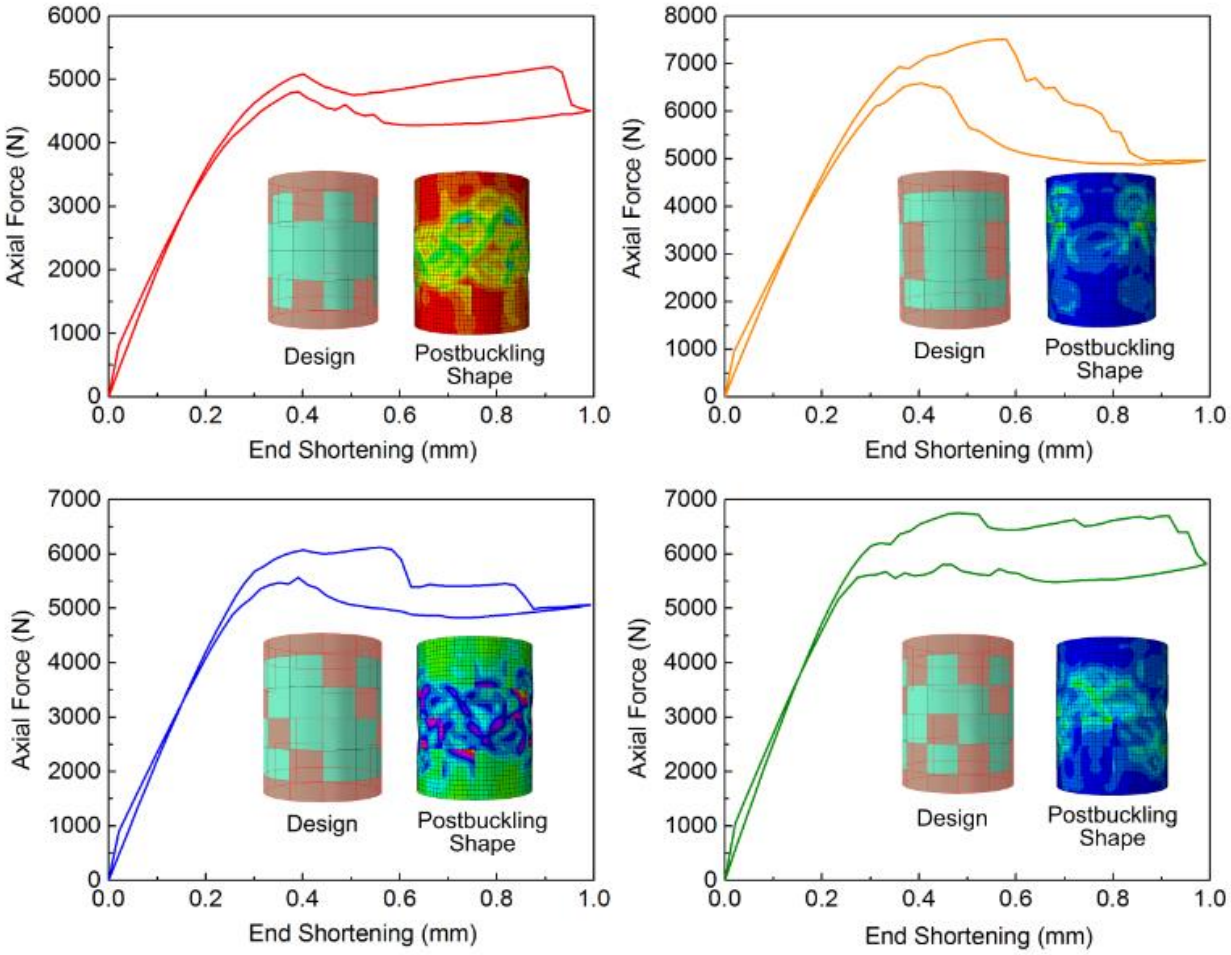

Figure 5-5: Effect of patterned material distributions on the global and local postbuckling response of hybrid cylinders under axial compression.

Using the same modeling approach, two additional simulations were conducted on cylinders with a uniform stiff material and with a uniform flexible material. Figure 5-6 shows that the postbuckling response of the stiff cylinder had only one significant mode jump event while no mode transition was observed on the response of the flexible cylinder. The response for NP cylinder case (c) is also plotted in Figure 5-6 and it can be seen that the NP cylinder had a larger number of mode transitions and dissipated more strain energy compared to the other two cases under the same seeded imperfection amplitude. Thus, the responses of the two uniform cylinders

can be considered upper and lower bounds to the postbuckling response of cylinders with patterned/hybrid material layouts using the same materials. The results show that cylinders with non-uniform material patterns open design opportunities to obtain material systems for a specific postbuckling response target.

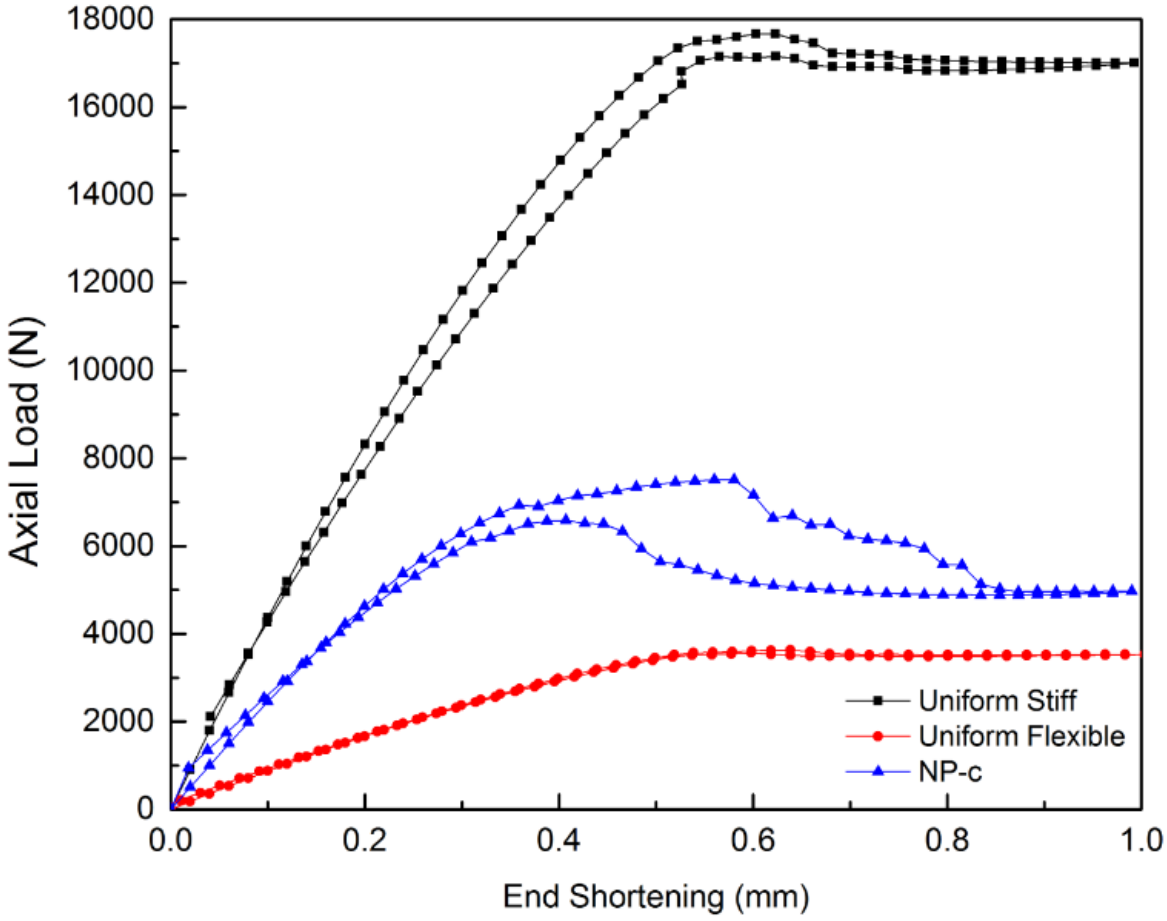

Figure 5-6: Predicted postbuckling response of hybrid cylinders with and without stiffness-patterned design.

5.3.2 Sensitivity analysis

Similar to the study presented in Section 4.3.2, a numerical simulation was conducted on a uniform cylindrical shell and an NSD cylindrical shell to evaluate the concept of NSD designs and its sensitivity to the initial imperfections. The selected geometry considered is relatively

smaller than the one used in Section 5.3.1, within the reasonable range as given in Table 3-1 ($L/R \leq 2$ and $R/t \geq 100$). The selected geometry also considered the size constraint for the fabrication of test specimens through 3D printing (see Section 3.4). Thus, the baseline cylindrical shell in this section had a length of 100 mm (including a 10 mm reinforced/thickened region at each end), a radius of 40 mm and a thickness of 0.5 mm. The cylinder had an L/R ratio of 2 and an R/t ratio of 80. The Young's modulus E was 1.8 GPa and the Poisson's ratio v was 0.2. The NSD cylinders had the same geometry but certain regions on the shell surface were thickened to 1 mm.

After fixing the geometry the imperfection profile and its amplitude has a bigger role on governing the postbuckling response. An NSD cylinder was created with a thickening ratio of 1/3 (i.e., the proportion of 1 mm patches with respect to the entire shell domain). Simulations were conducted for the uniform and NSD cylindrical shells to compare these two prototypes on their sensitivity to initial (random) imperfections.

It is known that the eigenvalues of cylindrical shells are closely spaced. In this case, the load of mode 200 is only 63% higher than mode one. Thus, a total of 200 mode shapes were considered to provide more geometric imperfection options for the baseline uniform cylinder. Both shells were provided with the same total imperfection amplitude but through five different imperfection sets, where each set was seeded from 5 mode shapes. The normalized postbuckling responses for both cases (loading phase only) are shown in Figure 5-7. It is interesting to see that the initial stiffness for both cases is similar. Also, the different imperfection sets lead to five postbuckling response curves after the first critical buckling, but all responses reach a similar stiffness towards the end of the loading phase. The response variability in the postbuckling regime is indicated by the size of the shaded area, which clearly shows that the NSD cylindrical shell has a lower sensitivity.

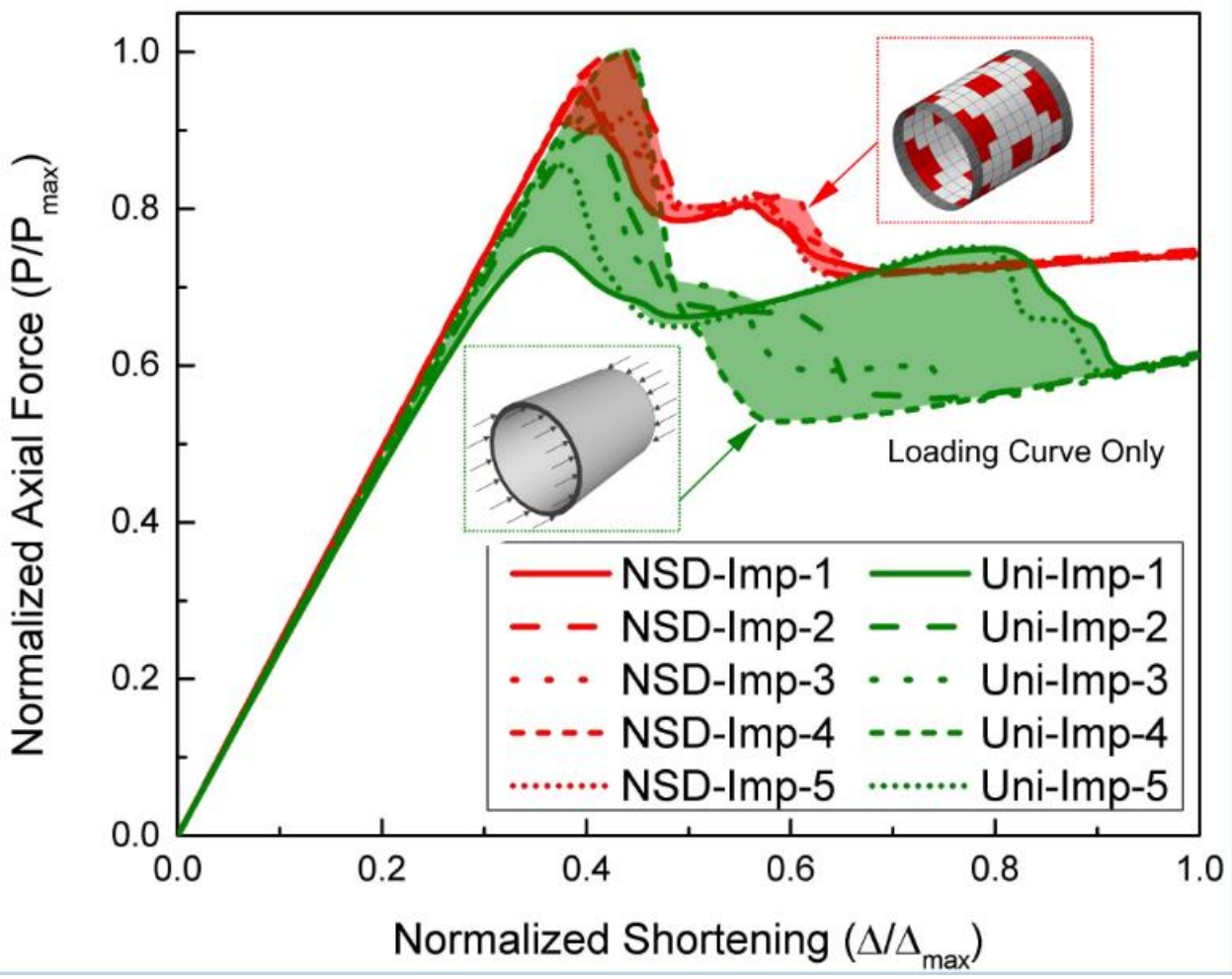

Figure 5-7: Numerical comparison of the sensitivity to initial imperfections between a uniform and a NSD cylinder subjected five imperfection set but same amplitude.

5.4 Experimental results: PLA cylinders

The evaluation presented in Section 5.3 showcased the opportunities of using discrete patches in the design of cylindrical shells. This section reports on the experimental evaluation of 11 NSD cylindrical shells, organized in two design groups (symmetric and asymmetric) that were fabricated via 3D printing and tested in axial compression.

5.4.1 Symmetric design

The first design group consisted of six baseline NSD cylindrical shells (cases NSD-A through NSD-F), as shown in Figure 5-8. The aim of this group was to systematically explore the cylinders' postbuckling response with various patch patterns and to recognize if mode transitions could be triggered in non-thickened regions.

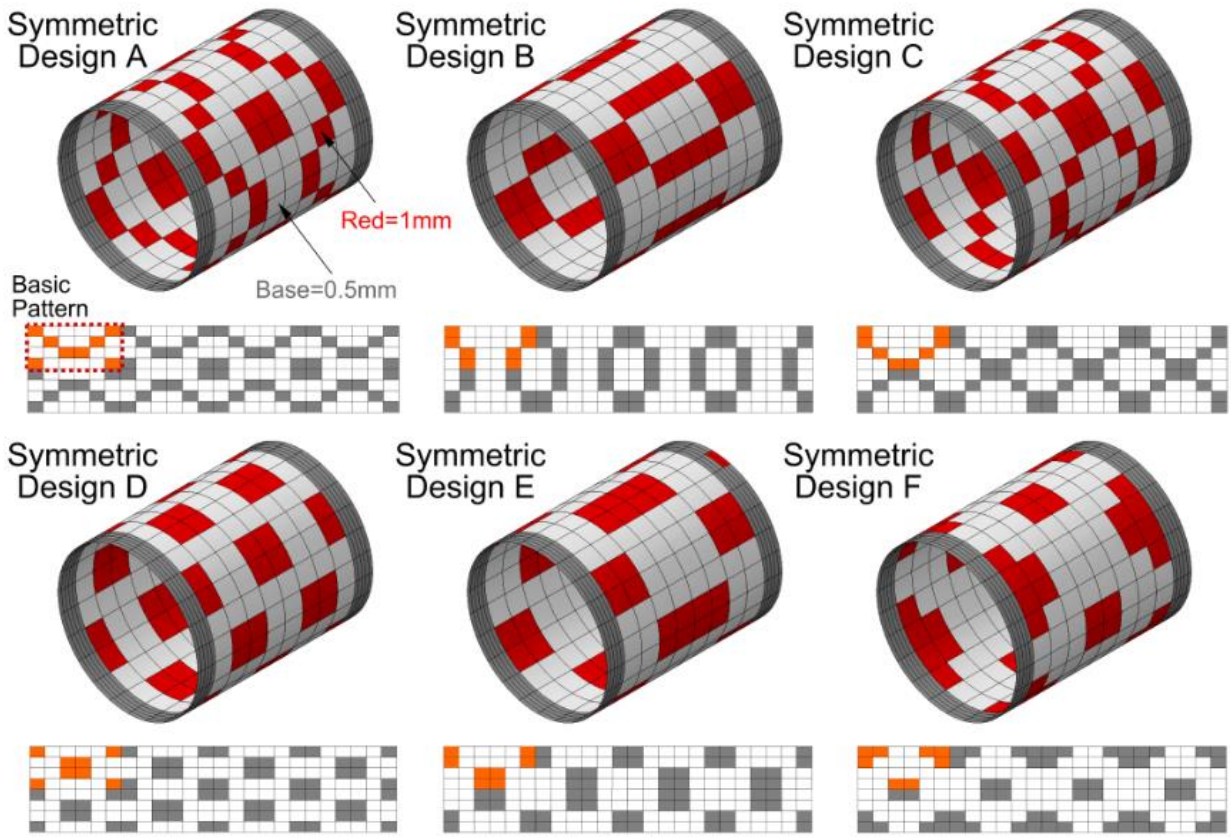

Figure 5-8: Baseline NSD cylinders with symmatric pattern.

The shell surface was discretized into 192 cells (8 in the axial direction by 24 in the circumferential direction). All six designs had symmetry in their patch pattern and the basic (i.e., repeating) pattern was assigned to one-eighth of the model, seen in Figure 5-8. Within the one-

eighth domain, 8 out of 24 cells were thickened to 1 mm and, which led to a thickening ratio of 1/3 for all six baseline NSD cylinders. These NSD cylinders were classified according to the layout of the thickening patches along the circumferential direction into two categories: "isolated" or "connected." Design cases NSD-A through NSD-C contain "isolated" flexible regions while the thickening regions of design cases NSD-D through NSD-F were arranged in a clustered pattern and well connected along circumferential directions.

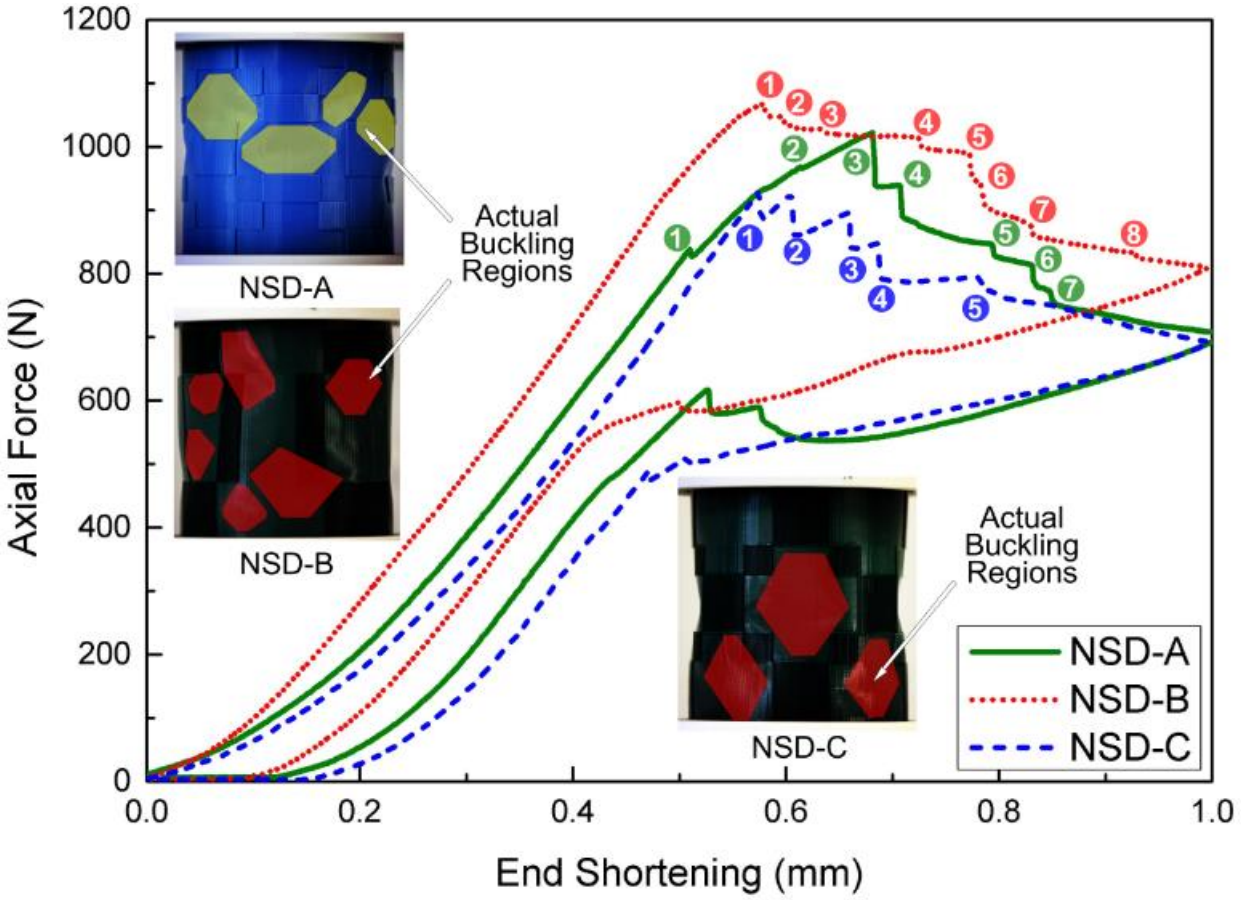

Figure 5-9: Obtained postbuckling responses of three NSD cylinders in isolated group.

The force-displacement responses of the six baseline NSD cylinders are shown in Figure 5-9 and Figure 5-10. It can be seen that the applied axial deformation and the initial stiffness were

recovered upon unloading in all six tests. As expected, several mode transitions after first buckling event were observed. The buckling events for the "isolated" designs (cylinders A through C) start within the flexible region and triggered a snap-buckling event (see shaded regions on the postbuckling shape insets in Figure 5-9). However, local buckling in these designs had difficulty propagating along the circumferential direction and buckling events are isolated or confined to the flexible regions. Compared to the "isolated" designs, the buckling events in the "connected" designs (cylinders D through F) could propagate along the circumferential direction due to the continuity among the flexible regions (see shaded regions).

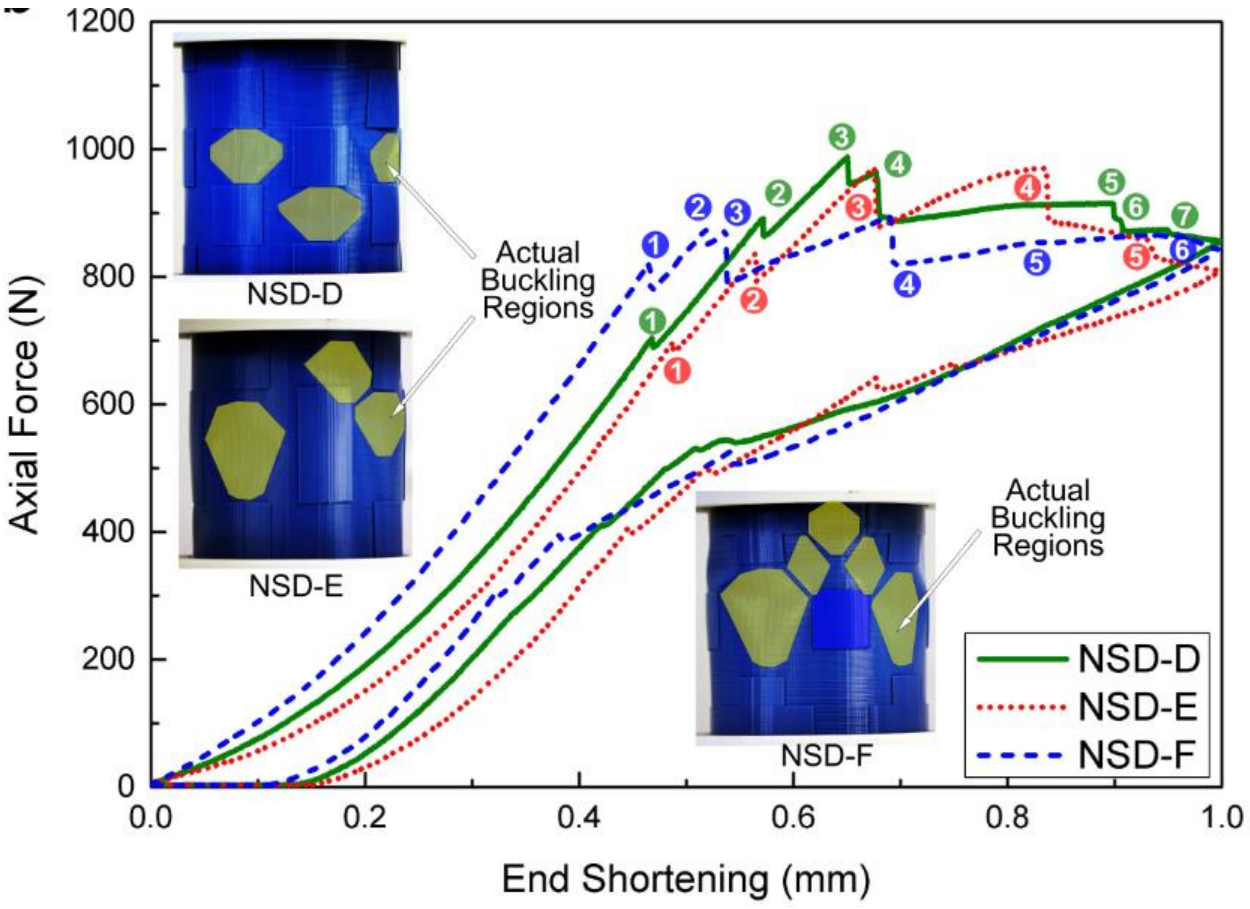

Figure 5-10: Obtained postbuckling responses of three NSD cylinders in conneceted group.

It can also be noted in Figure 5-9 and Figure 5-10 that the stiffness for the "isolated" designs (A through C) decreased significantly after each critical event, and that the end stiffness was nearly negative; while the stiffness for the "connected" designs (D through F) decreased more gradually and a residual stiffness was still observed at the end of the loading process. In other words, the "isolated" designs had a significant reduction in capacity during the postbuckling response and the first buckling load was usually the maximum critical load. Conversely, a stiffening post-buckling response was observed in the "connected" designs, with the load capacity tending to a plateau at a level that surpassed the initial buckling load. Another interesting observation is that for some design cases (NSD C and NSD E) the patch layout plays an important role in controlling the sequence of the localized buckling events. It can be seen that the postbuckling response curves in Figure 5-9 (dashed line) and in Figure 5-10 (dotted line) feature nearly equally-spaced buckling events for the first four load drops. These load drops are associated with the localized buckling events in the flexible regions on the middle region of the cylinder where the critical length is larger than in other flexible regions.

Table 5-3 gives a summary of the postbuckling response for the experimental cases in terms of the key parameters (K_i, P_{max}, ΔP_{max}, δ_{max}, A, and n_t) shown in Figure 3-12. It can be seen that all six cases has similar initial stiffness due to the equal thickening ratio (1/3) on the shell surface. Yet, as it is to be expected, the various layouts did affect the postbuckling behavior, e.g., the number of load drops, their magnitude and spacing, etc. Design NSD-B had the largest initial stiffness, first buckling load, enclosed area and total area below the response curve. A prior numerical study by the authors [250] found that initial stiffness has a strong correlation with ΔP_{max}, and A. These observations are confirmed by the tests reported here.

Table 5-3: Postbuckling response of six baseline NSD cylindrical shells with symmetric pattern.

Specimen	K_i (N/mm)	P_{max} (N)	ΔP_{max} (N)	δ_{max} (mm)	n	A (kJ)	A_t (kJ)
NSD-A	2011	1022	83.7	0.17	7	199	599
NSD-B	2061	1069	86.9	0.10	8	212	670
NSD-C	1992	930	66.6	0.10	5	173	540
NSD-D	2000	988	70.9	0.22	7	178	595
NSD-E	1967	972	94.2	0.16	5	175	567
NSD-F	2005	894	83.2	0.29	6	188	606
Mean	**2006**	**979**	**80.9**	**0.17**	**6**	**187**	**596**
CoV	**0.02**	**0.06**	**0.13**	**0.43**	**0.19**	**0.08**	**0.07**

5.4.2 Asymmetric design

The exploration on triggering the buckling events in certain regions was continued with four NSD cylinder designs that were slightly revised from cases NSD-A and NSD-F, as shown in Figure 5-11. The purpose of this design group was to evaluate simple cases with asymmetric patterned layouts and compare the locations of mode transitions with those observed in the baseline cylinders. These asymmetric designs were determined based on the lessons learned from the symmetric cases, which showed that localized buckling events did not take place in all of the non-thickened regions. For the "connected" designs (cylinders D through F), only one of two connected paths were active for the propagation of buckling events along the circumferential direction. Such phenomenon was observed in designs NSD-A (see insets in Figure 5-9). Thus, the rationale behind the four new asymmetric designs is to define a single propagation path such

that the location of buckling events is predictable and controllable. The only difference between design AA1 (or FA1) and AA2 (or FA2) is the size of the clustered patches in the middle region. As shown in Figure 5-11, the number of patches in the middle regions of design AA2 (or FA2) varies such that the sequence of buckling events may be predicted and controlled.

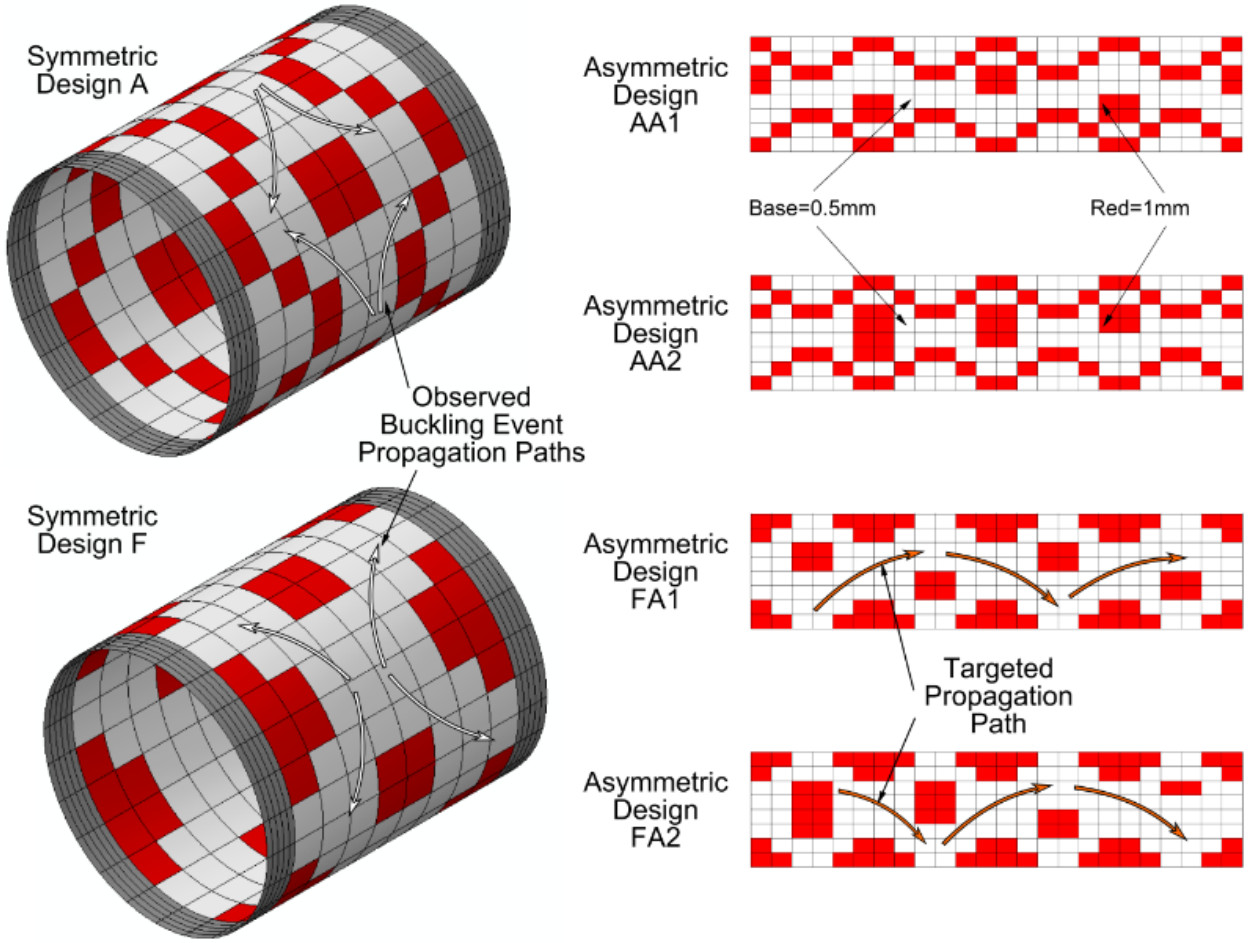

Figure 5-11: NSD cylinders with asymmatric pattern.

The axial load vs. end shortening responses of the four asymmetric designs versus two symmetric designs are shown in Figure 5-12 and Figure 5-13. The initial stiffness was similar for all cases due to the slight variation in the patch locations. The most interesting finding is that the

occurrence of the buckling events was quite different. A summary of results is provided in Table 5-4. It can be seen in Figure 5-12 that, compared to cylinder NSD-A, the postbuckling response of AA1 has a smaller number of the mode transitions while the postbuckling response of cylinder AA2 had a higher initial stiffness and a larger enclosed area. The insets of Figure 5-12 show the postbuckling shape of cylinder AA2, for which the buckling events were trigged in the targeted regions. In terms of the postbuckling response, cylinders FA1 and FA2 had the same number of mode transitions as cylinder NSD-F (see Figure 5-13) even though these three cases had a slightly different maximum load drop (ΔP_{max}) and enclosed area (A). The localized buckling events for designs FA1 and FA2 were also observed in the non-thickened regions.

Table 5-4: Postbuckling response variation between two NSD cylindrical shells with symmetric pattern and five NSD cylindrical shells with asymmetric pattern.

Specimen	K_i (N/mm)	P_{max} (N)	ΔP_{max} (N)	δ_{max} (mm)	n	A (kJ)	A_t (kJ)
NSD-A	2134	1022	83.7	0.17	7	199	599
AA1	2075	1074	61.3	0.22	4	200	612
AA2	2278	1341	150.8	0.11	6	264	773
NSD-F	2005	894	83.2	0.29	6	188	606
FA1	2339	1084	130.5	0.14	6	230	692
FA2	2272	842	60.4	0.15	6	182	534
FT	2344	1023	89.0	0.13	6	216	630

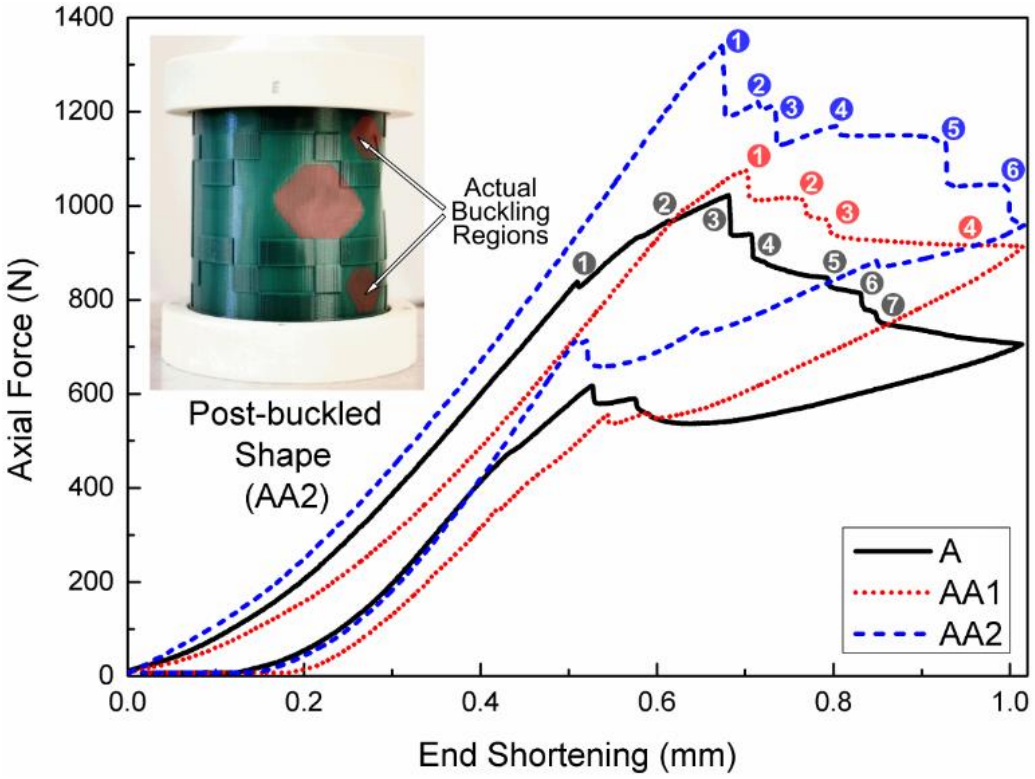

Figure 5-12: Effect of changing symmetry on the global postbuckling response of NSD cylinders (specimen series AA).

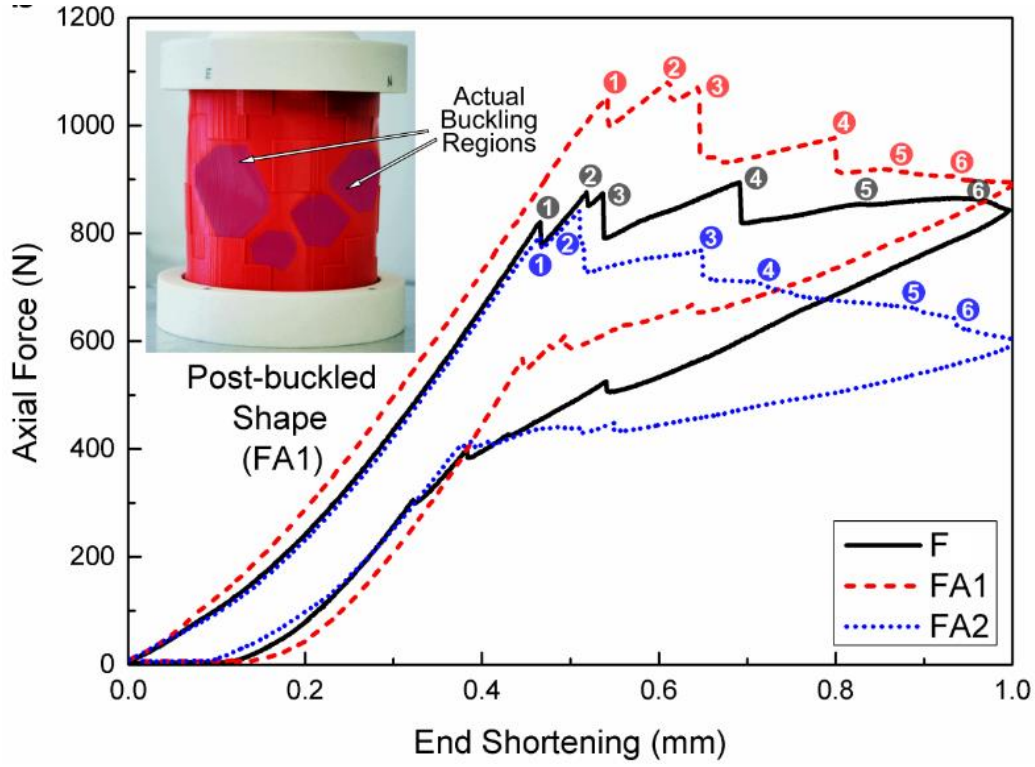

Figure 5-13: Effect of changing symmetry on the global postbuckling response of NSD cylinders (specimen series FA).

Maps indicating the propagation of local buckling events for the asymmetric designs and two baseline symmetric designs are shown in Figure 5-14 and Figure 5-15. It is clearly seen in this figures that buckling in the NSD cylinders occurred in specific regions rather than at random locations on the shell surface. For the baseline designs NSD-A and NSD-F it was observed that the buckling events were triggered on the upper side of the cylinder. Slight changes on the middle thickened patches in cylinders AA1 and FA1 created a single propagation path along the circumferential direction and the majority of the localized buckling events were triggered along this path. For cylinders AA2 and FA2 it can be seen that the first buckling event was triggered near the biggest thickened region and then propagate along the circumferential direction. Several buckling events did occur in "isolated" regions of cylinder AA2. Yet, overall, this experimental study indicated that NSD cylinders allow for localized buckling events to be triggered in certain regions of the shell by changing the pattern of stiffening patches on the shell surface.

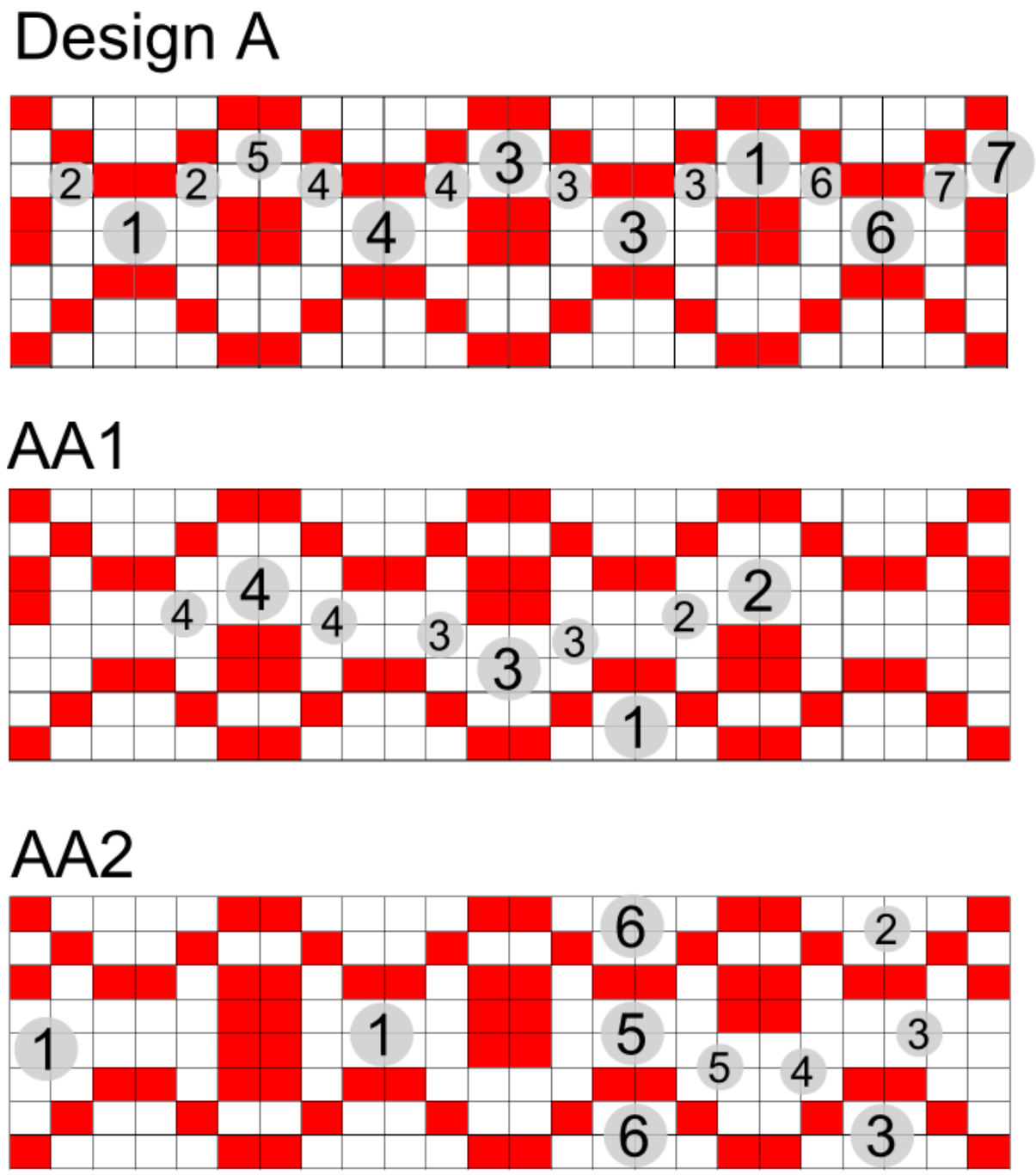

Figure 5-14: Propagation map of localized buckling events on NSD-A shell series.

Design F

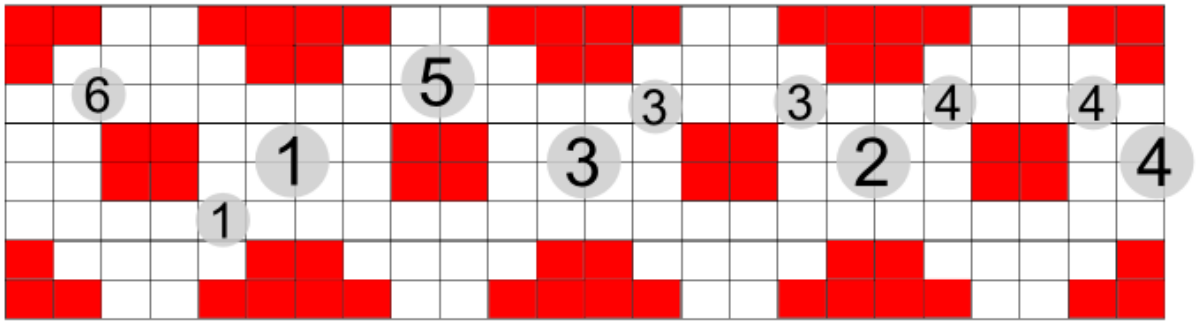

FA1

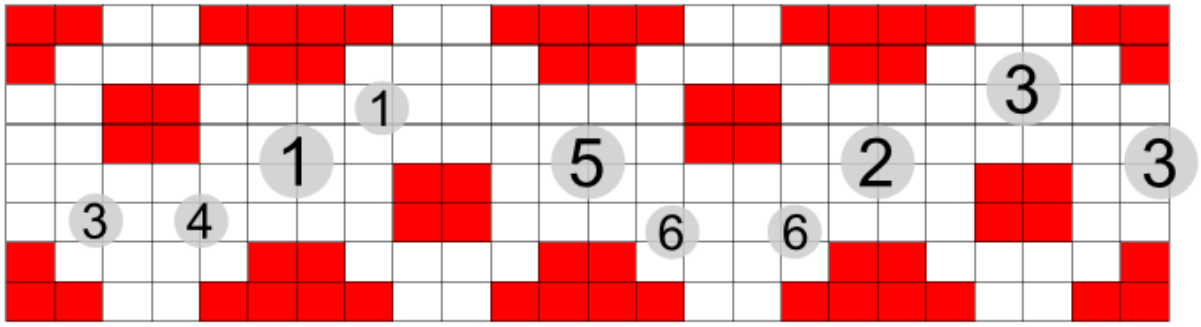

FA2

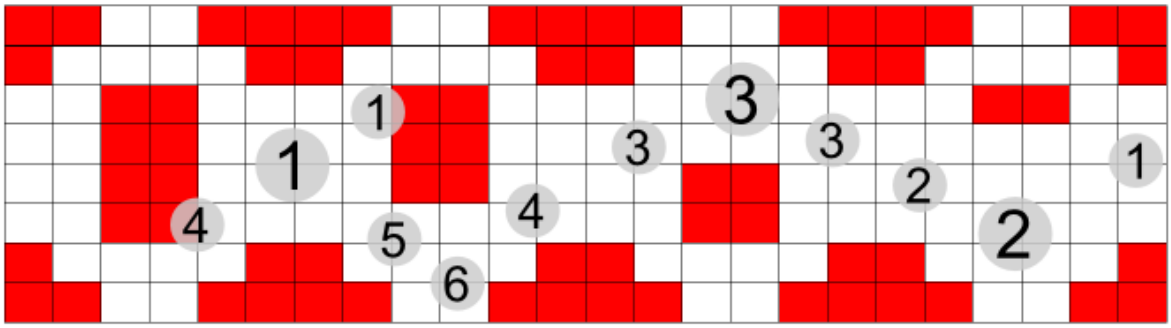

Figure 5-15: Propagation map of localized buckling events on NSD-F shell series.

The test series reported above shed some light on controlling not only the location of the buckling events but also the sequence of these events. An additional cylinder (FT) was designed based on baseline cylinder NSD-F, as shown in the inset of Figure 5-16.

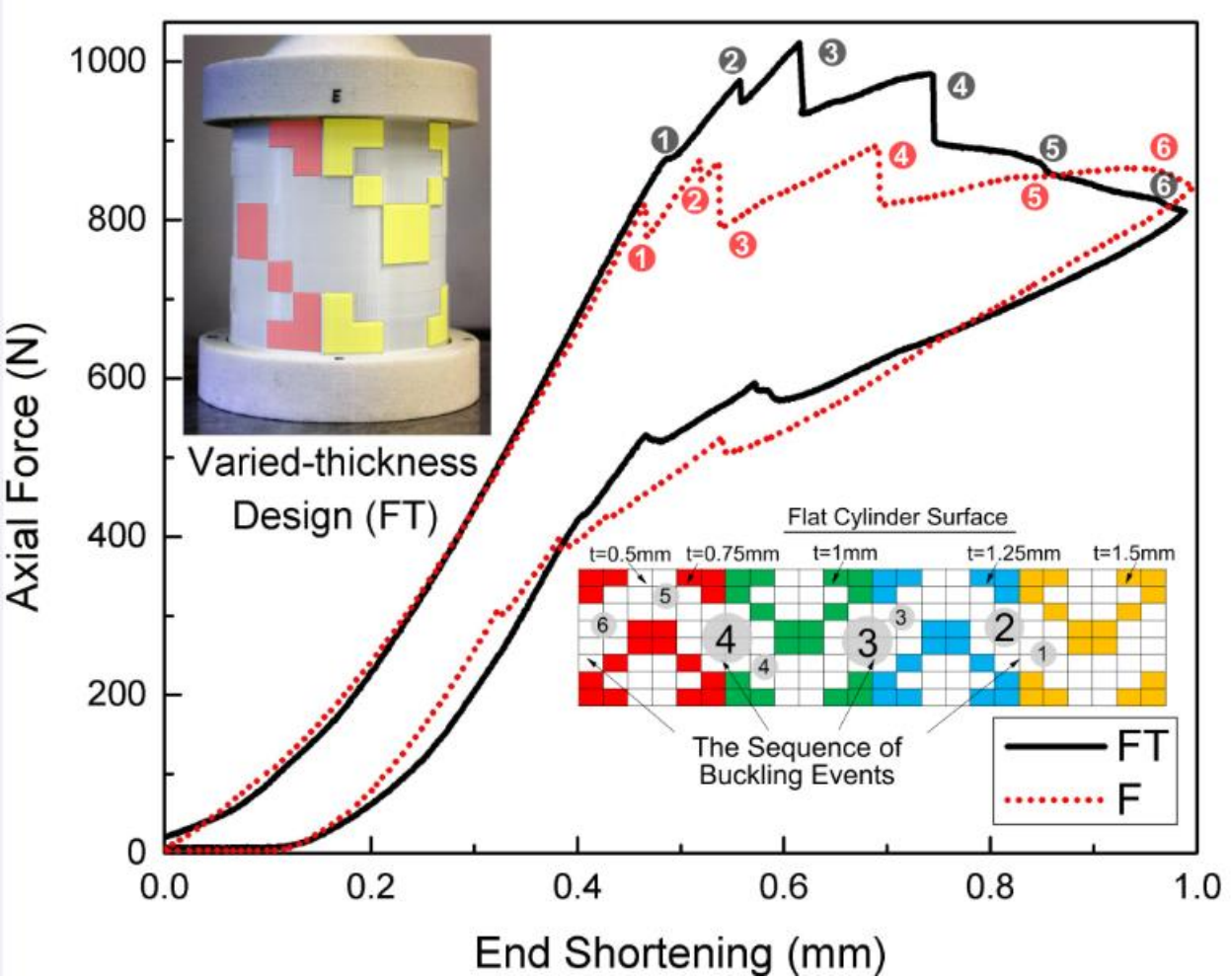

Figure 5-16: Effect of gradually varying thickness on the global postbuckling response and the sequence of buckling events of baseline cylinder NSD-F.

It can be seen that cylinder FT had four thickness variations along the circumferential direction of the shell surface, gradually thickening from 0.75 mm to 1.5 mm. The postbuckling response shown in Figure 5-16 and Table 5-4 indicates that cylinder FT had a bigger maximum load drop (ΔP_{max}) and enclosed area (A) but it had the same number of mode transitions compared to the baseline cylinder NSD-F. More importantly, this pilot test showed the buckling

events for cylinder FT started near the middle patches of the 1.5 mm thickened region and then propagated along the predefined path with multiple mode transitions. Therefore, in general, asymmetric stiffening patterns (in this case via varied thickness) can be used to control the time (i.e., sequence) and location of mode transitions in the elastic postbuckling regime.

5.4.3 Effect of thickened ratio

The six NSD cylinders discussed in Section 5.4.1 had the same thickening ratio of 1/3 (33.3%). Three additional cylinders with a uniform thickness of 0.5 mm (Uni-0.5), 0.75 mm (Uni-0.75) and 1 mm (Uni-1), which respectively represent uniform thickening ratios of 0%, 50%, and 100%, were printed and tested as described in the methods section (3.4.2). The aim of these tests was to showcase the variety of opportunities to modify the postbuckling response with different thickening ratios. Figure 5-17 compares the postbuckling response of these three uniform cylinders along with two NSD cylinders. It can be seen that the postbuckling response of cylinder Uni-0.5 and Uni-1 can be considered as lower and upper bound responses, respectively, for this cylinder geometry. No buckling event was observed in the test of cylinder Uni-1, while cylinder Uni-0.5 had multiple mode transitions. In between, the use of discrete patterned patches can lead to a postbuckling response with multiple mode transitions. Overall, it is clear that a targeted postbuckling behavior can be achieved if discrete pattern patches, which generate non-uniform stiffness distributions, are properly placed.

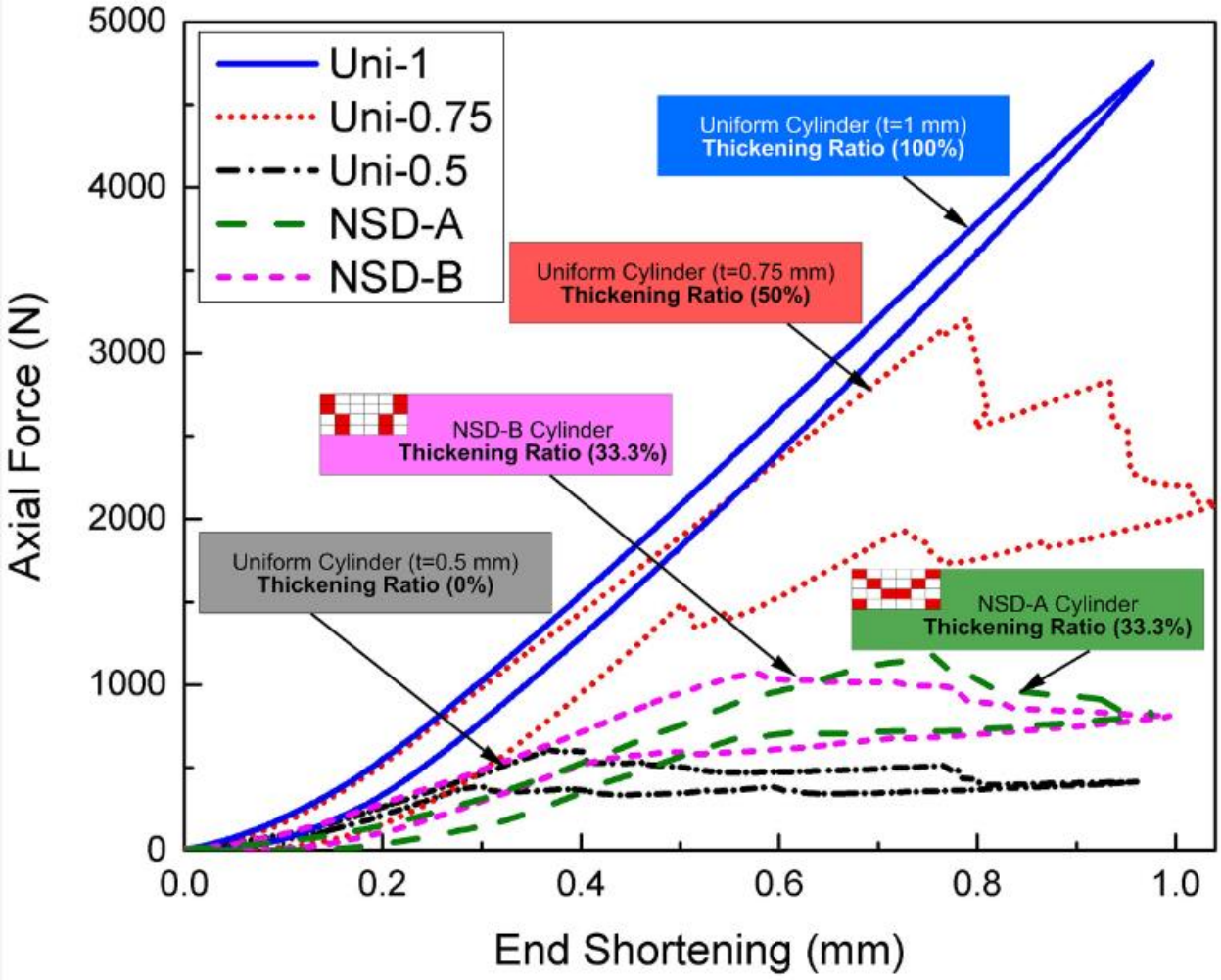

Figure 5-17: Effect of thickening ratio on the postbuckling response of NSD cylinders.

5.4.4 Effect of loading variation

A series of experiment were carried out on the six baseline NSD cylinder described in Section 5.4.3 to evaluate the sensitivity of their postbuckling responses to load variations. Load variation was assessed under two scenarios: (a) reloading in same position; and (b) reloading in a different position. As shown previously in Figure 3-10, an orientation label was marked on the loading fixture. The label "W" means that the front side of the specimen was facing west. Labels "N" and "E" represent north and east, and mean that the cylinder's position was rotated 90° and 180°,

respectively, from the position “W”. These orientation marks were added to the specimen’s identification name for the results presented herein.

The six baseline NSD cylinders were considered in two groups: NSD cylinders A, B and C were reloaded under three different positions, while cylinders D, E and F were reloaded in the same position (facing west.) The axial load vs. end shortening responses of cylinders NSD-A and NSD-F are shown in Figure 5-18 and Figure 5-19.

In Figure 5-18 the three postbuckling responses of cylinder NSD-F show the effect of loading variation within the same loading position. It can be seen that the first buckling load decreased after each loading-unloading cycle and the three responses show, in general, a decrease in capacity. This phenomenon may be caused by some localized damage due to the sharp corners of the thickened regions, which repeatedly trigger the postbuckling responses in the targeted regions possibly accumulating damage. Nonetheless, it is interesting to see that the overall features of the postbuckling response did not change significantly. Similar results were found from the reloading response of cylinders NSD-D and NSD-E. A summary of results is given in Table 5-5, which also provides mean response values in addition to those from the three tests.

The effect of changes in loading position on the postbuckling responses for cylinder NSD-A is shown in Figure 5-19. As expected, the postbuckling response variations were larger in this case because slight differences on the shell edge lead to a change on the pressure or loading distribution. It is clear that loading position changes leads to differences in the maximum load drop, the enclosed area, and even the location of the buckling events. However, the differences are small as shown by the coefficients of variation for the results summary in Table 5-6.

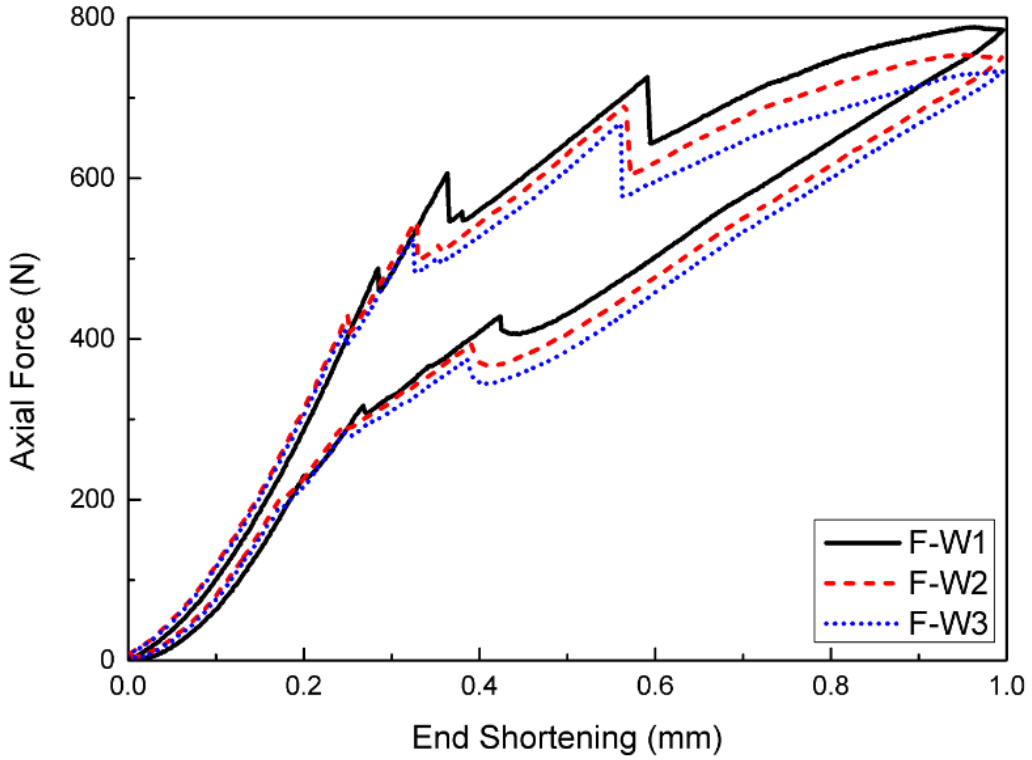

Figure 5-18: Sensitivity to loading variation of NSD cylinders under axial compression (reloading with same loading position).

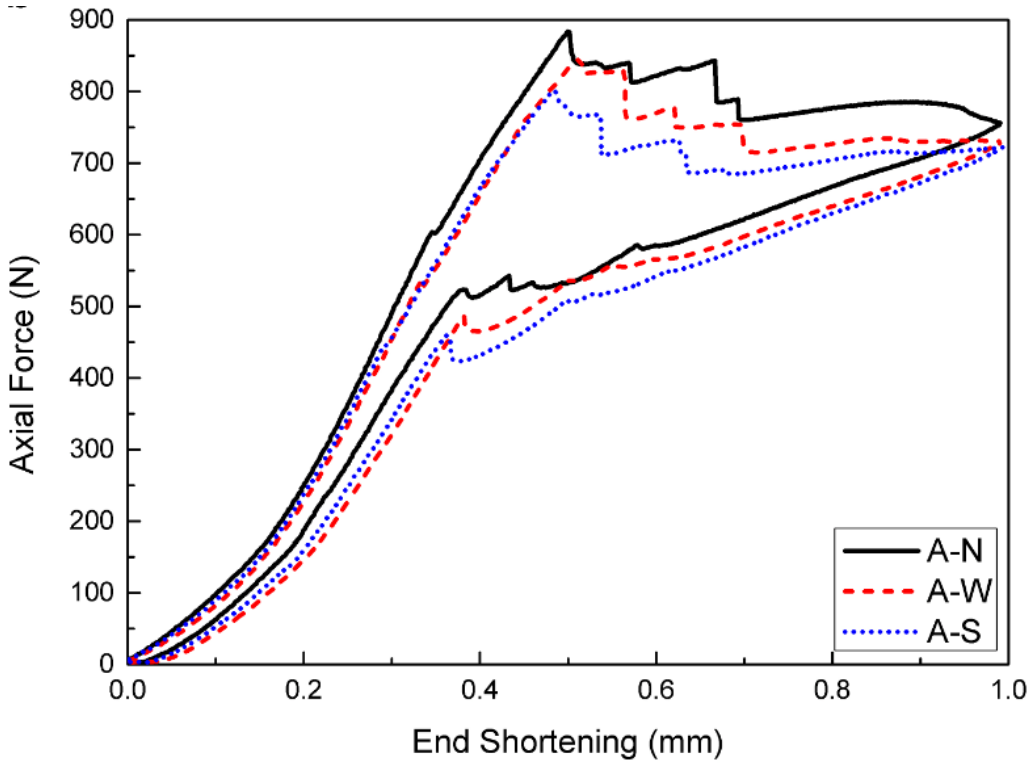

Figure 5-19: Sensitivity to loading variation of NSD cylinders under axial compression (varied loading position).

Table 5-5: Postbuckling response variation of NSD cylinders under same loading position.

Specimen	K_i (N/mm)	P_{max} (N)	ΔP_{max} (N)	δ_{max} (mm)	n	A (kJ)	A_t (kJ)
D-W1	1832	842	54.2	0.22	7	131	585
D-W2	1807	808	49.4	0.42	6	94	546
D-W3	1705	789	48.4	0.46	6	99	535
D-Mean	**1781**	**813**	**50.6**	**0.37**	**6**	**108**	**555**
D-CoV	**0.04**	**0.03**	**0.06**	**0.35**	**0.09**	**0.18**	**0.05**
E-W1	2148	879	104.2	0.17	5	148	589
E-W2	2137	795	88.9	0.21	5	121	543
E-W3	2129	754	86.9	0.20	6	115	528
E-Mean	**2138**	**810**	**82.7**	**0.24**	**6**	**123**	**554**
E-CoV	**0**	**0.08**	**0.10**	**0.09**	**0.11**	**0.14**	**0.06**
F-W1	2043	788	82.3	0.21	4	113	536
F-W2	1835	754	87.0	0.21	4	114	521
F-W3	1760	733	91.0	0.21	4	109	501
F-Mean	**1879**	**758**	**86.8**	**0.21**	**4**	**112**	**519**
F-CoV	**0.08**	**0.04**	**0.05**	**0.01**	**0**	**0.02**	**0.03**

Table 5-6: Postbuckling response variation of NSD cylinders under changing loading position.

Specimen	K_i (N/mm)	P_{max} (N)	ΔP_{max} (N)	δ_{max} (mm)	n	A (kJ)	A_t (kJ)
A-N	2327	884	58.2	0.26	7	130	587
A-W	2184	845	67.3	0.18	7	121	550
A-S	2121	800	57.1	0.09	7	113	535
A-Mean	**2211**	**843**	**60.9**	**0.18**	**7**	**121**	**557**
A-CoV	0.05	0.05	0.09	0.46	0	0.07	0.05
B-N	2436	844	32.4	0.16	7	124	613
B-W	2352	804	28.1	0.19	6	110	589
B-S	2322	790	28.9	0.20	6	109	593
B-Mean	**2394**	**824**	**30.3**	**0.18**	**7**	**117**	**601**
B-CoV	0.02	0.03	0.08	0.12	0.09	0.07	0.02
C-N	2348	693	46.4	0.17	8	129	503
C-W	2267	748	44.8	0.34	8	128	532
C-S	2239	650	58.0	0.15	7	108	476
C-Mean	**2253**	**589**	**36.4**	**0.17**	**8**	**98**	**425**
C-CoV	0.02	0.07	0.14	0.49	0.08	0.09	0.06

5.4.5 Uniform Shells vs. NSD Shells

Uniform cylindrical shells are well-known to suffer high degree imperfection sensitivity. It was an aim of this research to show that patterned patches is a viable strategy to design thin-walled cylindrical shells with a less sensitive postbuckling response. Test results in Section 5.4.1 and Section 5.4.2 have shown that an NSD cylinder still displays sensitivity effects in their elastic postbuckling response. From this perspective, it was worthwhile to compare the sensitivity of NSD cylinders with the two uniform cylinders described in Section 4.4.4.

The postbuckling responses for the uniform and NSD cylinders were normalized to allow their comparison. The normalized postbuckling responses, for repeating loading under the same position, of cylinders U1 and NSD-F are compared in Figure 5-20. Only the loading branch of the response curve is shown because the variations within the unloading branch are small. The shaded areas in indicate the response variation. It can be seen that the postbuckling response features are quite different, but both cylinders had a similar sensitivity (size of the shaded area) for this kind of load variation. The normalized postbuckling responses for cylinders U2 and NSD-A for load variations from different loading position are compared in Figure 5-21. The size of the shaded areas in Figure 5-21 indicates that the NSD cylinder had a smaller sensitivity to load changing variations than the uniform cylinder. Therefore, in general, the postbuckling response of NSD cylinders is less sensitive to loading variations.

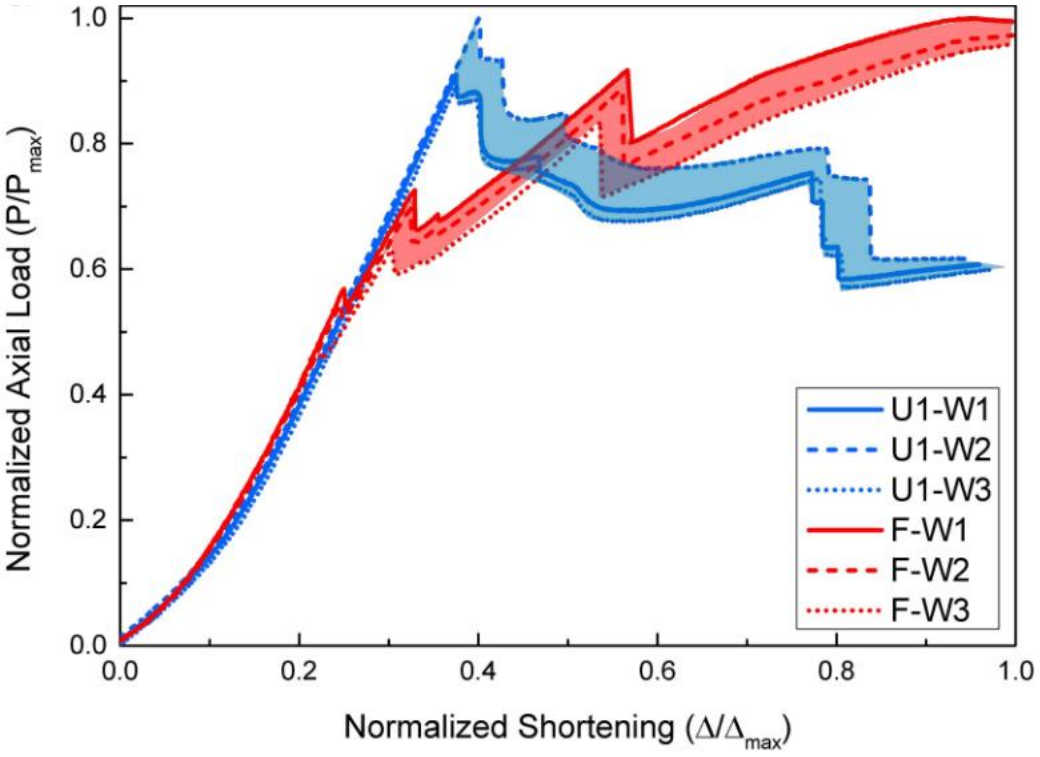

Figure 5-20: Experimental comparison of the sensitivity to initial imperfections between a uniform and a NSD cylinder (varied loading position).

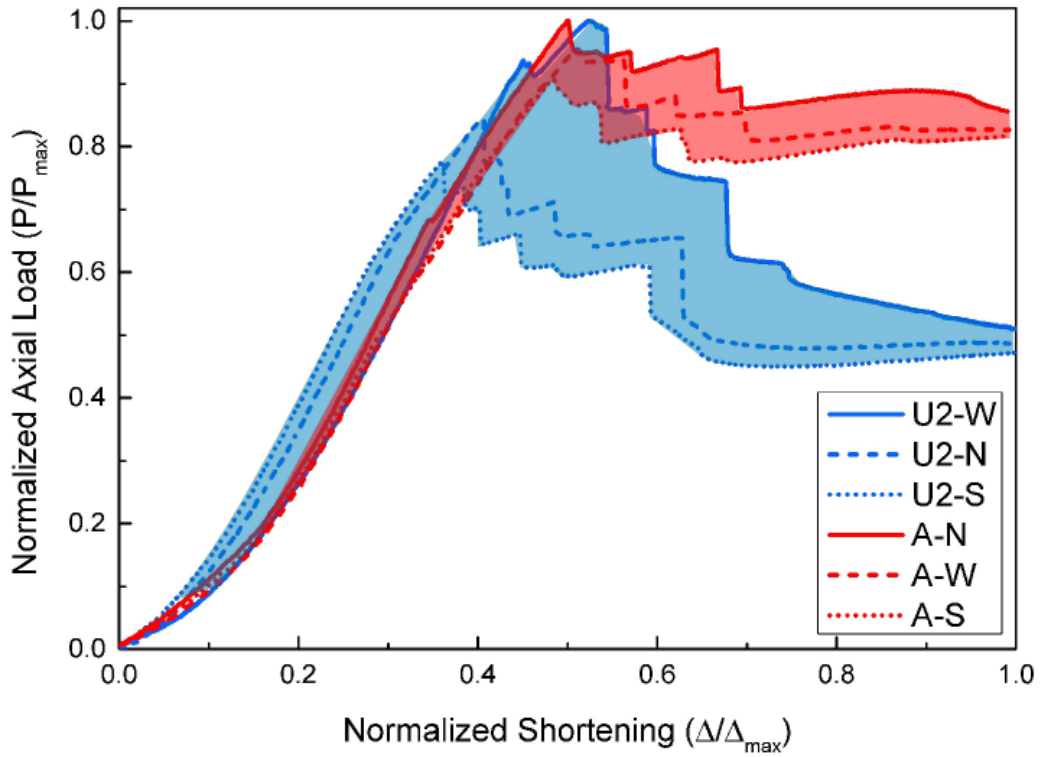

Figure 5-21: Experimental comparison of the sensitivity to initial imperfections between a uniform and a NSD cylinder (reloading with same loading position).

5.5 Summary

This chapter presented the evaluation of a concept for non-uniform stiffness distribution (NSD) on the surface of cylindrical shells by using patterned thickening patches (PTP), and introduced a novel role for such patterned stiffness distribution with the focus of triggering multiple mode transitions in the elastic postbuckling regime. Experimental and numerical studies showcased and evaluated the effect of patterned patches for modifying and controlling the postbuckling response of axially-compressed cylindrical shells. The results indicate new possibilities for the design of advanced materials, devices and structures. The following conclusions were drawn from the study presented in this chapter:

(1) The concept of NSD cylindrical shells was proposed. A predefined geometric imperfection was added to the shell's surface, in the form of patterned thickening patches (PTP), such that it has a governing role over other random imperfections on postbuckling behavior. Numerical simulations proved that the imperfection sensitivity of NSD cylinders is lower compared to that of uniform cylinders.

(2) The occurrences of buckling events in NSD cylinders are predictable. Experimental results on 3D printed cylindrical shells validated the hypothesis that an NSD design allows the postbuckling response of axially-compressed cylindrical shells to have multiple mode transitions in targeted regions. Both symmetric and asymmetric pattern cases were able to trigger the localized buckling events in the non-thickened regions. More importantly, some asymmetric pattern designs demonstrated the possibility of controlling not only the location of the buckling events but their sequence. This is a major step toward finding an optimal pattern distribution to achieve a predictable and controllable postbuckling response.

(3) The postbuckling response of NSD cylinders is less sensitivity to imperfections. Experimental and numerical results showed that NSD cylindrical shells were less sensitive to random and initial imperfection than uniform shells. It was of interest to note that NSD cylinders featured a similar (even equal for some designs) number of mode transitions from repeated loading-unloading cycles under the same loading position and rotated loading positions. Thus, NSD cylinders showed the advantage of using varied stiffness in the form of a patterned geometry for reducing their elastic postbuckling response sensitivity due to initial geometric imperfections and loading variations. In this way, NSD cylinders are favorable over a uniform cylinder because of their controllable postbuckling features.

Chapter 6

Lateral Constraints and Interactions (LCI)

6.1 Overview

The numerical and experimental results presented in Chapters 4 and 5 showed that the force-deformation response of the axially loaded cylindrical shells is characterized by a significant loss of stiffness and in some cases load-bearing capacity in the far postbuckling regime. This occurs as the buckling wave's amplitude increases without triggering additional localized mode transitions. This chapter presents a numerical and experimental study of the postbuckling response of cylindrical shells provided with a uniform inner lateral constraint as well the concept of multiple cylinders in nested assemblies. The later concept, termed lateral constraint interactions (LCI) cylinder, was motivated by the desire to gain further control of the postbuckling response through the cylindrical wall interactions. The hypothesis is that if the provision of lateral restraints on a compressed cylinder leads to modifications to the stiffness of the multiple postbuckled loading branches then the postbuckling stiffness of individual postbuckling branches and the overall postbuckling regime can be controlled by means of continuous constraints and the resulting interactions. Both inner-constrained laminated composite cylinders and multi-wall PLA cylinders were fabricated and tested. The study on inner-constrained cylinders presented in this chapter was published in the journal *Thin-walled Structures* [45] and study on multi-walled cylinder was published in the journal *Extreme Mechanics Letters* [251].

6.2 Numerical results

The baseline cylinder modeled for this evaluation was a [45°/-45°] carbon/epoxy cylinder with an effective length of 203 mm and internal diameter of 203 mm. The shell thickness was 0.28 mm. The ply properties were: E_{11} = 144.8 GPa, E_{22} = 9.655 GPa, G_{12} = 5.862 GPa, and ν_{12} = 0.25. The effects of unilateral and bilateral constraints on the cylindrical shell were studied by considering three conditions: unilateral outer and inner constraints, respectively, and bilateral constraints. In total, six cases were considered whereby the lateral constraint or the gap between the constraint and the cylinder were changed.

The lateral constraint was assumed to be rigid and was numerically modeled by defining a rigid cylinder, and contact interaction parameters were defined between the constraining surfaces and the cylindrical shell. The contact interaction properties were a no-penetration condition in the normal direction to the surfaces and a frictionless response in the tangential direction [10]. It should be noted that further investigation is needed to consider the effect of friction between the interacting surfaces. All models in this section were subjected to a 5 mm shortening in the axial direction. The analyses only considered nonlinear elastic response.

The postbuckling responses of Cases 2, 3 and 4 along with the base or unconstrained shell (Case 1) are plotted in Figure 6-1. It can be seen that the outer unilaterally constrained condition did not significantly improve the mode transition response of the base cylinder. Conversely, the unilateral inner constraint allowed the generation of multiple local mode transitions with a noticeable stiffening response, rather than a softening one, after the second major bifurcation event. The bilaterally constrained case did not significantly affect the response achieved with the

inner unilateral constraint. A summary of the postbuckling response characteristics of all cases is provided in Table 6-1.

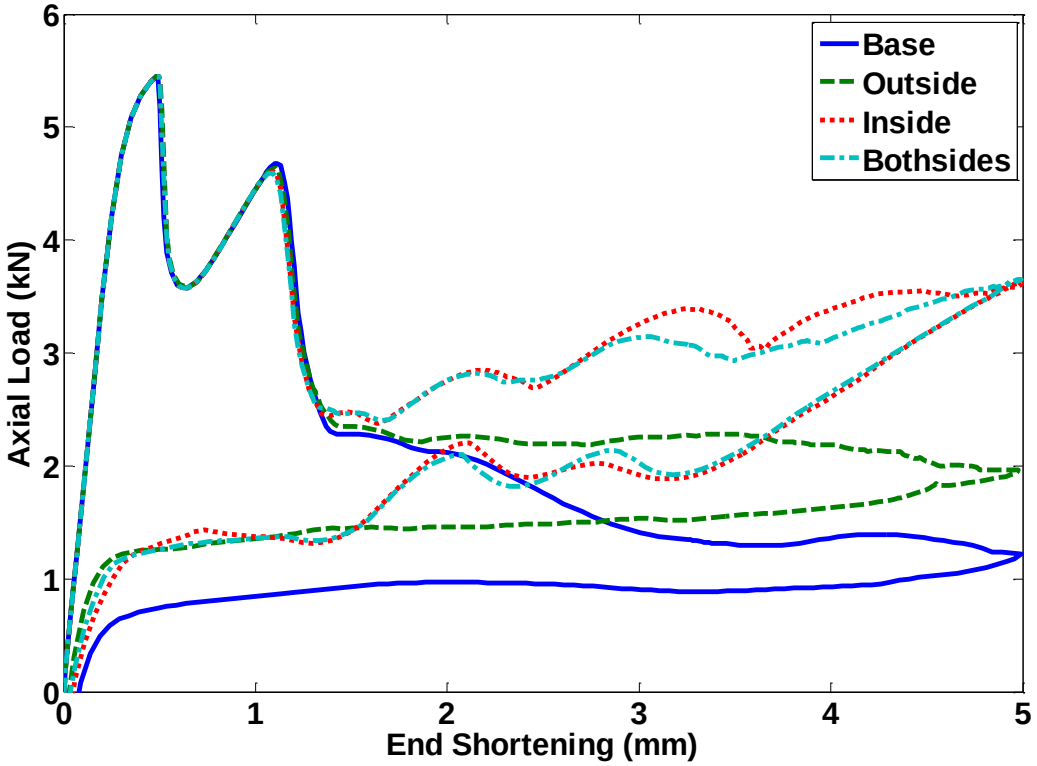

Figure 6-1: Predicted postbuckling response of laterally constrained CFRP cylindrical shells.

The postbuckling responses of Cases 5 and 6 along with the base specimen are plotted in Figure 6-2, which shows the influence of the gap size on the postbuckling behavior of the inner unilaterally constrained cases. It can be seen that reducing the gap increases the number of mode transitions and increases the post-buckling stiffening behavior to levels that even surpass the initial buckling load.

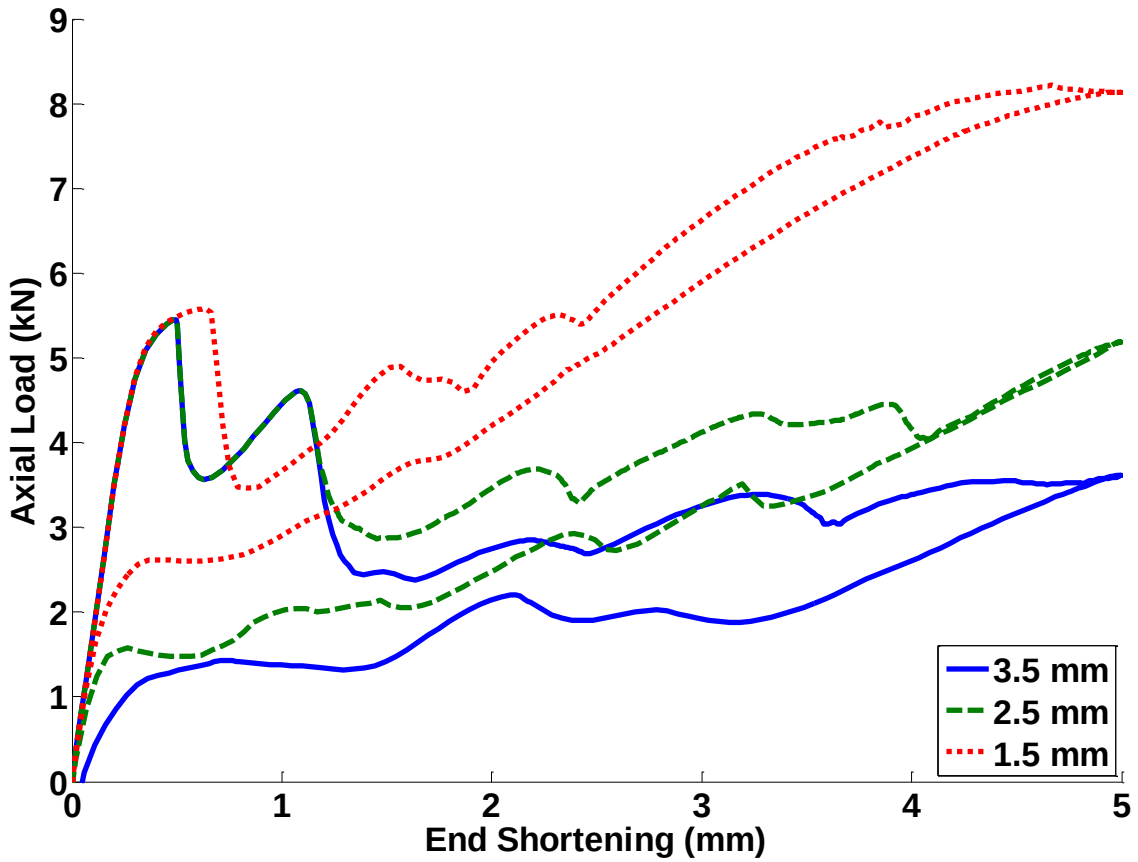

Figure 6-2: Effect of gap size on the postbuckling response of inner constrained cylinders.

Table 6-1: Postbuckling response of cylinders with lateral constraints.

#	Lateral constriant	Gap (mm)	P_1 (kN)	$\lvert\Delta P_1\rvert$ (kN)	δ_1 (mm)	A (J)	n
1	N/A	N/A	5.45	0.77	0.63	6.58	2
2	Outer	3.5	5.45	0.82	0.61	5.74	4
3	Inner	3.5	5.45	0.84	0.60	6.41	6
4	Both	3.5	5.45	0.86	0.59	6.04	5
5	Inner	2.5	5.45	0.84	0.60	5.19	6
6	Inner	1.5	5.59	0.69	0.93	4.18	5

6.3 Experimental results: inner-constrained cylinders

The effect of an inner constraint on postbuckling response was experimentally investigated on uniform (carbon/epoxy) and patterned hybrid (carbon/E-glass/epoxy) composite cylinders. The lateral constraint was an aluminum cylinder: (6.4 mm thick, 249 mm long and 203 mm in outer diameter). The inner constraining cylinder was machined to make it thinner in its center 224 mm region to create a gap between it and the test sample. The aluminum cylinder was placed inside the cylindrical shell test unit allowing for a space of 5 mm at the top for the end shortening of the specimen during testing. A photograph and schematic of the inner constraint setup is shown in Figure 6-3. The evaluation of uniform and patterned hybrid cylinder designs is presented in the following two sections, respectively.

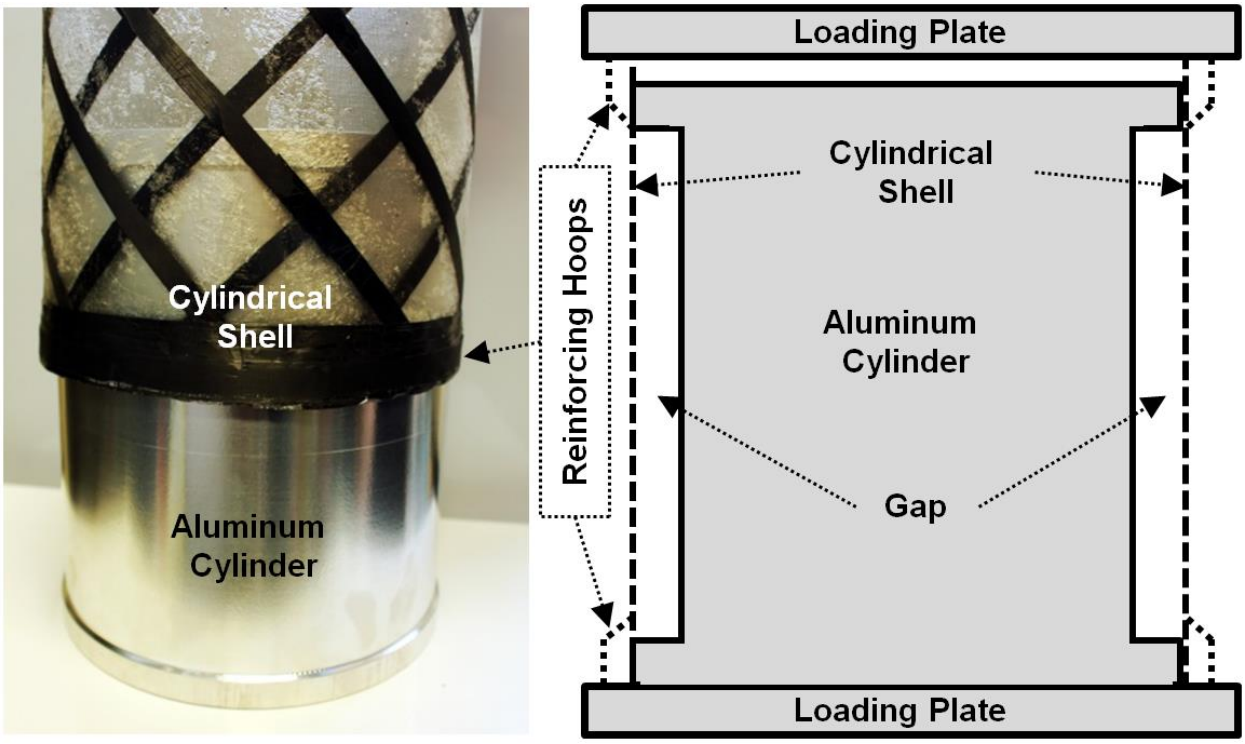

Figure 6-3: Photograph and details of continuous inner lateral constraint for cylindrical shells.

6.3.1 Angle-ply carbon/epoxy cylinders

Two test series on inner-constrained uniform laminated cylinders are reported in this section, including two new unconstrained shell tests (UC-1 and UC-2) as base cases. The test unit was a [45 °/-45 °] angle-ply carbon/epoxy cylinder.

The first constrained test was one in which the gap between the test unit and the inner constraint was 1.6 mm. The postbuckling responses of the constrained shell (C-1A) along with the unconstrained shell (UC-1) when subjected to a total end shortening of 0.55 mm are plotted in Figure 6-4(a). In the second test series the cylinders were axially shortened to 0.75 mm and the gap between the test unit and the inner constraint was increased to 2.4 mm. The constrained cylinder was tested three times to measure the effect of imperfection sensitivity. The position of the cylinder and aluminum plates in case C-2B was rotated in-plane by 90 ° from that of case C-2A. Case C-2C is the reloading cycle of case C-2B with same set-up. The postbuckling responses for these tests (except C-2C since the response was similar to that of C-2B) along with an unconstrained shell test (UC-2) are shown in Figure 6-4(b).

Several observations can be made on the force-displacement responses shown in Figure 6-4 and the summary of characteristic postbuckling features given in Table 6-2. First, it can be seen that the initial stiffness (K_i = 7133 N/mm) and first buckling load were the same for the constrained and unconstrained shells. However, after first the bifurcation the constrained cylinders were able to sustain increasing axial loads, surpassing the first bifurcation load and they experienced additional local snap-buckling events before a reduction in load capacity was observed. Conversely, the capacity of the unconstrained cylinders progressively reduced after the first bifurcation event. Nonetheless, it was interesting to observe that the number of mode transitions in the constrained and unconstrained cases was the same when subjected to an equal

total axial deformation. Another distinct feature is that the stiffness of the postbuckling equilibrium branches for the constrained cylinders did not degrade as rapidly as for the unconstrained cases and that the stiffness upon unloading was still significant (loss of about 36% from the initial stiffness). Therefore, further axial shortening, additional snap buckling events and higher energy dissipation may be possible for constrained cylinders (assuming that elastic response can still be preserved). However, the results for the second test series (Figure 6-4b) show that imperfections continue to have a large role even when transverse deformation are rigidly constrained.

Table 6-2: Experimental postbuckling response of inner-constrained carbon/epoxy cylinders.

Test ID	Gap	End Shorten (mm)	K_e (N/mm)	P_{cr1} (kN)	P_{max} (kN)	ΔP_{max} (kN)	δ_{max} (mm)	A (mJ)	n
UC-1	N/A	0.55	224	2103	2103	312	0.07	114	9
C-1A	1.6	0.55	4545	2075	2745	335	0.08	135	9
UC-2	N/A	0.75	127	1984	1984	349	0.19	163	11
C-2A	2.4	0.75	2194	1941	2475	459	0.09	208	11
C-2B	2.4	0.75	1696	2051	2591	923	0.11	248	11
C-2C	2.4	0.75	2679	2082	2662	771	0.10	189	11

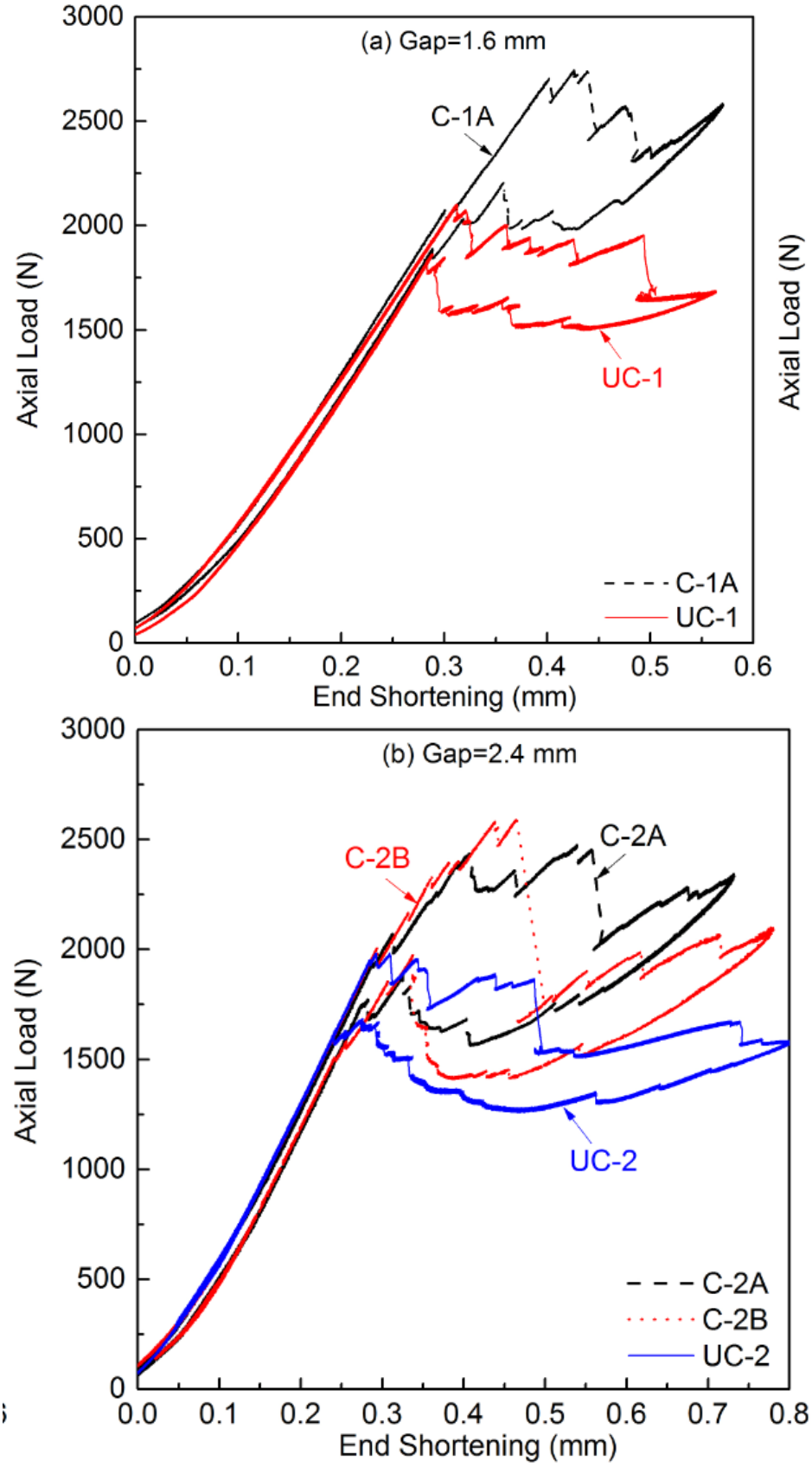

Figure 6-4: Observed postbuckling response of laterally constrained CFRP cylindrical shells.

6.3.2 Hybrid cylinders

The effect of a uniform inner rigid constraint on patterned hybrid cylinders is reported in this section. The test units were two of the hybrid carbon/E-glass/epoxy cylinders with patterned material stiffness presented in Section 5.2.3, namely designs [30/G/-30] and [0/G/90] (see Figure 5-2). Two test series were also conducted. The first test sequence evaluated the performance of the constrained [30/G/-30] hybrid cylinder (C30-1) with a gap of 1.6 mm between the test unit and the inner constraint. The force-deformation response for the C30-1 sample and the corresponding unconstrained test (UC-30) is plotted in Figure 6-5(a) and key postbuckling response values are given in Table 6-3. Similar to the observations made for the carbon/epoxy cylinders, the postbuckling response of the constrained hybrid cylinder surpassed the initial buckling load without a significant loss in stiffness. However, in this case the constrained cylinder was able to attain more mode-jumping events, although the load drops during these transitions were much smaller than those for the unconstrained cylinder. One of the reasons for this behavior is that the gap between the test specimen and lateral constraint restricted the full transverse deformations from the snap-through events.

The second test series evaluated the response of the [0/G/90] hybrid cylinder with a gap of 2.4 mm to the inner constraint. First, two independent constrained tests were performed (C90-A and C90-B) to evaluate repeatability of the behavior with an end axial shortening of 0.75 mm. For the third test in the series (C90-C) the constrained hybrid cylinder was subjected to a total end shortening of 1.1 mm. The force-deformation responses of these tests (except C90-A since its response was similar to that of C90-B) are compared to that of the corresponding unconstrained hybrid cylinder (UC-90) in Figure 6-5(b) and key postbuckling response values are listed in Table 6-3. All of the observations made previously for the [30/G/-30] tests apply to these test

series as well. A difference in this test series is that the stiffness in the first loading branch for the constrained and unconstrained cylinders diverges significantly before the first bifurcation. This is attributed to the larger transverse deformations experienced by the unconstrained cylinder in the first global buckling mode, a response particular for this material arrangement.

The other different feature in the [0/G/90] responses is that, while the load drops from the mode jumping events were still smaller for the constrained cylinders, this design did have larger load drops than what was observed in the C30-1 test. This is attributed to the 0^o oriented carbon/epoxy strips used in the [0/G/90] hybrid shells, which can accumulate more strain energy before reaching a critical instability point. Finally, the decrease of initial stiffness and first buckling load from test C90-A to C90-C may indicate some material-level damage. In fact, some fiber damage was visually observed in test C90-C when the specimen was subjected to a larger end shortening. The use of more flexible materials, perhaps other than laminated composites, may be necessary to avoid damage in the far elastic postbuckling response and allow the triggering of more snap-through events.

Table 6-3: Experimental postbuckling response of inner-constrained patterned hybrid cylinders.

Test ID	Gap	End Shorten (mm)	K_e (N/mm)	P_{cr1} (kN)	P_{max} (kN)	ΔP_{max} (kN)	δ_{max} (mm)	A (mJ)	n
UC-30	N/A	0.55	-475	4126	4163	904	0.16	1035	5
C30-1	1.6	0.55	3136	3760	5550	185	0.09	765	9
UC-90	N/A	0.75	75	3700	4671	1002	0.27	501	4
C90-A	2.4	0.75	7110	3477	5559	106	0.12	339	7
C90-B	2.4	0.75	6014	3476	5451	195	0.15	295	7
C90-C	2.4	1.1	4667	3223	5827	601	0.11	898	11

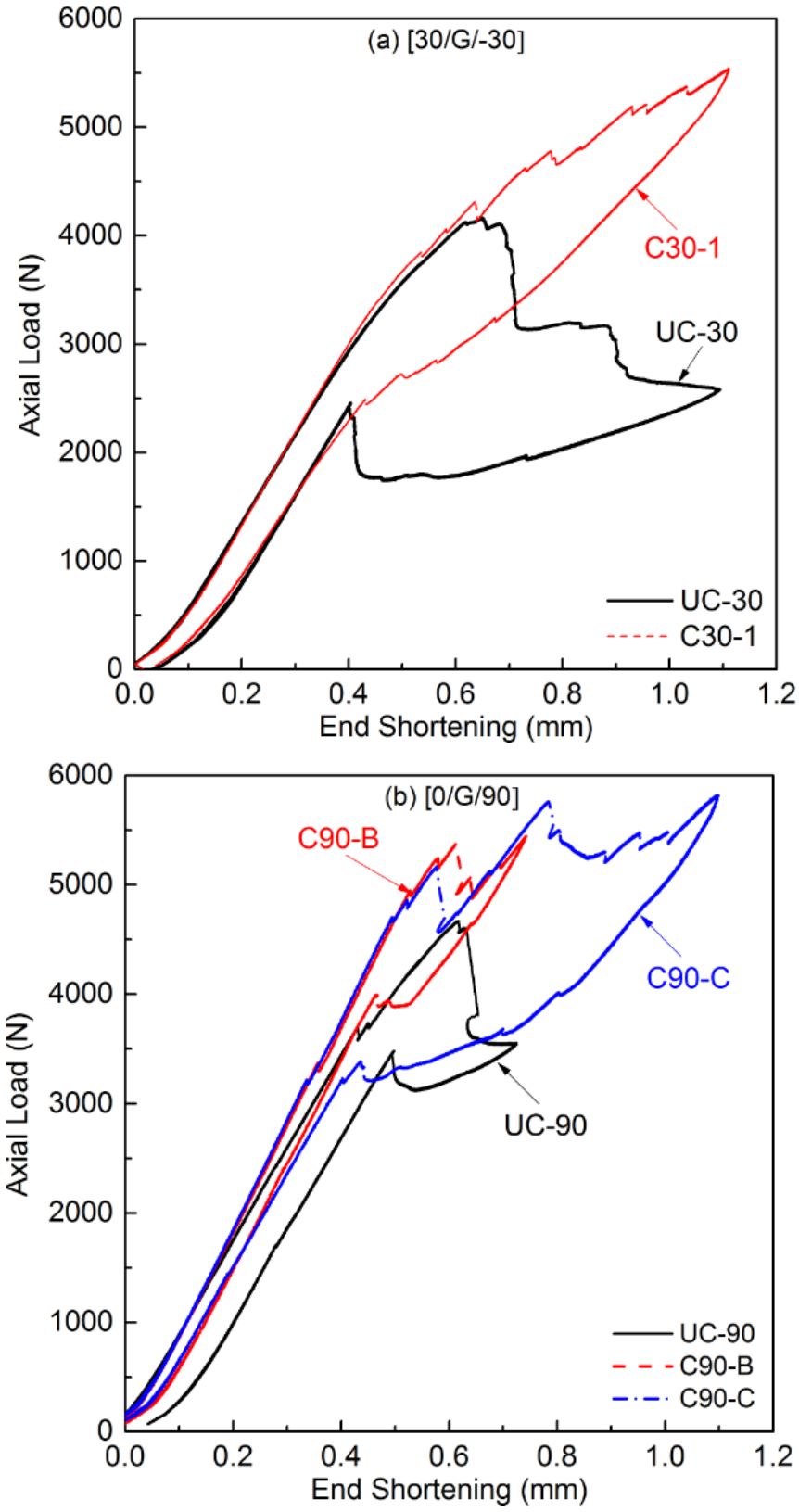

Figure 6-5: Observed postbuckling response of laterally constrained hybrid cylindrical shells.

6.4 Multi-walled cylinder

Results in Section 6.3 showed that a unilateral inner constraint to the transverse deformations during postbuckling response can increase the number of mode transitions and the post-buckling stiffening behavior to levels that even surpass the initial buckling load. In this section, the inner constraint was replaced by a deformable cylindrical shell in order to create interaction between the walls of both cylinders. Experimental tests and numerical results are presented.

The rationale behind the LCI concept is to take advantage of the collective response and interactions of an array of cylinders such that the postbuckling response of the system can be further modified and tailored. This concept is inspired by studies on the buckling of constrained columns [172, 252] and plates [74], as well the study presented in Section 6.3 [45]. The LCI cylinder was driven by obtaining more mode transitions in the postbuckling regime compared to SGI and NSD cylinders since the provision of multiple walls can lead to interactions in the elastic postbuckling regime. With variations in boundary conditions, the postbuckling responses of LCI cylinders are expected to be modified.

6.4.1 Experimental test

Two LCI cylinders were designed and fabricated to study the interaction between multi-wall cylinders. The pilot study reported in [45] showed that limiting the amplitude of transverse deformations can significantly modify the postbuckling response of cylindrical shells with a noticeable stiffening response, rather than a softening one in the far elastic postbuckling regime. In this study, a double-wall cylinder was designed from the uniform cylinder (inner diameter of 80 mm) and an inner cylinder with a smaller diameter (70 mm) was added thus creating a gap of 5 mm from the outer cylinder.

The resulting force-displacement responses of a double-wall LCI cylinder and a uniform cylinder with a thickness of 0.5 mm are shown in Figure 6-6. The presented results show that the force-deformation response of the LCI cylinder is characterized by a significant increase of stiffness, maximum load drop and enclosed area. The LCI cylinders were able to sustain increasing axial loads and attaining additional local snap-buckling events. It was interesting to observe that the number of mode transitions in the LCI cylinder is twice compared to those of the uniform cylinder when subjected to an equal total end shortening. Another distinct feature is that the stiffness of the postbuckling equilibrium branches for the LCI cylinders did not degrade as rapidly as for the uniform cylinder.

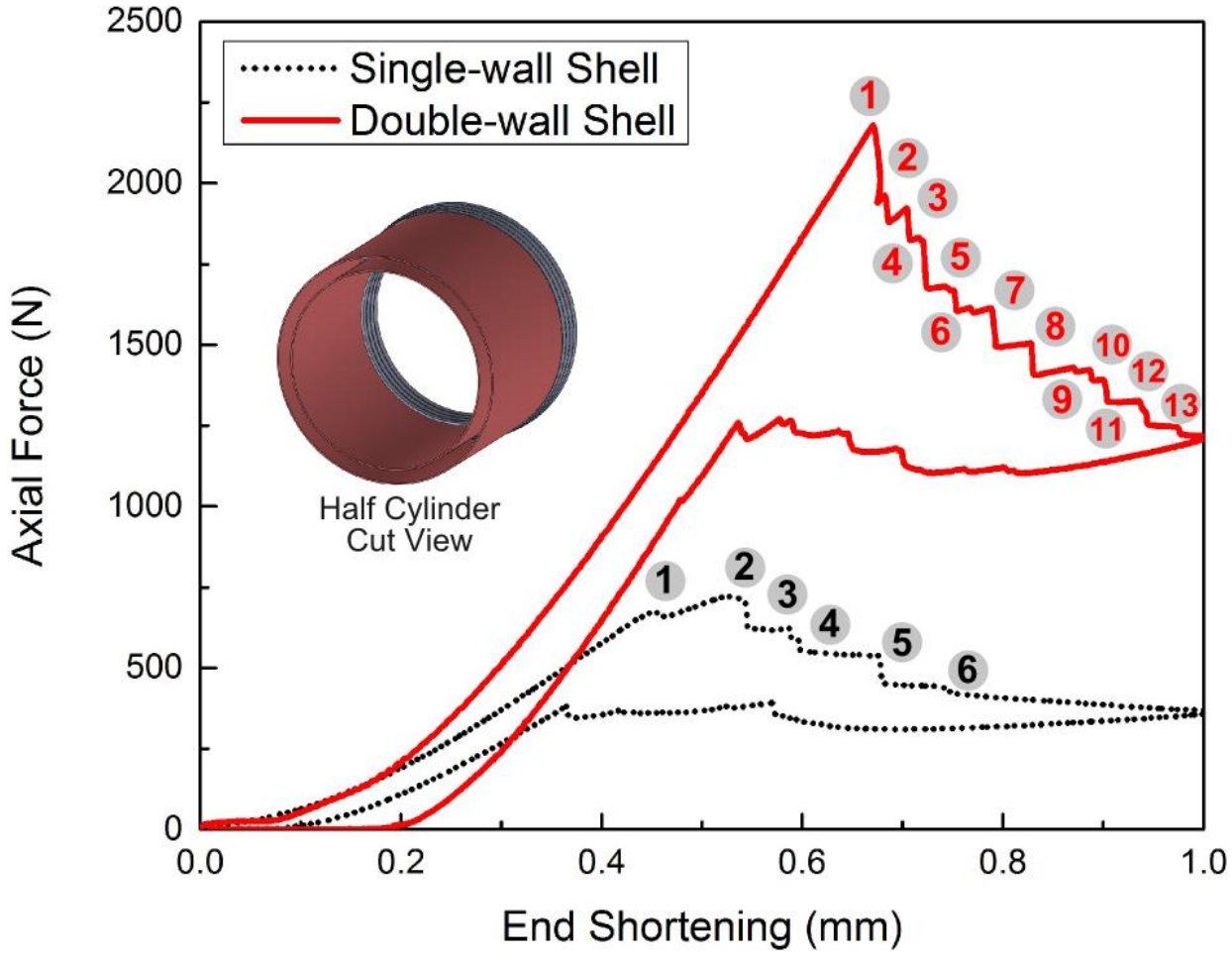

Figure 6-6: Obtained postbuckling responses of LCI double-walled cylinder.

It was hypothesized that reducing the gap may increase more mode transitions. Thus, an additional LCI cylinder was built with a triple-wall feature. In order to achieve, the length of the triple-wall cylinder was reduced to 60 mm and the radius was reduced to 20 mm in order to have similar stiffness of the double-wall cylinder. Figure 6-7 shows the load-shortening response and it can be seen that the initial stiffness up to a shortening of 0.5 mm was the same for both LCI cylinders. However, the triple-wall cylinder was able to sustain increasing axial loads and a larger enclosed area (hysteretic area) was achieved. It is interesting to see that the number of localized buckling events was same for both cases. Further, the use of different geometry and stiffness distribution for each wall may provide additional ways to control the localized buckling events. Overall, after first the bifurcation the interaction of nested cylinders was able to trigger a relatively higher number of mode transitions in the elastic postbuckling regime.

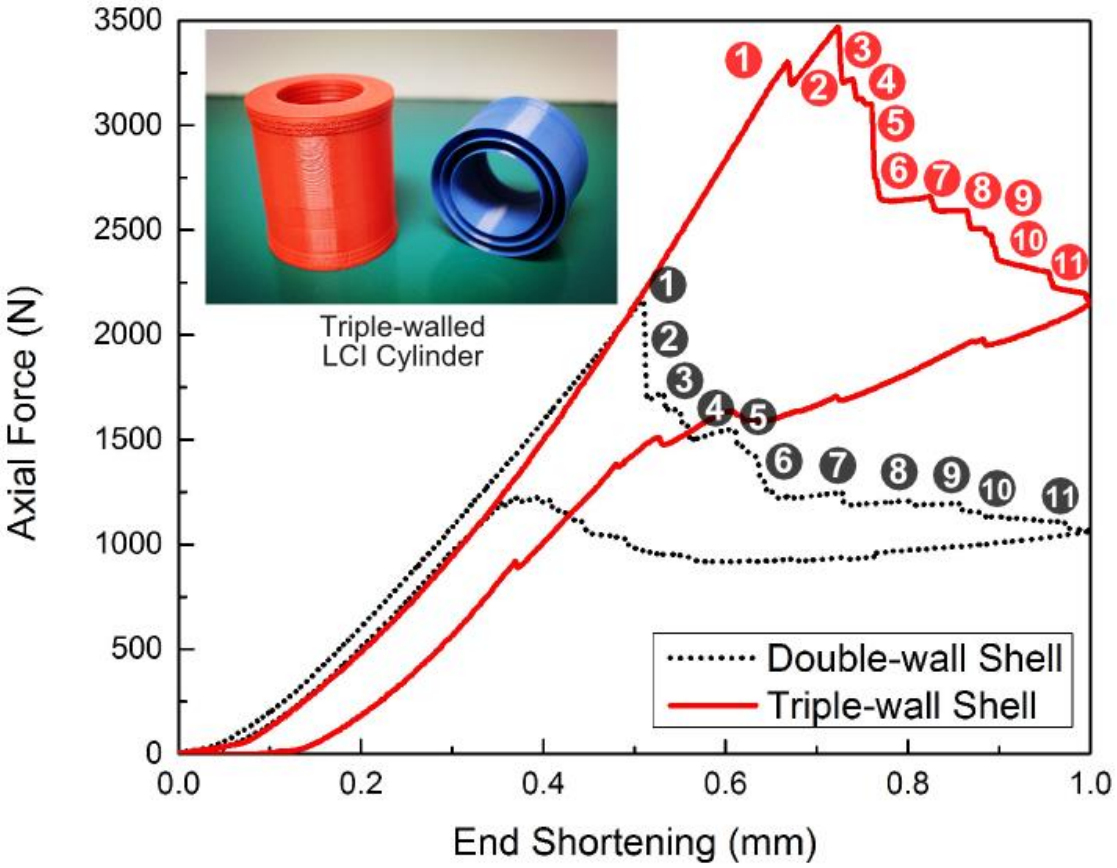

Figure 6-7: Obtained postbuckling responses of LCI triple-walled cylinder.

6.4.2 Numerical simulation

The results of Figure 6-6 seem to indicate that there was no interaction between walls. Thus, a numerical simulation was conducted on a double-walled SGI cylinder group to showcase the interaction between each SGI component. Two SGI designs were selected with different *m*–*n* combinations, one as M8N8 and the other as M4N10. Both cylinders had the same length and wall thickness, and a gap of 5 mm was defined by making the inside cylinder (M8N8) have a smaller diameter than the outside one (M4N10). The simulated force-deformation responses for the individual cylinders and the assembly (LCI design) for two different gap sizes (2 and 5 mm) are shown in Figure 6-8.

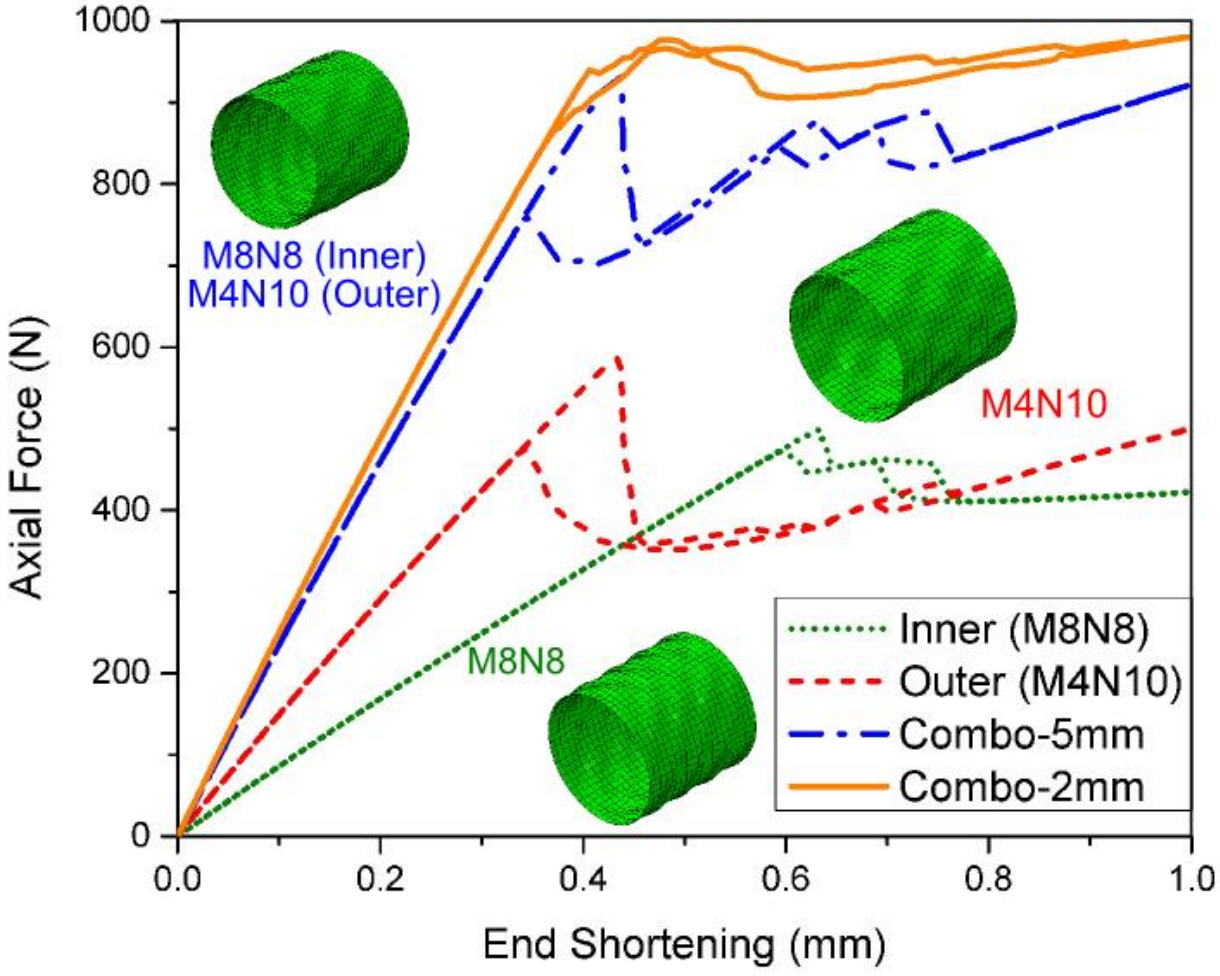

Figure 6-8: Estimated postbuckling responses of double-walled LCI cylinders.

It can be seen in Figure 6-8 that the individual responses of the cylinders show different characteristics: a large load drop for M4N10 versus two smaller drops for M8N8. As observed in the test, the simulated result for the LCI cylinder with a 5 mm gap had a combined response from each SGI cylinder without much interaction between the walls. The number of mode transition was the addition from those of each cylinder. However, the total load capacity, initial stiffness and enclosed area of the response curve were higher for the LCI cylinder than for either of the single cylinders.

Reducing the gap between the cylinders is expected to increase the number of mode transitions, see Section 6.3 and reference [45]. The results in Figure 6-8 show that the LCI cylinder with a 2 mm gap attained a larger number of mode transitions and a sustaining response type. Another distinct feature of the LCI design with a 2 mm gap is that the stiffness of the postbuckling equilibrium branches (individual loading paths between mode transitions) did not degrade as rapidly as for the LCI cylinder with a 5 mm gap due to interaction between cylinders. The postbuckling response summary of these four cases is given in Table 6-4.

Table 6-4: Postbuckling response of double-walled cylinder with SGI components.

Specimen	K_i (N/mm)	P_{max} (N)	ΔP_{max} (N)	δ_{max} (mm)	A (mJ)	n
M8N8-Inner	867.4	498.6	51.4	0.07	4.13	2
M4N10-Outer	1511	585.9	226.6	0.14	17.7	4
Combo-5mm	2378.2	939.0	207.6	0.14	21.8	5
Combo-2mm	2530.8	980.3	25.2	0.11	12.2	9

6.5 Summary

This chapter presented the evaluation of a concept for cylinders with lateral constraints and interactions (LCI) by providing uniform constraints and introducing a multi-wall cylinder group with the aim of triggering multiple mode transitions in the elastic postbuckling regime. Experimental and numerical studies showcased and evaluated such boundary condition for modifying and controlling the postbuckling response of axially-compressed cylindrical shells. The results indicate new possibilities for the design of advanced materials, devices and structures. The following conclusions were drawn from the study presented in this chapter:

(1) Although the initial stiffness was the same for the constrained and unconstrained shells, after first the bifurcation the constrained cylinders were able to sustain increasing axial loads, surpassing the first bifurcation load and attaining additional local snap-buckling events before a reduction in load capacity was observed.

(2) Constrained cylinders are able to attain more mode-jumping events, although the load drops during these transitions were smaller than those for the unconstrained one. Additional mode transitions and higher energy dissipation may be possible for constrained cylinders with further axial shortening.

(3) The possibility of further controlling the postbuckling reponse of cylinders through SGI designs was numerically demonstrated through a double-walled cylinder with two SGI components. It was shown that the postbuckling response of the double-walled cylinder can be further tailored by changing the “imperfect” geometry and the gap between nested cylinders. Assembly of multiple concentric SGI cylinders allows obtaining a more mode transitions in the elastic postbuckling regime, and reducing the gap between cylinders can create a sustaining postbuckling response due to their interaction.

Chapter 7

Tailoring Postbuckling Response toward Potential Applications

7.1 Overview

The experimental and numerical results in support of the three proposed design concepts presented in Chapter 4 to Chapter 6 indicate that cylindrical shell under axial compression are a viable structural prototype for obtaining an elastic postbuckling response with tailorable features. This chapter is an extension of the main research endeavor with the objective of exploring uses for the tailored postbuckling response of cylindrical shells. Optimization techniques were exploited to achieve the desired target response and benchmark experiments were used validate computational designs and simulations. The dynamic features of the postbuckling response are discussed and efforts on obtaining repeatable and scalable postbuckling behavior are presented. The knowledge gained provides guidance for the use of tailorable structural instability. The study presented in this chapter was submitted to the *International Journal of Solids and Structures* for consideration as a technical publication.

7.2 Response domain exploration

Chapter 4 presented the study of baseline SGI cylinders seeded from a single mode shape. This section presents different *m*–*n* combinations to further tailor the postbuckling behavior. A total of 14 SGI cylindrical shells were fabricated via 3D printing. The length, radius and

thickness of all cylinders were reported in Section 4.2.2. The selected mode shapes are well distributed on the Koiter circle, as seen by the labeled numbers in Figure 7-1(a) and final products are shown in Figure 7-1(b). These SGI cylinders were selected to represent the entire design domain, with the aim of studying the effect of axial and circumferential wavenumbers on the postbuckling response characteristics.

The postbuckling responses of three out of 14 SGI cylinders (M8N12, M11N2, and M11N8) are shown in Figure 7-2 and used to compare the variation of response type due to the SGI designs. All cylinders were subjected to a total shortening of 1.0 mm. As expected, the postbuckling behavior is quite different in terms of the key parameters (K_i, P_{max}, ΔP_{max}, δ_{max}, A, and n_t) given in Figure 3-12. Due to different number of waves on two directions, these designs showcased three different postbuckling characteristics under the same seeding amplitude, including softening (M11N8), sustaining (M8N12) and stiffening (M11N2) responses. It can be observed that cylinder M11N8 had more localized buckling events (seven), than the other two SGI cylinders. Cylinder M8N12 had four load drops in the response curve and cylinder M11N2 had only one small load drop., The maximum magnitude of single load drop was similar for cylinders M11N8 and M8N12, although they had a different number of mode transitions. In contrast, ΔP_{max} in cylinder M11N2 was very small. This result indicates that a larger load drop is usually associated with the shape of the inward region of the SGI cylinder. Due to the higher number of circumferential waves, the small inward regions on the surface of cylinders M11N8 and M8N12 have a diamond shape while cylinder M11N2 only has a large rectangular shape region with the short side along the axial direction

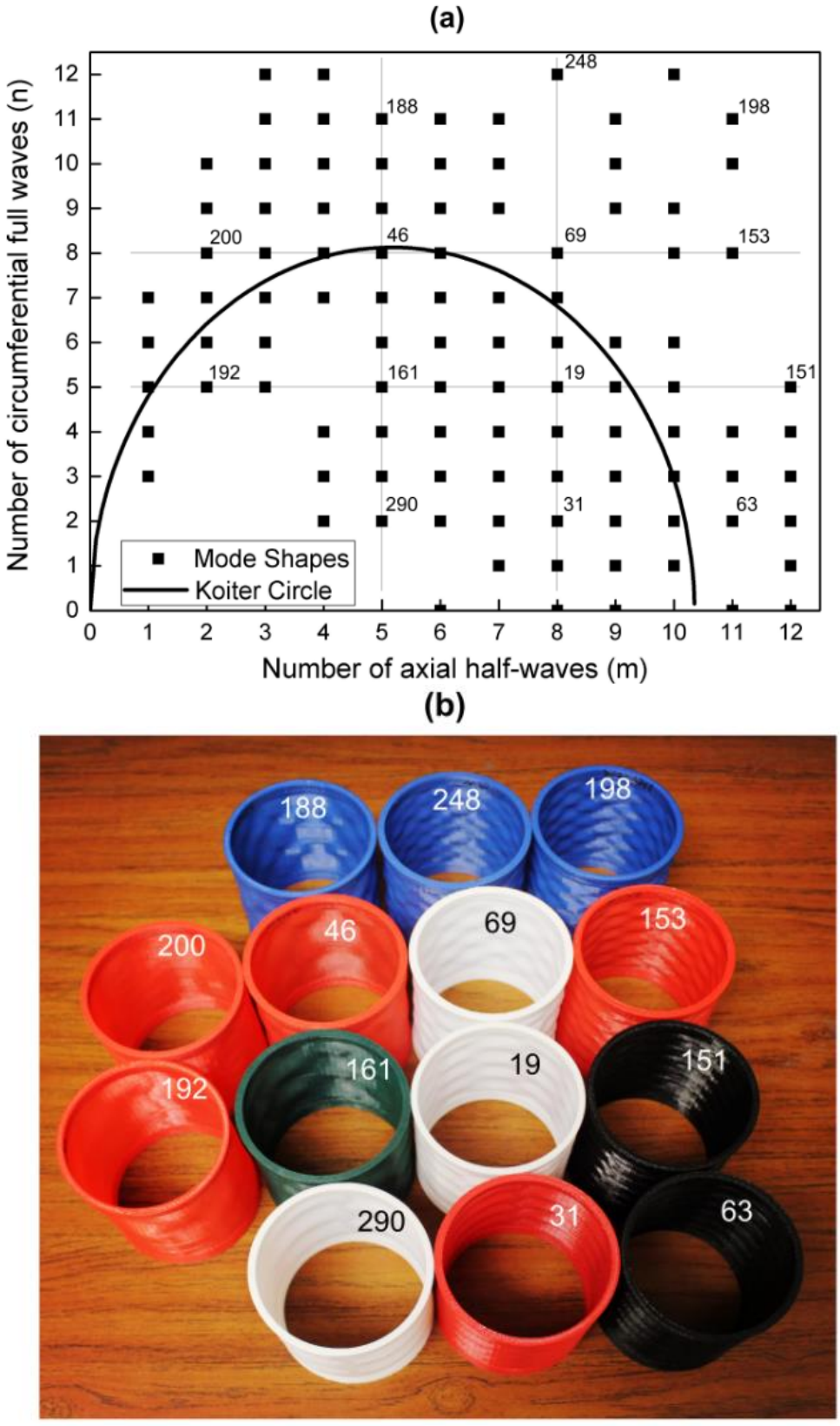

Figure 7-1: Effect of seeding shape (a) locations on the Koiter circle; (b) printed test units.

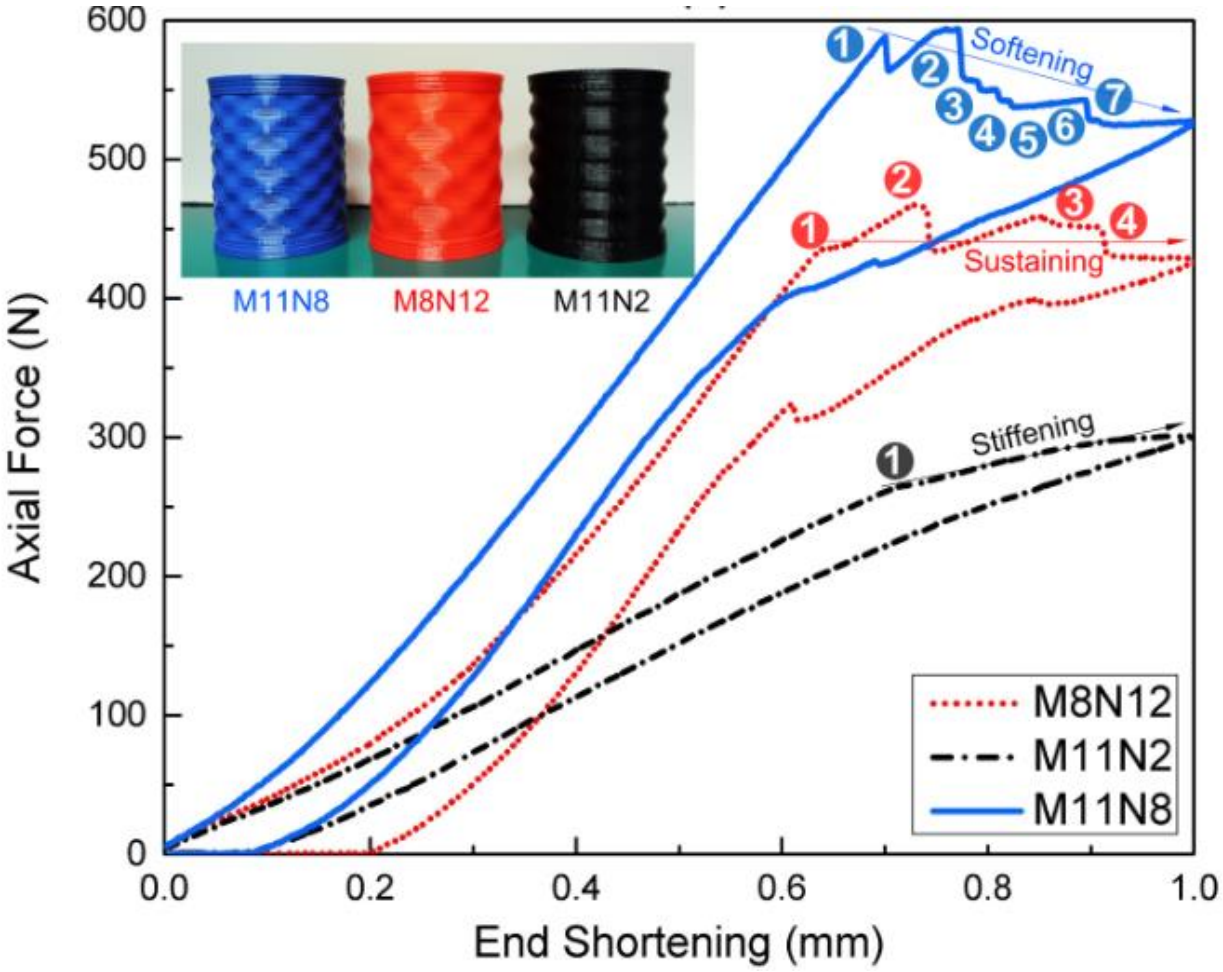

Figure 7-2: Postbuckling response of SGI cylinders with same amplitude but varied geometry.

A response contour based on the test data of all 14 SGI cylinders was plotted in terms of four key parameters: K_i, shown in Figure 7-3, ΔP_{max}, shown in Figure 7-4, A, shown in Figure 7-5 and n_t, shown in Figure 7-6. The intent of these contour maps is to understand the effect of wave numbers for the entire design domain using test results. It can be seen from the plots from Figure 7-3 to Figure 7-5 that the larger response values lie in the upper left corner, where the circumferential wave number is large and the axial wave number is small. This result indicates that a seeding geometry with a lower number of axial waves can achieve a higher stiffness, a higher single load drop and a larger enclosed area.

The numerical study presented in reference [231] found that there is a strong correlation between K_i, ΔP_{max}, and A. These observations are confirmed by the tests reported here. Another interesting finding from Figure 7-3 to Figure 7-5 is that the "hotspot" (i.e., the region with largest parameter value) was from the data of cylinder M5N8 which lies exactly on the top of the Koiter Circle. Further, the data in Figure 7-6 shows that multiple mode jumps in the postbuckling regime were more frequent when the seeded imperfection mode shapes had a relatively large number of waves in the circumferential direction. The "hotspot" in this case was from the cylinder M5N11. The summary of test results for all SGI cylinders is given in Table 7-1.

Based on observed experimental evidence it is proposed that the elastic postbuckling response of axially compressed cylindrical shells can be categorized in three types, as shown in Figure 7-7: stiffening, sustaining and softening. These definitions are based on a ratio of the total load drop (between the first buckling event and the end of the loading phase) to the magnitude of the first critical buckling load. As discussed later in this chapter, each postbuckling response type has its own potential application features.

Table 7-1: Postbuckling response of SGI cylinders with single mode shape as imperfection.

Mode	m	n	K_i (N/mm)	P_{max} (N)	ΔP_{max}(N)	δ_{max}(mm)	A(kJ)	n_t
192	2	5	1203.0	377.6	20.6	0.18	60.6	1
200	2	8	852.1	395.2	24.2	0.32	84.1	2
290	5	2	589.9	333.7	-	-	26.9	0
161	5	5	609.8	356.7	-	-	21.7	0
46	5	8	1153.4	706.5	129.5	0.10	92.0	3
188	5	11	943.2	456.5	24.4	0.14	39.2	8
31	8	2	478.5	304.6	2.5	-	29.8	1
19	8	5	559.7	390.0	1.9	-	40.1	1
69	8	8	676.3	392.4	41.9	0.16	41.9	5
248	8	12	974.0	428.8	25.6	0.24	52.8	3
63	11	2	408.5	299.4	11.2	-	29.0	1
151	11	8	981.4	561.4	23.6	0.09	58.9	5
153	11	11	815.4	402.1	4.8	0.10	44.8	2
198	12	5	610.1	500.4	70.2	-	49.9	1

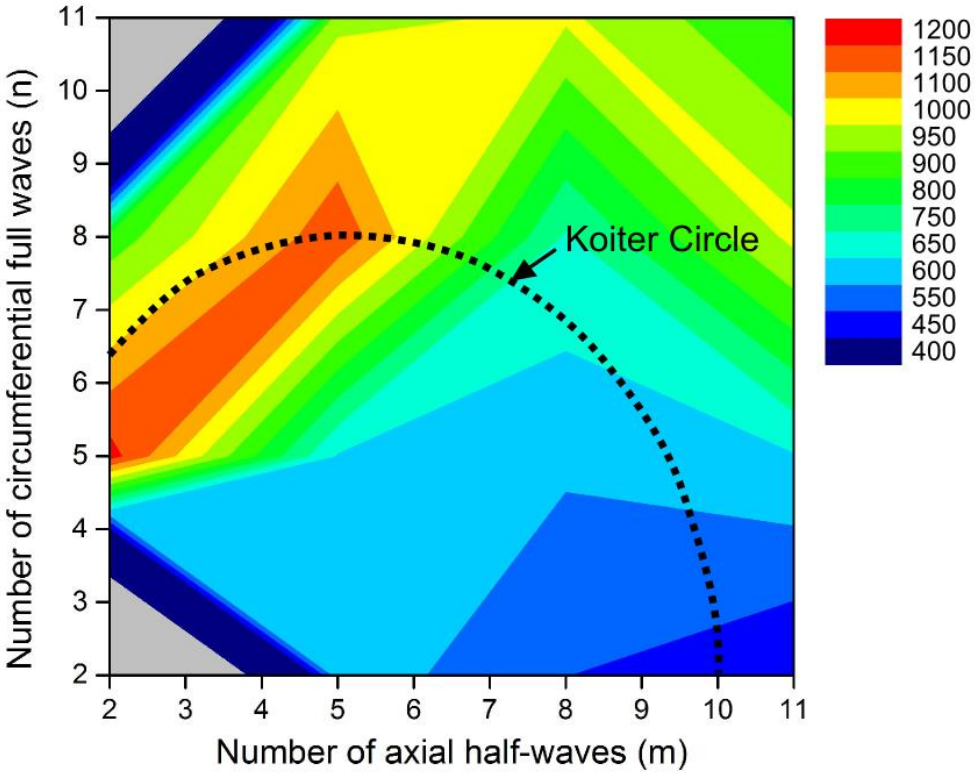

Figure 7-3: Obtained initial stiffness (*Ki*) contour of axially-loaded SGI cylinders.

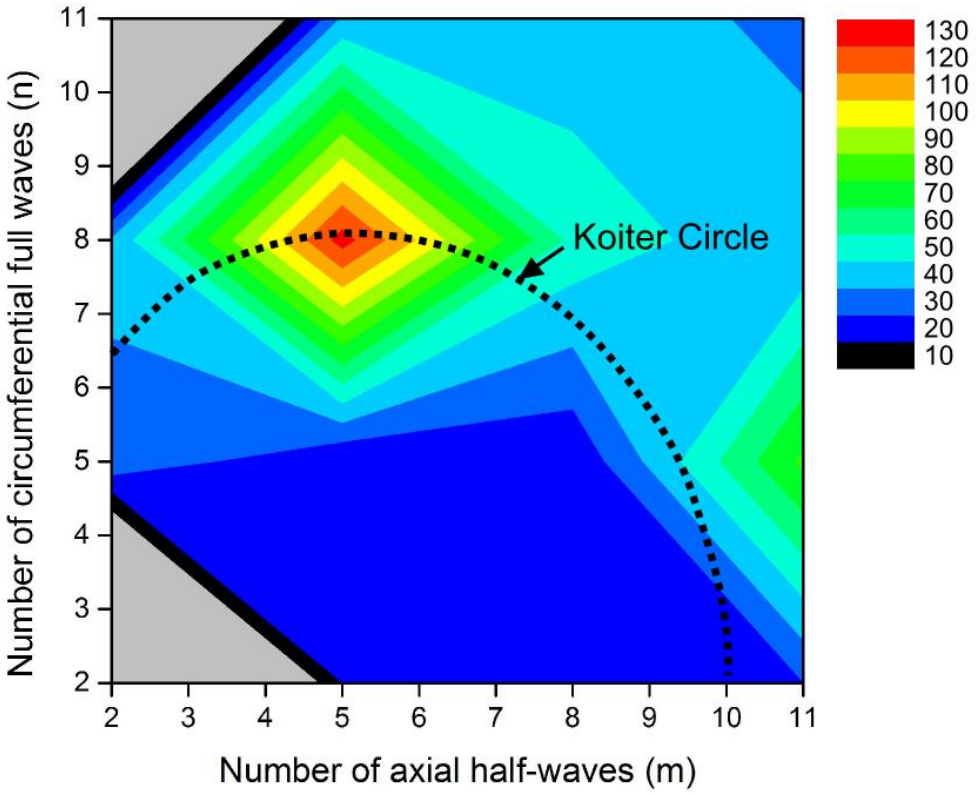

Figure 7-4: Obtained maximum single load drop (ΔP_{max}) contour of axially-loaded SGI cylinders.

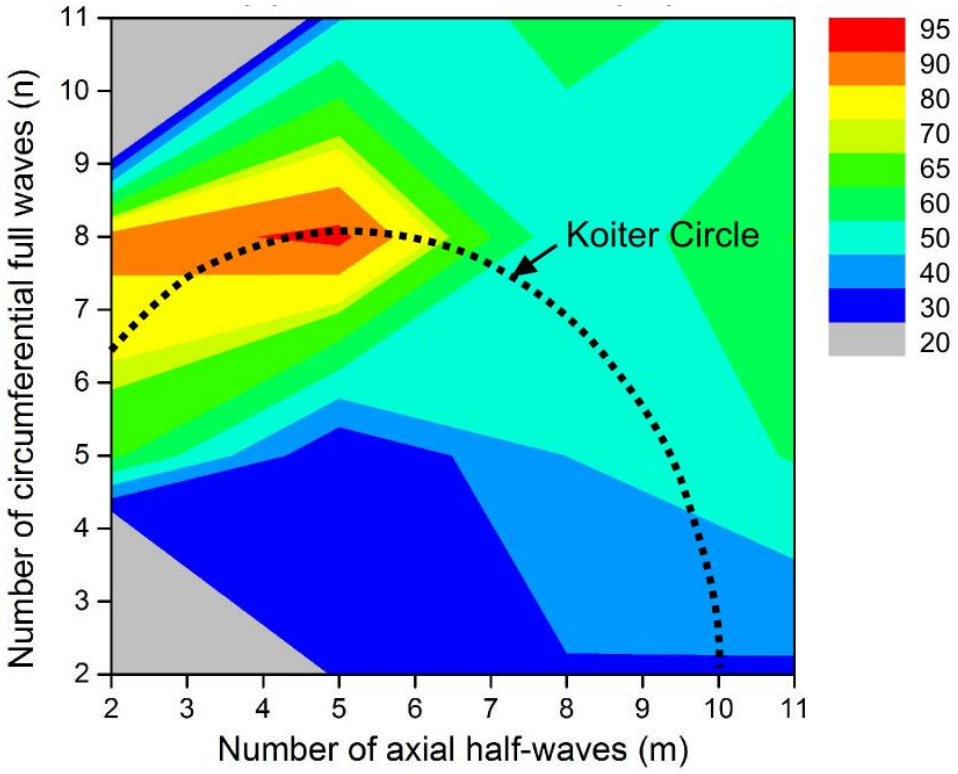

Figure 7-5: Obtained enclosed area (A) contour of axially-loaded SGI cylinders.

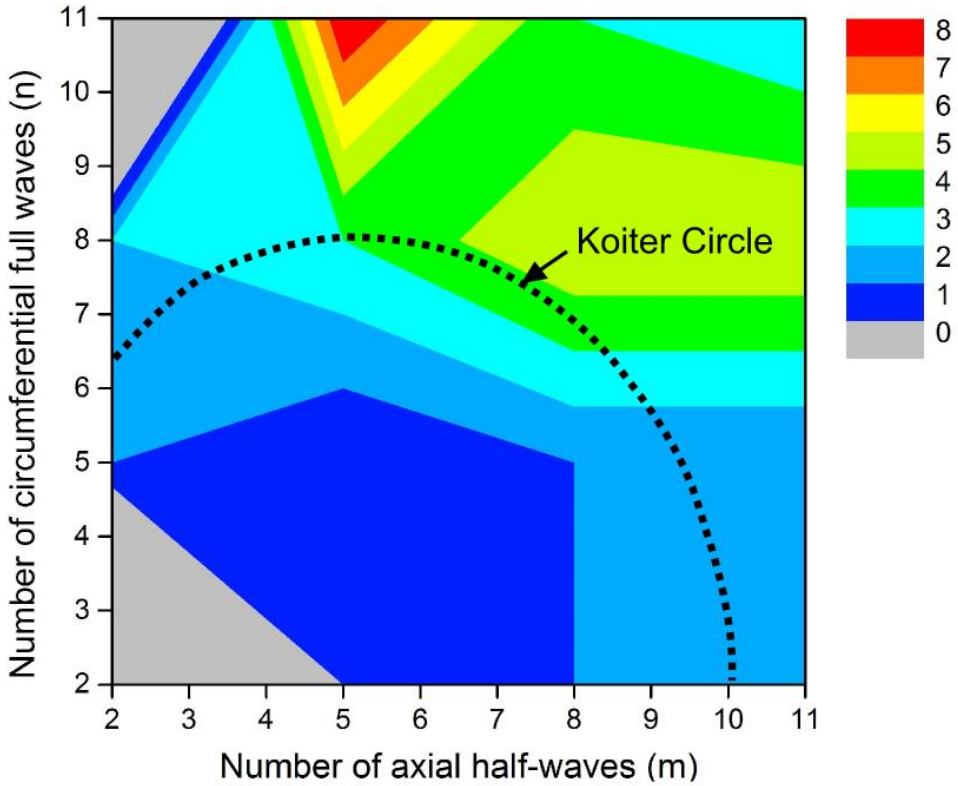

Figure 7-6: Obtained number of mode transitions (n_t) contour of axially-loaded SGI cylinders.

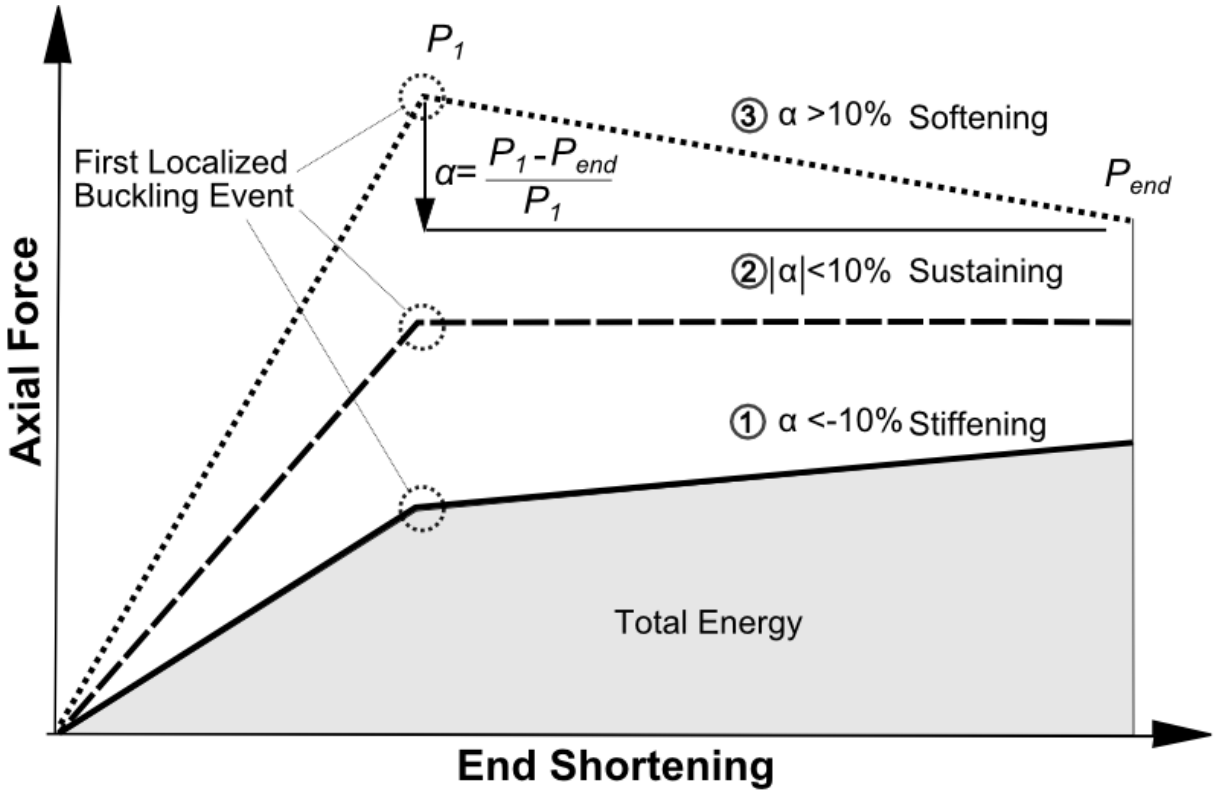

Figure 7-7: General postbuckling response types of an axially-compressed cylindrical shell.

7.3 Optimization for targeted response

It has been shown that an SGI cylinder with a given m-n combination can have a unique postbuckling response. The following section focuses on numerical modeling to explore the postbuckling response of SGI cylinders with different seeded shapes and amplitude through a design optimization process.

Before the optimization approach, a numerical simulation was conducted on the selected baseline SGI cylindrical shells to evaluate the efficiency of the modeling approach. Figure 7-8 shows experimental-numerical comparisons for two cases. The predicted postbuckling response curve for cylinder M5N2 is close to the one in the experiment, while there is larger discrepancy for cylinder M8N8. It is clear that the seeded geometry in cylinder M8N8 provided more

localized inward buckling regions (8×8 = 64) than cylinder M5N2 (5×2 = 10) such that cylinder M8N8 has a higher number of mode transitions, yet it is more vulnerable to initial imperfections. Nonetheless, it is interesting see that the numerical and experimental results for cylinder M8N8 attained the same number of mode transitions. The most important point from the compared responses is that the numerically simulated traces captured the general postbuckling behavior features for two rather different designs (M8N8: softening response; M5N2: stiffening response) even though curves did not exactly match.

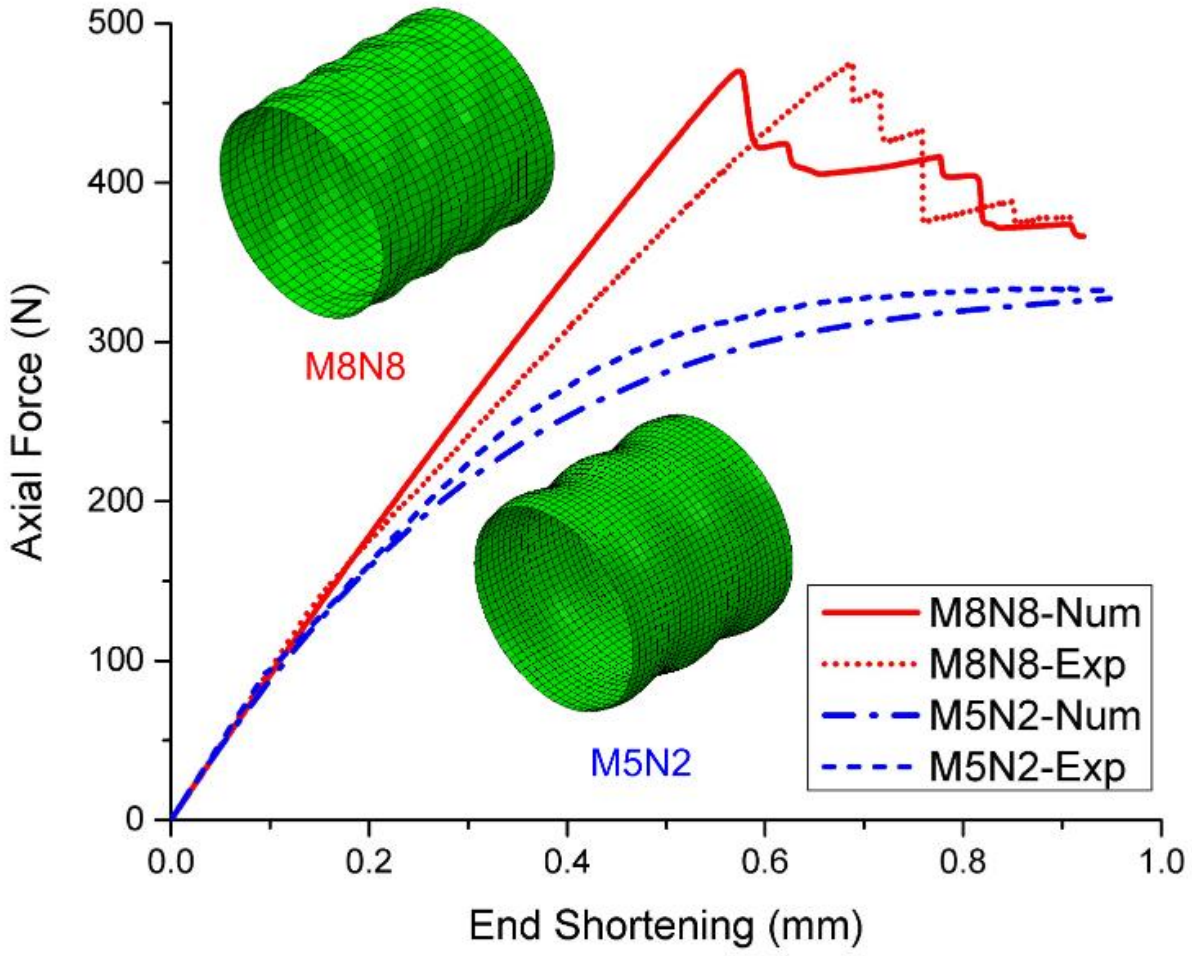

Figure 7-8: Obtained and predicted postbuckling responses of two baseline SGI cylinders.

Based on the numerical results of 14 tested cylinders (see in Section 7.2), response contours for K_i and n_t are shown, respectively, in Figure 7-9 and Figure 7-10. Only the K_i contour is presented given the correlation between K_i, ΔP_{max}, and A. It is interesting to see that these two predicted contours reveal a similar trend to the experimental ones in Figure 7-3 and Figure 7-6. While there are some differences in the actual values, the "hotspots" are predicted in the expected regions. Without measurement of the actual geometric imperfections, disagreement between predicted and measured responses still exists. Nonetheless, the difficulty in predicting the postbuckling behavior of SGI cylinders has been reduced, as compared to predicting the response of an uniform cylinder, due to the use of a governing mode shape as a seeded geometry.

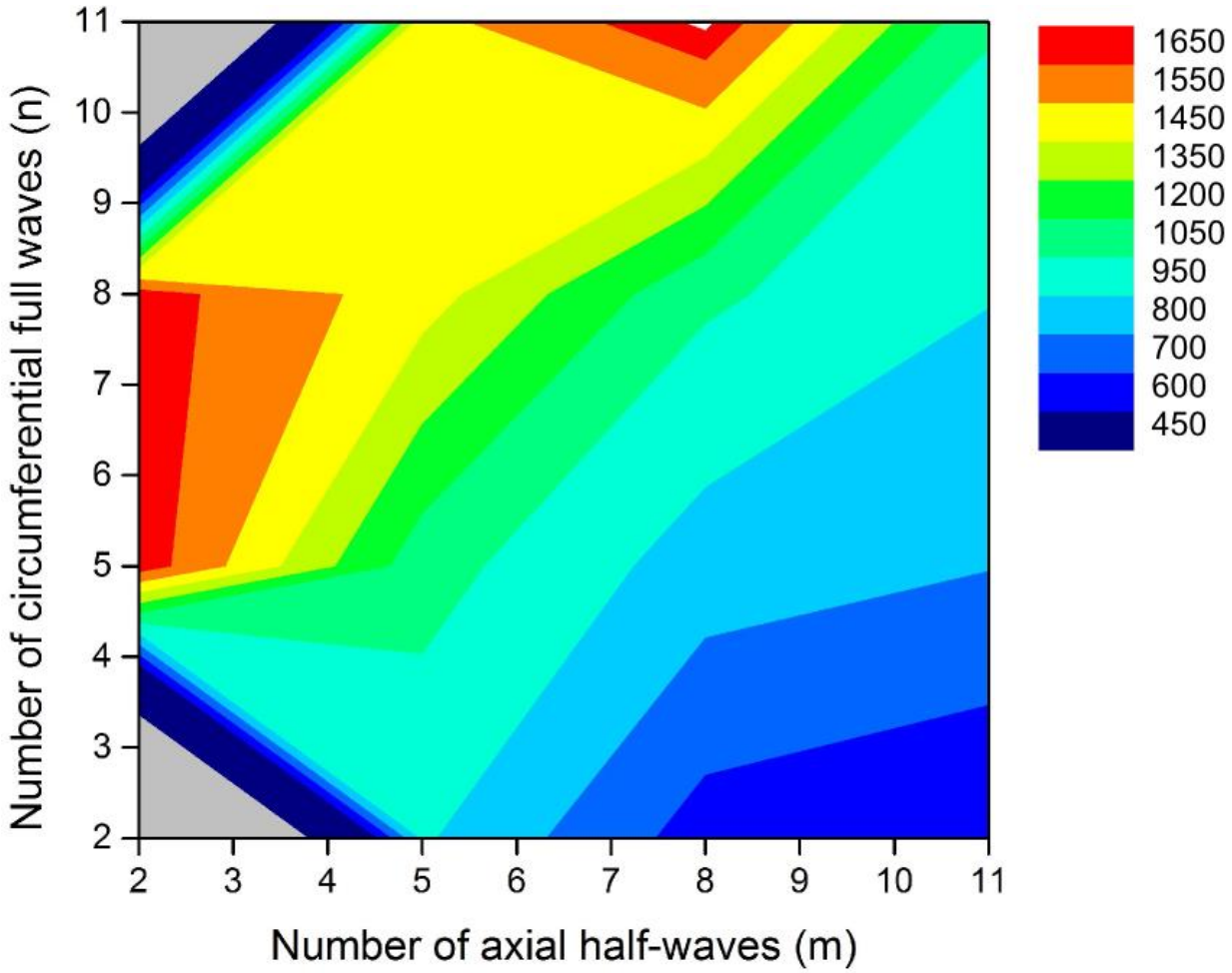

Figure 7-9: Predicted initial stiffness (K_i) contours of SGI cylinders.

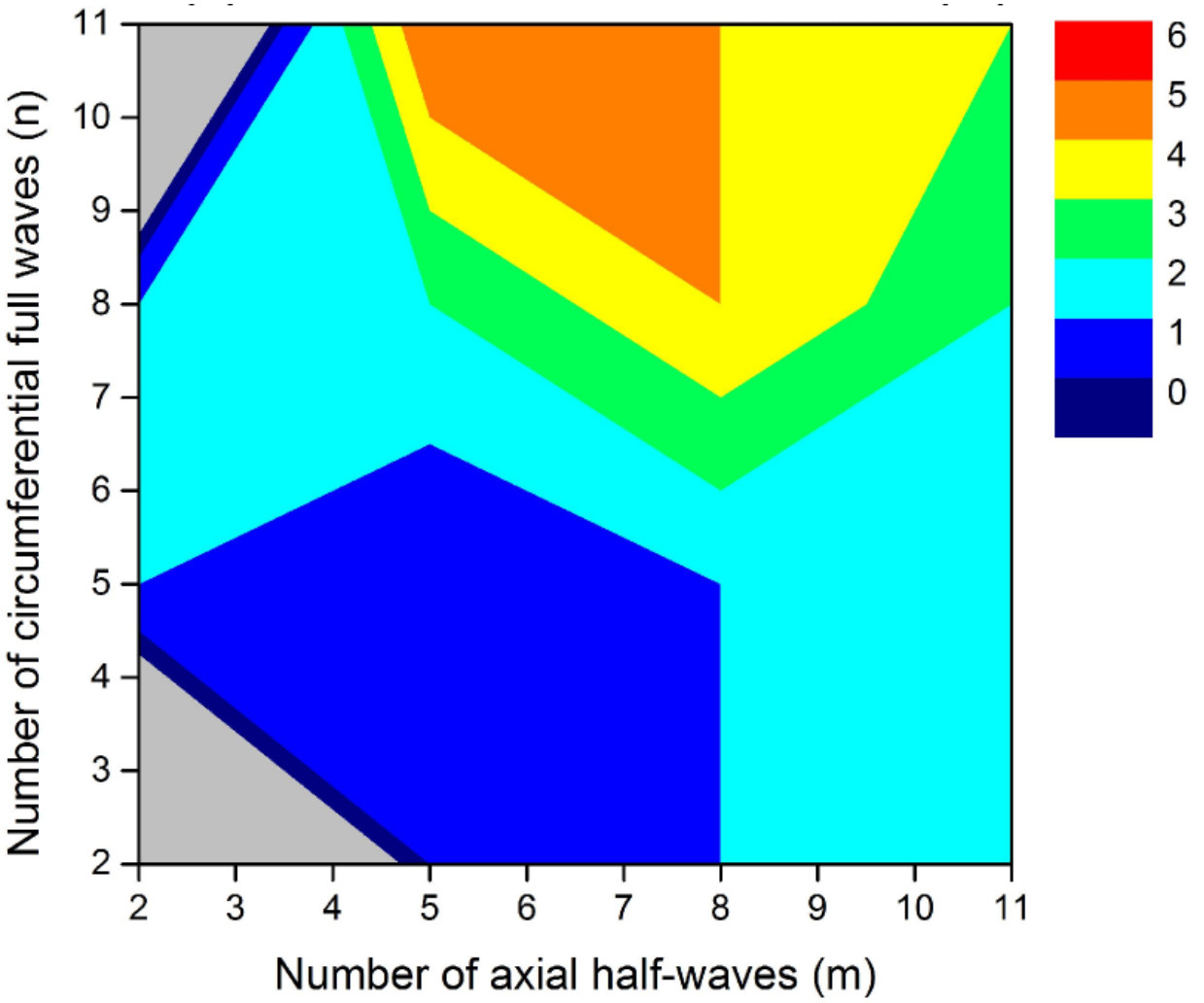

Figure 7-10: Predicted number of mode transitions (n_t) contours of SGI cylinders.

The evaluation presented in this section confirmed the simulation approach to trace and predict the postbuckling response and mode transitions in an SGI cylindrical shell. After such verification, the responses of two cylinder groups were numerically estimated for the entire Koiter Circle as shown in Figure 7-11 and Figure 7-12. The first simulation group, in Figure 7-11, featured SGI cylinders with an amplitude of 200% of the total shell thickness. According to the definition in Figure 5(a), the corresponding postbuckling response type for each *m*–*n* combination was plotted as a discrete response map. It can be seen that for a seeding amplitude

of 200% the majority of designs with softening response (type 3) are outside the Koiter Circle, while almost all designs with sustaining response (type 1) are along the perimeter of the half circle or inside the circle. Further, the number of designs with sustaining response (type 2) is limited and they are scattered both inside and outside the circle. It is also interesting to note from Figure 13(a) that a softening response can be achieved by seeding a geometry with either a large number of circumferential waves ($n > 10$) or a large number of axial waves ($m > 10$).

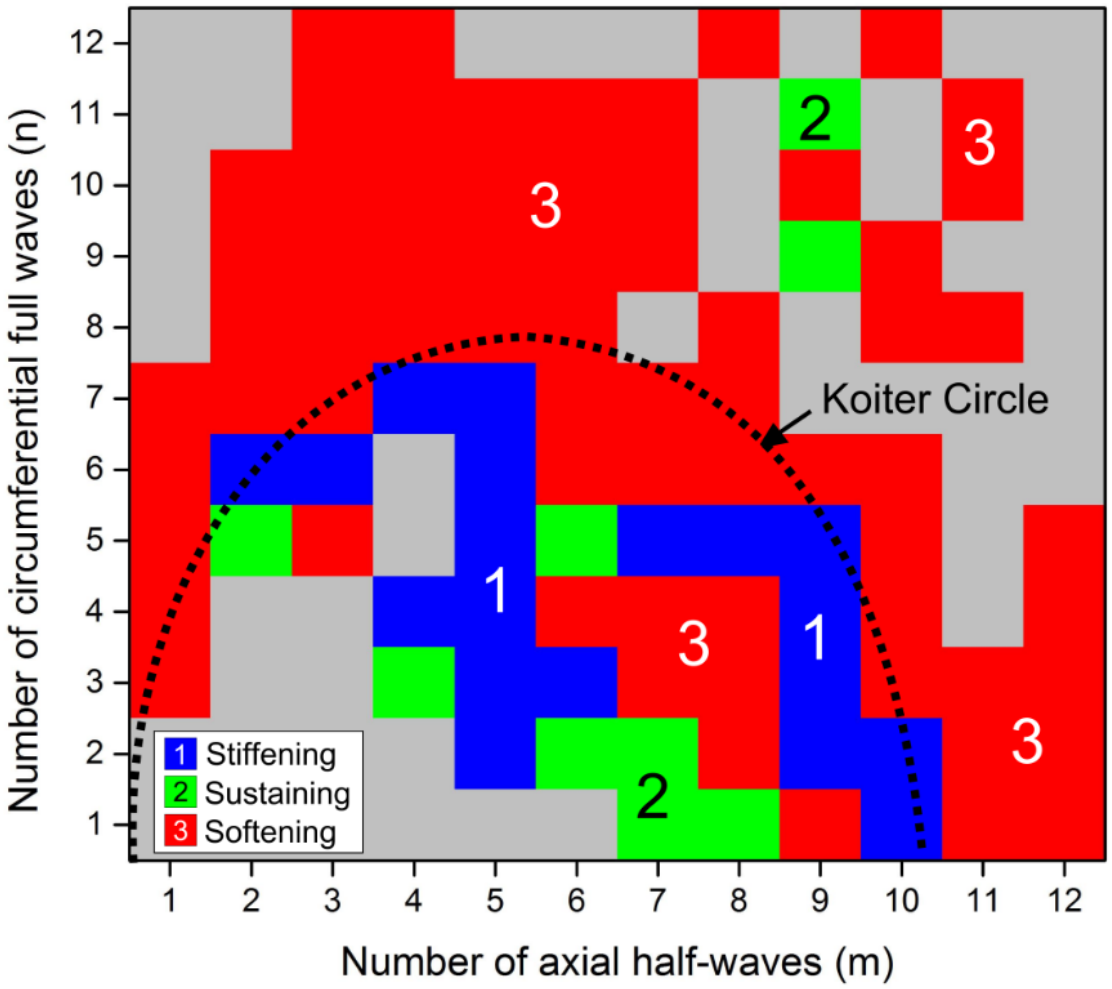

Figure 7-11: Discrete map of postbuckling responses type with 1 mm seeding amplitudes.

The second simulation group considered SGI cylinders with an amplitude of 500% of the total shell thickness. The discrete response map is plotted in Figure 7-12. It is noted that the number

of designs with sustaining type response (type 2) is significantly increased, particularly in the regime where the SGI cylinder was seeded with a large number of circumferential waves ($n > 8$). The reason is that changes in seeding amplitude can lead to a transition between response types. An increase in seeding amplitude has a significant knockdown effect on the first critical buckling load such that a softening response type transforms into a sustaining response, or even a stiffening response. Further, it should be noted that some SGI cylinders did not change their response type even if the amplitude was varied. Overall, the numerical results in this section show the opportunities of "imperfections by design" to tailor postbuckling response.

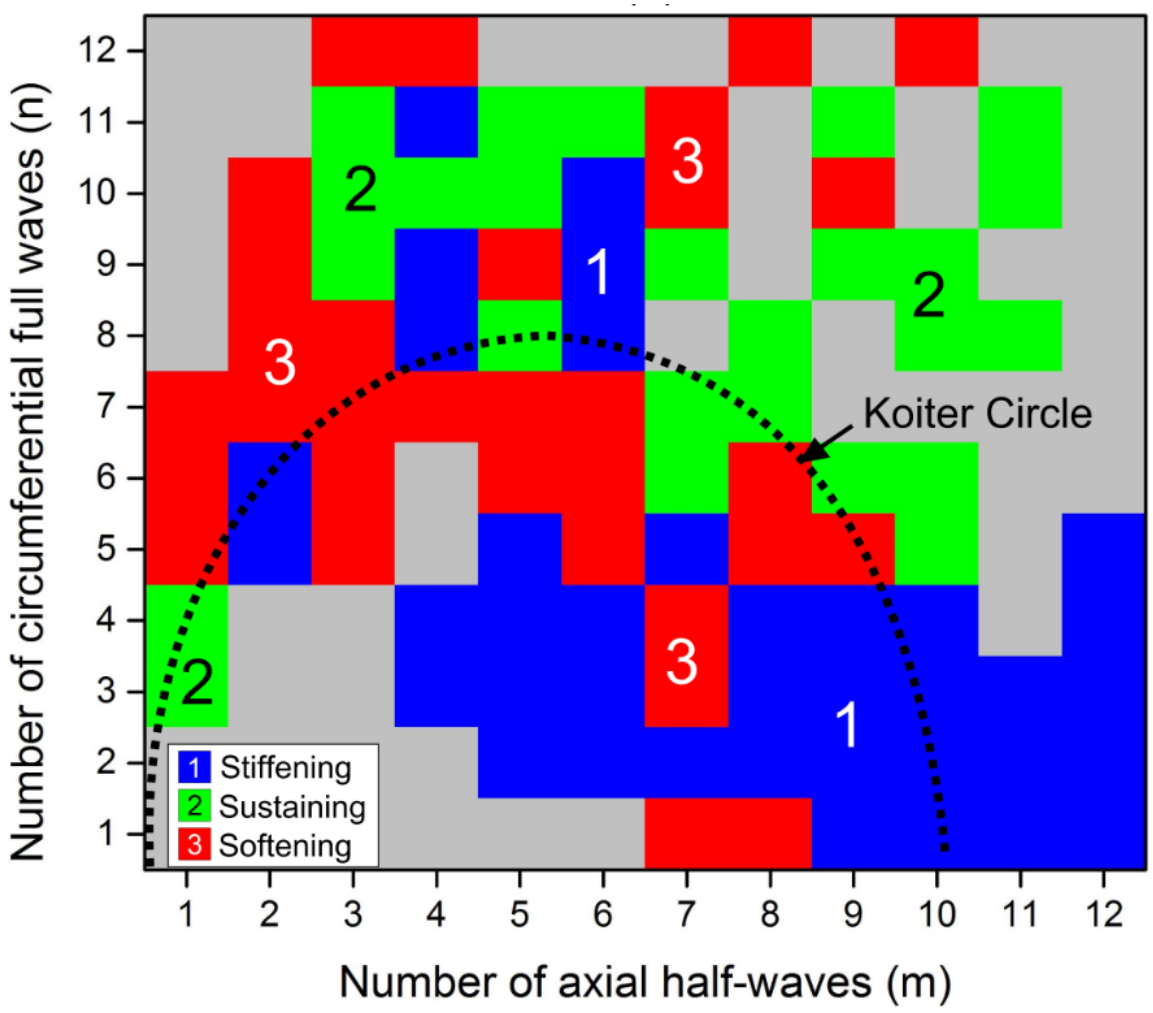

Figure 7-12: Discrete map of postbuckling responses type with 2.5 mm seeding amplitudes.

The form-finding of the SGI cylinder was completed from a three-step numerical procedure: (1) a finite element eigenvalue analysis and a nonlinear analysis using the finite element program ABAQUS [223]; (2) response evaluation through a custom code in Matlab [253]; and (3) sensitivity analysis and design updating through the design optimization software HEEDS [254].

Step 1 followed the same simulation procedure described in Figure 3-2 and the last two steps were used to find an optimal mode combination for a given design objective. For step 2, the custom code in Matlab reads the numerical results from ABAQUS and outputs the key parameters in Figure 7-13. In step 3 the program HEEDS was used to conduct the sensitivity analysis, update the design variables and modify the nonlinear analysis input for the ABAQUS model. HEEDS is a design optimization software that utilizes an iterative design process and an adaptive search strategy algorithm (SHERPA) to efficiently find optimized solutions., The SHERPA algorithm does not require solution gradients to exist during a single parametric optimization study and uses elements of multiple search methods simultaneously.

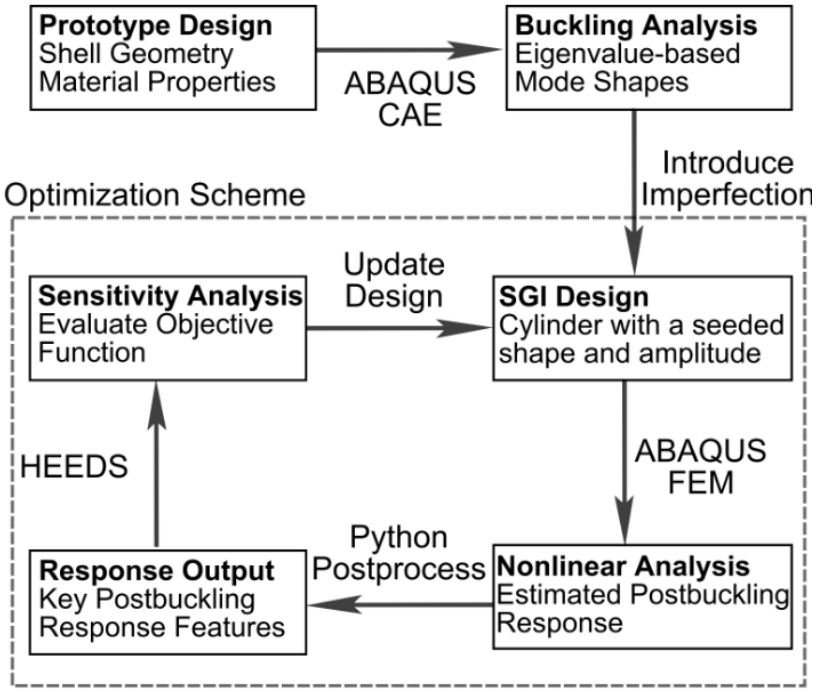

Figure 7-13: Optimization procedure for finding seeding geometry and amplitude.

Given that a key design feature of interest is to control the number of postbuckling mode transitions, one optimization case was conducted with the objective of obtaining a sustaining postbuckling response (i.e. $|\alpha|<0.1$) while maximizing the number of mode transitions. Two design variables were considered: (1) seeding mode shape and (2) seeding amplitude. A variable set sub-domain was selected out of the entire domain for the single mode shape, as shown in the shaded area of Figure 7-14. This sub-domain was chosen based on the response contour in Figure 7-9, which indicates the variable set that will most likely lead to attaining a higher number of mode transitions. As a result, a total of 29 modes were used for the mode shape design variable instead of the entire domain (95 mode shapes). For the seeding amplitude, the discrete maps in Figure 7-11 and Figure 7-12 provide knowledge on the transitions between response type and can be used as an upper and lower bounds on the postbuckling response. Thus, the seeding amplitude range was set to be between 200% and 500% of the total shell thickness.

A total of 250 iterations were requested in HEEDS and the best seeding mode for maximizing the number of mode transitions was determined to be mode 117, which has an axial half-wave number of six and a circumferential full wave number of ten (see dashed circle in Figure 7-14) and the simulated response had seven mode transitions. The postbuckling response is plotted in Figure 7-15. It can be seen that it is a sustaining postbuckling response, with the first buckling load being very similar to the load level at the end of loading phase. Such postbuckling response is attained due to the use of a large seeding amplitude. The seeding amplitude for the best design in the optimization process was 400% of the total shell thickness (0.5 mm), which implies a 2 mm maximum amplitude variation to the mid-plane of the shell. A sustaining postbuckling response is significantly different from the classic postbuckling response expected for cylindrical shells, which is known to have a large capacity loss in the postbuckling regime. Further, the

optimal seeding shape is consistent with the numerical response contour (see Figure 7-11 and Figure 7-12) as it is near the "hotspot" region. The results are also consistent with the previously noted finding that an increase in the circumferential wavenumber (*n*) for SGI cylinders will trigger a higher number of mode transitions. Overall, it is clear that a targeted postbuckling behavior can be achieved if a seeded shape is properly selected, offering a variety of opportunities within the design domain.

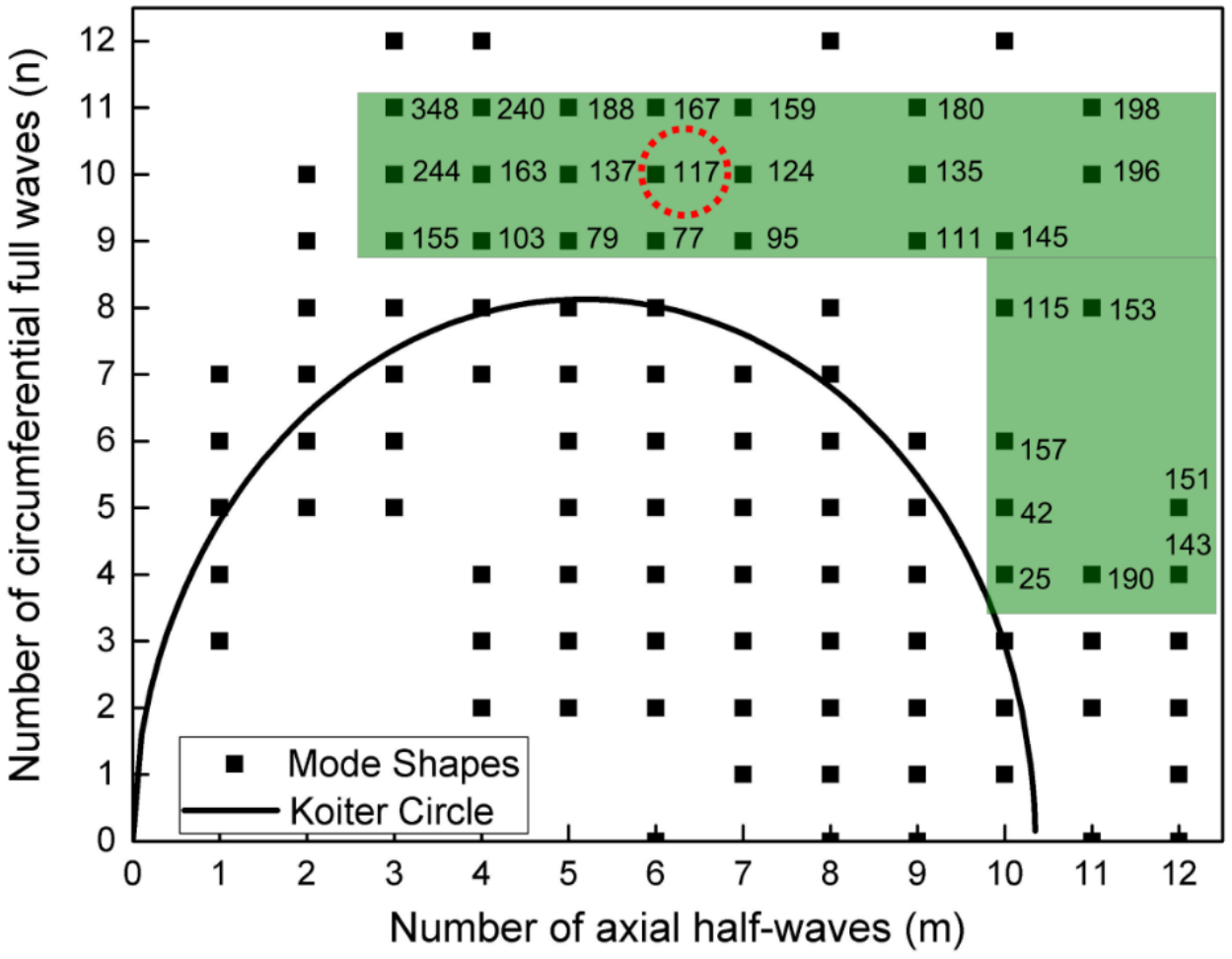

Figure 7-14: Sub-design variable domain of optimization case study.

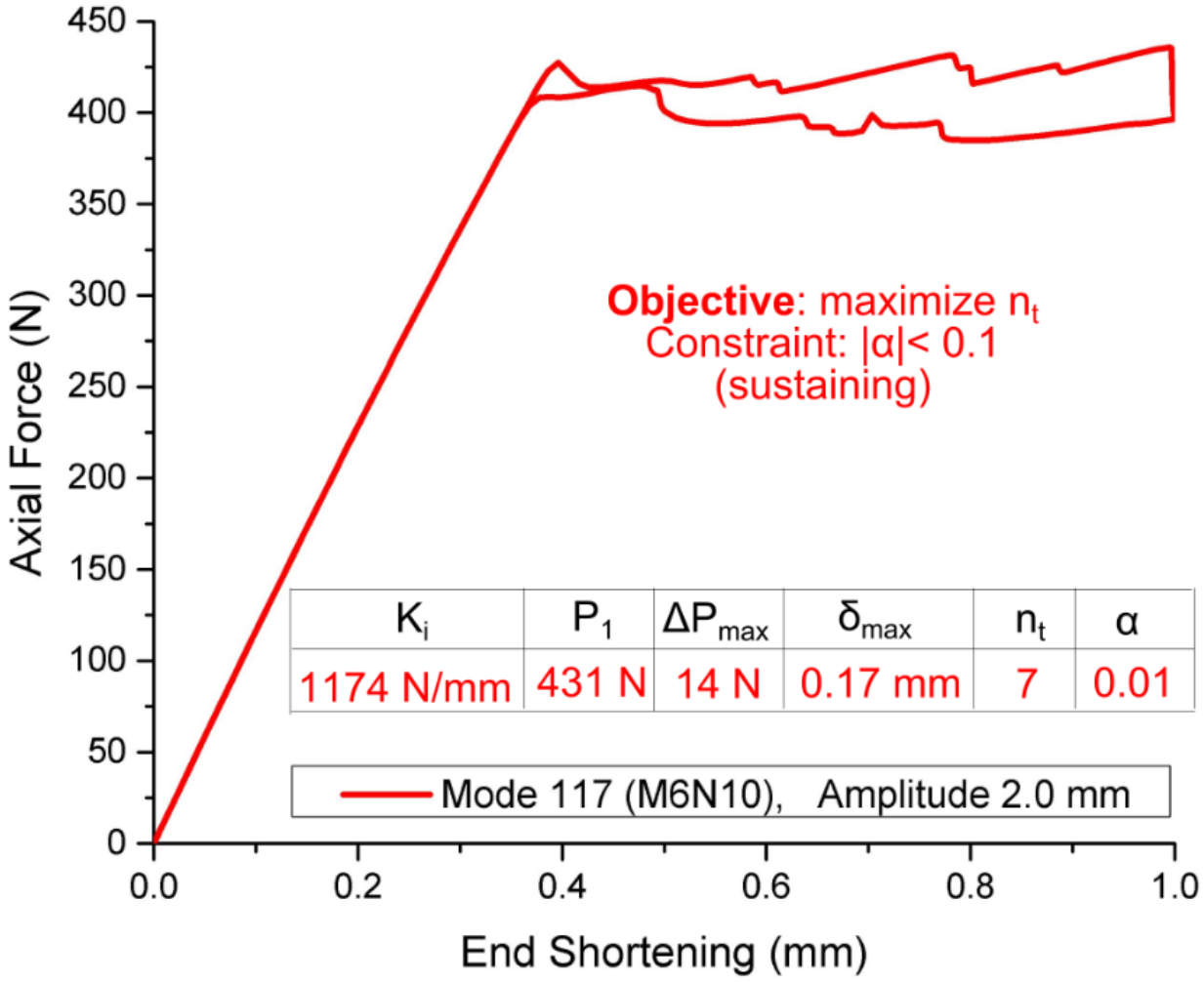

Figure 7-15: Postbuckling response of SGI cylinders with same amplitude but varied geometry.

7.4 Dynamic characteristics

Mode transitions in the elastic postbuckling response lead to partial release of stored strain energy in the axially-compressed cylindrical shell. The released energy is converted primarily into kinetic energy, allowing the cylinder to move from one potential energy well into another under increasing axial loading. Time histories of the strain and kinetic energies from the numerical results of an SGI cylinder design M69 (m = 8, n = 8, seeded from mode 69) are plotted

in Figure 7-16. The strain energy in the cylinder clearly accumulates with end shortening. Slope changes on the strain energy trace correspond to mode transition events, while the kinetic energy released during these events is clearly depicted by the spikes in its time history response curve.

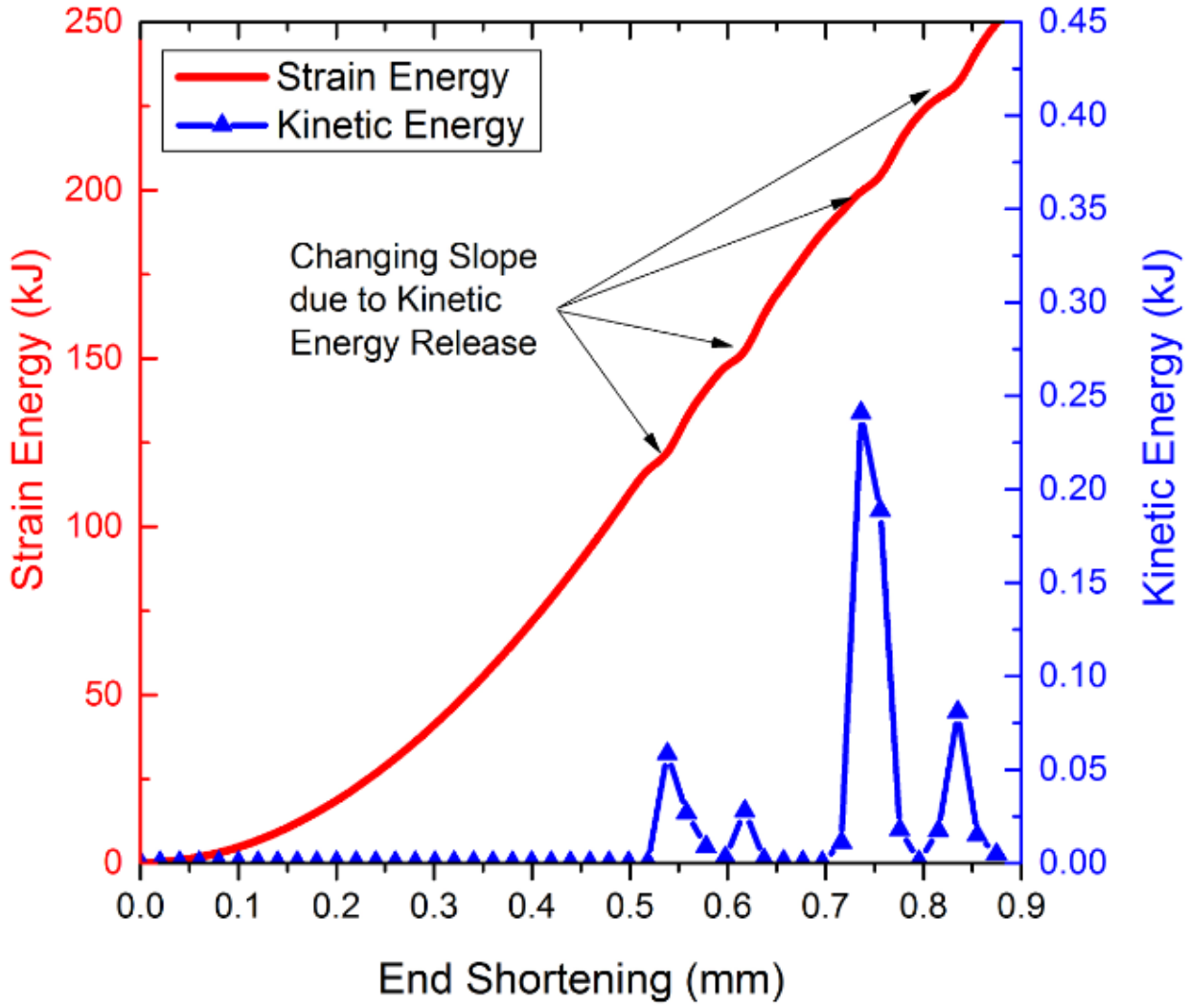

Figure 7-16: Strain energy versus kinetic energy of the SGI cylinder under axial compression.

As is to be expected, the kinetic energy release instances lead to discrete and localized events of high acceleration normal to the shell's surface, as shown in the acceleration time history responses in Figure 7-17 for three locations on cylinder M69. The noted dynamic response and

energetic features of the postbuckling response and the possibility of controlling them have great potential in the development of smart devices. Such concept has been explored for micro-energy harvesting and self-powered sensors by using the postbuckling response of bilaterally constrained columns [10, 118]. A similar buckling-induced energy harvesting concept is possible by using cylindrical shells. This study has shown that the number and location of localized buckling can be predefined in SGI cylinders, even if the exact occurrence of the buckling events has not been achieved yet. Thus, cylindrical shells with SGI designs can be turned into a promising prototype for smart applications by tailoring the time and location of buckling events in a controllable manner.

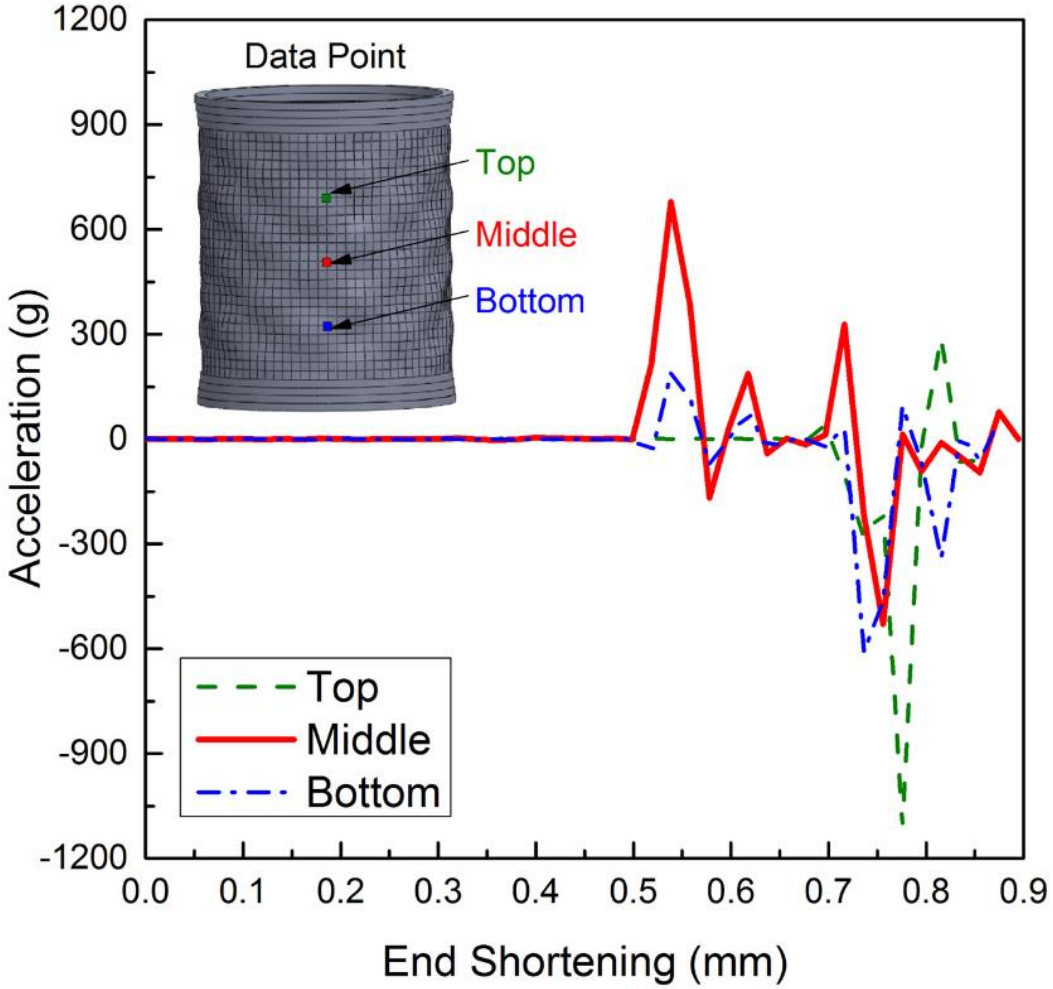

Figure 7-17: Key points' acceleration normal to the shell surface of the SGI cylinder.

Acceleration time-history responses obtained from numerical simulations for two sample points on the baseline cylinder NSD cylinder (NSD-A) as a function of end shortening are shown in Figure 7-18. It can be seen that the acceleration output from the point in the flexible region is much higher than the response in the stiff region, which is to be expected due to the localization of the snap-buckling events in the flexible zones. This results show that the sequence (time) and location (space) of localized buckling events can be predefined in NSD cylinders.

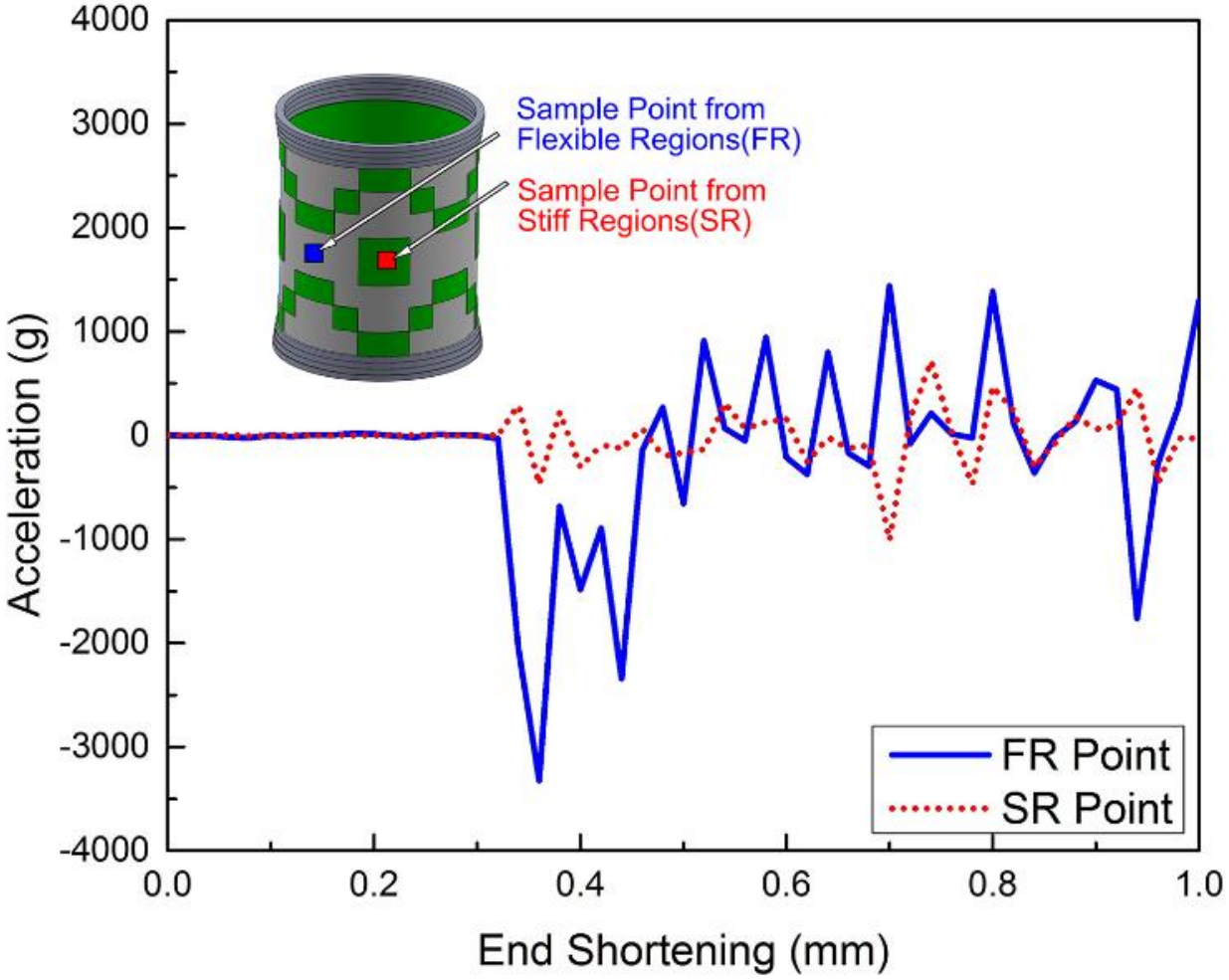

Figure 7-18: Comparison of acceleration normal to the shell surface between a point from a thickened region and from a non-thickened region of a NSD cylinder.

7.5 Miniaturization

The spectrum of interests in smart applications ranges from nanostructured materials to macro-scale structural elements. Thus, a further goal in the development of cylinders is to achieve a repeatable and recoverable elastic postbuckling response across scales. The size of the design domain can be changed with different *L/R* ratio and material properties. A numerical study on an isotropic cylinder NSD-G with the same geometry but for three Young's modulus values (E= 2, 5, 10 GPa) was conducted to illustrate this point. The modeling procedure was as described in Section 3.3. The loading phase of the postbuckling response is shown in Figure 7-19.

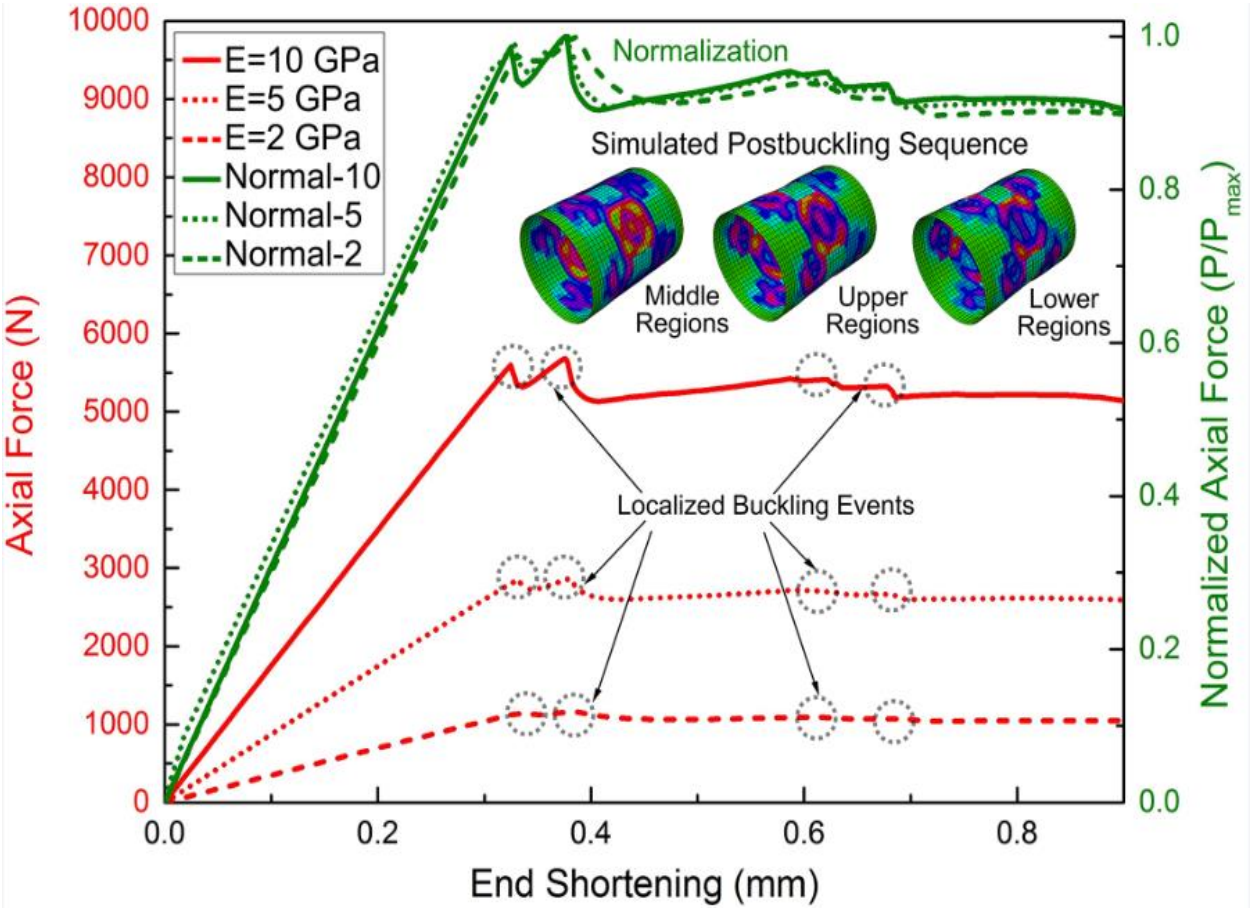

Figure 7-19: Predicted postbuckling responses of a baseline NSD cylinder with varied Young's modulus

As expected, changing the Young's modulus did not have a big effect on the magnitude of each drop but it is interesting to see that the number of mode transitions was the same (four) with decreasing material stiffness. If the postbuckling responses are normalized to their maximum critical load the curves essentially collapse to a single curve (see Figure 7-19), displaying similar values for the load drops (with respect to the total load drop) at the snap buckling events. This indicates a scale invariance in the underlying postbuckling behavior for a given shell geometry. Such scale invariance for elastic postbuckling behavior has also been emphasized by other studies [255]. Overall, it is clear that a targeted postbuckling behavior, with multiple opportunities within a design domain, can be achieved if patterned patches (i.e., non-uniform stiffness distributions) are properly distributed.

Another aspect of interest for exploring uses is the miniaturization of the design concepts developed through this study. Two prototype cylinders were discussed in this dissertation. The dimension of the first prototyped cylinders (laminate graphite/epoxy) was 254 mm long by 203 mm in diameter. The second prototype, the 3D printed PLA cylinder, had an effective length of 80 mm, a radius of 40 mm and a thickness of 0.5 mm, which were scaled down by a factor of 2.5. Thus, as shown in Figure 7-20 the research endeavor summarized in this dissertation started with relatively large cylinder prototypes (L = 254 mm and R = 101.5 mm) and with the use of 3D printing the scale of the baseline cylinder was reduced by a factor of 100.

Achieving a similar postbuckling response by keeping the same geometric features (L/R ratio and R/t ratio) would bring strong practical implications to the use of cylinders at different scales. A prototype multi-material multi-scale cylinder (Figure 7-21) with an effective length of 20 mm, a radius of 10 mm and a thickness of 1 mm was built by using a multi-material 3D printer (Objet Connex350). This printer allows part fabrication from different materials (up to 14)

in the same tray and it is ideal to fabricate components with varying material properties. The prototype cylinder had only two materials: a thermoplastic material on stiff regions and a rubber-like material on flexible regions. It should be noted that the fabrication cost on this multi-material printer is much higher than for the 3D polymer-based printer (MakerBot Replicator 2), which is why it was not used for the main prototype samples evaluated in this research.

Figure 7-20: Test units showcasing the miniaturization potential of cylinder prototypes.

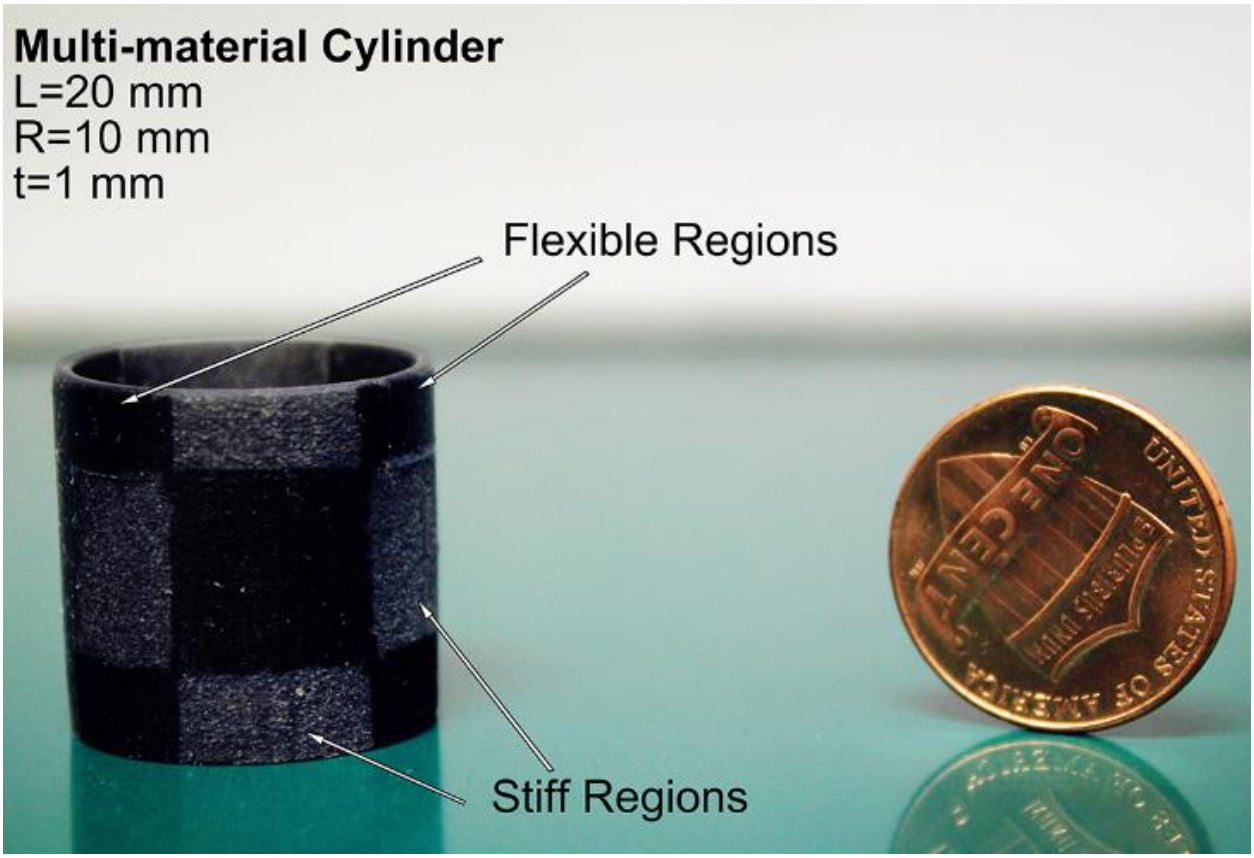

Figure 7-21: Prototype multi-material cylinder in a reducing scale.

7.6 Summary

This chapter presented a numerical and experimental study on further tailoring the postbuckling response of cylindrical shells for its potential use in the design of smart and adaptive materials and structures. Increasing interest has pushed the limits on the understanding of cylindrical shells as a traditional structural component, and they may now turn into a promising prototype for smart applications. The following conclusions were drawn from the study in this chapter:

(1) An extension work on SGI cylinders showed that SGI designs provide advantages for controlling the elastic postbuckling response of axially compressed cylindrical shells by changing the shape and amplitude of the seeded imperfection. A response contour was presented using experimental results for a baseline SGI cylinder; and it was observed that

multiple mode jumps in the postbuckling regime were more likely to occur when the seeded imperfection mode shape had a relatively large number of waves in the circumferential direction. Further, a seeding geometry with a lower number of axial waves can lead to a shell with higher stiffness, higher single load drop from postbuckling mode jumps and larger energy dissipation from the elastic loading/unloading cycle.

(2) Numerical predictions seem to reasonably capture the key postbuckling characteristics and response type, as judged by comparisons with experimental data. With this verification, SGI designs for all seeding shapes were numerically simulated and presented as a discrete response map. This map, along with a response contour, can be used to guide the design of SGI cylinders for a targeted postbuckling response. This approach was verified by an optimization study to find an optimal design for maximizing the number of mode transitions. It was shown that a targeted postbuckling behavior can be achieved if a seeded shape is properly selected, thus offering a variety of opportunities within the design domain

(3) The dynamic features of the mode transitions in the elastic postbuckling response were discussed based on numerical results based on time histories of the strain and kinetic energies of SGI cylinder. As is to be expected, the kinetic energy release instances lead to discrete and localized events of high acceleration normal to the shells' surface. The noted dynamic response and energetic features of the postbuckling response and the possibility of controlling them have great potential in the development of smart devices.

(4) Based on evidence from numerical simulations and prototype fabrication it is envisioned that the three design concepts (SGI, NSD and LCI) could be used across scales and the postbuckling response is expected be repeatable and recoverable by selecting appropriate materials and fabrication techniques.

Chapter 8

Conclusions

8.1 Research significance

The research presented in this dissertation has led to knowledge on the possibilities, extent and means to control (and thus design) the elastic far postbuckling response of cylindrical shells by means of variations in geometry, stiffness and boundary conditions. Full characterization and understanding of these variables in the attainment and control of postbuckling response with desirable features can promote the use of the presented cylindrical shell concepts for a variety of purposes of emerging interest and across scales for various applications. The research findings are expected open new avenues for the development of materials and devices that use instabilities for applications such as sensing, actuation, control, energy harvesting, and energy dissipation, advances that in turn could also facilitate the development of novel smart, active and multifunctional materials and structures.

8.2 Conclusions

Based on the discussions in previous chapters, the following overall conclusions were reached:

1) **Cylinders as a prototype**: Cylindrical shells under axial compression were investigated to be considered as a viable structural prototype for the purpose of designing smart and adaptive devices. The positive features of the resulting unstable postbuckling response were recognized in this dissertation, for which mode transitions lead to sudden and high-

rate deformations from generally smaller changes in the controlling load or displacement input to the system. Compared to other existing prototypes, cylindrical shells can attain a higher number multiple stable configurations (also known as mode transitions) without the need of additional constraints due to the natural transverse deformation restraint provided by their geometry. Such geometric nonlinear responses allow cylindrical shells to be considered as a viable structural prototype for purposes such as energy harvesting, sensing, actuation, etc.

2) **Imperfection as a tool**: The existence of initial imperfections due to the manufacturing process has limited the potential use of cylindrical shells for smart applications. However, *imperfection* in this dissertation played a governing role in the design of cylindrical shells by using two concepts (seeded geometric imperfections, SGI; and non-uniform stiffness distributions, NSD). Numerical and experimental results indicate that both SGI and NSD cylinders can attain a controllable postbuckling response for which the localized buckling events can be triggered in predefined regions and in certain sequence. In addition, the postbuckling response of SGI and NSD cylinders was shown to be less sensitive to initial (manufacturing) imperfections as well as loading variations compared to that of uniform cylinders. Further, the difficulty of predicting and modeling the postbuckling response of cylindrical shells is reduced by the presence of the governing, purposely introduced, imperfection. In this way, imperfections do not have a detrimental effect but lead to a predictable, tailorable and controllable postbuckling response in cylindrical shells.

3) **Postbuckling as a regime of interest**: Buckling of cylindrical shells has been mainly regarded as a failure limit and the afterward response (postbuckling) as a safeguard. Rather than a well-known capacity loss, the postbuckling behavior of cylindrical shells in

this dissertation was tailored into three response types (softening, sustaining and stiffening) through careful selection of the geometry and stiffness distribution, as well as the provision of constraints and interactions; which lead to diverse design opportunities. Rather than predicting the critical buckling load, several key parameters were of primary interest, including the number of mode transitions, the maximum single load drop, the maximum separation of the critical points and the dissipated energy from the equilibrium path transitions. These parameters were evaluated and tailored through experimental testing, numerical simulations and optimization studies. In addition to documenting the feasibility of controlling the postbuckling response of axially loaded shells by the noted approaches, design guidelines were also developed to achieve the targeted behavior.

8.3 Future research

The current study and investigation was motivated by the increased interest in using the instabilities of flexible systems for the development of smart materials and structures. Within this context, this dissertation only focused on exploring the use of cylindrical shells as a potential structural prototype but further study requires identifying specific applications. Related research endeavors have demonstrated that the attainment of a stable postbuckling response in bilaterally constrained columns can be used to harvest energy for local use in devices such as sensors without the need for external vibration as the energy source [10, 118]. This is possible by using the kinetic energy released during the mode transitions events in the postbuckling response to excite piezoelectric oscillators, which transform the vibration energy caused by the sudden motion into power. Use of the postbuckling response from cylinders is a clear extension but one

that requires validation and characterization, particularly for optimized designs as the ones presented in this dissertation.

The issue of selecting an appropriate material for the cylindrical shell was also raised. A further goal in the development of cylinders for the purposes reported in this study is to achieve a repeatable and recoverable postbuckling response in the elastic range. The studied cylinders (laminated composite and PLA) exhibited decreasing performance upon load cycling, such as the maximum load drop and the enclosed force-deformation area, which indicates that the material may have suffered minor damage in the postbuckling regime. Further applications will also depend on using materials with either the ability of shape change or the ability of shape memory. A material may have these two features separately or simultaneously. Thus, a smart material such as a shape memory alloy (SMA) could be a good candidate manufacture cylinders for smart purposes.

Controlling the location of buckling events was proven to be possible, yet the sequence of buckling events can be further tailored under each of the proposed structural prototypes. This, however, requires further understanding of the interaction and transition between the predefined geometrical and material patterns. If modifications on the distribution of material/stiffness and the seeding of dominating imperfections can individually modify the elastic postbuckling response then the combination of both effects is expected to provide additional levels of control. A combined shape and topology optimization algorithm could be useful for the design of cylindrical shells with the objective of obtaining a predefined elastic postbuckling response.

The postbuckling response of cylindrical shells was evaluated at the component level (i.e., a single shell) and fabricated at a desktop scale. It should be noted that axial compression is only of the loading scenario and other cases (such as twisting, internal pressure, etc) should also be

explored. Further, hybrid systems (cylinder groups or cylinders with other structural types) should be considered based on a specific application across scales. With more advanced additive manufacturing techniques, further development and use of cylinders across dimensional scales seems promising and the expansion of designing for and using a targeted buckling and postbuckling response is likely to be advanced.

BIBLIOGRAPHY

BIBLIOGRAPHY

[1] S. P. Timoshenko and J. M. Gere, *Theory of elastic stability*. London: Dover Publications, 2012.

[2] J. M. T. Thompson and G. W. Hunt, *A general theory of elastic stability*. London-New York-Sydney-Toronto: John Wiley & Sons Ltd, 1973.

[3] B. Li, Y.-P. Cao, X.-Q. Feng, and H. Gao, "Mechanics of morphological instabilities and surface wrinkling in soft materials: a review," *Soft Matter,* vol. 8, pp. 5728-5745, 2012.

[4] N. Friedman and A. Ibrahimbegovic, "Overview of highly flexible, deployable lattice structures used in architecture and civil engineering undergoing large displacements," *YBL Journal of Built Environment,* vol. 1, pp. 85-103, 2013.

[5] I. K. Kuder, A. F. Arrieta, W. E. Raither, and P. Ermanni, "Variable stiffness material and structural concepts for morphing applications," *Progress in Aerospace Sciences,* vol. 63, pp. 33-55, 11// 2013.

[6] W. M. Huang, H. B. Lu, Y. Zhao, Z. Ding, C. C. Wang, J. L. Zhang, *et al.*, "Instability/collapse of polymeric materials and their structures in stimulus-induced shape/surface morphology switching," *Materials & Design,* vol. 59, pp. 176-192, 7// 2014.

[7] S. P. Pellegrini, N. Tolou, M. Schenk, and J. L. Herder, "Bistable vibration energy harvesters: A review," *Journal of Intelligent Material Systems and Structures,* vol. 24, pp. 1303-1312, July 1, 2013 2013.

[8] A. Mita and S. Takhira, "A smart sensor using a mechanical memory for structural health monitoring of a damage-controlled building," *Smart Materials and Structures,* vol. 12, p. 204, 2003.

[9] M. R. Begley and N. S. Barker, "Analysis and design of kinked (bent) beam sensors," *Journal of Micromechanics and Microengineering,* vol. 17, p. 350, 2007.

[10] N. Lajnef, R. Burgueño, W. Borchani, and Y. Sun, "A concept for energy harvesting from quasi-static structural deformations through axially loaded bilaterally constrained columns with multiple bifurcation points," *Smart Materials and Structures,* vol. 23, p. 055005, 2014.

[11] B. J. Hansen, C. J. Carron, B. D. Jensen, A. R. Hawkins, and S. M. Schultz, "Plastic latching accelerometer based on bistable compliant mechanisms," *Smart Materials and Structures,* vol. 16, p. 1967, 2007.

[12] C. G. Xia, H. Lee, and N. Fang, "Solvent-driven polymeric micro beam device," *Journal of Micromechanics and Microengineering,* vol. 20, p. 085030, 2010.

[13] N. Lindahl, D. Midtvedt, J. Svensson, O. A. Nerushev, N. Lindvall, A. Isacsson, *et al.*, "Determination of the Bending Rigidity of Graphene via Electrostatic Actuation of Buckled Membranes," *Nano Letters,* vol. 12, pp. 3526-3531, 2012/07/11 2012.

[14] P. B. Da Costa Teixeira, P. B. Gonçalves, I. A. Cestari, A. A. Leirner, and D. Pamplona, "Mechanical Behavior and Stability of the Internal Membrane of the InCor Ventricular Assist Device," *Artificial Organs,* vol. 25, pp. 912-921, 2001.

[15] P. B. Gonçalves, D. Pamplona, P. B. C. Teixeira, R. L. C. Jerusalmi, I. A. Cestari, and A. A. Leirner, "Dynamic non-linear behavior and stability of a ventricular assist device," *International Journal of Solids and Structures,* vol. 40, pp. 5017-5035, 9// 2003.

[16] J.-H. Jang, C. Y. Koh, K. Bertoldi, M. C. Boyce, and E. L. Thomas, "Combining pattern instability and shape-memory hysteresis for phononic switching," *Nano Letters,* vol. 9, pp. 2113-2119, 2009/05/13 2009.

[17] K. Bertoldi, P. M. Reis, S. Willshaw, and T. Mullin, "Negative Poisson's ratio behavior induced by an elastic instability," *Advanced Materials,* vol. 22, pp. 361-366, 2010.

[18] Y. Zhang, E. A. Matsumoto, A. Peter, P.-C. Lin, R. D. Kamien, and S. Yang, "One-Step Nanoscale Assembly of Complex Structures via Harnessing of an Elastic Instability," *Nano Letters,* vol. 8, pp. 1192-1196, 2008/04/01 2008.

[19] W. Shan and Z. Chen, "Mechanical instability of thin elastic rods," *Journal of Postdoctoral Research February,* vol. 1, p. 8, 2013.

[20] F. Cottone, L. Gammaitoni, H. Vocca, M. Ferrari, and V. Ferrari, "Piezoelectric buckled beams for random vibration energy harvesting," *Smart Materials and Structures,* vol. 21, p. 035021, 2012.

[21] S. Boisseau, G. Despesse, S. Monfray, O. Puscasu, and T. Skotnicki, "Semi-flexible bimetal-based thermal energy harvesters," *Smart Materials and Structures,* vol. 22, p. 025021, 2013.

[22] Y. Zhu and J. W. Zu, "Enhanced buckled-beam piezoelectric energy harvesting using midpoint magnetic force," *Applied Physics Letters,* vol. 103, p. 041905, 2013.

[23] R. L. Harne and K. W. Wang, "A review of the recent research on vibration energy harvesting via bistable systems," *Smart Materials and Structures,* vol. 22, p. 023001, 2013.

[24] S. Chen, S. Gonella, W. Chen, and W. K. Liu, "A level set approach for optimal design of smart energy harvesters," *Computer Methods in Applied Mechanics and Engineering,* vol. 199, pp. 2532-2543, 8/1/ 2010.

[25] L. F. Shen, Y. S. Cha, A. Shams, and M. Porfiri, "Fabrication and buckling analysis of ionic polymer metal composite pipes," *Smart Materials and Structures,* vol. 22, p. 105032, 2013.

[26] L. Dong and R. Lakes, "Advanced damper with high stiffness and high hysteresis damping based on negative structural stiffness," *International Journal of Solids and Structures,* vol. 50, pp. 2416-2423, 7// 2013.

[27] H. Kalathur and R. S. Lakes, "Column dampers with negative stiffness: high damping at small amplitude," *Smart Materials and Structures,* vol. 22, p. 084013, 2013.

[28] J. Winterflood, T. A. Barber, and D. G. Blair, "Mathematical analysis of an Euler spring vibration isolator," *Physics Letters A,* vol. 300, pp. 131-139, 7/29/ 2002.

[29] L. H. Donnell, "A new theory for the buckling of thin cylinders under axial compression and bending," *Trans. Asme,* vol. 56, pp. 795-806, 1934.

[30] T. von Karman and H.-S. Tsien, "The Buckling of Thin Cylindrical Shells under Axial Compression," *Journal of Aeronautical Sciences,* vol. 8, pp. 303-312, 1941.

[31] J. Hutchinson and W. Koiter, "Postbuckling theory," *Appl. Mech. Rev,* vol. 23, pp. 1353-1366, 1970.

[32] N. Yamaki, K. Otomo, and K. Matsuda, "Experiments on the postbuckling behavior of circular cylindrical shells under compression," *Experimental Mechanics,* vol. 15, pp. 23-28, 1975/01/01 1975.

[33] W. T. Koiter, "The stability of elastic equilibrium," DTIC Document1970.

[34] I. Sheinman and G. J. Simitses, "Buckling and postbuckling of imperfect cylindrical shells under axial compression," *Computers & Structures,* vol. 17, pp. 277-285, // 1983.

[35] S. Yamada and J. G. A. Croll, "Buckling and Post-buckling Characteristics of Pressure-Loaded Cylinders," *Journal of Applied Mechanics,* vol. 60, pp. 290-299, 1993.

[36] M. Jamal, L. Lahlou, M. Midani, H. Zahrouni, A. Limam, N. Damil, *et al.*, "A semi-analytical buckling analysis of imperfect cylindrical shells under axial compression," *International Journal of Solids and Structures,* vol. 40, pp. 1311-1327, 3// 2003.

[37] H. S. Shen, "Boundary layer theory for the buckling and postbuckling of an anisotropic laminated cylindrical shell. Part I: Prediction under axial compression," *Composite Structures,* vol. 82, pp. 346-361, Feb 2008.

[38] C. Bisagni and P. Cordisco, "An experimental investigation into the buckling and post-buckling of CFRP shells under combined axial and torsion loading," *Composite Structures,* vol. 60, pp. 391-402, 6// 2003.

[39] R. Degenhardt, A. Kling, K. Rohwer, A. C. Orifici, and R. S. Thomson, "Design and analysis of stiffened composite panels including post-buckling and collapse," *Computers & Structures,* vol. 86, pp. 919-929, 5// 2008.

[40] E. Riks, C. C. Rankin, and F. A. Brogan, "On the solution of mode jumping phenomena in thin-walled shell structures," *Computer Methods in Applied Mechanics and Engineering,* vol. 136, pp. 59-92, 9/15/ 1996.

[41] F. Fujii, H. Noguchi, and E. Ramm, "Static path jumping to attain postbuckling equilibria of a compressed circular cylinder," *Computational Mechanics,* vol. 26, pp. 259-266, 2000/09/01 2000.

[42] G. Hunt, G. J. Lord, and M. A. Peletier, "Cylindrical shell buckling: a characterization of localization and periodicity," *Discrete and Continuous Dynamical Systems Series B,* vol. 3, pp. 505-518, 2003.

[43] J. G. Teng and T. Hong, "Postbuckling analysis of elastic shells of revolution considering mode switching and interaction," *International Journal of Solids and Structures,* vol. 43, pp. 551-568, 2// 2006.

[44] C. Hühne, R. Rolfes, E. Breitbach, and J. Teßmer, "Robust design of composite cylindrical shells under axial compression — Simulation and validation," *Thin-Walled Structures,* vol. 46, pp. 947-962, 7// 2008.

[45] R. Burgueño, N. Hu, A. Heeringa, and N. Lajnef, "Tailoring the elastic postbuckling response of thin-walled cylindrical composite shells under axial compression," *Thin-Walled Structures,* vol. 84, pp. 14-25, 11// 2014.

[46] C. Bisagni, "Numerical analysis and experimental correlation of composite shell buckling and post-buckling," *Composites Part B: Engineering,* vol. 31, pp. 655-667, // 2000.

[47] G. J. Simitses, "Buckling and Postbuckling of Imperfect Cylindrical Shells: A Review," *Applied Mechanics Reviews,* vol. 39, pp. 1517-1524, 1986.

[48] J. G. Teng, "Buckling of Thin Shells: Recent Advances and Trends," *Applied Mechanics Reviews,* vol. 49, pp. 263-274, 1996.

[49] B. L. O. Edlund, "Buckling of metallic shells: Buckling and postbuckling behaviour of isotropic shells, especially cylinders," *Structural Control and Health Monitoring,* vol. 14, pp. 693-713, 2007.

[50] R. Degenhardt, A. Kling, A. Bethge, J. Orf, L. Kärger, R. Zimmermann, *et al.*, "Investigations on imperfection sensitivity and deduction of improved knock-down factors for unstiffened CFRP cylindrical shells," *Composite Structures,* vol. 92, pp. 1939-1946, 7// 2010.

[51] S. G. P. Castro, R. Zimmermann, M. A. Arbelo, R. Khakimova, M. W. Hilburger, and R. Degenhardt, "Geometric imperfections and lower-bound methods used to calculate knock-down factors for axially compressed composite cylindrical shells," *Thin-Walled Structures,* vol. 74, pp. 118-132, 1// 2014.

[52] B. Kriegesmann, M. Möhle, and R. Rolfes, "Sample size dependent probabilistic design of axially compressed cylindrical shells," *Thin-Walled Structures,* vol. 74, pp. 222-231, 1// 2014.

[53] H. S. Shen, P. Zhou, and T. Y. Chen, "Postbuckling analysis of stiffened cylindrical shells under combined external pressure and axial compression," *Thin-Walled Structures,* vol. 15, pp. 43-63, // 1993.

[54] H. A. Mang, C. Schranz, and P. Mackenzie-Helnwein, "Conversion from imperfection-sensitive into imperfection-insensitive elastic structures I: Theory," *Computer Methods in Applied Mechanics and Engineering,* vol. 195, pp. 1422-1457, 2/15/ 2006.

[55] C. Schranz, B. Krenn, and H. A. Mang, "Conversion from imperfection-sensitive into imperfection-insensitive elastic structures. II: Numerical investigation," *Computer Methods in Applied Mechanics and Engineering,* vol. 195, pp. 1458-1479, 2/15/ 2006.

[56] E. Lindgaard, E. Lund, and K. Rasmussen, "Nonlinear buckling optimization of composite structures considering “worst” shape imperfections," *International Journal of Solids and Structures,* vol. 47, pp. 3186-3202, 11// 2010.

[57] X. Ning and S. Pellegrino, "Design and testing of imperfection-insensitive monocoque cylindrical shells," in *54th AIAA/ASME/ASCE/AHS/ASC Structures, Structural Dynamics, and Materials Conference*, ed: American Institute of Aeronautics and Astronautics, 2013.

[58] S. D. Guest and S. Pellegrino, "Analytical models for bistable cylindrical shells," *Proceedings of the Royal Society A: Mathematical, Physical and Engineering Science,* vol. 462, pp. 839-854, March 8, 2006 2006.

[59] A. D. Norman, K. A. Seffen, and S. D. Guest, "Multistable corrugated shells," *Proceedings of the Royal Society A: Mathematical, Physical and Engineering Science,* vol. 464, pp. 1653-1672, July 8, 2008 2008.

[60] S. Vidoli and C. Maurini, "Tristability of thin orthotropic shells with uniform initial curvature," *Proceedings of the Royal Society A: Mathematical, Physical and Engineering Science,* vol. 464, pp. 2949-2966, November 8, 2008 2008.

[61] B. H. Coburn, A. Pirrera, P. M. Weaver, and S. Vidoli, "Tristability of an orthotropic doubly curved shell," *Composite Structures,* vol. 96, pp. 446-454, 2// 2013.

[62] H.-T. Pham and D.-A. Wang, "A quadristable compliant mechanism with a bistable structure embedded in a surrounding beam structure," *Sensors and Actuators A: Physical,* vol. 167, pp. 438-448, 6// 2011.

[63] P. A. Porter and T. A. Berfield, "A bi-stable buckled energy harvesting device actuated via torque arms," *Smart Materials and Structures,* vol. 23, p. 075003, 2014.

[64] F. Dai, H. Li, and S. Du, "A multi-stable lattice structure and its snap-through behavior among multiple states," *Composite Structures,* vol. 97, pp. 56-63, 3// 2013.

[65] H. J. Lee and J. J. Lee, "A numerical analysis of the buckling and postbuckling behavior of laminated composite shells with embedded shape memory alloy wire actuators," *Smart Materials and Structures,* vol. 9, p. 780, 2000.

[66] M. Hübler, M. Gurka, S. Schmeer, and U. P. Breuer, "Performance range of SMA actuator wires and SMA–FRP structure in terms of manufacturing, modeling and actuation," *Smart Materials and Structures,* vol. 22, p. 094002, 2013.

[67] V. Dimitris and A. S. Dimitris, "Nonlinear coupled mechanics and initial buckling of composite plates with piezoelectric actuators and sensors," *Smart Materials and Structures,* vol. 11, p. 330, 2002.

[68] P. F. Giddings, H. A. Kim, A. I. T. Salo, and C. R. Bowen, "Modelling of piezoelectrically actuated bistable composites," *Materials Letters,* vol. 65, pp. 1261-1263, 5/15/ 2011.

[69] Y. Yang, L. Tang, and H. Li, "Vibration energy harvesting using macro-fiber composites," *Smart Materials and Structures,* vol. 18, p. 115025, 2009.

[70] J. Mohd Jani, M. Leary, A. Subic, and M. A. Gibson, "A review of shape memory alloy research, applications and opportunities," *Materials & Design,* vol. 56, pp. 1078-1113, 4// 2014.

[71] J. Leng, X. Lan, Y. Liu, and S. Du, "Shape-memory polymers and their composites: Stimulus methods and applications," *Progress in Materials Science,* vol. 56, pp. 1077-1135, 9// 2011.

[72] L. Sun, W. M. Huang, Z. Ding, Y. Zhao, C. C. Wang, H. Purnawali, *et al.*, "Stimulus-responsive shape memory materials: A review," *Materials & Design,* vol. 33, pp. 577-640, 1// 2012.

[73] W. Krzys and A. Muc, "Buckling and post-buckling behavior of shells under unilateral constraints," in *Post-Buckling of Elastic Structures: Proceedings of the Euromech Colloquium No. 200,* Mátrafüred, Hungary, 1985, pp. 171-184.

[74] H. Chai, "On the post-buckling behavior of bilaterally constrained plates," *International Journal of Solids and Structures,* vol. 39, pp. 2911-2926, 6// 2002.

[75] M. Piñeirua, M. Adda-Bedia, and S. Moulinet, "Spooling and disordered packing of elastic rods in cylindrical cavities," *EPL (Europhysics Letters),* vol. 104, p. 14005, 2013.

[76] H. A. Eschenauer and N. Olhoff, "Topology optimization of continuum structures: a review," *Applied Mechanics Reviews,* vol. 54, pp. 331-389, 2001.

[77] M. P. Bendsoe and O. Sigmund, *Topology optimization: theory, methods and applications*: Springer, 2003.

[78] J. Deaton and R. Grandhi, "A survey of structural and multidisciplinary continuum topology optimization: post 2000," *Structural and Multidisciplinary Optimization,* pp. 1-38, 2013/07/04 2013.

[79] T. Sekimoto and H. Noguchi, "Homologous Topology Optimization in Large Displacement and Buckling Problems," *JSME International Journal Series A Solid Mechanics and Material Engineering,* vol. 44, pp. 616-622, 2001.

[80] T. E. Bruns, O. Sigmund, and D. A. Tortorelli, "Numerical methods for the topology optimization of structures that exhibit snap-through," *International Journal for Numerical Methods in Engineering,* vol. 55, pp. 1215-1237, 2002.

[81] T. E. Bruns and O. Sigmund, "Toward the topology design of mechanisms that exhibit snap-through behavior," *Computer Methods in Applied Mechanics and Engineering,* vol. 193, pp. 3973-4000, 9/10/ 2004.

[82] R. Kemmler, A. Lipka, and E. Ramm, "Large deformations and stability in topology optimization," *Structural and Multidisciplinary Optimization,* vol. 30, pp. 459-476, 2005/12/01 2005.

[83] M. Kegl, B. Brank, B. Harl, and M. M. Oblak, "Efficient handling of stability problems in shell optimization by asymmetric 'worst-case' shape imperfection," *International Journal for Numerical Methods in Engineering,* vol. 73, pp. 1197-1216, 2008.

[84] M. Kögl and E. C. N. Silva, "Topology optimization of smart structures: design of piezoelectric plate and shell actuators," *Smart Materials and Structures,* vol. 14, p. 387, 2005.

[85] Z. Luo, Q. Luo, L. Tong, W. Gao, and C. Song, "Shape morphing of laminated composite structures with photostrictive actuators via topology optimization," *Composite Structures,* vol. 93, pp. 406-418, 1// 2011.

[86] C. Y. Kiyono, E. C. N. Silva, and J. N. Reddy, "Design of laminated piezocomposite shell transducers with arbitrary fiber orientation using topology optimization approach," *International Journal for Numerical Methods in Engineering,* vol. 90, pp. 1452-1484, 2012.

[87] J. S. Han, J. S. Ko, and J. G. Korvink, "Structural optimization of a large-displacement electromagnetic Lorentz force microactuator for optical switching applications," *Journal of Micromechanics and Microengineering,* vol. 14, p. 1585, 2004.

[88] M. Howard, J. Pajot, K. Maute, and M. L. Dunn, "A computational design methodology for assembly and actuation of thin-film structures via patterning of eigenstrains," *Microelectromechanical Systems, Journal of,* vol. 18, pp. 1137-1148, 2009.

[89] D. N. Betts, H. A. Kim, C. R. Bowen, and D. J. Inman, "Optimal configurations of bistable piezo-composites for energy harvesting," *Applied Physics Letters,* vol. 100, p. 114104, 2012.

[90] A. Takezawa, M. Kitamura, S. L. Vatanabe, and E. C. N. Silva, "Design methodology of piezoelectric energy-harvesting skin using topology optimization," *Structural and Multidisciplinary Optimization,* vol. 49, pp. 281-297, 2014/02/01 2014.

[91] S. Y. Kim, C. K. Mechefske, and I. Y. Kim, "Optimal damping layout in a shell structure using topology optimization," *Journal of Sound and Vibration,* vol. 332, pp. 2873-2883, 6/10/ 2013.

[92] M. Ohsaki and S. Nishiwaki, "Shape design of pin-jointed multistable compliant mechanisms using snapthrough behavior," *Structural and Multidisciplinary Optimization,* vol. 30, pp. 327-334, 2005/10/01 2005.

[93] B. Zhu and X. Zhang, "A new level set method for topology optimization of distributed compliant mechanisms," *International Journal for Numerical Methods in Engineering,* vol. 91, pp. 843-871, 2012.

[94] A. Takezawa and M. Kitamura, "Geometrical design of thermoelectric generators based on topology optimization," *International Journal for Numerical Methods in Engineering,* vol. 90, pp. 1363-1392, 2012.

[95] B. Stanford and P. Beran, "Aerothermoelastic topology optimization with flutter and buckling metrics," *Structural and Multidisciplinary Optimization,* vol. 48, pp. 149-171, 2013/07/01 2013.

[96] N. Hu and R. Burgueño, "Buckling-induced smart applications: recent advances and trends," *Smart Materials and Structures,* vol. 24, p. 063001, 2015.

[97] H. Kim, J.-H. Kim, and J. Kim, "A review of piezoelectric energy harvesting based on vibration," *International Journal of Precision Engineering and Manufacturing,* vol. 12, pp. 1129-1141, 2011/12/01 2011.

[98] A. Harb, "Energy harvesting: State-of-the-art," *Renewable Energy,* vol. 36, pp. 2641-2654, 10// 2011.

[99] R. C. Batra, M. Porfiri, and D. Spinello, "Review of modeling electrostatically actuated microelectromechanical systems," *Smart Materials and Structures,* vol. 16, p. R23, 2007.

[100] W.-M. Zhang, H. Yan, Z.-K. Peng, and G. Meng, "Electrostatic pull-in instability in MEMS/NEMS: A review," *Sensors and Actuators A: Physical,* vol. 214, pp. 187-218, 8/1/ 2014.

[101] J. P. Lynch and K. J. Loh, "A summary review of wireless sensors and sensor networks for structural health monitoring," *Shock and Vibration Digest,* vol. 38, pp. 91-130, 2006.

[102] S. C. Yuen and G. N. Nurick, "The energy-absorbing characteristics of tubular structures with geometric and material modifications: an overview," *Applied Mechanics Reviews,* vol. 61, p. 020802, 2008.

[103] C. Winkelmann, S. S. Kim, and V. La Saponara, "Design and development of hybrid composite bistable structures for energy absorption under quasi-static tensile loading," *Composite Structures,* vol. 93, pp. 171-178, 12// 2010.

[104] K. V. Avramov and Y. V. Mikhlin, "Snap-through truss as a vibration absorber," *Journal of Vibration and Control,* vol. 10, pp. 291-308, February 1, 2004 2004.

[105] J. Winterflood, D. G. Blair, and B. Slagmolen, "High performance vibration isolation using springs in Euler column buckling mode," *Physics Letters A,* vol. 300, pp. 122-130, 7/29/ 2002.

[106] A. Carrella, M. J. Brennan, and T. P. Waters, "Static analysis of a passive vibration isolator with quasi-zero-stiffness characteristic," *Journal of Sound and Vibration,* vol. 301, pp. 678-689, 4/3/ 2007.

[107] R. A. Ibrahim, "Recent advances in nonlinear passive vibration isolators," *Journal of Sound and Vibration,* vol. 314, pp. 371-452, 7/22/ 2008.

[108] H. Sadeghian, Y. Chung-Kai, J. F. L. Goosen, E. Van der Drift, A. Bossche, P. J. French, *et al.,* "Characterizing size-dependent effective elastic modulus of silicon nanocantilevers using electrostatic pull-in instability," *Applied Physics Letters,* vol. 94, p. 221903, 2009.

[109] D. P. Holmes and A. J. Crosby, "Snapping Surfaces," *Advanced Materials,* vol. 19, pp. 3589-3593, 2007.

[110] K. Bertoldi and M. C. Boyce, "Mechanically triggered transformations of phononic band gaps in periodic elastomeric structures," *Physical Review B,* vol. 77, p. 052105, 02/27/ 2008.

[111] J. Prasad and A. R. Diaz, "A concept for a material that softens with frequency," *Journal of Mechanical Design,* vol. 130, p. 091703, 2008.

[112] Z. Zhang and T. Li, "Graphene morphology regulated by nanowires patterned in parallel on a substrate surface," *Journal of Applied Physics,* vol. 107, p. 103519, 2010.

[113] P. Pour Shahid Saeed Abadi, S. B. Hutchens, J. R. Greer, B. A. Cola, and S. Graham, "Buckling-driven delamination of carbon nanotube forests," *Applied Physics Letters,* vol. 102, p. 223103, 2013.

[114] N. Elvin, G., N. Lajnef, and A. Elvin, A. , "Feasibility of structural monitoring with vibration powered sensors," *Smart Materials and Structures,* vol. 15, p. 977, 2006.

[115] G. Park, T. Rosing, M. Todd, C. Farrar, and W. Hodgkiss, "Energy Harvesting for Structural Health Monitoring Sensor Networks," *Journal of Infrastructure Systems,* vol. 14, pp. 64-79, 2008.

[116] W. K. G. Seah, E. Zhi Ang, and H. Tan, "Wireless sensor networks powered by ambient energy harvesting (WSN-HEAP) - Survey and challenges," in *Wireless Communication,*

Vehicular Technology, Information Theory and Aerospace & Electronic Systems Technology, 2009. Wireless VITAE 2009. 1st International Conference on, 2009, pp. 1-5.

[117] S. F. Ali, M. I. Friswell, and S. Adhikari, "Analysis of energy harvesters for highway bridges," *Journal of Intelligent Material Systems and Structures,* vol. 22, pp. 1929-1938, November 1, 2011 2011.

[118] N. Lajnef, W. Borchani, R. Burgueno, and S. Chakrabartty, "Self-Powered Piezo-Floating-Gate Smart-Gauges Based on Quasi-Static Mechanical Energy Concentrators and Triggers," *Sensors Journal, IEEE,* vol. 15, pp. 676-683, 2015.

[119] S. Daynes and P. M. Weaver, "Review of shape-morphing automobile structures: concepts and outlook," *Proceedings of the Institution of Mechanical Engineers, Part D: Journal of Automobile Engineering,* vol. 227, pp. 1603-1622, November 1, 2013 2013.

[120] X. Lachenal, S. Daynes, and P. M. Weaver, "Review of morphing concepts and materials for wind turbine blade applications," *Wind Energy,* vol. 16, pp. 283-307, 2013.

[121] G. Georgios, M. Javier, and V. John, "Snap-through buckling behavior of piezoelectric bimorph beams: II. Experimental verification," *Smart Materials and Structures,* vol. 16, p. 1158, 2007.

[122] G. Georgios, M. Javier, and V. John, "Snap-through buckling behavior of piezoelectric bimorph beams: I. Analytical and numerical modeling," *Smart Materials and Structures,* vol. 16, p. 1148, 2007.

[123] C. Maurini, J. Pouget, and S. Vidoli, "Distributed piezoelectric actuation of a bistable buckled beam," *European Journal of Mechanics - A/Solids,* vol. 26, pp. 837-853, 9// 2007.

[124] X. Chen, L. S. Ma, Y. M. Zheng, X. X. Li, and D. W. Lee, "The influences of transverse loads on electrothermal post-buckling microbeams," *Journal of Micromechanics and Microengineering,* vol. 22, p. 015011, 2012.

[125] A. B. Pippard, "The elastic arch and its modes of instability," *European Journal of Physics,* vol. 11, p. 359, 1990.

[126] Y. Zhang, Y. Wang, and Z. Li, "Analytical method of predicating the instabilities of a micro arch-shaped beam under electrostatic loading," *Microsystem Technologies,* vol. 16, pp. 909-918, 2010/06/01 2010.

[127] F. Cellini, Y. Cha, and M. Porfiri, "Energy harvesting from fluid-induced buckling of ionic polymer metal composites," *Journal of Intelligent Material Systems and Structures,* vol. 25, pp. 1496-1510, 2014.

[128] F. Cottone, P. Basset, H. Vocca, L. Gammaitoni, and T. Bourouina, "Bistable electromagnetic generator based on buckled beams for vibration energy harvesting," *Journal of Intelligent Material Systems and Structures,* October 25, 2013 2013.

[129] A. Fargette, S. Neukirch, and A. Antkowiak, "Elastocapillary Snapping: Capillarity Induces Snap-Through Instabilities in Small Elastic Beams," *Physical Review Letters,* vol. 112, p. 137802, 04/04/ 2014.

[130] S. Krylov, B. Ilic, and S. Lulinsky, "Bistability of curved microbeams actuated by fringing electrostatic fields," *Nonlinear Dynamics,* vol. 66, pp. 403-426, 2011/11/01 2011.

[131] C.-Y. Lee and J.-H. Kim, "Thermal post-buckling and snap-through instabilities of FGM panels in hypersonic flows," *Aerospace Science and Technology,* vol. 30, pp. 175-182, 10// 2013.

[132] A. Pirrera, D. Avitabile, and P. M. Weaver, "On the thermally induced bistability of composite cylindrical shells for morphing structures," *International Journal of Solids and Structures,* vol. 49, pp. 685-700, 3/1/ 2012.

[133] R. Ramlan, M. J. Brennan, B. R. Mace, and S. G. Burrow, "On the performance of a dual-mode non-linear vibration energy harvesting device," *Journal of Intelligent Material Systems and Structures,* May 6, 2012 2012.

[134] M. R. Shankar, M. L. Smith, V. P. Tondiglia, K. M. Lee, M. E. McConney, D. H. Wang, *et al.*, "Contactless, photoinitiated snap-through in azobenzene-functionalized polymers," *Proceedings of the National Academy of Sciences,* vol. 110, pp. 18792-18797, November 19, 2013 2013.

[135] C. Bisagni and P. Cordisco, "Post-buckling and collapse experiments of stiffened composite cylindrical shells subjected to axial loading and torque," *Composite Structures,* vol. 73, pp. 138-149, 5// 2006.

[136] M. Yazdani and G. H. Rahimi, "The Effects of Helical Ribs' Number and Grid Types on the Buckling of Thin-walled GFRP-stiffened Shells under Axial Loading," *Journal of Reinforced Plastics and Composites,* vol. 29, pp. 2568-2575, September 1, 2010 2010.

[137] W. Miller, C. W. Smith, F. Scarpa, and K. E. Evans, "Flatwise buckling optimization of hexachiral and tetrachiral honeycombs," *Composites Science and Technology,* vol. 70, pp. 1049-1056, 7// 2010.

[138] J. Błachut, "Experimental Perspective on the Buckling of Pressure Vessel Components," *Applied Mechanics Reviews,* vol. 66, pp. 010803-010803, 2013.

[139] A. D. Shaw, S. A. Neild, D. J. Wagg, P. M. Weaver, and A. Carrella, "A nonlinear spring mechanism incorporating a bistable composite plate for vibration isolation," *Journal of Sound and Vibration,* vol. 332, pp. 6265-6275, 11/25/ 2013.

[140] D. Pasala, A. Sarlis, S. Nagarajaiah, A. Reinhorn, M. Constantinou, and D. Taylor, "Adaptive Negative Stiffness: New Structural Modification Approach for Seismic Protection," *Journal of Structural Engineering,* vol. 139, pp. 1112-1123, 2013.

[141] A. Sarlis, D. Pasala, M. Constantinou, A. Reinhorn, S. Nagarajaiah, and D. Taylor, "Negative Stiffness Device for Seismic Protection of Structures," *Journal of Structural Engineering*, vol. 139, pp. 1124-1133, 2013.

[142] A. Brinkmeyer, M. Santer, A. Pirrera, and P. M. Weaver, "Pseudo-bistable self-actuated domes for morphing applications," *International Journal of Solids and Structures*, vol. 49, pp. 1077-1087, 5/1/ 2012.

[143] M. K. Ramasubramanian, O. M. Barham, and V. Swaminathan, "Mechanics of a mosquito bite with applications to microneedle design," *Bioinspiration & Biomimetics*, vol. 3, p. 046001, 2008.

[144] Y. Forterre, J. M. Skotheim, J. Dumais, and L. Mahadevan, "How the Venus flytrap snaps," *Nature*, vol. 433, pp. 421-425, 01/27/print 2005.

[145] J. Lienhard, S. Schleicher, S. Poppinga, T. Masselter, M. Milwich, T. Speck, *et al.*, "Flectofin: a hingeless flapping mechanism inspired by nature," *Bioinspiration & Biomimetics*, vol. 6, p. 045001, 2011.

[146] K. Seung-Won, K. Je-Sung, L. Jong-Gu, R. Junghyun, C. Maenghyo, and C. Kyu-Jin, "Flytrap-inspired robot using structurally integrated actuation based on bistability and a developable surface," *Bioinspiration & Biomimetics*, vol. 9, p. 036004, 2014.

[147] S. Armon, E. Efrati, R. Kupferman, and E. Sharon, "Geometry and Mechanics in the Opening of Chiral Seed Pods," *Science*, vol. 333, pp. 1726-1730, September 23, 2011 2011.

[148] S. Mukherjee and R. Ganguli, "Nonlinear dynamic analysis of dragonfly-inspired piezoelectric unimorph actuated flapping and twisting wing," *International Journal of Smart and Nano Materials*, vol. 3, pp. 103-122, 2012/06/01 2012.

[149] D. S. A. De Focatiis and S. D. Guest, "Deployable membranes designed from folding tree leaves," *Philosophical Transactions of the Royal Society of London. Series A: Mathematical, Physical and Engineering Sciences*, vol. 360, pp. 227-238, February 15, 2002 2002.

[150] A. Pirrera, X. Lachenal, S. Daynes, P. M. Weaver, and I. V. Chenchiah, "Multi-stable cylindrical lattices," *Journal of the Mechanics and Physics of Solids*, vol. 61, pp. 2087-2107, 11// 2013.

[151] S. Daynes, A. Grisdale, A. Seddon, and R. Trask, "Morphing structures using soft polymers for active deployment," *Smart Materials and Structures*, vol. 23, p. 012001, 2014.

[152] V. G. A. Goss, G. H. M. Heijden, J. M. T. Thompson, and S. Neukirch, "Experiments on snap buckling, hysteresis and loop formation in twisted rods," *Experimental Mechanics*, vol. 45, pp. 101-111, 2005/04/01 2005.

[153] D. Bigoni, F. Bosi, F. Dal Corso, and D. Misseroni, "Instability of a penetrating blade," *Journal of the Mechanics and Physics of Solids,* vol. 64, pp. 411-425, 3// 2014.

[154] A. Pandey, D. E. Moulton, D. Vella, and D. P. Holmes, "Dynamics of snapping beams and jumping poppers," *EPL (Europhysics Letters),* vol. 105, p. 24001, 2014.

[155] J. Huang, J. Liu, B. Kroll, K. Bertoldi, and D. R. Clarke, "Spontaneous and deterministic three-dimensional curling of pre-strained elastomeric bi-strips," *Soft Matter,* vol. 8, pp. 6291-6300, 2012.

[156] P.-O. Mouthuy, M. Coulombier, T. Pardoen, J.-P. Raskin, and A. M. Jonas, "Overcurvature describes the buckling and folding of rings from curved origami to foldable tents," *Nat Commun,* vol. 3, p. 1290, 12/18/online 2012.

[157] Y. Klein, E. Efrati, and E. Sharon, "Shaping of Elastic Sheets by Prescription of Non-Euclidean Metrics," *Science,* vol. 315, pp. 1116-1120, February 23, 2007 2007.

[158] C. D. Santangelo, "Buckling thin disks and ribbons with non-Euclidean metrics," *EPL (Europhysics Letters),* vol. 86, p. 34003, 2009.

[159] Z. W. Yao, M. Bowick, X. Ma, and R. Sknepnek, "Planar sheets meet negative-curvature liquid interfaces," *EPL (Europhysics Letters),* vol. 101, p. 44007, 2013.

[160] M. Dias, A. and C. D. Santangelo, "The shape and mechanics of curved-fold origami structures," *EPL (Europhysics Letters),* vol. 100, p. 54005, 2012.

[161] Q. Guo, A. K. Mehta, M. A. Grover, W. Chen, D. G. Lynn, and Z. Chen, "Shape selection and multi-stability in helical ribbons," *Applied Physics Letters,* vol. 104, p. 211901, 2014.

[162] G. W. Hunt and I. Ario, "Twist buckling and the foldable cylinder: an exercise in origami," *International Journal of Non-Linear Mechanics,* vol. 40, pp. 833-843, 7// 2005.

[163] J. Shim, C. Perdigou, E. R. Chen, K. Bertoldi, and P. M. Reis, "Buckling-induced encapsulation of structured elastic shells under pressure," *Proceedings of the National Academy of Sciences,* vol. 109, pp. 5978-5983, April 17, 2012 2012.

[164] S. Knoche and J. Kierfeld, "Secondary polygonal instability of buckled spherical shells," *EPL (Europhysics Letters),* vol. 106, p. 24004, 2014.

[165] P. Wang, F. Casadei, S. H. Kang, and K. Bertoldi, "Locally resonant band gaps in periodic beam lattices by tuning connectivity," *Physical Review B,* vol. 91, p. 020103, 01/26/ 2015.

[166] S. Shan, S. H. Kang, P. Wang, C. Qu, S. Shian, E. R. Chen, *et al.*, "Harnessing Multiple Folding Mechanisms in Soft Periodic Structures for Tunable Control of Elastic Waves," *Advanced Functional Materials,* vol. 24, pp. 4935-4942, 2014.

[167] P. Portela, P. Camanho, P. Weaver, and I. Bond, "Analysis of morphing, multi stable structures actuated by piezoelectric patches," *Computers & Structures,* vol. 86, pp. 347-356, 2// 2008.

[168] C. R. McInnes and T. J. Waters, "Reconfiguring smart structures using phase space connections," *Smart Materials and Structures,* vol. 17, p. 025030, 2008.

[169] K. Seffen, "Bi-stable Concepts for Reconfigurable Structures," in *45th AIAA/ASME/ASCE/AHS/ASC Structures, Structural Dynamics & Materials Conference*, ed: American Institute of Aeronautics and Astronautics, 2004.

[170] A. F. Arrieta, O. Bilgen, M. I. Friswell, and P. Hagedorn, "Dynamic control for morphing of bi-stable composites," *Journal of Intelligent Material Systems and Structures,* June 27, 2012 2012.

[171] B. Onur, F. A. Andres, I. F. Michael, and H. Peter, "Dynamic control of a bistable wing under aerodynamic loading," *Smart Materials and Structures,* vol. 22, p. 025020, 2013.

[172] H. Chai, "The post-buckling response of a bi-laterally constrained column," *Journal of the Mechanics and Physics of Solids,* vol. 46, pp. 1155-1181, 7// 1998.

[173] J. D. Deaton and R. Grandhi, "A survey of structural and multidisciplinary continuum topology optimization: post 2000," *Structural and Multidisciplinary Optimization,* pp. 1-38, 2013/07/04 2013.

[174] S. Daynes and P. M. Weaver, "Stiffness tailoring using prestress in adaptive composite structures," *Composite Structures,* vol. 106, pp. 282-287, 12// 2013.

[175] R. A. Steven and A. S. Henry, "A review of power harvesting using piezoelectric materials (2003–2006)," *Smart Materials and Structures,* vol. 16, p. R1, 2007.

[176] S. Saadon and O. Sidek, "A review of vibration-based MEMS piezoelectric energy harvesters," *Energy Conversion and Management,* vol. 52, pp. 500-504, 1// 2011.

[177] C. R. Bowen, H. A. Kim, P. M. Weaver, and S. Dunn, "Piezoelectric and ferroelectric materials and structures for energy harvesting applications," *Energy & Environmental Science,* vol. 7, pp. 25-44, 2014.

[178] A. Mukherjee and A. S. Chaudhuri, "Active control of dynamic instability of piezolaminated imperfect columns," *Smart Materials and Structures,* vol. 11, p. 874, 2002.

[179] S. Srinivasan and K. Sunjung, "Piezoelectric control of columns prone to instabilities and nonlinear modal interaction," *Smart Materials and Structures,* vol. 17, p. 035001, 2008.

[180] Q. S. Wang, "Active buckling control of beams using piezoelectric actuators and strain gauge sensors," *Smart Materials and Structures,* vol. 19, p. 065022, 2010.

[181] I. Karaman, B. Basaran, H. E. Karaca, A. I. Karsilayan, and Y. I. Chumlyakov, "Energy harvesting using martensite variant reorientation mechanism in a NiMnGa magnetic shape memory alloy," *Applied Physics Letters,* vol. 90, p. 172505, 2007.

[182] A. Nespoli, S. Besseghini, S. Pittaccio, E. Villa, and S. Viscuso, "The high potential of shape memory alloys in developing miniature mechanical devices: A review on shape memory alloy mini-actuators," *Sensors and Actuators A: Physical,* vol. 158, pp. 149-160, 3// 2010.

[183] O. E. Ozbulut, S. Hurlebaus, and R. DesRoches, "Seismic Response Control Using Shape Memory Alloys: A Review," *Journal of Intelligent Material Systems and Structures,* August 5, 2011 2011.

[184] Z. Suo, "Theory of dielectric elastomers," *Acta Mechanica Solida Sinica,* vol. 23, pp. 549-578, 12// 2010.

[185] L. Liu, Z. Zhang, Y. Liu, and J. Leng, "Electroactive Polymer Soft Material Based on Dielectric Elastomer," in *Responsive Membranes and Materials*, ed: John Wiley & Sons, Ltd., 2012, pp. 315-384.

[186] B. Li, L. Liu, and Z. Suo, "Extension limit, polarization saturation, and snap-through instability of dielectric elastomers," *International Journal of Smart and Nano Materials,* vol. 2, pp. 59-67, 2011/04/19 2011.

[187] H. S. Park, Q. Wang, X. Zhao, and P. A. Klein, "Electromechanical instability on dielectric polymer surface: Modeling and experiment," *Computer Methods in Applied Mechanics and Engineering,* vol. 260, pp. 40-49, 6/15/ 2013.

[188] C. Keplinger, T. Li, R. Baumgartner, Z. Suo, and S. Bauer, "Harnessing snap-through instability in soft dielectrics to achieve giant voltage-triggered deformation," *Soft Matter,* vol. 8, pp. 285-288, 2012.

[189] B. Li, H. Chen, J. Qiang, and J. Zhou, "A model for conditional polarization of the actuation enhancement of a dielectric elastomer," *Soft Matter,* vol. 8, pp. 311-317, 2012.

[190] L. Liu, Y. Liu, B. Li, K. Yang, T. Li, and J. Leng, "Thermo-electro-mechanical instability of dielectric elastomers," *Smart Materials and Structures,* vol. 20, p. 075004, 2011.

[191] V. Rocco, F. Antonio, B. Massimo, C. Federico, F. Gabriele, and R. Danilo De, "Modeling and experimental validation of buckling dielectric elastomer actuators," *Smart Materials and Structures,* vol. 21, p. 094005, 2012.

[192] B. Tavakol, M. Bozlar, C. Punckt, G. Froehlicher, H. A. Stone, I. A. Aksay, *et al.*, "Buckling of dielectric elastomeric plates for soft, electrically active microfluidic pumps," *Soft Matter,* vol. 10, pp. 4789-4794, 2014.

[193] T. Li, S. Qu, and W. Yang, "Energy harvesting of dielectric elastomer generators concerning inhomogeneous fields and viscoelastic deformation," *Journal of Applied Physics,* vol. 112, p. 034119, 2012.

[194] D. L. Henann, S. A. Chester, and K. Bertoldi, "Modeling of dielectric elastomers: Design of actuators and energy harvesting devices," *Journal of the Mechanics and Physics of Solids,* vol. 61, pp. 2047-2066, 10// 2013.

[195] G. Kang, K.-S. Kim, and S. Kim, "Note: Analysis of the efficiency of a dielectric elastomer generator for energy harvesting," *Review of Scientific Instruments,* vol. 82, p. 046101, 2011.

[196] T. G. McKay, B. M. O'Brien, E. P. Calius, and I. A. Anderson, "Soft generators using dielectric elastomers," *Applied Physics Letters,* vol. 98, p. 142903, 2011.

[197] L. Liu, Y. Liu, and J. Leng, "Theory progress and applications of dielectric elastomers," *International Journal of Smart and Nano Materials,* vol. 4, pp. 199-209, 2013/09/01 2013.

[198] X. Zhao and Q. Wang, "Harnessing large deformation and instabilities of soft dielectrics: Theory, experiment, and application," *Applied Physics Reviews,* vol. 1, p. 021304, 2014.

[199] T. Li and Z. Zhang, "Snap-Through Instability of Graphene on Substrates," *Nanoscale Research Letters,* vol. 5, pp. 169-173, 2010/01/01 2010.

[200] S. Scharfenberg, N. Mansukhani, C. Chialvo, R. L. Weaver, and N. Mason, "Observation of a snap-through instability in graphene," *Applied Physics Letters,* vol. 100, p. 021910, 2012.

[201] N. G. Boddeti, X. Liu, R. Long, J. Xiao, J. S. Bunch, and M. L. Dunn, "Graphene Blisters with Switchable Shapes Controlled by Pressure and Adhesion," *Nano Letters,* vol. 13, pp. 6216-6221, 2013/12/11 2013.

[202] J.-H. Jeon, T.-H. Cheng, and I.-K. Oh, "Snap-through dynamics of buckled IPMC actuator," *Sensors and Actuators A: Physical,* vol. 158, pp. 300-305, 3// 2010.

[203] B. Bhandari, G.-Y. Lee, and S.-H. Ahn, "A review on IPMC material as actuators and sensors: Fabrications, characteristics and applications," *International Journal of Precision Engineering and Manufacturing,* vol. 13, pp. 141-163, 2012/01/01 2012.

[204] D. Bushnell, *Computerized buckling analysis of shells* vol. 9: Springer Science & Business Media, 1985.

[205] W. T. Koiter, "Over de stabiliteit van het elastisch evenwicht," 1945.

[206] B. Budiansky and J. W. Hutchinson, "Buckling of circular cylindrical shells under axial compression," *Contributions to the Theory of Aircraft Structures Delft University Press,* pp. 239-259, 1972.

[207] W. T. Koiter, I. Elishakoff, Y. W. Li, and J. H. Starnes Jr, "Buckling of an axially compressed cylindrical shell of variable thickness," *International Journal of Solids and Structures,* vol. 31, pp. 797-805, 3// 1994.

[208] Y. W. Li, I. Elishakoff, and J. H. Starnes Jr, "Axial buckling of composite cylindrical shells with periodic thickness variation," *Computers & Structures,* vol. 56, pp. 65-74, 7/3/ 1995.

[209] Y.-W. Li, I. Elishakoff, J. H. Starnes Jr, and D. Bushnell, "Effect of the thickness variation and initial imperfection on buckling of composite cylindrical shells: Asymptotic analysis and numerical results by BOSOR4 and PANDA2," *International Journal of Solids and Structures,* vol. 34, pp. 3755-3767, 10// 1997.

[210] Z. Chen, L. Yang, G. Cao, and W. Guo, "Buckling of the axially compressed cylindrical shells with arbitrary axisymmetric thickness variation," *Thin-Walled Structures,* vol. 60, pp. 38-45, 11// 2012.

[211] J. M. T. Thompson and A. C. Walker, "A general theory for the branching analysis of discrete structural systems," *International Journal of Solids and Structures,* vol. 5, pp. 281-288, 4// 1969.

[212] P. T. Pedersen, "On the Collapse Load of Cylindrical Shells," in *Buckling of Structures*, B. Budiansky, Ed., ed: Springer Berlin Heidelberg, 1976, pp. 27-39.

[213] R. C. Tennyson and K. C. Chan, "Buckling of imperfect sandwich cylinders under axial compression," *International Journal of Solids and Structures,* vol. 26, pp. 1017-1036, // 1990.

[214] H. Huang and Q. Han, "Nonlinear buckling and postbuckling of heated functionally graded cylindrical shells under combined axial compression and radial pressure," *International Journal of Non-Linear Mechanics,* vol. 44, pp. 209-218, 3// 2009.

[215] T. Kobayashi, Y. Mihara, and F. Fujii, "Path-tracing analysis for post-buckling process of elastic cylindrical shells under axial compression," *Thin-Walled Structures,* vol. 61, pp. 180-187, 12// 2012.

[216] R. S. Priyadarsini, V. Kalyanaraman, and S. M. Srinivasan, "Numerical and experimental study of buckling of advanced fiber composite cylinders under axial compression," *International Journal of Structural Stability and Dynamics,* vol. 12, p. 1250028, Jul 2012.

[217] T. A. Winterstetter and H. Schmidt, "Stability of circular cylindrical steel shells under combined loading," *Thin-Walled Structures,* vol. 40, pp. 893-910, 10// 2002.

[218] R. Burgueño, N. Hu, and N. Lajnef, "Title," unpublished|.

[219] T. Zhang and W. Gu, "The Secondary Buckling and Design Criterion of Composite Laminated Cylindrical Shells," *Applied Composite Materials,* vol. 19, pp. 203-217, 2012/06/01 2012.

[220] C. Fang and G. S. Springer, "Design of Composite Laminates by a Monte Carlo Method," *Journal of Composite Materials,* vol. 27, pp. 721-753, July 1, 1993 1993.

[221] C. A. Schenk and G. I. Schu ller, "Buckling analysis of cylindrical shells with random geometric imperfections," *International Journal of Non-Linear Mechanics,* vol. 38, pp. 1119-1132, 10// 2003.

[222] M. Broggi and G. I. Schu ller, "Efficient modeling of imperfections for buckling analysis of composite cylindrical shells," *Engineering Structures,* vol. 33, pp. 1796-1806, 5// 2011.

[223] Dassault Syst èmes, *ABAQUS, User Manual Version 6.12,* 2012.

[224] C. Bisagni, "Dynamic buckling of fiber composite shells under impulsive axial compression," *Thin-Walled Structures,* vol. 43, pp. 499-514, 3// 2005.

[225] M. K. Chryssanthopoulos, A. Y. Elghazouli, and I. E. Esong, "Compression tests on anti-symmetric two-ply GFRP cylinders," *Composites Part B: Engineering,* vol. 30, pp. 335-350, 6// 1999.

[226] E. Eglītis, K. Kalniņš, and O. Ozoliņš, "Experimental and numerical study on buckling of axially compressed composite cylinders," *Scientific Journal of Riga Technical University. Construction Science,* vol. 10, pp. 33-49, 2009.

[227] C. York, "Unified Approach to the Characterization of Coupled Composite Laminates: Benchmark Configurations and Special Cases," *Journal of Aerospace Engineering,* vol. 23, pp. 219-242, 2010.

[228] C. Jiang and G. F. Zhao, "A Preliminary Study of 3D Printing on Rock Mechanics," *Rock Mechanics and Rock Engineering,* pp. 1-10, 2014/06/18 2014.

[229] A. R. Torrado Perez, D. A. Roberson, and R. B. Wicker, "Fracture Surface Analysis of 3D-Printed Tensile Specimens of Novel ABS-Based Materials," *Journal of Failure Analysis and Prevention,* vol. 14, pp. 343-353, 2014/06/01 2014.

[230] Dassault Syst èmes, "SolidWorks 2013 x64 Edition," Waltham, Massachusetts, USA2013.

[231] N. Hu, R. Burgue ño, and N. Lajnef, "Structural optimization and form-finding of cylindrical shell for a targeted elastic postbuckling response," presented at the In: Proceeding of ASME Smart Materials, Adaptive Structures and Intelligent Systems, SMASIS2014, Newport, Rhode Island, USA., 2014.

[232] J. C. Amazigo and J. W. Hutchinson, "Imperfection-sensitivity of eccentrically stiffened cylindrical shells," *AIAA Journal,* vol. 5, pp. 392-401, 1967/03/01 1967.

[233] Y. W. Li, I. Elishakoff, J. H. Starnes Jr, and D. Bushnell, "Effect of the thickness variation and initial imperfection on buckling of composite cylindrical shells: Asymptotic analysis and numerical results by BOSOR4 and PANDA2," *International Journal of Solids and Structures,* vol. 34, pp. 3755-3767, 10// 1997.

[234] Z.-M. Li and D.-Q. Yang, "Postbuckling of shear deformable stiffened anisotropic laminated cylindrical shell under axial compression," *Ocean Engineering,* vol. 38, pp. 1246-1255, 7// 2011.

[235] J. F. Ma, W. Y. Chen, L. Zhao, and D. H. Zhao, "Elastic Buckling of Bionic Cylindrical Shells Based on Bamboo," *Journal of Bionic Engineering,* vol. 5, pp. 231-238, 9// 2008.

[236] H. Ghiasi, K. Fayazbakhsh, D. Pasini, and L. Lessard, "Optimum stacking sequence design of composite materials Part II: Variable stiffness design," *Composite Structures,* vol. 93, pp. 1-13, 12// 2010.

[237] E. Lund, "Buckling topology optimization of laminated multi-material composite shell structures," *Composite Structures,* vol. 91, pp. 158-167, 11// 2009.

[238] A. W. Blom, P. B. Stickler, and Z. Gürdal, "Optimization of a composite cylinder under bending by tailoring stiffness properties in circumferential direction," *Composites Part B: Engineering,* vol. 41, pp. 157-165, 3// 2010.

[239] J. Díaz, C. Fagiano, M. M. Abdalla, Z. Gürdal, and S. Hernández, "A study of interlaminar stresses in variable stiffness plates," *Composite Structures,* vol. 94, pp. 1192-1199, 2// 2012.

[240] J. Sliseris and K. Rocens, "Optimal design of composite plates with discrete variable stiffness," *Composite Structures,* vol. 98, pp. 15-23, 4// 2013.

[241] O. Stodieck, J. E. Cooper, P. M. Weaver, and P. Kealy, "Improved aeroelastic tailoring using tow-steered composites," *Composite Structures,* vol. 106, pp. 703-715, 12// 2013.

[242] O. Falcó, J. A. Mayugo, C. S. Lopes, N. Gascons, A. Turon, and J. Costa, "Variable-stiffness composite panels: As-manufactured modeling and its influence on the failure behavior," *Composites Part B: Engineering,* vol. 56, pp. 660-669, 1// 2014.

[243] K. Miura, "Proposition of pseudo-cylindrical concave polyhedral shells," in *Proceedings of IASS Symposium on Folded Plates and Prismatic Structures*, 1970.

[244] S. Lukasiewicz and W. Szyszkowski, "Geometrical analysis of large elastic deflections of axially compressed cylindrical and conical shells," *International Journal of Non-Linear Mechanics,* vol. 14, pp. 273-284, // 1979.

[245] T. Nojima, "Modelling of Folding Patterns in Flat Membranes and Cylinders by Origami," *JSME International Journal Series C Mechanical Systems, Machine Elements and Manufacturing,* vol. 45, pp. 364-370, 2002.

[246] J. Marsolek and H. G. Reimerdes, "Energy absorption of metallic cylindrical shells with induced non-axisymmetric folding patterns," *International Journal of Impact Engineering,* vol. 30, pp. 1209-1223, 9// 2004.

[247] J. Song, Y. Chen, and G. Lu, "Axial crushing of thin-walled structures with origami patterns," *Thin-Walled Structures,* vol. 54, pp. 65-71, 5// 2012.

[248] J. Song, Y. Chen, and G. Lu, "Light-weight thin-walled structures with patterned windows under axial crushing," *International Journal of Mechanical Sciences,* vol. 66, pp. 239-248, 1// 2013.

[249] Y. Chen, J. Sun, Y. Liu, and J. Leng, "Variable stiffness property study on shape memory polymer composite tube," *Smart Materials and Structures,* vol. 21, p. 094021, 2012.

[250] N. Hu, R. Burgueño, and N. Lajnef, "Structural Optimization and Form-Finding of Cylindrical Shells for Targeted Elastic Postbuckling Response," in *ASME 2014 Conference on Smart Materials, Adaptive Structures and Intelligent Systems*, 2014, pp. V001T03A008-V001T03A008.

[251] N. Hu and R. Burgueño, "Tailoring the elastic postbuckling response of cylindrical shells: A route for exploiting instabilities in materials and mechanical systems," *Extreme Mechanics Letters,* 2015.

[252] P. Holmes, G. Domokos, J. Schmitt, and I. Szeberényi, "Constrained Euler buckling: an interplay of computation and analysis," *Computer Methods in Applied Mechanics and Engineering,* vol. 170, pp. 175-207, 3/12/ 1999.

[253] Mathworks, "Matlab Version 8.2 (R2013b)," ed, 2013.

[254] Red Cedar Technology. Getting Started with HEEDS MDO 7.2 [Online].

[255] A. Lazarus and P. M. Reis, "Soft Actuation of Structured Cylinders through Auxetic Behavior," *Advanced Engineering Materials,* pp. n/a-n/a, 2015.